Titre: Title:	Development and validation of burnup dependent computational schemes for the analysis of assemblies with advanced lattice codes
Auteur: Author:	Karthikeyan Ramamoorthy
Date:	2006
Type:	Mémoire ou thèse / Dissertation or Thesis
Référence: Citation:	Ramamoorthy, K. (2006). Development and validation of burnup dependent computational schemes for the analysis of assemblies with advanced lattice codes [Thèse de doctorat, École Polytechnique de Montréal]. PolyPublie. https://publications.polymtl.ca/7782/

URL de PolyPublie: PolyPublie URL:	https://publications.polymtl.ca/7782/
Directeurs de recherche: Advisors:	
Programme: Program:	Non spécifié

UNIVERSITÉ DE MONTRÉAL

DEVELOPMENT AND VALIDATION OF BURNUP DEPENDENT COMPUTATIONAL SCHEMES FOR THE ANALYSIS OF ASSEMBLIES WITH ADVANCED LATTICE CODES

KARTHIKEYAN RAMAMOORTHY
DÉPARTEMENT DE GENIE PHYSIQUE
ÉCOLE POLYTECHNIQUE DE MONTRÉAL

THÈSE PRÉSENTÉE EN VUE DE L'OBTENTION
DU DIPLÔME DE PHILOSOPHIÆ DOCTOR
(GENIE NUCLÉAIRE)
OCTOBER 2006

Your file Votre référence
ISBN: 978-0-494-24548-4
Our file Notre référence
ISBN: 978-0-494-24548-4

UNIVERSITÉ DE MONTRÉAL

ÉCOLE POLYTECHNIQUE DE MONTRÉAL

Cette thèse intitulée:

DEVELOPMENT AND VALIDATION OF BURNUP DEPENDENT COMPUTATIONAL SCHEMES FOR THE ANALYSIS OF ASSEMBLIES WITH ADVANCED LATTICE CODES

présentée par: RAMAMOORTHY Karthikeyan
en vue de l'obtention du diplôme de: Philosophiæ Doctor
a été dûment acceptée par le jury d'examen constitué de:

M. KOCLAS Jean, Ph.D., président
M. HÉBERT Alain, D.Ing., membre et directeur de recherche
M. MARLEAU Guy, Ph.D., membre
M. ROUBEN Benjamin, Ph.D., membre

To my family, friends and almighty

ACKNOWLEDGMENTS

This research wouldn't have been possible but for the sacrifice of my family, particularly my wife, K. Srividhya, my mother R. Mythili and my daughters K. Manasvini and K. Tejasvini. I wish to sincerely thank my senior colleague, Dr. V. Jagannathan, for granting me the permission to go to Canada for two years, at a time when he needed my assistance the most for completion of important projects. His constant encouragement and valuable guidance has made me into what I am today. Thanks are due to Dr. S. Ganesan for recommending my name for the research at École Polytechnique de Montréal, Dr. R. Srivenkatesan for pursuing it and Shri R. K. Sinha for obtaining the permission at the highest level. I would like to thank my department, Bhabha Atomic Research Centre (BARC) for standing by me and protecting my interests at the professional and personal level. My special thanks to all my relatives, colleagues and friends who stood by my family during the two years when I was away from them.

I wish to sincerely thank Professor Alain Hébert, for persevering with my research and providing me all the support that a student needs to perform good research. I thank him for patiently waiting for me to join in January 2004, after accepting me as a student in September 2002. I also sincerely wish to thank Dr. Guy Marleau for the various discussions I had with him. I would also like to thank Romain Le Tellier for all the discussions we had on the subject and introducing me to the usage of all the relevant packages for my research. I would also like to thank all my friends in Montréal, for their constant emotional support during my stay of two years in Montréal. My special thanks to G. Ramkiran for providing me much needed emotional support and make me feel Montréal, a home away from home.

Last, but not the least, all this wouldn't have been possible without divine intervention, for which I sincerely thank my father, Late C. Ramamoorthy and the almighty.

RÉSUMÉ

Le but principal de cette recherche est le développement et la validation de schémas de calcul dédiés aux codes de réseaux avancés. Le code de réseau avancé faisant l'objet de cette recherche est "DRAGON Version4". Ce code possède des caractéristiques uniques, tels qu'un modèle d'autoprotection capable de représenter les effets de distribution en espace et ceux de protection mutuelle, un modèle de fuites dépendant de l'espace avec effets de *streaming* isotrope ou anisotrope, la disponibilité de la méthode des caractéristiques (MOC), une résolution des équations d'évolution iosotopique avec prise en compte des énergies correspondant à chaque réaction, etc.

Des codes de physique des réacteurs qualifiés sont requis pour l'étude de tous les réacteurs nucléaires existants ou en cours de design. Tout nouveau design requiert une analyse détaillée des paramètres de sureté du réacteur et de son comportement sous irradiation. Tout calcul de physique des réacteurs nécessite le calcul du flux neutronique correspondant à diverses régions spatiales. Ce calcul est réalisé en plusieurs étapes, la dernière permettant d'obtenir la solution recherchée. Chaque niveau du calcul de réseau est essentiel et tout compromis sur l'un d'eux est succeptible de mener à un résultat final de piètre qualité. Ces différents niveaux sont: 1. choix de la bibliothèque de données nucléaires et du découpage multigroupe sur lequel ces données sont condensées; 2. autoprotection des données nucléaires en fonction des caractéristiques géométriques et des concentrations isotopiques; 3. traçage de la géométrie de façon à conserver les erreurs surfaciques et volumiques à un niveau acceptable; 4. génération et normalisation des probabilités de collision, ou de l'information requis par la méthode des caractéristiques, en espace et en énergie; 5. solution de l'équation de transport en utilisant l'information multigroupe calculée précédemment et obtention des flux et des taux de réaction en divers endroits du réseau; 6. évolution du combustible et des autres matériaux avec normalisation à puissance ou flux constant. Parmis eux, nous allons principalement porter attention aux deux niveaux relatifs à l'autoprotection

et à l'évolution isotopique.

Le comportement du système est affecté par la composition des isotopes résonnants et des isotopes légers participant au ralentissement neutronique. Lorsque la concentration d'un isotope résonnant est faible, sa présence affecte peu la courbe de flux qui demeure non-résonnante. Lorsque sa concentration augmente, on observe une dépression locale dans la courbe de flux à l'endroit de la résonance. Cet effet de creusement va affecter les taux de réaction car ils sont égaux au produit de sections efficaces par le flux. Les taux de réaction seront donc plus faibles que si le flux était non-résonnant. Cet effet est appelé *autoprotection des résonances.* Le calcul de l'autoprotection des résonances est donc une étape essentielle du calcul de réseau. Cet effet d'autoprotection doit être correctement modélisé afin d'obtenir une solution physiquement acceptable. Dans cette recherche, nous allons analyser le comportement des modèles d'autoprotection avancés disponibles dans le code DRAGON Version4. Les modèles d'autoprotection existants sont principalement divisés en deux catégories selons qu'ils sont basés sur une *equivalence en dilution* ou sur la *méthode des sous-groupes.* Différents modèles d'autoprotection seront testés sur une variété de réseaux, tels ceux des réacteurs *Canada Deuterium Uranium* (CANDU-6), *CANDU new-generation* (CANDU-NG), à eau légère (LWR) et *à eau légère et à conversion élevée* (HCLWR). La composition du combustible va varier entre l'oxyde d'uranium naturel, l'oxyde d'uranium enrichi et l'oxyde mixte uranium-plutonium (MOX). Nous allons également analyser la présence de forts absorbants netroniques tels le Dysprosium et le Gadolinium dans le réseau. Le caloporteur/modérateur choisi dans ces analyses sera de l'eau légère ou lourde, ou une combinaison des deux. La géométrie du réseau va varier de carrée, hexagonale ou circulaire. Un large spectre de réseaux seront donc analysés, permettant de valider le comportement des modèles d'autoprotection avancés. Les résultats obtenus par DRAGON seront validés par rapport au code de Monte-Carlo MCNP5. Les solutions de référence correspondant à chaque cas seront calculées par MCNP5.

L'évolution isotopique des isotopes présents dans le réseau va dépendre de la normalisation à puissance ou flux constant qui sera utilisée. En général, le flux est obtenu à l'étape 5. pour un neutron absorbé unique, puis est normalisé ultérieurement à la puissance réelle du réseau. La normalisation de puissance est principalement faite en égalant le produit de l'énergie par fission par le taux de fission à une valeur de puissance donnée. Dans cette recherche, nous allons prendre en compte toutes les réactions neutron-noyau produisant de l'énergie et incluant l'énergie de décroissance radioactive. Ces différentes valeurs seront récupérées de l'évaluation en format ENDF et seront copiées dans la bibliothèque multigroupe en amont du calcul de réseau. Nous allons évaluer les contributions de chaque réaction nucléaire apportées par chacun des isotopes présents dans le réseau. Nous allons valider ce modèle sur des benchmarks de cellules CANDU-6, cellule unique PWR avec thorium et cellule unique avec Gadolinium. Le comportement en évolution du benchmark PWR avec thorium sera validé par rapport à des calculs de reference obtenus à l'aide du code MONTEBURNS qui relie MCNP5 et ORIGEN, un code d'évolution isotopique.

ABSTRACT

The main aim of this research is the development and validation of computational schemes for advanced lattice codes. The advanced lattice code which forms the primary part of this research is "DRAGON Version4". The code has unique features like self shielding calculation with capabilities to represent distributed and mutual resonance shielding effects, leakage models with space-dependent isotropic or anisotropic streaming effect, availability of the method of characteristics (MOC), burnup calculation with reaction-detailed energy production etc.

Qualified reactor physics codes are essential for the study of all existing and envisaged designs of nuclear reactors. Any new design would require a thorough analysis of all the safety parameters and burnup dependent behaviour. Any reactor physics calculation requires the estimation of neutron fluxes in various regions of the problem domain. The calculation goes through several levels before the desired solution is obtained. Each level of the lattice calculation has its own significance and any compromise at any step will lead to poor final result. The various levels include choice of nuclear data library and energy group boundaries into which the multigroup library is cast; self shielding of nuclear data depending on the heterogeneous geometry and composition; tracking of geometry, keeping error in volume and surface to an acceptable minimum; generation of regionwise and groupwise collision probabilities or MOC-related information and their subsequent normalization thereof; solution of transport equation using the previously generated groupwise information and obtaining the fluxes and reaction rates in various regions of the lattice; depletion of fuel and of other materials based on normalization with constant power or constant flux. Of the above mentioned levels, the present research will mainly focus on two aspects, namely self shielding and depletion.

The behaviour of the system is determined by composition of resonant and predomi-

nantly scattering isotopes. When the concentration of resonant isotopes is small, its presence does not affect the flux shape which is smooth. But when the concentration becomes high, there will be dips in the flux where resonances of the isotopes occur. This will affect the reaction rate, which is a product of cross section and flux. The reaction rate will thus be lower than that when one does not consider the flux dip. This is the phenomenon of self shielding. Self shielding treatment is thus a very important aspect of reactor lattice analysis code. This needs to be correctly modelled to obtain a physically sound and acceptable solution. In this research we will be looking into behaviour of the advanced self shielding models that have been incorporated in the code DRAGON Version4. The self shielding models are primarily classified into two broad groups, which are based on "equivalence in dilution" and "subgroup approach". These self shielding models will be tested against a variety of lattices which include Canada Deuterium Uranium (CANDU-6), CANDU-New Generation (CANDU-NG), Light Water Reactor (LWR), and High Conversion Light Water Reactor (HCLWR). The fuel composition will vary from natural uranium oxide to enriched uranium oxide and plutonium-uranium mixed oxide (MOX). We will also consider the presence of strong neutron absorbers like gadolinium and dysprosium in the lattice. The coolant/moderator chosen for the analysis will be light water/heavy water or a combination. The lattice geometry will vary from square, hexagonal and annular. Thus a broad spectrum of lattices will be analysed to assess the behaviour of advanced self shielding models. The results obtained using DRAGON will be validated against that obtained using Monte Carlo code MCNP5. The reference solutions for all situations will be provided by MCNP5.

The depletion behaviour of any lattice will depend on the power or flux normalization that is considered. In general the flux in various regions is estimated with reference to a single neutron absorbed and is normalized subsequently to the power produced by the lattice. Power normalization is predominantly performed by equating the product of energy per fission and fission reaction rate to constant power. But in this research work, we will be normalizing the power using decay energy and energies from most neutron induced reactions. These energy

values are obtained from the basic evaluated nuclear datafiles and are built into the custom cross section library. We will also be estimating the individual contribution due to each neutron induced reaction and also the contribution to each reaction type by each element. We will be analysing CANDU-6, PWR thorium pincell and gadolinium pincell benchmarks for validating depletion model. The burnup dependent behaviour of the PWR thorium pincell will be validated against the reference results obtained using code MONTEBURNS which links codes MCNP and ORIGEN, an isotopic depletion code.

CONDENSÉ EN FRANÇAIS

Les codes de calcul en physique des réacteurs ont pour but premier de prédire la distribution des neutrons et des photons gamma sur l'espace du coeur, en énergie et en temps. Ces codes résolvent numériquement la forme linéaire de l'équation du transport, originellement développée par Boltzmann en théorie cinétique des gas. Les techniques de résolution numériques sont basées sur quelques approximations, telles que les différences finies appliquées aux opérateurs différentiels, les formules de quadratures pour les opérateurs intégraux, et les méthodes de dévelopement. Les codes utilisés en physique des réacteur se classifient en codes de réseau et codes de coeur.

Les codes de réseau permettent d'étudier les valeurs caractéristiques d'une cellule unitaire représentative du coeur. Celle-ci peut être une simple cellule crayon de combustible unique, une super-cellule ou un assemblage complet. Les divers paramètres pris en compte sont l'enrichissement du combustible, la composition matérielle du combustible, de la gaine et du modérateur, les températures, la concentration en poisons consommables, le burnup, etc. Ce calcul est réalisé en plusieurs étapes, la dernière permettant d'obtenir la solution recherchée. Chaque niveau du calcul de réseau est essentiel et tout compromis sur l'un d'eux est succeptible de mener à un résultat final de piètre qualité. Ces différents niveaux sont: 1. choix de la bibliothèque de données nucléaires et du découpage multigroupe sur lequel ces données sont condensées; 2. autoprotection des données nucléaires en fonction des caractéristiques géométriques et des concentrations isotopiques; 3. traçage de la géométrie de façon à conserver les erreurs surfaciques et volumiques à un niveau acceptable; 4. génération et normalisation des probabilités de collision, ou de l'information requise par la méthode des caractéristiques, en espace et en énergie; 5. solution de l'équation de transport en utilisant l'information multigroupe calculée précédemment et obtention des flux et des taux de réaction en divers endroits du réseau; 6. évolution du combustible et des autres matériaux avec normalisation à puissance ou flux constant. Parmis eux, nous allons principalement porter attention aux deux niveaux relatifs à l'autoprotection et à l'évolution isotopique.

Le but principal de cette recherche est le développement et la validation de schémas de calcul dédiés aux codes de réseaux avancés. Le code de réseau avancé faisant l'objet de cette recherche est "DRAGON Version4". Ce code possède des caractéristiques uniques, tels qu'un modèle d'autoprotection capable de représenter les effets de distribution en espace et ceux de protection mutuelle, un modèle de fuites dépendant de l'espace avec effets de *streaming* isotrope ou anisotrope, la disponibilité de la méthode des caractéristiques (MOC), une résolution des équations d'évolution isotopique avec prise en compte des énergies correspondant à chaque réaction, etc.

L'information la plus importante, en amont de la chaîne de calcul, sont les données nucléaires. Un ensemble complet et validé de données nucléaires est requis pour pouvoir estimer les valeurs caractéristiques du réacteur de la façon la plus réaliste possible. Les données nucléaires utilisées en physique des réacteurs sont traitées par un code, tel NJOY [MacFarlane 2000], qui utilise un *fichier de données nucléaires évaluées* comme point de départ. On désigne par *évaluation* le processus d'analyse des données nucléaires acquises de façon expérimentale, en combinant ces valeurs avec des prédictions de modèles nucléaires théoriques, dans le but d'obtenir les vraies valeurs des sections efficaces. La paramétrisation et la réduction des données nucléai-res en tableaux produisent un ensemble de données nucléaires évaluées. Le système *Evaluated Nuclear Data File* (ENDF) [MCSEWG 2001] a été développé pour permettre la stockage et la récupération des données nucléaires évaluées requises par les applications en amont en physique des réacteurs. Ces applications gèrent plusieurs caractéristiques du système, incluant le choix des matériaux sélectionnés, les données utilisées, le format utilisé, et les tests de vérifications devant être réalisés avant la mise en disponibilité d'une bibliothèque ENDF. Les bibliothèques ENDF sont disponibles dans divers *centres de données nucléaires* à travers le monde. La bibliothèque américaine ENDF/B est gérée au *National Nuclear Data Center* (NNDC) et contient les évaluations recommandés pour chaque matériel. D'autres centres sont situés au *Nuclear Energy Agency* (NEA) en Europe, au *International Atomic Energy Agency* (IAEA), au *Brookhaven National Laboratory* (BNL), au *Japanese Atomic Energy Research Institute* (JAERI), au *Korean Atomic Energy*

Research Institute (KAERI), et dans des centres russes et chinois. Chaque matériel inclus dans une bibliothèque est aussi complet que possible et procure des données évaluées pour toutes les réactions nucléaires induites par neutrons et couvrant un domaine étendu d'énergies du neutron incident. La bibliothèque contient également des informations telles que les distributions angulaires et énergétiques des neutrons secondaires, les données de décroissance radioactive, des rendements de produits de fission, etc. Chaque bibliothèque évaluée est périodiquement revisée ou remplacée, mais seulement après une période suffisante de revue et de tests. On obtient ainsi une nouvelle référence standardisée pouvant être utilisée lors d'analyses ultérieures en physique des réacteurs. Lorsqu'une nouvelle bibliothèque évaluée est rendue disponible en format ENDF, elle peut être convertie sous une forme plus appropriée pour des applications de tests ou réelles, en utilisant un code de traitement de type NJOY.

Le code NJOY contient plusieurs fonctions tels que la reconstruction des sections efficaces résonnantes, l'élargissement Doppler des résonances, le calcul de moyennes multi-groupes, la traduction de l'information nucléaire en formats d'interfaces spécifiques, et permet donc de générer des sections efficaces, multi-groupes ou continues en énergie, adaptées à un calcul neutronique. Les formats d'interfaces les plus utilisés sont le format WIMSLIB adapté aux codes WIMS (*Winfrith Improved Multigroup Scheme*) [Askew 1966] et WIMS-E, le format ACE (*A Compact ENDF*) [MacFarlane 2000] adapté au code MCNP [X-5 Monte Carlo Team 2003] et certains formats multi-groupes standardisés pour des codes tels DTF-IV. Le code MCNP a été développé aux laboratoires de Los Alamos et est basé sur la méthode de Monte Carlo avec représentation en énergie continue des sections efficaces. Récemment un nouveau module appelé DRAGR [Hébert 1992] a été introduit dans NJOY pour permettre la génération de données nucléaires multi-groupes en format DRAGLIB [Hébert 2004] adapté au code DRAGON. Pour la présente recherche, nous avons choisi d'utiliser des données évaluées pour chaque isotope selon la recommandation du *co-ordinated research project* (CRP) de l'IAEA pour le *WIMS library update project* (WLUP).

Le comportement du système est affecté par la composition des isotopes résonnants

et des isotopes légers participant au ralentissement neutronique. Lorsque la concentration d'un isotope résonnant est faible, sa présence affecte peu la courbe de flux qui demeure non-résonnante. Lorsque sa concentration augmente, on observe une dépression locale dans la courbe de flux à l'endroit de la résonance. Cet effet de creusement va affecter les taux de réaction car ils sont égaux au produit de sections efficaces par le flux. Les taux de réaction seront donc plus faibles que si le flux était non-résonnant. Cet effet est appelé *autoprotection des résonances.* Le calcul de l'autoprotection des résonances est donc une étape essentielle du calcul de réseau. Cet effet d'autoprotection doit être correctement modélisé afin d'obtenir une solution physiquement acceptable. Dans cette recherche, nous allons analyser le comportement des modèles d'autoprotection avancés disponibles dans le code DRAGON Version4. Les modèles d'autoprotection existants sont principalement divisés en deux catégories selons qu'ils sont basés sur une *equivalence en dilution* ou sur la *méthode des sous-groupes.* Différents modèles d'autoprotection seront testés sur une variété de réseaux, tels ceux des réacteurs *Canada Deuterium Uranium* (CANDU-6), *CANDU new-generation* (CANDU-NG), à eau légère (LWR) et *à eau légère et à conversion élevée* (HCLWR). La composition du combustible va varier entre l'oxyde d'uranium naturel, l'oxyde d'uranium enrichi, l'oxyde mixte uranium-plutonium (MOX) et l'oxyde mixte uranium-thorium. Nous allons également analyser la présence de poisons consommables tels le Dysprosium et le Gadolinium dans le réseau. Le caloporteur/modérateur choisi dans ces analyses sera de l'eau légère ou lourde, ou une combinaison des deux. La géométrie du réseau va varier de carrée, hexagonale ou circulaire. Un large spectre de réseaux seront donc analysés, permettant de valider le comportement des modèles d'autoprotection avancés. Les résultats obtenus par DRAGON seront validés par rapport au code de Monte-Carlo MCNP5. Les solutions de référence correspondant à chaque cas seront calculées par MCNP5.

L'évolution isotopique des isotopes présents dans le réseau va dépendre de la normalisation à puissance ou flux constant qui sera utilisée. En général, le flux est obtenu à l'étape 5. pour un neutron absorbé unique, puis est normalisé ultérieurement à la puissance réelle du réseau. La normalisation de puissance est principalement faite en égallant le produit de

l'énergie par fission par le taux de fission à une valeur de puissance donnée. Dans cette recherche, nous allons prendre en compte toutes les réactions neutron-noyau produisant de l'énergie et incluant l'énergie de décroissance radioactive. Ces différentes valeurs seront récupérées de l'évaluation en format ENDF et seront copiées dans la bibliothèque multi-groupe en amont du calcul de réseau. Nous allons évaluer les contributions de chaque réaction nucléaire apportées par chacun des isotopes présents dans le réseau. Nous allons valider ce modèle sur des benchmarks de cellules CANDU-6, cellule unique PWR avec thorium et cellule unique avec Gadolinium. Le comportement en évolution de ces benchmarks sera validé par rapport à des calculs de reference obtenus à l'aide du code MONTEBURNS qui relie MCNP5 et ORIGEN, un code d'évolution isotopique.

La qualité des codes développés pour l'analyse des systèmes de réacteurs nucléaires est démontrée par leur validation relative à des benchmarks standardisés. Les benchmarks sont généralement choisis en fonction de la nature des applications par rapport auxquelles le code est appliqué. Les benchmarks utilisés pour valider le code de réseau doivent couvrir un domaine d'application étendu. Un benchmark est requis principalement pour isoler la contribution relative des erreurs sur les caractéristiques intégrales du réacteur provenant des données nucléaires de bases, des limitations dues au format des bibliothèques, des hypothèses de traitement des données et des approximations relatives aux modèles de calcul du code. Le choix des benchmarks a été fait sur la base d'une bonne représentation des types de combustibles et des géométriers les plus répendus dans les réacteurs de recherche et de puissance actuels. Ce choix inclut une combinaison de combustibles ^{232}Th, ^{233}U, ^{235}U, ^{238}U, ^{239}Pu, ainsi que des géométries de réseaux carrés ou hexagonaux et des cellules unitaires de Wigner-Seitz. Les réacteurs à eau pressurisés (PWR) utilisés aux États-Unis utilisent un combustible à l'uranium enrichi en ^{235}U avec de l'eau légère comme caloporteur et modérateur et une disposition du combustible en réseau carré. Les réacteurs à eau pressurisés (WWER) utilisés en Russie sont similaires mais utilisent une disposition du combustible en réseau hexagonal. Les réacteurs à tube de force tels le CANDU-6 utilisent de l'uranium naturel comme combustible et de l'eau lourde comme caloporteur et modérateur. La géométrie du combustible

dans un CANDU-6 a la forme d'une grappe circulaire de 37 crayons. Certaines propositions futuristes de réacteurs envisagent d'utiliser le thorium comme combustible et certaines activités de recherche sont en cours dans des pays tels l'Inde. Le réacteur de recherche KAMINI, développé en Inde, utilise un combustible à base d'^{233}U. L'Inde poursuit également le développement du *Advanced Heavy Water Reactor* (AHWR) [Kakodkar 1998] permettant une utilisation étendue de ses ressources en thorium. D'autres propositions d'utilisation du thorium ont également été publiées [Jagannathan 2001]. Certains benchmarks incluant des poisons consommables ont été proposés. Le choix d'utiliser le Gadolinium comme poison consommable a été fait dans la plupart des PWR modernes. Ce poison permet d'éliminer l'excès initial de réactivité et permet d'atteindre des burnup de sortie plus élevés. Des isotopes du Gadolinium, principalement ^{155}Gd et ^{157}Gd, sont mélangés au combustible en forme oxyde. Ce type de poison consommable diffère du bore qui est généralement mélangé au modérateur des PWR où il agit comme mécanisme de réactivité chimique.

Un total de cinq types de réseaux ont été analysés dans le câdre de cette recherche. Ce choix a été motivé par les caractéristiques décrites au tableau I. On peut observer que les benchmarks choisis couvrent une gamme étendue d'énergies du neutron incident, une exigence décrite précédemment. On voit que le réseau CANDU-6 représente un système bien thermalisé alors que la cellule PWR avec Gadolinium possède la fraction la plus élevee de neutrons dont l'énergie est supérieure à 100 keV. Un benchmark inspiré du réacteur à haut taux de conversion (HCLWR) a été sélectionné car il représente la plus grande fraction de fissions dans la région des résonances où les modèles d'autoprotection opèrent. Une description plus détaillée de chaque benchmark est disponible dans les divers chapitres de la thèse.

Validation des modèles d'autoprotection

CANDU-6 – Les paramètres relatives à la sûreté, tels le coefficient de température du combustible (FTC), le coefficient de vide caloporteur (CVR),le coefficient d'ingression du tube de force (PTI) et le coefficient d'ingression du tube de calandre (CTI) ont été évalués pour une géométrie représentative d'une cellule CANDU-6. Cette cellule comporte une grappe

Table 1 Fractions de fissions dans chaque domaine d'énergie

Réseau	Thermal (< 0.625 eV)	Résonnant (0.625 eV – 100 KeV)	Rapide (> 100 keV)
CANDU-6	93%	2%	5%
CANDU-NG	89%	7%	4%
PWR Thorium	76%	20%	4%
PWR avec Gadolinium	20%	43%	37%
HCLWR	34%	46%	20%

circulaire de 37 crayons de combustible d'oxyde d'uranium naturel et utilise des gaines de zircalloy. Les tubes de force et de calandre sont faits de zircalloy. Le caloporteur et le modérateur sont de l'eau lourde. La frontière externe de la cellule unitaire, correspondant à un réseau carré de 28.575 cm, a été annularisée et une condition de réflexion isotrope a été utilisée. Une discrétisation de quatre couronne par crayon de combustible a été utilisée, en suivant la recommandation de la référence [Santamarina 2004], afin d'améliorer la prédiction des effets d'autoprotection distribués. Les crayons de combustible sont donc subdivisés en couronnes représentant 50%, 30%, 15% et 5% du volume total du crayon. Deux valeurs de burnup ont été utilisées lors des analyses. La première valeur correspond à du combustible frais alors que la seconde valeur correspond à un burnup de sortie de 7993 MW-jour/tonne. Dans cette analyse, nous avons analysé les isotopes suivants du combustible: ^{235}U, ^{238}U, ^{239}Pu, ^{240}Pu, ^{241}Pu, ^{242}Pu, ^{135}Xe, ^{149}Sm et ^{16}O. Même si un plus grand nombre de produits de fission et d'actinides sont produits avec le burnup, nous avons limité notre analyse aux isotopes précédents qui, selon notre connaissance, vont jouer un rôle important lors des transitoires de réactivité. Le choix de ces éléments est basé sur leur valeur du rapport de capture, égal au taux de capture dans un isotope unique divisé par le taux de capture total, dans le domaine d'énergie situé entre 2.7679 eV et 677.29 eV, correspondant au domaine des résonances résolues. Le rapport de capture varie de 100% lorsque le combustible est frais à 90% au burnup de sortie. Le choix de ces neuf éléments est donc suffisant pour valider la précision du modèle et les effets d'autoprotection sur les taux de capture dans le domaine

des résonances résolues. Ce choix permet aussi de comprendre l'effet d'autoprotection sur chaque élément individuel.

Les valeurs de base de k_∞ de tous les paramètres de sûreté sont sous-évaluées par chacun des modèles d'autoprotection. La méthode de Stamm'ler généralisée, implémentée dans la Version 3 de Dragon, prédit mieux k_∞ que les variantes de cette méthode avec les modèles de Nordheim ou d'intégration de Riemann lorsque la normalisation de Livolant-Jeanpierre est désactivée. Cette tendance est renversée lorsque la normalisation de Livolant-Jeanpierre est activée. En fait, la méthode de Stamm'ler généralisée avec les modèles de Nordheim et d'intégration de Riemann et avec la normalisation de Livolant-Jeanpierre fonctionne mieux que les modèles d'autoprotection avec sous-groupes, excepté dans le cas de vidange du caloporteur. Le modèle d'autoprotection avec sous-groupes et tables de probabilités physiques fonctionne aussi bien que la méthode avec tables de probabilité mathématiques pour la prédiction de k_∞. Nous avons observé que toutes les méthodes d'autoprotection sous-estiment les paramètres de sûreté d'un CANDU-6. On devra se souvenir de cette observation lors de l'utilisation de ces méthodes pour le design de réacteur. La variation des paramètres de sûreté avec le burnup est correctement prise en compte par toutes les méthodes d'autoprotection. La réactivité du vide est nettement sous-estimée lorsque la méthode de Stamm'ler généralisée est utilisée avec les modèles de Nordheim et d'intégration de Riemann et avec la normalisation de Livolant-Jeanpierre. Nous avons observé que les modèles d'autoprotection avec sous-groupes prédisent correctement tous les paramètres de sûreté d'un CANDU-6. En général, le taux de capture dans le domaine des résonances résolues est mieux estimé par les modèles d'autoprotection avec sous-groupes, en comparaison des modèles d'équivalence en dilution. Par contre, l'effet de la vidange caloporteur sur les taux de capture n'est pas correctement prédit, quelque soit la méthode d'autoprotection. En général, parmi toutes les méthodes d'autoprotection, celles basées sur les sous-groupes et tables de probabilités physiques performent bien dans toutes les situations. Il est également possible d'utiliser une approche de sous-groupes et tables de probabilités mathématiques, mais cette dernière option est plus coûteuse et nécessite d'utiliser une bibliothèque de sections efficaces

comportant des données *Autolib*.

CANDU-NG – Le réseau de type *New Generation CANDU* (CANDU-NG) a été proposé lors d'un stage préliminaire du développement du *Advanced CANDU Reactor* (ACR) et est maintenant utilisé à des fins de benchmarking [Chan 2001]. Le crayon central de la grappe à 43 crayons contient du dysprosium (4.6 %) dans de l'uranium naturel. Le crayon central et les sept crayons de l'anneau 1 sont plus épais (diamètres interne/externe – 0.627/0.675 cm) comparé aux 14 crayons de l'anneau 2 et aux 21 crayons de l'anneau 3 (diamètres interne/externe – 0.533/0.575 cm). La densité de combustible des 8 crayons centraux est plus élevée (10.12 g/cc) comparée à celle des autres crayons (9.825 g/cc). Les dimensions du tube de force sont les mêmes que celles du CANDU-6. Deux changements importants ont été apporté au réseau CANDU-NG. Le pas de réseau a été réduit à 22 cm. De plus, les dimensions du tube de calandre (diamètres interne/externe –7.5/7.8 cm) ont été augmentées en comparaison de celles d'un CANDU-6 (6.45/6.59 cm). En conséquence, l'espace annulaire est très augmentée et le volume de modérateur est réduit d'autant plus. Le caloporteur est de l'eau légère alors que le modérateur est de l'eau lourde. L'espace annulaire est remplie d'hélium. Deux ensembles d'études ont été menées dans le câdre de la présente recherche. Dans le premier ensemble, le coefficient de vide caloporteur d'une cellule CANDU-NG a été estimé en utilisant DRAGON. Deux variétés de cellule unique ont été analysées, selon que le crayon central de la grappe comporte du dysprosium ou non, en plus de l'uranium naturel. Ces tests aident à comprendre l'effet du dysprosium lors de la vidange du caloporteur et permettent de valider les modèles d'autoprotection en présence de forts absorbants de neutrons. Le second ensemble d'études est relatif à un motif de 2×2 cellules CANDU-NG. Nous avons validé DRAGON Version4 pour des cas de vidange complète et pour des cas de vidanges en damier. Les cas de vidange en damier supposent l'absence de caloporteur dans deux cellules diagonales et la présence dans les deux autres cellules.

Nous avons observé que les modèles d'autoprotection basés sur la méthode des sous-groupes avec tables de probabilités physiques prédisent k_∞, le coefficient de vide caloporteur et les taux de réaction mieux que tous les autres modèles. Cette approche a été utilisée pour

effertuer les calculs de motif 2×2 et le coefficient de vide caloporteur a ainsi pu être évalué. Ces calculs avec DRAGON ont été rendu possible par l'introduction du nouveau module de traçage NXT. En utilisant DRAGON, nous avons observé le phénomène d'augmentation du coefficient de vide caloporteur, en présence de dysprosium dans le crayon central, lorsque la vidange est réalisée en damier plutôt que complète.

HCLWR – Un réseau de réacteur à eau légère et à haut taux de conversion a été choisi pour valider les modèles d'autoprotection, compte tenu du fait que les principales contributions de fission (46%) se produisent dans le domaine des résonances. Le combustible est enrichi en oxyde de plutonium (7%) mélangé à de l'oxyde d'uranium usé. Le réseau est hexagonal, avec un pas de 1.2204 cm, ce qui est petit en comparaison du pas des réacteurs à eau légère conventionnels. Dans cette recherche, nous avons principalement étudié des réseaux hexagonaux de burnup nul dont le rapport V_m/V_f est de 1.1.

Nous avons observé que les valeurs de k_∞ obtenues avec diverses méthodes d'autoprotection présentent un large écart par rapport aux références MCNP5. Le plus grand écart correspond à la méthode de Stamm'ler généralisée avec modèle de Nordheim et sans normalisation de Livolant-Jeanpierre. La déviation la plus faible correspond à la méthode de Ribon étendue avec modèle de correlation prenant en compte l'effet de protection mutuelle. En général, les méthodes de type sous-groupe fonctionnent mieux que celles basées sur une équivalence en dilution. La valeur calculée de k_∞ est plus élevée lorsque la normalisation de Livolant-Jeanpierre est utilisée. L'importance du phénomène de protection mutuelle provient de deux causes: le rapport de concentrations $^{238}U/^{240}Pu$ et l'indice de spectre. On doit prendre en compte la protection mutuelle lorsque le rapport de concentration est inférieur à 300 et que le spectre est dur. L'effet de protection mutuelle entre ^{239}Pu et ^{240}Pu joue également un rôle sur la précision des taux de capture et de k_∞. Les meilleurs résultats sont obtenus avec la prise en compte des correlations entre ^{238}U, ^{239}Pu et ^{240}Pu. Lorsque le spectre devient plus mou, l'effet de protection mutuelle devient moins important. Une autre observation importante est relative à la méthode de Stamm'ler généralisée. Dans ces cas, le taux de fission est réduit d'avantage lorsque la normalisation de Livolant-Jeanpierre est utilisée avec la méthode

de Nordheim, plutôt qu'avec les deux autres variantes de la méthode de Stamm'ler.

Validation des modèles d'évolution isotopique

CANDU-6 – Des analyses en évolution ont été réalisées pour le réseau CANDU-6 décrit plus haut. La normalisation de puissance est traditionnellement basée sur la connaissance des taux de fission et de l'énergie correspondante. Dans les bibliothèques multigroupes WLUP, il est mentionné que l'énergie de fission utilisée pour la normalisation provient de l'énergie de fission, moins l'énergie des neutrinos, en prenant en compte implicitement l'énergie de capture radiative et celle des neutrons incidents. Dans la présente étude, nous avons tenté d'effectuer une normalisation de puissance en prenant en compte de façon explicite l'énergie de décroissance radioactive et celle de chaque réaction nucléaire induite par neutron. Trois ensembles d'études ont été effectués. Dans les deux premières, nous avons généré des chaines d'évolution isotopiques complètes et inclu chaque énergie de façon explicite. Dans la première étude, nous avons effectué la normalisation de puissance en prenant en compte uniquement l'énergie libérée dans le combustible (option `'NOGL'`), alors que dans la seconde étude, nous avons pris en compte la totalité de l'énergie libérée (option `'GLOB'`). Dans la troisième étude, nous avons utilisé les valeurs d'énergie de fission implicites recommandées par le projet WLUP. Dans ce dernier cas, les valeurs recommandées ont été multipliées par les taux de fission des actinides pour calculer la puissance du réseau. Dans tous les cas, nous avons utilisé une valeur de puissance de référence égale à 31.9713 kW/kg.

Nous avons observé que la valeur de k_∞ est surestimée en fonction du burnup lorsque les valeurs recommandées par le projet WLUP sont utilisées pour la normalisation de puissance. La plus grande déviation est de 1.6 mk au burnup de sortie pour l'option `'NOGL'` et de 1.1 mk à 7 GW-jour/tonne. Nous avons de plus estimé la contribution de chaque réaction au calcul de puissance du réseau. Au burnup de sortie, la fission compte pour 95.3% de l'énergie produite, alors que 4.7% provient de la capture radiative, incluant la contribution de 0.8% en provenance des produits de fission.

Cellule PWR avec thorium – Nous avons étudié le comportement en évolution d'une cellule

de réseau PWR avec thorium, en extrayant un crayon d'un assemblage 17×17 de type Westinghouse. Ce calcul a été réalisé avec DRAGON Version4 et les résultats ont été validés à l'aide du code MONTEBURNS, qui permet un couplage entre MCNP5 et ORIGEN. La puissance du réseau a été normalisée à 38.1347 kW/kg(métal lourd). Le calcul d'évolution du crayon de combustible a été réalisé de trois façons differentes. Pour le premier calcul, dénoté par `'MODEL-1'`, nous avons généré des chaines d'évolution isotopiques complètes et inclu chaque énergie de façon explicite. Pour le second calcul, dénoté par `'MODEL-2'`, nous avons utilisé les valeurs d'énergie de fission implicites recommandées par le projet WLUP. Pour le troisième calcul, dénoté par `'MODEL-3'`, nous avons utilisé une version modifiée du code MONTEBURNS de façon à prendre en compte les énergies explicites de chaque réaction, comme dans `'MODEL-1'`. Cette modification est présentée à l'annexe V. Les valeurs de k_∞ et les densités isotopiques des actinides et produits de fission les plus importants obtenues par DRAGON ont été comparées à celles obtenues par MONTEBURNS.

Nous avons observé que le k_∞ prédit par DRAGON est proche de celui obtenu avec MONTEBURNS. Les densités isotopiques sont prédites avec un écart inférieur à 5% pour la plupart des actinides. Nous pouvons donc conclure que les effets de burnup cont correctement modélisés par DRAGON, en comparaison avec MONTEBURNS. Nous avons également observé que la combustion du combustible est augmentée lorsque toutes les énergies sont modélisés de façon explicite. Finalement, les composantes d'énergies provenant de la fission, de la capture radiative et des réactions $(n, 2n)$, obtenues par les deux codes, sont de valeurs voisines.

Benchmark Sidorenko – Ce benchmark est une étude d'un crayon de gadolinium en évolution avec DRAGON Version4 et MONTEBURNS. Il est intéressant d'étudier la génération d'éner-gie par la capture radiative *en plus* de celle générée pas fission dans l'^{235}U. Pour nos calculs, le crayon a été divisé en un, quatre, six ou dix régions de volumes égaux. Les pas d'évolution sélectionnés varient entre 50, 100, 200, 250, 500 et 1000 MW-jour/tonne. Nous avons comparé le k_∞ et les densités isotopiques de ^{155}Gd, ^{157}Gd, ^{235}U, ^{239}Pu, ^{240}Pu, ^{241}Pu et ^{242}Pu en diverses situations. Le crayon est considéré être placé dans un réseau hexagonal.

Nous avons observé que l'utilisation d'un minimum de 10 régions de volumes égaux est requise pour obtenir un comportement correct en évolution. Il faut également utiliser des pas d'évolution fins, de l'ordre de 50 MW-jour/tonne, jusqu'à l'élimination du gadolinium. Deux modèles de normalisation de puissance ont été étudiés et nous avons observé que la combustion du combustible est augmentée lorsque toutes les énergies sont modélisés de façon explicite, du à un flux plus élevé. Cependant, lorsque du gadolinium est introduit dans le combustible, ce type de normalisation provoque une diminution de la combustion du combustible, du à un flux moins élevé. Ce flux plus faible est du à la composante d'énergie produite par capture radiative dans le combustible qui peut atteindre 21 % en début d'évolution. Il est donc important d'inclure, dans la bibliothèque multigroupe, les données d'énergie pour le gadolinium et d'utiliser ces valeurs pour effectuer correctement la normalisation de puissance.

Conclusions

En général, nous avons observé que les modèles d'autoprotection basés sur une méthode de sous-groupes se comportent mieux, en toutes situations, que ceux basés sur une équivalence en dilution. Les écarts de k_∞ et des taux de réaction par rapport à MCNP5 sont plus faibles lorsqu'une méthode de sous-groupes est utilisée. Dans certaines situations, la méthode de Stamm'ler généralisée avec modèles de Nordheim et d'intégration de Riemann prédit mieux le k_∞, mais moins bien les taux de capture. Les paramètres de sûreté, tels le coefficient de vide caloporteur, le coefficient de température combustible et les coefficients d'ingression du tube de force et de calandre sont mieux prédits avec une méthode de sous-groupes. Cependant, toutes les valeurs obtenues sont plus faibles que celles prédites par MCNP5. Il est donc important de noter que les paramètres de sûreté sont généralement sous-estimés par DRAGON Version4. On a également observé que les méthodes d'équivalence en dilution fonctionnent mieux en présence de normalisation de Livolant-Jeanpierre.

La méthode de sous-groupes basée sur les tables de probabilités mathématiques est aussi précise que celle basée sur les tables physiques mais est plus coûteuse et nécessite

d'utiliser une bibliothèque de sections efficaces comportant des données *Autolib*. Cependant, dans les cas où le combustible comporte une forte concentration des isotopes ^{238}U, ^{239}Pu et ^{240}Pu, il peut devenir nécessaire d'utiliser des tables de probabilités mathématiques avec le modèle de correlation. Seul ce modèle d'autoprotection est capable de prendre en compte l'effet de protection mutuelle. Nous avons observé que cet effet devient non-négligeable lorsque le rapport de concentrations ^{238}U/^{240}Pu est de l'ordre de 300 ou plus faible. De plus, l'effet de protection mutuelle diminue lorsque le rapport $V_{\mathrm{m}}/V_{\mathrm{f}}$ augmente.

Afin d'effectuer la validation des modèles dévolution isotopique, nous avons apporté une importante modification dans le code MONTEBURNS. En plus du calcul d'énergie de fission déjà disponible, nous avons ajouté la possibilité de calculer les composantes d'énergies issues de la décroissance radioactive, de l'énergie de capture radiative et de celle des réactions $(n, 2n)$. Ces valeurs peuvent ensuite être utilisées pour calculer les taux de réaction correspondants et pour effectuer la normalisation de puissance.

Les modèles dévolution isotopique ont été validés à l'aide d'une bibliothèque multigroupe alternative qui contient seulement des composantes modifiées d'énergie de fission pour les actinides présents dans la chaîne d'évolution. La valeur modifiée de chaque énergie de fission prend en compte, de façon implicite, les énergies provenant des autres sources d'énergie en utilisant les valeurs proposées par le projet WLUP. Lors des études de validation, nous avons observé que la combustion du combustible est augmentée lorsque toutes les énergies sont modélisés de façon explicite. Cet effet est inversé lorsque lorsqu'un isotope, autre qu'un actinide, contribue de façon importante à la production d'énergie. Lors de nos tests, nous avons étudié le gadolinium qui est utilisé dans les réacteurs à eau légère pour compenser l'excès initial de réactivité. Il est intéressant de constater que la représentation explicite des énergies provoque une diminution de la combustion du gadolinium de telle sorte que le combustible demeure sur-critique au delà du point où les autres modèles prédisent la disparition du gadolinium.

Le comportement en évolution d'une cellule à eau légère et combustible thorium a été étudié avec DRAGON et comparé à un calcul MONTEBURNS. Nous avons observé que le

k_∞ prédit par DRAGON est dans un voisinage de 0.5% de la valeur estimée par MONTE-BURNS. Les densités isotopiques des actinides sont semblables dans un voisinage de 10%. Quelques produits de fission ont cependant des écarts plus importants. Ces écarts sont dus principalement aux différences de rendements de fission entre ceux fournis avec ORIGEN et ceux générés par nous à l'aide du module DRAGR.

Des tendances intéressantes sont observées lorsque du gadolinium est ajouté au combustible. Il est important d'utiliser au moins 10 couronnes d'égal volume dans le crayon afin de calculer correctement la combustion en *pelure d'oignon*. Les pas de calcul en evolution doivent être aussi petits que possible, de l'ordre de 50 MW-jour/tonne, jusqu'à ce que le gadolinium soit complètement brulé. Lorsque du gadolinium est mélangé à de l'uranium, il a pour effet de favoriser la production d'isotopes du plutonium. Cet effet est du au durcissement du spectre qui provoque une augmentation des captures neutroniques dans les résonances de l'^{238}U.

Nous avons calculé les contributions de chaque réaction à la normalisation de puissance. Lorsque seulement des actinides sont présents dans le combustible, la contribution de la fission à l'énergie produite est de l'ordre de 95–96%, le restant provenant de la capture radiative. Lorsque du gadolinium est ajouté au combustible, près de 25% de l'énergie provient de la capture radiative dans ^{155}Gd et ^{157}Gd. Une petite contribution négative provient des réactions $(n, 2n)$. En conséquence, il apparaît important pour les codes de réseau de prendre en compte la contribution des réactions de fission, capture radiative et $(n, 2n)$ à la normalisation de puissance.

Perspectives futures

Les valeurs de k_∞ calculées pour le réseau CANDU-NG demeurent différentes des valeurs obtenues avec MCNP5, même lorsque des modèles d'autoprotection avancés sont utilisés. Il serait souhaitable de proposer un benchmark et d'initier des collaborations avec d'autres laboratoires sur ce thème.

Presque tous les benchmarks étudiés dans cette recherche ont utilisé un partitionnement

du combustible en quatre anneaux de volumes 50%, 30%, 15% et 5%, selon la recommandation de Santamarina. Il serait intéressant d'étudier l'effet du choix du nombre de volumes et de leurs valeurs sur le spectre.

Nous avons utilisé un découpage énergétique à 172 groupes pour tous nos calculs DRAGON. Il serait intéressant d'implémenter le maillage *Santamarina-Hfaiedh energy mesh* (SHEM) [Hfaiedh 2005] dans NJOY et d'étudier son comportement en autoprotection. Lorsque 172 groupes sont utilisés, la limite inférieure des données Autolib a été fixée à 2.76 eV, correspondant à une résonance de ^{242}Pu. Comme aucun de nos benchmarks ne contient de concentration importante de ^{242}Pu, aucun effet indésirable n'a été observé. Si un benchmark comportant une concentration élevée de ^{242}Pu était réalisé, nous pourrions justifier le choix d'une limite inférieure à 2.76 eV.

Les modèles d'autoprotection de DRAGON Version4 n'ont pas été testés pour des réseaux de réacteurs rapides. Il serait intéressant de vérifier l'effet du choix des groupes d'énergie dans le domaine des résonances non résolues. Les calculs d'évolution ont été réalisés en supposant que l'énergie des rayons gamma est déposée à l'endroit où elle est émise. Cependant, dans la réalité, cette énergie est transportée plus loin. Il serait intéressant d'étudier le transport gamma et son effet sur la répartition de puissance. Le modèle d'évolution de DRAGON Version4 devrait être validé pour un réseau d'assemblages BWR/PWR comportant plusieurs crayons avec gadolinium. On devrait également valider ce modèle pour un réseau CANDU-NG comportant du dysprosium dans le crayon central. Le dysprosium, tout comme le gadolinium, possède une section efficace de capture radiative élevée et la fraction d'énergie produite par cette réaction est aussi élevée que celle du gadolinium. On pourrait également étudier la combustion du gadolinium lorsque celui-ci n'est pas mélangé au combustible. Nous avons utilisé 150 produits de fission dans notre chaîne d'évolution, sans inclure de pseudo-produits de fission. Nous avons observé que la contribution à l'absorption totale de plusieurs produits de fission était négligeable. Il serait intéressant de sélectionner les produits de fission selon un critère de réactivité et selon celui de la radio-toxicité. Les rendements de fission utilisés avec ORIGEN devraient être remis en question. Certains écarts

de validations avec MONTEBURNS pourraient être éliminés si on utilisait les rendements de fission de DRAGON dans ORIGEN.

Il serait intéressant d'étudier l'énergie produite dans le combustible irradié avec DRAGON Version4, lorsque le combustible est sorti du réacteur. Cet effet a également été modélisé dans MONTEBURNS. Une telle validation pour du combustible hors coeur est donc possible.

TABLE OF CONTENTS

DEDICATION iv

ACKNOWLEDGMENTS v

RÉSUMÉ vi

ABSTRACT ix

CONDENSÉ EN FRANÇAIS xii

TABLE OF CONTENTS xxix

LIST OF FIGURES xxxiii

LIST OF TABLES xxxviii

LIST OF APPENDICES xli

INTRODUCTION 1

CHAPTER 1 DRAGON VERSION4 12

1.1 Self shielding models based on equivalence in dilution principle 13

1.1.1 Generalized Stamm'ler Model 13

1.1.2 Improved Generalized Stamm'ler Method 18

1.1.2.1 Nordheim Model 18

1.1.2.2 Riemann Integration Method 20

1.2 Models based on subgroup approach 22

1.2.1 The Statistical Subgroup Model 22

1.2.2 Ribon Extended Self Shielding Model 24

1.3 Burnup models 28

1.3.1 Power normalization in DRAGON Version4 28
1.3.2 Depletion calculation in DRAGON Version4 29
1.4 The Saturation models in Dragon 31

CHAPTER 2 REFERENCE CODES 33
2.1 NJOY99 33
2.2 MCNP5 37
2.3 ORIGEN2 37
2.4 MONTEBURNS 38
2.4.1 Calculation methodology in MONTEBURNS 39
2.4.1.1 Modification in MONTEBURNS 42

CHAPTER 3 CANDU-6 45
3.1 Description of Problem 46
3.2 Nuclear Data 49
3.2.1 MCNP Library Generation 49
3.2.2 Library in DRAGLIB Format 50
3.3 Calculational methodology using MCNP5 50
3.4 Computational scheme used for DRAGON analysis 52
3.4.1 Calculational methodology in DRAGON 52
3.5 Numerical Results 53
3.6 Conclusions 57

CHAPTER 4 CANDU-NG 74
4.1 Scope of study 75
4.2 Computational scheme used for DRAGON analysis 76
4.3 Results and Discussions 78
4.4 Conclusions 81

CHAPTER 5 HCLWR 94
5.1 Reference solution 95
5.2 Computational scheme used for DRAGON analysis 95
5.3 Optimization studies 96
5.4 Results obtained using various self shielding models 96
5.5 Conclusions 100

CHAPTER 6 BURNUP OF CANDU-6 CLUSTER 115
6.1 Computational scheme used for DRAGON analysis 115
6.2 Scope of study 116
6.3 Numerical results 118
6.4 Conclusions 120

CHAPTER 7 BURNUP OF PWR THORIUM PINCELL 126
7.1 Computational scheme used for DRAGON analysis 127
7.2 Scope of study 128
7.3 Validation using MONTEBURNS 128
7.4 Numerical results 129
7.5 Conclusions 132

CHAPTER 8 BURNUP OF GADOLINIUM PINCELL 146
8.1 Computational scheme used for DRAGON analysis 147
8.2 Effect of burnup step 148
8.3 Effect of number of rings per pin 150
8.4 Effect of gadolinium 151
8.5 Burnup of important actinides 152
8.6 Contribution due to different neutron induced reactions 152
8.7 Effect of power normalization 154
8.8 Reference solution using MCNP5 at zero burnup 155

8.9 Conclusions 155

CONCLUSION 175

REFERENCES 181

APPENDICES 189

LIST OF FIGURES

Figure 2.1	Flowchart for DRAGLIB/ACELIB Production	34
Figure 2.2	Spectrum used for collapsing cross sections into multigroup	36
Figure 3.1	Cross section of 37 element fuel assembly	59
Figure 3.2	Single pin with 4 layers in fuel	59
Figure 3.3	Typical spectrum in a CANDU-6 lattice	60
Figure 3.4	k_∞ curve for natural uranium CANDU fuel as a function of burnup	61
Figure 3.5	Ratio of capture rate in nine elements in fuel to all the elements as a function of burnup	61
Figure 3.6	Comparison of capture rate for CVR at 'B0' in resolved resonance group for representative pins in CANDU-6 lattice	62
Figure 3.7	Capture cross section in resolved resonance group for ^{238}U	63
Figure 4.1	Cross section of CANDU-NG unit cell and single pin	82
Figure 4.2	Cross section of 2×2 CANDU-NG assembly	83
Figure 4.3	Typical spectrum in CANDU-NG lattice	84
Figure 4.4	Capture rate in four layers of pins in four rings	85
Figure 5.1	High conversion light water reactor lattice	101
Figure 5.2	Typical spectrum in a high conversion light water reactor lattice . .	102
Figure 5.3	Variation of δK as a function of ratio of number densities of ^{238}U and ^{240}Pu	103
Figure 5.4	Capture rate in the resonances of ^{238}U in groups between 2.7679 eV and 677.287 eV	103
Figure 5.5	Capture rate in the resonances of ^{239}Pu in groups between 2.7679 eV and 677.287 eV	104
Figure 5.6	Capture rate in the resonances of ^{240}Pu in groups between 2.7679 eV and 677.287 eV	104
Figure 5.7	Resonances of ^{238}U and ^{240}Pu between 2.7 eV and 100 eV	105

Figure 5.8	Resonances of ^{239}Pu and ^{240}Pu between 2.7 eV and 100 eV	105
Figure 6.1	Variation in k_∞ as a function of burnup	121
Figure 6.2	Variation in δk_∞ of 'MODEL-2' w.r.t 'MODEL-1' and 'GLOB' option as a function of burnup	121
Figure 6.3	Variation in normalized flux as a function of burnup	122
Figure 6.4	Contribution of (n, f) to power normalization ('MODEL-1') as a function of burnup	122
Figure 6.5	Contribution of (n, γ) to power normalization ('MODEL-1') as a function of burnup	123
Figure 6.6	Contribution of $(n, 2n)$ to power normalization ('MODEL-1') as a function of burnup	123
Figure 6.7	Contribution of (n, f) to power normalization by selected actinides ('MODEL-1') as a function of burnup	124
Figure 6.8	Contribution of (n, γ) to power normalization by selected actinides ('MODEL-1') as a function of burnup	124
Figure 6.9	Pinwise contribution to power normalization ('MODEL-1') as a function of burnup	125
Figure 6.10	Variation in ΔE_p as a function of burnup	125
Figure 7.1	PWR thorium pincell	133
Figure 7.2	Typical spectrum in a PWR thorium pincell	134
Figure 7.3	Variation of k_∞ as a function of burnup	134
Figure 7.4	Variation of δk_∞ as a function of burnup	135
Figure 7.5	Comparison of fluxes as a function of burnup obtained using various models	135
Figure 7.6	Contribution (in %) to absorption rate from fission products and actinides as a function of burnup	136
Figure 7.7	Comparison of ^{232}Th number density as a function of burnup	136
Figure 7.8	Comparison of ^{238}U number density as a function of burnup	137

Figure 7.9	Comparison of ^{235}U number density as a function of burnup	137
Figure 7.10	Comparison of ^{239}Pu number density as a function of burnup	138
Figure 7.11	Comparison of ^{240}Pu number density as a function of burnup	138
Figure 7.12	Comparison of ^{135}Xe number density as a function of burnup	139
Figure 7.13	Comparison of ^{149}Sm number density as a function of burnup	139
Figure 7.14	Contribution to power normalization due to energy from fission	140
Figure 7.15	Contribution towards power normalization due to energy from (n, γ) reaction	140
Figure 7.16	Contribution to power normalization due to energy from $(n, 2n)$ reaction	141
Figure 7.17	Contribution to power normalization due to energy from fission of important actinides	141
Figure 7.18	Contribution to power normalization due to energy from (n, γ) reaction of important actinides	142
Figure 7.19	Contribution to power normalization due to energy from (n, γ) reaction of ^{232}Th and ^{238}U	142
Figure 8.1	Sidorenko lattice	156
Figure 8.2	Typical spectrum in Sidorenko lattice	157
Figure 8.3	Dependence of k_∞ on burnup step and its variation as a function of burnup	158
Figure 8.4	Variation of ΔK, with reference to 50 MWd/T burnup step, as a function of burnup	158
Figure 8.5	Dependence of k_∞ on choice of different rings per pin and its variation as a function of burnup	159
Figure 8.6	Variation of ΔK, with reference to ten rings per pin, as a function of burnup	159
Figure 8.7	Thermal absorption rate ($cm^{-3}s^{-1}$) as a function of number of rings per pin	160

Figure 8.8 Thermal absorption rate ($cm^{-3}s^{-1}$) up to 10,000 MWd/T in fuel pin with 10 rings 160
Figure 8.9 Thermal absorption rate ($cm^{-3}s^{-1}$) beyond 10,000 MWd/T in fuel pin with 10 rings 161
Figure 8.10 Resonance absorption rate ($cm^{-3}s^{-1}$) as a function of number of rings per pin 161
Figure 8.11 Resonance absorption rate ($cm^{-3}s^{-1}$) up to 10,000 MWd/T in fuel pin with 10 rings 162
Figure 8.12 Resonance absorption rate ($cm^{-3}s^{-1}$) beyond 10,000 MWd/T in fuel pin with 10 rings 162
Figure 8.13 k_∞ variation as a function of burnup for pin with and without gadolinium 163
Figure 8.14 Δ^{235}U variation as a function of burnup for pin with and without gadolinium 163
Figure 8.15 Δ^{239}Pu variation as a function of burnup for pin with and without gadolinium 164
Figure 8.16 Δ^{240}Pu variation as a function of burnup for pin with and without gadolinium 164
Figure 8.17 Δ^{241}Pu variation as a function of burnup for pin with and without gadolinium 165
Figure 8.18 Δ^{242}Pu variation as a function of burnup for pin with and without gadolinium 165
Figure 8.19 Contribution to power normalization due to energy from fission reaction 166
Figure 8.20 Contribution towards power normalization due to energy from (n, γ) reaction 166
Figure 8.21 Contribution towards power normalization due to energy from (n, γ) reaction in ^{155}Gd and ^{157}Gd 167

Figure 8.22 Contribution towards power normalization due to energy from (n, γ) reaction in ^{154}Gd,^{156}Gd and ^{158}Gd 167

Figure 8.23 Contribution to power normalization due to energy from fission of important actinides 168

Figure 8.24 Contribution to power normalization due to energy from (n, γ) reaction of important actinides 168

Figure 8.25 Contribution to power normalization due to energy from $(n, 2n)$ reaction 169

Figure 8.26 k_∞ variation as a function of burnup using two different models of power normalization 169

Figure 8.27 Variation of δK, with 'MODEL-2' as reference, as a function of burnup 170

Figure 8.28 Comparison of normalization flux using two different models of power normalization 170

Figure 8.29 Comparison of ^{155}Gd number density using two different models of power normalization 171

Figure 8.30 Comparison of ^{157}Gd number density using two different models of power normalization 171

Figure 8.31 Comparison of ^{235}U number density using two different models of power normalization 172

Figure 8.32 Comparison of ^{239}Pu number density using two different models of power normalization 172

Figure III.1 Lumping of isotopes in DRAGR 202

Figure III.2 COMPLOT - Total cross section of ^{235}U 213

Figure III.3 COMPLOT - Elastic cross section of ^{235}U 213

Figure III.4 COMPLOT - N,2N cross section of ^{235}U 214

LIST OF TABLES

Table 1	Fractions de fissions dans chaque domaine d'énergie	xviii
Table 2	Percentage fissions in each of the energy groups	11
Table 3.1	CANDU benchmark specifications	64
Table 3.2	Information on the elements used in the analysis	65
Table 3.3	Concentration of nuclides (in atoms per barn-cm) in each ring in fuel assembly of CANDU-6	66
Table 3.4	FTC estimation for CANDU-6 using various self shielding models .	67
Table 3.5	Comparison of k_∞ for various safety related parameters of CANDU-6	68
Table 3.6	Comparison of CTIR, PTIR and CVR of CANDU-6 using various self shielding models	69
Table 3.7	Comparison of capture rate ($cm^{-3}s^{-1}$) in resolved resonance group for CVR at B0	70
Table 3.8	Comparison of capture rate ($cm^{-3}s^{-1}$) in resolved resonance group for CVR at B1	71
Table 3.9	Elementwise contribution to capture rate ($cm^{-3}s^{-1}$) for CVR estimation of CANDU-6	72
Table 3.10	Groupwise breakdown of capture rate ($cm^{-3}s^{-1}$) for ^{238}U for CVR case at B1 for outermost layer of outermost pin	73
Table 4.1	CANDU-NG benchmark Specifications	86
Table 4.2	Comparison of k_∞ for single CANDU-NG lattice	87
Table 4.3	Comparison of the capture rate in the resolved resonance energy group for single CANDU-NG lattice with natural uranium in the central pin	88
Table 4.4	Comparison of the capture rate in the resolved resonance energy group for single CANDU-NG lattice with dysprosium in natural uranium in the central pin	89

Table 4.5 Comparison of k_∞ for assembly calculation in 2×2 pattern for CANDU-NG 90
Table 4.6 Comparison of capture rate in resolved resonance energy group for assembly calculation in 2x2 pattern (all cells cooled) for CANDU-NG with central pin having Dy in natural uranium 91
Table 4.7 Comparison of capture rate in resolved resonance energy group for assembly calculation in 2x2 pattern (all cells voided) for CANDU-NG with central pin having Dy in natural uranium 92
Table 4.8 Comparison of capture rate in resolved resonance energy group for assembly calculation in 2x2 pattern (checkerboard) for CANDU-NG with central pin having Dy in natural uranium 93
Table 5.1 Modified high conversion light water reactor benchmark specifications 106
Table 5.2 Optimization of quadrature parameter and track density 107
Table 5.3 k_∞ obtained using various self shielding models for HCLWR lattice 108
Table 5.4 Capture rate in resolved resonance group and nu-fission rate in thermal group obtained using various self shielding models 109
Table 5.5 Contribution (in %) to capture rate due to each element in each layer of fuel pin and in each broad energy group obtained using 'RIB-CORR' model 110
Table 5.6 Capture rate in ^{238}U in resolved resonance group obtained using various self shielding models 111
Table 5.7 Capture rate in ^{239}Pu in resolved resonance group obtained using various self shielding models 112
Table 5.8 Capture rate in ^{240}Pu in resolved resonance group obtained using various self shielding models 113
Table 5.9 Capture rate and nu-fission rate in four groups obtained using various self shielding models 114
Table 7.1 Modified PWR thorium pincell benchmark specifications 143

Table 7.2	Comparison of number densities of fission products at 60,000 MWd/T	144
Table 7.3	Comparison of number densities of actinides at 60,000 MWd/T . .	145
Table 7.4	Comparison of energies for power normalization obtained from MONTEBURNS and DRAGON	145
Table 8.1	Modified Sidorenko benchmark specifications	173
Table 8.2	k_∞ obtained using MCNP5 and δK (in pcm) with respect to MCNP5 obtained using various self shielding models	173
Table 8.3	Comparison of capture rate and fission rate (in $cm^{-3}s^{-1}$) in resolved resonance and thermal groups	174
Table I.1	Temperature (in K) at which cross sections were generated	189
Table I.2	Dilutions (in barns) chosen for cross section generation	189
Table I.3	Elements in the library without dilution	190
Table I.4	Elements in the library with dilution	193
Table II.1	French XMAS neutron energy group structure (in eV)	194
Table IV.1	Energy(in MeV) from various neutron induced reactions on respective elements	215

LIST OF APPENDICES

APPENDIX I	NUCLEAR DATA USED IN RESEARCH	189
APPENDIX II	GROUP STRUCTURE FOR DRAGLIB	194
APPENDIX III	PYTHON SCRIPT	197
APPENDIX IV	ENERGY FOR NORMALIZATION OF POWER IN BURNUP CALCULATIONS	215
APPENDIX V	MODIFICATIONS IN MONTEBURNS	223

INTRODUCTION

The fundamental aim in development of codes in reactor analysis is to estimate the neutron and gamma distributions in space, energy and time throughout the core. The codes numerically solve the linearized version of the particle transport equation originally developed by Boltzmann for the kinetic theory of gases. These numerical methods are based on a few approximation techniques, such as finite differences for differential operators, quadrature formulas for integral operators, or expansion methods. The codes for reactor analysis can be broadly classified as lattice level codes, and core level codes. Lattice level codes primarily involve the generation of characteristics of representative cell in the core. It could be a simple pincell, or a supercell or a complete assembly. Various parameters that are taken into consideration are the fuel enrichment, material composition of the fuel, clad, moderator, temperature, burnable poison concentration, burnup etc. The cell calculation is followed by both a spatial homogenization and an energy condensation of nuclear cross sections and diffusion coefficients. The spatial homogenization gets rid of the geometrical description of the cell for subsequent diffusion theory calculations. The cell is effectively replaced by a homogeneous material whose cross sections and diffusion coefficients are constant on the complete cell volume. The energy condensation will generate these homogeneous properties in fewer groups as a function of all the above mentioned parameters. The lattice level code thus plays a very important role in the reactor analysis.

The core level code uses the cell homogenized cross sections developed by the lattice code and analyses the overall behaviour of the core as a function of burnup. The analysis also includes the presence/absence of control absorbers, reflector material in estimating the flux and power distribution.

The most important starting point for reactor analysis is the nuclear data. A complete and validated set of nuclear data is required for estimating various reactor parameters as

close to the actual situation as possible. The nuclear data used for reactor analysis is processed by codes such as NJOY [MacFarlane 2000], which uses the evaluated nuclear data files as the starting point. An evaluation is the process of analyzing experimentally measured cross-section data, combining them with the predictions of nuclear model calculations, and attempting to extract the true value of a cross section. Parameterization and reduction of the data to tabular form produces an evaluated data set. The Evaluated Nuclear Data File (ENDF) system [MCSEWG 2001] was developed for the storage and retrieval of evaluated nuclear data to be used for applications of nuclear technology. These applications control many features of the system including the choice of materials to be included, the data used, the formats used, and the testing required before a library is released. Nuclear data libraries are made available at various nuclear data centers. The ENDF/B library is maintained at the National Nuclear Data Center (NNDC) and it contains the recommended evaluation for each material. Other centers include Nuclear Energy Agency (NEA) data bank, International Atomic Energy Agency (IAEA), Brookhaven National Laboratory (BNL), Japanese Atomic Energy Research Institute (JAERI), Korean Atomic Energy Research Institute (KAERI), Russian NDC, Chinese NDC etc. Each material included in the libraries is as complete as possible providing evaluated data for all neutron-induced reactions, covering the full range of incident neutron energies. The file also contains information such as the angular and energy distributions for secondary neutrons, radioactive decay data, fission product yield data etc. The datasets are periodically revised or replaced only after extensive review and testing, thus making them a standard reference data for subsequent analyses. Once the evaluated data sets have been prepared in ENDF format, they can be converted to forms appropriate for testing and actual applications using processing codes such as NJOY.

NJOY includes functions such as resonance reconstruction, Doppler broadening, multigroup averaging, and/or rearrangement into specified interface formats, and thus generates group-averaged cross sections for use in neutronics calculations. Of these most prevalently used are data libraries in Winfrith Improved Multigroup Scheme (WIMS) [Askew 1966] for-

mat for codes like WIMS-D and WIMS-E, "A Compact ENDF" (ACE) format [MacFarlane 2000] for the Los Alamos continuous-energy Monte Carlo code MCNP [X-5 Monte Carlo Team 2003], multigroup data for transport codes that accept formats based in the DTF-IV code etc. Recently a new module called DRAGR [Hébert 1992] has been introduced in NJOY which generates cross section in DRAGLIB format [Hébert 2004] suitable for codes like DRAGON.

Neutron energies can be broadly classified into three groups. They are the fast region with energies above 100 keV, resonance region for energies between 4 eV to 100 keV and thermal region below 4 eV. The resonance region displays sharp peaks in cross sections for various elements that are of interest in reactor analysis. The elements mainly include thorium and its chain of nuclides, uranium isotopes, plutonium isotopes, burnable absorbers like gadolinium, dysprosium, and control materials like silver, indium, cadmium etc. The cross sections of these elements are represented in the libraries in certain energy group structures like that of 69 group, or 172 group. The resonance region is represented by 13 groups in 69 group formalism, while there are 47 groups in 172 group formalism.

Neutron spectrum is dependent upon the type of reactor that is considered. In case of fast reactors, the neutron spectrum is predominantly in the keV range and above, and depends upon the loss in energy due to scattering by heavy nuclides. The thermal reactors have neutrons mainly in the eV region and generally has a Maxwellian spectrum corresponding to the temperature of the moderator/coolant. In thermal reactors, the moderator material is used to slow down high energy neutrons to thermal energies, so that they could be effectively utilised in fission reactions. The fission cross section of nuclides like ^{233}U, ^{235}U, ^{239}Pu etc are very high at thermal energies. But the main problem while slowing down the neutrons is the neutron captures in the resonances of fertile nuclides. In natural uranium reactors, for e.g. in Canada Deuterium Uranium (CANDU), it is found that the resonance escape probability is of the order of 0.9 despite having a large concentration of ^{238}U which has large resonances. This is mainly due to the self shielding effects with regard to both energy and space, i.e. the

greater the cross section means smaller the neutron flux and consequently a relatively constant capture rate. It is very difficult to calculate the resonance escape probability accurately due to the complicated structure of the absorption cross section in the resonance range. It has always been a challenge to estimate the reaction rates in the resonance energy range while doing multigroup calculations. A large number of methods have been developed over the years in order to estimate the resonance absorption rates as accurately as possible, without consuming too much computing time.

Bibliographical review

Various self shielding models have been considered for calculating the microscopic cross section in the resonance region. Of them, the Stamm'ler method was used for the self shielding calculations for arbitrary two and three dimensional geometries [Hébert 1991]. Stamm'ler method is based on a simple two term rational approximation for the fuel to fuel collision probability and leads to the computation of an averaged macroscopic dilution cross section that can be used to interpolate pretabulated effective resonance integrals [Stamm'ler 1983]. Rational approximations for regular lattices of slabs or pincells have been obtained and the method was found to accurately simulate the self shielding phenomenon. The authors [Hébert 1991] have generalized the Stamm'ler method, and have suggested that it will enable the treatment of any geometry for which standard collision probabilities (CP) can be obtained. They have considered three-term rational approximation for fuel to fuel CPs and have obtained microscopic dilution cross section, carrying out complex algebra, and thence obtaining the absorption cross section after interpolation of effective resonance integrals. This paper is limited to the study of a lattice that incorporates a single spatial resonant region. This spatial region is a collection of one or more volumes containing the same mixture of light isotopes with a single resonant isotope. Three benchmarks were analysed. The first benchmark was a pure homogeneous case of a mixture of ^{238}U with hydrogen and oxygen. Second benchmark was a pure two region cylindrical geometry with fuel, moderator and no

clad and the third one was a simplified 5X5 PWR assembly, featuring a water hole surrounded by square and rectangular fuel cells that include cladded fuel rods of different diameters.

The paper compared the absorption rates in ^{238}U calculated using two methods. One using code CESCOL, which finds the solution of fixed source slowing down equation, using an elastic slowing down operator for heavy resonant isotopes in the resolved energy domain. The second method was using a self shielding model based on the Stamm'ler method in the code DRAGON. The resonant behaviour was adequately represented by thousands of energy groups for code CESCOL, while the self shielded cross section were obtained for a coarse energy grid in DRAGON. The same collision probability module for calculation of flux was used in both the modules.

It was observed that the maximum error in the absorption rates was 4.6% and 5.4% in group 40 for all the benchmarks. It increased to 7.4% and 7.7% respectively in absence of Livolant Jeanpierre normalization. All the calculations were made for a single resonant isotope. It was proposed to perform calculations taking into account many heavy isotopes mixed together and distributed over many resonant regions. It was also proposed to perform a study of a CANDU cluster and the influence of cylinderization approximation.

It was found that the generalized Stamm'ler method which was based on narrow resonance approximation and on the assumption that the effective resonance integrals are linear functions of the square root of the dilution, was responsible for a large part of the error. Thus a new technique was proposed [Saygin 1996], where the dilution cross section was chosen such that the absorption rate in the narrow resonance approximation for closely spaced resonances in each energy group is preserved. This formalism of Riemann integration led to the improvement of the accuracy of the self shielding model, but requires non-standard cross section library called "autolib data". It consists of point-ENDF (PENDF) data averaged over a very fine mesh using the DRAGR interface module developed at École Polytechnique. The same set of benchmarks (except the homogeneous case) were analysed like that in the pa-

per [Hébert 1991]. It was observed that average error between CESCOL and generalized Stamm'ler method for absorption rates in ^{238}U got reduced from 4.6% to 1.6%, and 5.4% to 3.3% in benchmarks considered before, due to introduction of Riemann integration formalism. But this method is limited to resolved energy domain and it was proposed that the Riemann integration could be replaced by a Lebesgue integration in the unresolved energy domain. This method also was tested for single resonant isotope and a proposal for testing it for a mixture of resonant isotopes was made.

The generalized Stamm'ler method was found to be unable to represent the distributed self shielding effects in a fuel rod or across the fuel bundle. In order to improve the resonance treatment based on the generalized Stamm'ler method, it was proposed to introduce the Nordheim approximation, to gain distributed self shielding capabilities [Hébert 2004a]. The Nordheim approximation is used to uncouple the various resonant regions present in the domain and to represent distributed self shielding effects. A set of four benchmarks were analysed. Three were the same as those previously analysed [Hébert 1991]. In order to study the distributed self shielding effects within the fuel rod, a fourth benchmark was analysed by dividing the fuel rod into six annular volumes and absorption rate was computed in each subvolume. It was observed that by introduction of Nordheim approximation, some distributed self shielding capabilities were brought to the Stamm'ler method. It was observed that the equivalent dilution calculated, played a role in limiting the estimation of absorption rate in the outer fuel ring. By using both the Nordheim approximation and Riemann integration, a better representation of the distributed effects was observed, i.e. -66.3% reduced to -8.1%. Numerical tests presented in this paper were limited to fuel rods with a single resonant isotope of (^{238}U).

In the paper [Hébert 2005], the lattice calculations were performed using a development version of DRAGON, activating different self-shielding models, i.e. the Universal Self Shielding (USS) model, the Sanchez-Coste model [Hébert 2002], and the Ribon extended model (RIB). The Sanchez-Coste model is based on the mathematical probability tables and

is used in APOLLO2 [Loubiére 1999]. The main difference between the Sanchez-Coste and Ribon extended methods, is that the latter is a pure subgroup method and that the former relies on computing averaged dilutions to interpolate NJOY tables. In a pure subgroup method, an averaged dilution is not computed. The results were compared with those obtained using code CESCOL. In the paper [Hébert 2005], the author has chosen a set of eight benchmarks. The benchmarks analysed were similar to those chosen in the previous work [Hébert 2004a], except that one more isotope ^{240}Pu was considered along with ^{238}U and cases were repeated. This was done especially to bring out the effect of mutual self shielding effects between resonant isotopes. Other than the eight benchmarks, the Rowlands pincell benchmark [Rowlands 1999] was also analysed. This benchmark has a combination of UO_2 fuelled (UOX) and $UPuO_2$ fueled with two different isotopic compositions of the mixed oxide. It was observed that with first four set of benchmarks, which had only ^{238}U in the fuel, the absorption rates, calculated with models described, matched well with that of CESCOL and of them, the most accurate one was the RIB model, with a maximum integrated error of 0.6%. The next four benchmarks were analysed for mutual self shielding effects with new correlation model to that with no correlation. A small improvement on integrated ^{238}U rate errors (from 2% to 0.6%) and a more substantial improvement on ^{240}Pu rates errors (from 15.7% to 4.5%) was observed using the RIB model with correlation.

A study to investigate the accuracy of the new probability tables on the Rowlands pincell benchmark [Rowlands 1999] was carried out by the author [Hébert 2005]. The results were compared with the Monte Carlo code TRIPOLI [Both 1996]. The generalized Stamm'ler approach, currently programmed in DRAGON 3.05 [Marleau 2006], was also tested along with the other models described above. The parameter that was compared was the infinite multiplication factor. It was observed that the numerical results obtained using RIB model were close to those obtained using code TRIPOLI, after considering the distributed self shielding effects and the correlation effects between pair of resonant isotopes (^{238}U and ^{240}Pu). It was noted that the results obtained using generalized Stamm'ler model

were off by many hundreds of pcm, and was attributed to the crude approximations used in the Stamm'ler method, and the inability of the model to represent the distributed self shielding effects within a rod.

A summary of development on computational models used in France for neutron resonance absorption in light water lattices was provided [Reuss 2003]. The authors have concentrated on the methods developed especially in France and has given a brief description of each of the methods. In the paper [Reuss 2003], two sets of benchmarks have been chosen. The benchmarks have been analysed using various methods, that range from, no self shielding, to performing self shielding calculation with six resonant regions, a homogenization with the all resonances ("AR") model in each resonant group and an exact direct method ("DM") diagonalization which is the recommended model for APOLLO-2. The reaction rates of ^{238}U was compared using each of the models with that of the reference. Group histograms of the resonant capture rates was also presented. The idea of using statistics on macrogroup reaction rates as proposed in [Reuss 2003] would be used, so as to enable us to perform extensive validation of the methods selected for this research.

In an earlier related work [Hajjami 2001] of generating cross section libraries inhouse at the Institute of Nuclear Engineering (IGN), 69 group cross section library in WIMS-D4 format was generated using the evaluated datafiles obtained from NNDC, Brookhaven. This work was primarily taken up to generate cross section libraries in house and test it against standard benchmarks. The benchmarks chosen were that of Mosteller [Mosteller 1991], Rowlands [Rowlands 1999] and feedback effects in CANDU-6. The feedback effects included void and fuel temperature. The main conclusion of this work was that the diffusion cross section of ^{16}O was primarily responsible for eigenvalue discrepancies.

In most of the reactor codes, burnup calculations are performed considering energy per fission and fission rate to normalize power and obtain fluxes to deplete the fuel. Under the auspices of the WIMS Library Update Project (WLUP) [Leszczynski 2003], information on

energy released from fission of important actinides has been provided. The energy released per fission includes the contributions from the kinetic energy of incident neutrons and from the decay of the capture products. The energy released from other neutron induced reactions or energies released due to neutron induced reactions with other elements are not provided in the library.

In the code MONTEBURNS [Poston 1999], there is a discussion of choice of energy used for power normalization. It is mentioned that the user can provide the average energy deposited per fission or allow the code to calculate the value based on production of actinides as a function of burnup. The amount of energy per fission of each actinide is provided as a fraction with respect to energy released due to fission of ^{235}U atom. The value of energy provided by user must include all modes of energy deposition, including fission gammas, capture gammas, and neutron kinetic energy. This energy value is used along with the fission rate to obtain the flux for depletion calculations using ORIGEN. It was however concluded that MONTEBURNS may be modified to include necessary tallies for other reactions like capture, (n, 2n) etc. so that energies from all reactions could be used for power normalization.

It can thus be seen from the bibliographical review that the self shielding models incorporated in DRAGON has been tried against limited sets of lattices. In this work we propose to do a more exhaustive studies analysing lattices in vogue and having a variety of fuel, lattice pitch, coolant/moderator to bring out the performance of the models and provide an opportunity for the user to chose a self shielding model for a particular type of analysis.

We will be generating cross section libraries inhouse using a Python script which automatically creates the inputs for NJOY to produce libraries in DRAGLIB and ACE formats.

It will also be seen in the present research, the need to perform power normalization using energy from all neutron induced reactions in the context of fuel having actinides and fuel having actinides and burnable absorbers like gadolinium, which contributes to heat by

neutron capture. The code MONTEBURNS will be appropriately modified to include tallies for capture and $(n, 2n)$ reactions and utilize energy of these reactions to perform power normalization and will be used for validation studies.

Benchmarks analysed

The quality assurance of the codes developed for analysis of reactor systems is mainly achieved by validating them against experimental data or if such data is not available, against some standard numerical benchmarks. These benchmarks are generally chosen as a function of the nature of application to which the code is to be applied. The benchmarks against which the lattice code is to be validated has to have a broad spectrum. A benchmark is required mainly to decouple the relative contribution to the error in the calculated integral parameters originating from the basic nuclear data and those arising from the library format limitations, data processing assumptions and approximations in the calculational models in the code. The choices of the benchmarks have been done on the basis that they include fuel types, geometries in vogue in the current power and research reactors. They include a combination of ^{232}Th, ^{233}U, ^{235}U,^{238}U, ^{239}Pu, as fuel, and the geometries include square, hexagonal and Wigner-Seitz unit cells. The pressurized water reactors in the USA use enriched ^{235}U as fuel with light water as coolant and moderator and are having square geometry, while the Russian PWRs, i.e WWERs have hexagonal geometry. The pressure tube reactors, i. e. CANDU-6, use natural uranium as fuel and use heavy water as moderator and coolant. The fuel geometry is annular and the presently used fuel bundles in CANDU-6 are the 37 rod type cluster. The futuristic reactors envisage the use of thorium as fuel and development activities are underway in countries like India. KAMINI, a research reactor in India, is based on ^{233}U as fuel. India is also pursuing Advanced Heavy Water Reactor (AHWR) [Kakodkar 1998] for large scale utilisation of its thorium resources. Other parallel ideas on effective utilisation of thorium has been published [Jagannathan 2001]. Certain benchmarks have been considered with burnable poison. The choice is made as in most of the modern PWRs burnable poison like gadolinium

is used along with fuel. This helps in suppressing the initial excess reactivity and allows to go for higher discharge burnup. Isotopes of gadolinium mainly ^{155}Gd and ^{157}Gd are mixed with the fuel in the oxide form. They differ from other burnable poison like boron which are generally mixed with moderator, as in PWRs where it acts as a chemical shim.

A total of five types of lattices have been analysed as part of this research. Very interesting information regarding these lattices is provided in Table 2. It can be seen from the table that the benchmarks chosen cover a wide range of behaviour of neutron energies as mentioned earlier for choice of benchmarks. It can be seen that CANDU-6 lattice represents a well thermalised system, while PWR pin with gadolinium, in comparison to other lattices, has the largest fraction of fissions happening in energy range greater than 100 keV. A high conversion light water reactor (HCLWR) benchmark has been chosen mainly because it represents the highest amount of fissions in the resonance energy range where we are testing our self shielding models. A more detailed description on each of the benchmark is provided in the respective chapters.

Table 2 Percentage fissions in each of the energy groups

Lattice	Thermal (< 0.625 eV)	Resonance (0.625 ev - 100 keV)	Fast (> 100 keV)
CANDU-6	93%	2%	5%
CANDU-NG	89%	7%	4%
PWR Thorium	76%	20%	4%
PWR pin with Gd	20%	43%	37%
HCLWR	34%	46%	20%

Chapter 1 gives a brief introduction to the self shielding and burnup models that have been incorporated in DRAGON Version4. A brief description of the codes that will provide reference solutions for this research is mentioned in chapter 2. Chapters 3 to 8 give the description and analysis of chosen benchmarks. It will be followed by conclusions and appendices.

CHAPTER 1

DRAGON VERSION4

The computer code DRAGON solves the integral transport equation using collision probability method, interface current method or the method of characteristics. The code has been built as a modular structure with ease of addition of new models in the existing framework. The code has all the functions that characterize a reactor lattice physics code. It includes the interpolation of microscopic cross sections which are supplied by means of standard libraries like MATXS [MacFarlane 1992], WIMS-D4 [Askew 1966], WIMS-AECL [Donnelly 1986], APOLLO [Loubiére 1999] and DRAGLIB. Several advanced resonance self-shielding models (that are being validated as part of this research) are incorporated in the code. The self shielding models are broadly classified under two categories, i.e models based on "equivalence in dilution" or "subgroup approach". A more elaborate discussion will be provided in the following sections. The collision probabilities are obtained using interface current method for 2-D cartesian or hexagonal assemblies or collision probability method for simple one dimensional (1-D) or two dimensional (2-D) pin-cell cartesian or hexagonal geometries or for more general 2-D geometries and for three dimensional (3-D) assemblies. The power iteration method is used to obtain effective multiplication factor k_{eff} and fluxes in various regions. Depletion calculations are also performed by normalizing for constant flux or power. Power normalization using decay energy and energies from most neutron induced reactions forms an important part of the modeling in DRAGON and is being validated as part of this research.

1.1 Self shielding models based on equivalence in dilution principle

1.1.1 Generalized Stamm'ler Model

Self shielding models for simple geometries were based on equivalence principle proposed by Stamm'ler. This approach is based on a two-term rational approximation for fuel to fuel collision probability (CP) and leads to the computation of an averaged macroscopic dilution cross section that can be used to interpolate pretabulated effective resonance integrals. In order to apply the method for complex geometries, a general method was introduced in the DRAGON lattice code [Hébert 1991]. A brief description of the model is mentioned below.

The ultimate goal of self shielding calculation is to evaluate $\bar{\sigma}_y(g)$, the self shielded microscopic cross section for any nuclear reaction y. $\bar{\sigma}_y(g)$ is defined as

$$\bar{\sigma}_y(g) = \mu_g \frac{\int_{u_{g-1}}^{u_g} du \sigma_y(u)\phi(u)}{\int_{u_{g-1}}^{u_g} du \phi(u)} \tag{1.1}$$

where

u	=	lethargy
g	=	coarse energy group that may include many resonances and that will be used after completion of the self shielding calculation
u_{g-1}, u_g	=	lethargy limits of this group
$\phi(u)$	=	neutron flux
$\sigma_y(u)$	=	microscopic cross section for nuclear reaction y
μ_g	=	Super Homogenisation (SPH) equivalence factor [Hébert 1993]

The collision probability form of the transport equation can be used to describe an heterogeneous case. In the one resonant isotope case, we obtain

$$\phi_i(u) = \sum_{j=1}^{I} p_{ij}(u) \left\{ R_j^+ \{\phi_j(u)\} + R_j^* \{\phi_j(u)\} \right\} \quad ; \quad i = 1, I \tag{1.2}$$

where

$\phi_i(u)$	=	neutron flux in region i
$p_{ij}(u)$	=	reduced CP for neutrons born in region i to collide in region j; the corresponding CP matrix should be computed in a closed domain, i.e., with an albedo set to 1
$R_j^+ \{\phi_j(u)\}$	=	Slowing down operator in region j for nuclear reactions with light isotopes, as defined in Eq. 1.3
$R_j^* \{\phi_j(u)\}$	=	Slowing down operator in resonant region j for nuclear reactions with a single heavy isotope, as defined in Eq. 1.3 .

Slowing down operator is generally defined as

$$R\{\phi(u)\} = \frac{1}{1-\alpha} \int_{u-\epsilon}^{u} du' e^{u'-u} \sigma_s(u') \phi(u') \ . \tag{1.3}$$

The reduced collision probability is defined as

$$p_{ij}(u) = \frac{P_{ij}(u)}{\Sigma_j(u)} \tag{1.4}$$

where P_{ij} is the element of the complete CP matrix and $\Sigma_j(u)$ is the total macroscopic cross section of the resonant region and is given as

$$\Sigma_j(u) = \Sigma_j^+(u) + \Sigma_j^*(u) \tag{1.5}$$

where $\Sigma_j^*(u)$ is the macroscopic total cross section of the heavy isotope contained in region j and $\Sigma_j^+(u)$ is the macroscopic total cross section of light isotopes contained in region j.

Three assumptions due to Livolant-Jeanpierre were used to simplify neutron slowing down equation. First one factorizes the neutron flux into a product of resonant fine structure function $\varphi_i(u)$ with a regular distribution $\psi_i(u)$. Second one assumes that the slowing down operator for the heavy isotope acts over a short lethargy range, and third one assumes a spatially flat value of distribution $\psi_i(u)$ across the domain. The simplified form of slowing down equation thus was

$$\varphi_i(u) = \sum_{j=1}^{I} p_{ij}(u) \left\{ \Sigma_j^+(u) + R_j^* \left\{ \varphi_j(u) \right\} \right\} \quad ; \quad i = 1, I \ . \tag{1.6}$$

The problem domain is divided into regular and resonant regions, where a regular region contains heavy isotope mixed with light isotopes. The resonant regions are merged into a single resonant region denoted as index x, even if they are unconnected. The fuel to fuel resonant collision probability for the resonant region is written as

$$p_{xx}(u) = \frac{\sum\limits_{i \in G_x} V_i \sum\limits_{j \in G_x} p_{ij}(u) \Sigma_j(u)}{\sum\limits_{i \in G_x} V_i \Sigma_i(u)} \tag{1.7}$$

where G_x is the set of indices (i, j) belonging to the resonant region x and V_i is the volume of the resonant region i.

Subsequently an expression for fine structure function is obtained for the resonant region as,

$$p_{xx}(u)\left\{\Sigma_x^*(u) - R_x^*\left\{\varphi_x(u)\right\}\right\} = 1 - \varphi_x(u) \ . \tag{1.8}$$

A three-term rational approximation is considered for the reduced collision probability against the two term rational approximation considered by Stamm'ler in the original theory. It is represented as

$$p_{xx}[\Sigma_x^*(u)] \simeq \frac{1}{\Sigma_x^*(u) + E[\Sigma_x^*(u)]} \simeq \sum_{n=1}^{3} \frac{\alpha_n(g)}{\Sigma_x^*(u) + \Sigma_{en}(g)} \tag{1.9}$$

with

$$\sum_{n=1}^{3} \alpha_n(g) = 1 \tag{1.10}$$

where $E[\Sigma_x^*(u)]$ is the escape function and $\Sigma_{en}(g)$ is the background scattering cross section.

The typical behaviour of escape function is represented using a quadratic rational approximation as

$$E[\Sigma_x^*(u)] = \frac{a[\Sigma_x^*(u)]^2 + b[\Sigma_x^*(u)] + c}{[\Sigma_x^*(u)]^2 + d[\Sigma_x^*(u)] + e} \tag{1.11}$$

with

$$\lim_{[\Sigma_x^*(u)]\to\infty} E[\Sigma_x^*(u)] = a \ . \tag{1.12}$$

The narrow resonance model for slowing down operator $R_x^*\left\{\varphi_x(u)\right\}$ is assumed. Hence

$$R_x^*\left\{\varphi_x(u)\right\} = \Sigma_{px}, \tag{1.13}$$

where Σ_{px} is macroscopic potential cross section of the resonant isotope.

On substitution of equations 1.9 and 1.13 in 1.8, we get the fine structure function for the heterogeneous case as

$$\varphi_x(u) = \sum_{n=1}^{3} \alpha_n(g) \frac{\Sigma_{px} + \Sigma_{en}}{\Sigma_x^*(u) + \Sigma_{en}} \tag{1.14}$$

where the dilution, σ_{en}, which is used as NJOY input in GROUPR module, is Σ_{en}/N^*, where N^* is the number density of the resonant isotope.

The fine structure function is used in the definition of effective resonance integral $I_y(g)$ for nuclear reaction y, which is written as

$$I_y(g) = \int_{u_{g-1}}^{u_g} du \sigma_y(u) \varphi_x(u) \ . \tag{1.15}$$

In order to evaluate the averaged (equivalent) microscopic dilution cross section $\bar{\sigma}_e(g)$, a mathematical recipe is followed that is mentioned in [Hébert 1991]. It is given as

$$\bar{\sigma}_e = \frac{1}{N^*} \left\{ \alpha_1 (\Sigma_{e1})^{1/2} + \alpha_2 (\Sigma_{e2})^{1/2} + \alpha_3 (\Sigma_{e3})^{1/2} \right\}^2 \ . \tag{1.16}$$

The dilution $\bar{\sigma}_e(g)$ thus obtained can be used to interpolate all the effective resonance integrals in the cross section library. Using these effective resonance integrals, the averaged fine structure function $\bar{\varphi}_x(g)$ can be calculated based on a procedure known as Livolant-Jeanpierre normalization (LJ) as

$$\bar{\varphi}_x(g) = 1 - \frac{1}{E[\bar{\Sigma}_x^*(g)]} \left\{ I(g) - \sum_h \frac{U_h}{U_g} I_s(g \leftarrow h) \right\} \tag{1.17}$$

where $E[\bar{\Sigma}_x^*(g)]$ is the value of the escape function interpolated at the self-shielded macroscopic cross section $\bar{\Sigma}_x^*(g)$

The new self shielded microscopic cross section is then computed using

$$\bar{\sigma}_y^*(g) = \frac{I_y(g)}{\bar{\varphi}(g)} \ . \tag{1.18}$$

It can be noted that the SPH equivalence factor defined in Eq. 1.1 is not seen explicitly in Eq.1.18. The value of the SPH factors are taken as unity when one does not consider LJ normalization. But when one considers LJ normalization, the SPH equivalence factor is the ratio of fine flux obtained using LJ normalization to that obtained without using LJ normalization. The Generalized Stamm'ler method is used for resonance treatment in DRAGON 3.05 [Marleau 2006].

1.1.2 Improved Generalized Stamm'ler Method

The generalized Stamm'ler method is based on narrow resonance model (equation 1.13) and on the assumption that the effective resonance integrals are linear functions of the square root of dilution (equation 1.16). A detailed error analysis showed that the two assumptions made were responsible for a large part of error [Saygin 1996]. Improvements were made to the generalized Stamm'ler method to achieve better accuracy (using Riemann integration method) and to represent distributed self shielding effects in a fuel rod or across a fuel bundle (using Nordheim Model) [Hébert 2004a, Nordheim 1961].

1.1.2.1 Nordheim Model

Starting from equation 1.2 and using equations 1.4 and 1.5 , we have

$$\phi(u) = \sum_{j \in G_x} \frac{P_{ij}(u)}{\Sigma_j^+ + N_j^* \sigma^*(u)} N_j^* r_j \{\phi_j(u)\} + \sum_{j=1}^{I} \frac{P_{ij}(u)}{\Sigma_j^+ + N_j^* \sigma^*(u)} \Sigma_j^+ \ . \tag{1.19}$$

It is assumed that

$$r_i \{\phi_i(u)\} = r_j \{\phi_j(u)\} \tag{1.20}$$

for $i \in G_x$ and $j \in G_x$, where G_x is the set of indices i pointing to a resonant region.

The Nordheim equation is obtained as

$$\phi_i(u) = \frac{1 - P_i(u)}{\sigma^*(u)} r_i \{\phi_i(u)\} + P_i(u) \ ; \ i \in G_x \tag{1.21}$$

where $P_i(u)$ is the probability that a neutron born in the fuel region i has the next collision on a non-resonant isotope.

$$P_i(u) = \sum_{j=1}^{I} P_{ij}(u) \frac{\Sigma_j^+}{\Sigma_j^+ + N_j^* \sigma^*(u)} \ . \tag{1.22}$$

A three term rational approximation similar to generalized Stamm'ler model is considered, where

$$\frac{1 - P_i(u)}{\sigma^*(u)} = \sum_{n=1}^{3} \frac{\alpha_{n,i}}{\sigma^*(u) + \sigma_{en,i}} \tag{1.23}$$

where

$$\sum_{n=1}^{3} \alpha_{n,i} = 1 \ . \tag{1.24}$$

With the above approximation, the Nordheim equation is written as

$$\phi_i(u) = \sum_{n=1}^{3} \frac{\alpha_{n,i}}{\sigma^*(u) + \sigma_{en,i}} \left\{ r_i \left\{ \phi_i(u) \right\} + \sigma_{en,i} \right\} \;\; ; \;\; i \in G_x \tag{1.25}$$

so that

$$\phi_i(u) = \sum_{n=1}^{3} \alpha_{n,i} \varphi_{n,i}(u) \tag{1.26}$$

where the partial flux $\varphi_{n,i}$ is assumed to be the solution of the following equation:

$$r_i \left\{ \phi_i(u) \right\} + \sigma_{en,i} = \left\{ \sigma^*(u) + \sigma_{en,i} \right\} \varphi_{n,i}(u) \;\; . \tag{1.27}$$

Using a mathematical recipe similar to the one mentioned for generalized Stamm'ler model, we obtain a set of values $\{\alpha_{n,i}, \Sigma_{en,i}, n = 1,3\}$ for each index $i \in G_x$. The difference from the generalized Stamm'ler model is that microscopic dilution factor is found for each region instead of a single value found in the earlier model. $\bar{\sigma}_{e,i}$ is thus obtained using $\{\alpha_{n,i}, \Sigma_{en,i}, n = 1,3\}$ in equation 1.16, and self shielded cross section is evaluated for each resonant region.

1.1.2.2 Riemann Integration Method

The recipe to calculate an average dilution based on Stamm'ler approximation is known to be accurate only for high values of $\bar{\sigma}_{e,i}$ and for energy domains where the distributed self shielding effects can be neglected. The method involves use of Statistical (ST) and Wide Resonance (WR) slowing down models, different from equation (1.13). It is represented as

$$r_i \left\{ \varphi_{n,i}(u) \right\} = \lambda_g \left\langle \sigma_s^* \varphi_{n,i} \right\rangle_g + (1 - \lambda_g) \sigma_s^* \varphi_{n,i}(u) \tag{1.28}$$

where λ_g is the Goldstein-Cohen parameter [Goldstein 1962] of the resonant isotope in group g.

Substituting equation (1.28) in equation (1.27) we have

$$\phi_i(u) = \sum_{n=1}^{3} \alpha_{n,i} \varphi_{n,i}(u) \tag{1.29}$$

with

$$\varphi_{n,i}(u) = \frac{\lambda_g \langle \sigma_s^* \varphi_{n,i} \rangle_g + \sigma_{en,i}}{\sigma_a^*(u) + \lambda_g \sigma_s^*(u) + \sigma_{en,i}} \ . \tag{1.30}$$

Using the value of flux obtained, one estimates the value of reference absorption rate $T_{a,g}$ as following.

$$T_{a,g} = \sum_{n=1}^{3} \alpha_{n,i} \sigma_{en,i} \frac{\left\langle \dfrac{\sigma_a^*}{\sigma_a^* + \lambda_g \sigma_s^* + \sigma_{en,i}} \right\rangle_g}{1 - \lambda_g \left\langle \dfrac{\sigma_s^*}{\sigma_a^* + \lambda_g \sigma_s^* + \sigma_{en,i}} \right\rangle_g} \ . \tag{1.31}$$

The reference absorption rate $T_{a,g}$ is computed as a function of detailed cross section data $\sigma_s^*(u)$ and $\sigma_a^*(u)$ in group g of the resolved energy domain. This information, called "autolib data", is available in cross section libraries built with NJOY and post processed with the DRAGR module. If "autolib data" is not available in an energy group, equation 1.16 is used to compute $\bar{\sigma}_{e,i}$.

The Riemann integration method consists in computing the equivalent dilution $\bar{\sigma}_{e,i}$ as

the root of the following non-linear equation:

$$T_{a,g}\left\{1-\lambda_g\left\langle\frac{\sigma_s^*}{\sigma_a^*+\lambda_g\sigma_s^*+\bar{\sigma}_{e,i}}\right\rangle_g\right\}-\bar{\sigma}_{e,i}\left\langle\frac{\sigma_s^*}{\sigma_a^*+\lambda_g\sigma_s^*+\bar{\sigma}_{e,i}}\right\rangle_g=0\ . \tag{1.32}$$

After obtaining the equivalent dilution $\bar{\sigma}_{e,i}$, using Newton-Raphson iteration, the procedure similar to generalized Stamm'ler method is used and the self shielded cross sections are found.

The improved Generalized Stamm'ler Method with Nordheim model (GSM1) and Generalized Stamm'ler Method with Nordheim model and Riemann integration (GSM2) has been incorporated in DRAGON Version4 [Marleau 2006].

1.2 Models based on subgroup approach

1.2.1 The Statistical Subgroup Model

The statistical subgroup model (SUBG) is similar to the self-shielding model used in codes WIMS-7 [Halsall 1996] and Helios [Casal 1991]. It is based on a subgroup equation with *physical probability tables*, obtained by fitting tables of dilution-dependent cross sections. It is currently considered as the state-of-the-art approach for computing self-shielded cross sections. The probability table corresponding to the total cross section is computed so as to match the numerical integration results with the tabulated values for specific values of the microscopic dilution cross section σ_e to a given accuracy using the following fitting

function:

$$\bar{\sigma}(\sigma_e) = \frac{\left\langle \frac{\sigma}{\sigma+\sigma_e} \right\rangle_g}{\left\langle \frac{1}{\sigma+\sigma_e} \right\rangle_g} = \frac{\sum_{k=1}^{K} \frac{\omega_k \sigma_k}{\sigma_k+\sigma_e}}{\sum_{k=1}^{K} \frac{\omega_k}{\sigma_k+\sigma_e}} \tag{1.33}$$

with the infinite dilution microscopic total cross section defined as

$$\bar{\sigma}(\infty) = \frac{1}{\Delta u_g} \int_{u_{g-1}}^{u_g} du \sigma(u) = \sum_{k=1}^{K} \omega_k \sigma_k \ . \tag{1.34}$$

Determination of probability table coefficients in equation 1.33 is a curve fitting problem and is carried out using Padé regression method [Hébert 1998]. The creation of physical probability tables is mentioned in [Hébert 2005]. It is subsequently used to solve for the fluxes, starting from equation 1.2. The slowing down operator considered is as per ST-WR model as shown in equation 1.28, as proposed by Cullen [Cullen 1977]. The Goldstein-Cohen parameter λ_g is recovered as input data to the self shielding operator as there are no capabilities in DRAGON for computing the λ_g. This approach is limited in its incapability to represent mutual resonance shielding effects. The flux in each region i and subgroup k is calculated using probability tables as follows.

$$\phi_{i,k} = \sum_{j=1}^{I} p_{ij,k} \left\{ \Sigma_{s,j}^{+} + N_j^* \left\{ \lambda_g \sum_{l=1}^{K} \omega_l \sigma_{s,j,l}^* \phi_{j,l} + (1-\lambda_g) \sigma_{s,j,k}^* \phi_{j,k} \right\} \right\} \tag{1.35}$$

where $\sigma_{s,j,l}^*$ is the microscopic P_0 scattering cross section of the resonant isotope in subgroup l and region j. $p_{ij,k}$ is a component of the collision probability matrix computed using the cross sections of the k-th subgroup. Equation 1.35 is written in terms of collision probabilities but its use with other solution techniques of the transport equation is straightforward.

Subsequently integrated flux $\langle \phi_i \rangle_g$ and reaction rates $\langle \sigma_{\rho,i} \phi_i \rangle_g$ are computed as follows. The

detailed procedure is mentioned in [Hébert 2005].

$$\langle \phi_i \rangle_g = \sum_{k=1}^{K} \omega_k \phi_{i,k} \quad and \quad \langle \sigma_{\rho,i} \phi_i \rangle_g = \sum_{k=1}^{K} \omega_k \phi_{i,k} \sigma_{\rho,i,k} \ . \tag{1.36}$$

As before, the flux-volume averaged cross sections thus obtained cannot be used directly in a coarse group calculation as the reaction rates are not conserved. A multigroup equivalence procedure is subsequently performed and an SPH corrective factor is introduced for each region and coarse energy group and equivalent cross sections are determined, as mentioned in [Hébert 2005].

1.2.2 Ribon Extended Self Shielding Model

The Ribon extended self-shielding model (RIB) is a new-generation approach with improved accuracy and capabilities for representing both the *distributed self-shielding effect* and the *mutual resonance shielding effect.* The RIB model is based on subgroup flux equation with mathematical probability tables taking into account negative and positive moments of the resonant cross sections, as proposed in the CALENDF approach [Ribon 1989]. A new type of correlated 2D probability table is used for the representation of the slowing down effect in the resolved energy domain. The resulting formalism gives a better representation of distributed self shielding effect. Also, a numerical scheme to represent mutual shielding effect of overlapping resonances between different isotopes, are represented by a correlated weight matrix also computed using a CALENDF approach. Detailed cross section information for the total and P_0 scattering reactions, known as "autolib data", allows the computation of these probability tables in the resolved energy domain. The RIB model is used in all energy groups where "autolib data" is available. The RIB model uses *mathematical probability tables*, which are introduced in [Ribon 1989] and used in [Hébert 2005].

Probability tables corresponding to the microscopic total cross section $\sigma(u)$ can be defined from the probability density $\Pi(\sigma)$. $\Pi(\sigma)d\sigma$ is the probability for the microscopic total cross section of the resonant isotope, to have a value between σ and $\sigma + d\sigma$. Using this definition, any Riemann integral in lethargy, with a σ dependent integrand, can be replaced by an equivalent Lebesgue integral:

$$\frac{1}{\Delta u_g}\int_{u_{g-1}}^{u_g} du f[\sigma(u)] = \int_0^{max(\sigma)} d\sigma \Pi(\sigma) f(\sigma) \tag{1.37}$$

where $\Delta u_g = u_g - u_{g-1}$

The probability density $\Pi(\sigma)$ is represented by a series of K Dirac distributions centered at discrete values σ_k of the microscopic total cross section for the resonant isotope. Each discrete level is called a subgroup and is also characterized by a discrete weight ω_k. The probability density is written

$$\Pi(\sigma) = \sum_{k=1}^{K} \delta(\sigma - \sigma_k)\omega_k \tag{1.38}$$

which leads to discretization of Riemann integral in lethargy as

$$\frac{1}{\Delta u_g}\int_{u_{g-1}}^{u_g} du f[\sigma(u)] = \sum_{k=1}^{K} \omega_k f(\sigma_k) \ . \tag{1.39}$$

The sets of values $\{\omega_k, \sigma_k; k = 1, K\}$ corresponding to energy group g is called a probability table, for the variable σ. The mathematical probability table is generated using the CALENDF approach, where the position of the base points σ_k and the values of the weights ω_k are simultaneously determined [Hébert 2005, Hébert 2002]. Similarly probability tables for other reactions like elastic scattering are generated and used in the solution for slow-

ing down equation and subsequent calculation of self shielded cross sections for a particular reaction. The subgroup flux equation is thus written using the probability tables as follows.

$$\phi_{i,k} = \sum_{j=1}^{I} p_{ij,k} \left\{ \Sigma_{s,j}^{+} + N_j^* \sum_{l=1}^{K} \frac{W_{k,l}}{\omega_k} \sigma_{w,j,l}^* \phi_{j,l} \right\} \tag{1.40}$$

where $\sigma_{w,j,l}^*$ is the microscopic secondary scattering cross section of the resonant isotope in subgroup l and region j. $W_{k,l}$ is the slowing down correlated weight matrix. Subsequently the integrated flux and reaction rates are calculated as mentioned before. SPH correction is applied before calculating the self shielded cross sections.

Mutual resonance shielding model has been developed in order to represent the correlation effect between pairs of different resonant isotopes such that it is compatible with RIB model. The generation of probability tables for resonant isotopes, correlated weight matrices, and their subsequent use in determining the self shielded cross sections is mentioned in [Hébert 2005]. The salient points of the model is described here for the sake of continuity.

The collision probability form of transport equation considering two resonant isotopes can be written as

$$\phi_i(u) = \sum_{j=1}^{I} p_{ij}(u) \left\{ \Sigma_{s,j}^{+} + N_j^{*a} r_j^a \left\{ \phi_j(u) \right\} + N_j^{*b} r_j^b \left\{ \phi_j(u) \right\} \right\} \ , \quad i = 1, I \tag{1.41}$$

where

I	=	number of regions
$p_{ij}(u)$	=	lethargy dependent reduced collision probability
$\Sigma^{+}_{s,j}$	=	macroscopic P_0 scattering cross section of the non resonant isotopes in region j
N^{*a}_j, N^{*b}_j	=	number density of the two resonant isotopes in region j
r^a_j,r^b_j	=	slowing down operators defined in Equation 1.3

The mutual resonance shielding model consists of computing the flux component $\phi^a_{i,k}$ in region i and subgroup k for element a, taking into account the correlation effect. If ST heavy slowing down model is chosen, then $\phi^a_{i,k}$ is obtained as

$$\phi^a_{i,k} = \sum_{j=1}^{I} \bar{p}^a_{ij,k} \left\{ \Sigma^{+}_{s,j} + N^{*b}_j \bar{\sigma}^b_{s,j} + N^{*a}_j \sum_{l=1}^{K} \frac{W^a_{k,l}}{\omega^a_k} \sigma^{*a}_{w,j,l} \phi^a_{j,l} \right\} \quad , \quad k = 1, K \tag{1.42}$$

where $\bar{\sigma}^b_{s,j}$ is the self shielded scattering P_0 cross section of isotope b recovered from the previous self shielding iteration. This approximation assumes that the slowing down correlation and two isotope correlation effects are independent. The flux solution is obtained after an iterative procedure [Hébert 2005]. After convergence of the subgroup fluxes $\phi^a_{i,k}$ and $\phi^b_{i,k}$, the self shielded cross sections are obtained using Equation 1.36. This model is generally considered only when isotopes having correlation are in large concentration. For example, RIB method with correlation will be effective when one considers mixed oxide (MOX) fuel of uranium oxide and plutonium oxide with a large concentration of ^{240}Pu.

1.3 Burnup models

1.3.1 Power normalization in DRAGON Version4

The fluxes obtained as a solution for the eigen value transport problem is of arbitrary normalization and cannot be directly used for depletion calculation. In order to obtain the flux for depletion calculations, a normalization for constant power or constant flux is performed. We will focus mainly on flux obtained for constant power normalization. Power normalization is done in DRAGON Version4 as

$$A\phi = B - D \tag{1.43}$$

where $A\phi$ is the contribution due to neutron induced reactions, D is the contribution due to decay, and B is the reference power to which fluxes are normalized. By considering energy released due to decay as part of normalization, one can analyze the behavior of fuel assembly and heat generated thereof when it is cooled away from the reactor. In general,

$$A\phi = \sum_{m=1}^{MIX} \sum_{l=1}^{L} \sum_{x=1}^{NREAC} Q_{xlm} \left\langle \sigma_{\mathrm{x},lm}\phi \right\rangle N_{lm} \tag{1.44}$$

where Q_{xlm} is energy associated with reaction x for element l of mixture m, while $\sigma_{\mathrm{x},lm}$ is the microscopic cross section of element l for reaction x of mixture m and N_{lm} is the number density of element l of mixture m. $\langle \sigma_{\mathrm{x},lm}\phi \rangle$ represents summation of reaction rates over all energy groups. 'NREAC' represents the eleven types of reactions taken into consideration, including (n,γ), (n,f), $(n,2n)$, $(n,3n)$, $(n,4n)$, (n,α), (n,p), $(n,2\alpha)$, (n,np), (n,d), and (n,t). L represents all the fission products and actinides considered in burnup chain. MIX represents the different mixtures in the study.

1.3.2 Depletion calculation in DRAGON Version4

A very important parameter in reactor calculations is the variation of number density of isotopes as a function of time. The elements that are mainly considered include the actinides, like ^{232}Th and its chain, or ^{238}U and its chain and fission products along with burnable absorbers if any. The depletion calculations are carried out using the flux calculated using Equation 1.43 for constant power. In general the set of equations that need to be solved as a function of burnup are as follows:

$$\frac{dN_k}{dt} + N_k(t)\,\Lambda_k(t) = S_k(t) \quad ; \; k = 1, K \tag{1.45}$$

with

$$\Lambda_k(t) = \lambda_k + \langle \sigma_{\mathrm{a},k}(t)\phi(t) \rangle \;, \tag{1.46}$$

$$S_k(t) = \sum_{l=1}^{L} Y_{kl}\, \langle \sigma_{\mathrm{f},l}(t)\phi(t) \rangle\, N_l(t) + \sum_{l=1}^{K} m_{kl}(t)\, N_l(t) \;, \tag{1.47}$$

$$\langle \sigma_{\mathrm{x},l}(t)\phi(t) \rangle = \int_0^\infty \sigma_{\mathrm{x},l}(u)\phi(t,u)du \tag{1.48}$$

and

$$\sigma_{\mathrm{x},k}(t,u)\phi(t,u) = \sigma_{\mathrm{x},k}(t_0,u)\phi(t_0,u) + \frac{\sigma_{\mathrm{x},k}(t_f,u)\phi(t_f,u) - \sigma_{\mathrm{x},k}(t_0,u)\phi(t_0,u)}{t_f - t_0}(t - t_0) \tag{1.49}$$

or

$$\sigma_{x,k}(t,u)\phi(t,u) = \sigma_{x,k}(t_0,u)\phi(t_0,u) \tag{1.50}$$

where

K = number of depleting isotopes

L = number of fissile isotopes producing fission products

$N_k(t)$ = time dependent number density for k^{th} isotope

λ_k = radioactive decay constant for k^{th} isotope in s^{-1}

$\sigma_{x,k}(t,u)$ = time and lethargy dependent microscopic cross section for nuclear reaction x on k^{th} isotope.
$x = a$, $x = f$ and $x = \gamma$ respectively stands for absorption, fission and radiative capture cross sections

$\phi(t,u)$ = time and lethargy dependent neutron flux

Y_{kl} = fission yield for production of fission product k by fissile isotope l

$m_{kl}(t)$ = radioactive decay constant or $\langle \sigma_{x,l}(t)\phi(t) \rangle$ term for production of isotope k by isotope l.

Equation 1.49 is used when one considers 'EXTR' option, which is a linear extrapolation of the microscopic reaction rates, using the information in the preceding time step while Equation 1.50 is used when one considers 'NOEX' option.

1.4 The Saturation models in Dragon

Depleting isotopes with $\Lambda_k(t_0)\,[t_f - t_0] \geq$ valexp and $\Lambda_k(t_f)\,[t_f - t_0] \geq$ valexp are considered to be at saturation, where valexp is a user input value, whose default value is 80.0 and to remove the saturation approximation, it is set to a very high value such as 1.0 x 10^5. They are described by making $\frac{dN_k}{dt} = 0$ in Eq. 1.45 to obtain

$$N_k(t) = \frac{S_k(t)}{\Lambda_k(t)} \quad ; \text{ if } k \text{ is at saturation.} \tag{1.51}$$

If the saturation option is to be considered, then beginning-of-stage and end-of-stage Dirac contributions are added to the previous equation (option 'DIRA' in DRAGON Version4):

$$N_k(t) = \frac{1}{\Lambda_k(t)} \left[a\delta(t - t_0) + S_k(t) + b\delta(t - t_f)\right] \quad ; \text{ if } k \text{ is at saturation} \tag{1.52}$$

where a and b are chosen in order to satisfy the time integral of Eq. 1.45:

$$N_k(t_f^+) - N_k(t_0^-) + \int_{t_0^-}^{t_f^+} N_k(t)\,\Lambda_k(t)\,dt = \int_{t_0^-}^{t_f^+} S_k(t)\,dt \tag{1.53}$$

It is numerically convenient to chose the following values of a and b:

$$a = N_k(t_0^-) - \frac{S_k(t_0^+)}{\Lambda_k(t_0^+)} \tag{1.54}$$

and

$$b = \frac{S_k(t_0^+)}{\Lambda_k(t_0^+)} - \frac{S_k(t_f^+)}{\Lambda_k(t_f^+)} \tag{1.55}$$

Very short period isotopes are taken at saturation and are solved apart from non-saturating isotopes. The lumped depletion matrix system containing the non-saturating isotopes is solved using either a fifth order Cash-Karp algorithm or a fourth order Kaps-Rentrop algorithm [Press 1994], taking care to perform all matrix operations in sparse matrix algebra. Matrices $[m_{kl}(t_0)]$ and $[m_{kl}(t_f)]$ are therefore represented in diagonal banded storage and kept apart from the yield matrix $[Y_{kl}]$. Every matrix multiplication or linear system solution is obtained via the LU algorithm.

CHAPTER 2

REFERENCE CODES

The codes that will be used for validating the advanced self shielding and burnup models, mentioned in the previous chapter, are MCNP5 [X-5 Monte Carlo Team 2003] and MONTEBURNS [Poston 1999], which links codes MCNP5 and ORIGEN [Croff 1980]. The code NJOY [MacFarlane 2000] will be used for generation of cross section libraries needed for validation. A brief description of each of the codes will be provided in this chapter.

2.1 NJOY99

The NJOY nuclear data processing system is a modular computer code used for converting evaluated nuclear data in the Evaluated Nuclear Data File (ENDF) format into libraries useful for nuclear reactor calculations. There are several laboratories around the world which provide evaluated nuclear data, of which the most important ones are National Nuclear Data Center, Brookhaven National Laboratory (for ENDF/B-VII) in the US; Nuclear Energy Agency data bank, (for JEF-2.2 and JEFF-3.1) in Europe; Nuclear data center, Japan Atomic Energy Agency (for JENDL-3.2) in Japan; and Obninsk data center (for BROND-2.2) in Russia. The evaluated data are processed and are made available in certain formats specific for codes like continuous-energy Monte Carlo code (MCNP), through deterministic transport codes (DANT [Alcouffe 1995], ANISN [Engle 1967], DORT [Rhoades 1988]), to reactor lattice codes (WIMS [Askew 1966]). The modular nature of NJOY makes it easier to add output for other kinds of application libraries or to add new computational features. This feature has been used for development of module DRAGR for generation of libraries compatible with code DRAGON.

NJOY has been used to generate the cross sections for selected elements relevant for the benchmarks analysed as part of this research. The evaluated nuclear data files for the elements have been chosen on the basis of recommendations by the WIMS Library Update Project (WLUP) [Leszczynski 2003] and JEF-2.2. The data libraries that were generated using NJOY, were written in DRAGLIB format, compatible with code DRAGON Version4, and in "A Compact ENDF" (ACE) format compatible with MCNP5. The modules of the NJOY code system that were invoked for library generation are MODER, RECONR, BROADR, UNRESR/PURR, THERMR, GROUPR, DRAGR and ACER. The flow chart to generate libraries using NJOY is depicted in Figure 2.1.

A gist of the main function of the modules are mentioned as follows:

MODER: A file format conversion utility, to convert ascii to binary and vice versa.

RECONR: Reconstructs pointwise (energy-dependent) cross sections from ENDF resonance parameters and interpolation schemes.

BROADR: Doppler broadens and thins pointwise cross sections corresponding to temperature of interest. The same temperature input list is also required by UNRESR, THERMR and GROUPR.

UNRESR: Computes effective self-shielded pointwise cross sections in the unresolved energy range.

PURR: Generates unresolved resonance probability tables and Bondarenko moments.

THERMR: Produces cross sections and energy-to-energy matrices for free or bound scatterers in the thermal energy range.

GROUPR: Generates self-shielded multigroup cross sections, group-to-group scattering matrices, photon-production matrices, and charged-particle cross sections from pointwise input. For resonant isotopes, the flux calculator is activated for homogeneous mixtures of the resonant isotope with hydrogen from 0.1 eV up to the upper limit of the resolved resonance range; the narrow resonance approximation is used above this energy.

DRAGR: Designed to produce nuclear data in the DRAGLIB format.

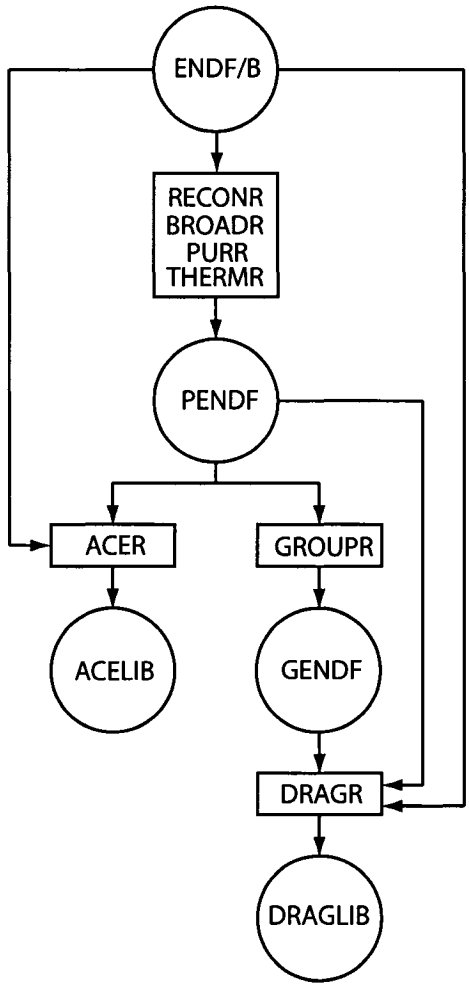

Figure 2.1 Flowchart for DRAGLIB/ACELIB Production

ACER: Prepares libraries in ACE format for the Los Alamos continuous-energy Monte Carlo code MCNP.

The evaluated datafiles, temperatures and dilution values used for generation of cross section libraries in DRAGLIB and ACE format are given in Appendix I. The group structure parameter in GROUPR is set to 22 (x-mas scheme) for 172 group libraries. Appendix II gives the energy values corresponding to the group boundaries. Figure 2.2 shows the weighting spectrum used in **GROUPR:** module for collapsing pointwise evaluated nuclear data files

into groupwise evaluated nuclear data files. The parameters used to generate the weighting spectrum were a thermal temperature of 0.0253 eV joined to 1/E at 0.1 eV, and a fission temperature of 1.40 MeV joined to 1/E at 820.3 keV.

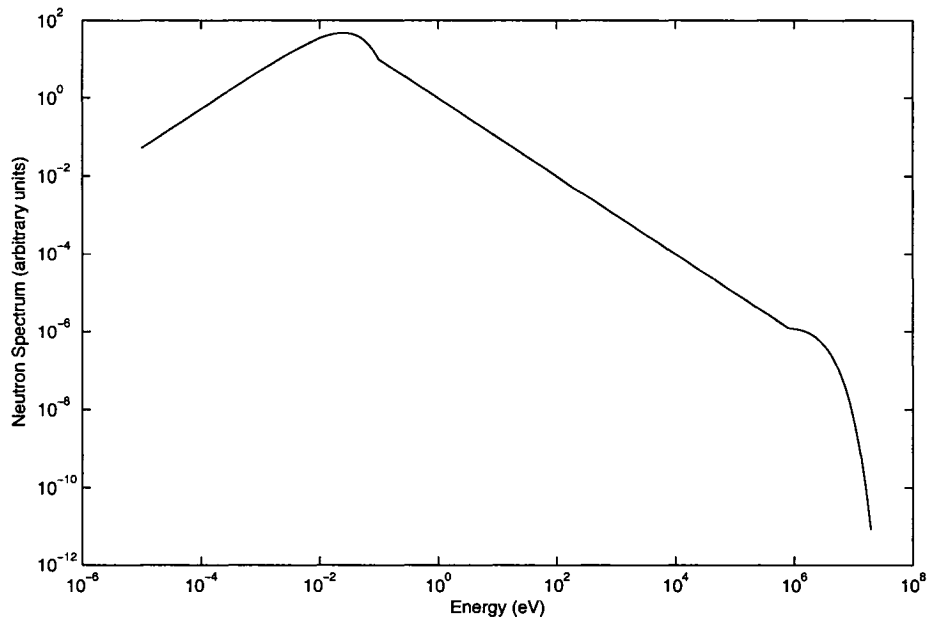

Figure 2.2 Spectrum used for collapsing cross sections into multigroup

Appendix III provides the Python script that was used to generate the cross section libraries in DRAGLIB and ACE formats. It also has a section which provides the examples for generation of libraries for certain specific elements representative of moderator, clad, fuel and reactor poison. An important addition in Appendix III is a scheme provided by IAEA for verification of the generated ACE files using the codes included in the PREPRO code system [Cullen 2002].

2.2 MCNP5

The results obtained using lattice code DRAGON needs to be compared with the results of code that has closest representation of the actual situation in terms of accurateness in geometry and data. This is made possible with codes like MCNP5 [X-5 Monte Carlo Team 2003]. MCNP is a well known and widely used Monte Carlo code for neutron, photon, and electron transport simulations. MCNP Version 5 is the outcome of an effort to modernize MCNP. MCNP5 has been tested against a suite of 42 regression tests, a suite of 26 criticality benchmark problems, a suite of 10 analytic benchmarks for criticality, and a suite of 19 radiation shielding validation problems. It was observed that in nearly all problems, the MCNP5 results exactly match those of MCNP4C2 and the few that differ agreed well within statistics [X-5 Monte Carlo Team 2003]. The conclusion was that MCNP5 is verified to be as reliable and accurate as previous versions and that all previously-existing capabilities have been preserved.

We have thus used MCNP5 to provide the benchmark results against which the results obtained using DRAGON will be validated.

2.3 ORIGEN2

The ORIGEN2.1 isotope generation and depletion code uses either the matrix exponential method or the Bateman equations to solve a set of coupled ordinary differential equations that describe the transmutation and decay of radionuclides [Croff 1980]. An isotope and photon decay library and a large number of one-group cross-section libraries are provided for different reactor systems. Use of the code requires specification of the initial material inventories, continuous material feed and removal rates when applicable, and the irradiation history (power or total flux and duration). The output at each time step includes detailed material

inventories for actinides, fission and activation products, and various other parameters.

In order to analyse burnup benchmarks, a coupled utility code of MCNP5 and ORIGEN2 would be used. The details will be mentioned in section on MONTEBURNS.

2.4 MONTEBURNS

MONTEBURNS is a fully automated tool that links MCNP with ORIGEN [Poston 1999]. The code consists of a Perl script, which manipulate the inputs and outputs of MCNP and ORIGEN in an automated burnup sequence. MCNP provides one-group microscopic cross-sections and fluxes halfway through each step to ORIGEN for depletion calculations, and ORIGEN is used to calculate isotopic inventories both halfway through and at the end of each step. MCNP calculates the effective one-group cross-sections for the system modeled, for user-specified isotopes and/or isotopes that contribute significantly to the absorption, fission, mass, or atom fraction of materials in the system. Because MCNP cross-section libraries do not exist for all isotopes tracked in ORIGEN, default cross-sections are used for the missing isotopes.

MONTEBURNS that links MCNP/MCNPX and ORIGEN has been used in analysis of assembly available as a part of the ARIANE project [Lebenhaft 2003]. It was concluded in the paper that the results obtained using MONTEBURNS compared well with the experimental results. An excessive depletion of ^{238}U and hence production of ^{239}Pu was observed and was attributed to statistical variations in the cross section calculations and spectrum effects. It was also concluded that it is the modern technique that can be used for accurate three dimensional depletion analyses of high burnup MOX fuel.

MONTEBURNS has thus been chosen for the analysis of burnup benchmarks.

2.4.1 Calculation methodology in MONTEBURNS

Power normalization in MONTEBURNS is done in the following way. The user has the option to provide the Q-value, i.e. amount of energy deposited per fission for a system. MONTEBURNS internally calculates the average energy deposited per fission of each material. The Q-value essentially includes all modes of energy deposition, including fission gammas, capture gammas, and neutron kinetic energy. The Q-value thus calculated is used to estimate the Q_{ave} considering the fission reaction rate. The Q_{ave}, obtained using Equations 2.1 to 2.4, is subsequently used to calculate the normalization factor for the flux. The normalization factor obtained using Equation 2.5 is multiplied to the flux calculated using MCNP and provided to ORIGEN for burning the mixture (see Equations 2.6 and 2.7). In this research, we have modified the code MONTEBURNS in order to perform power normalization using energies from mainly three reactions viz. (n, f), (n, γ) and $(n, 2n)$. The energies for these reactions are provided by an external file which was created using DRAGR module. The file also includes the decay energy and decay constant of all the actinides and fission products included in the analysis. In order to calculate the Q_{ave} for all reactions, we have added the product of reaction rate of each of the reactions with its corresponding energy (see Equation 2.8). The sum is subsequently used for power normalization (see Equations 2.9 to 2.10). We have also considered decay energy in the calculations. Eventhough its contribution is quite low when the reactor is in operation, it will be interesting to study the effect for cooling of fuel, which can be considered as future work.

In MONTEBURNS, the total amount of recoverable energy per fission (Q_{fis}) is calculated as

$$Q_{fis} = \mid Q_{U-235} \mid \times Q_{rat} \tag{2.1}$$

where

Q_{U-235} =recoverable energy per fission for ^{235}U

Q_{rat} =weighting factor to include recoverable fission energy for all actinides present

In order to obtain Q_{rat}, MONTEBURNS uses Equation 2.2, which is

$$Q_{rat} = \sum_{i=1}^{n} q_{rat}(i) \times f_{rat}(i) \tag{2.2}$$

where

n =number of isotopes being considered

$q_{rat}(i)$ =ratio of recoverable energy per fission for isotope i divided by the recoverable energy per fission for ^{235}U

$f_{rat}(i)$ =ratio of fissions resulting from isotope i to total number of fissions

where

$$f_{rat}(i) = \frac{\sigma_f(i) \times n(i)}{\sum_{i=1}^{n} \sigma_f(i) \times n(i)} \tag{2.3}$$

with

$\sigma_f(i)$ =one group microscopic fission cross section of isotope and

$n(i)$ =number density of isotope i in the system (in units of gram-atoms)

The average recoverable energy per fission of all materials, Q_{ave}, is calculated in MONTEBURNS as

$$Q_{ave} = \frac{\sum_{j=1}^{m}(Q_{fis}^{j} \times \phi_n^j \times \Sigma_f^j \times V^j)}{\sum_{j=1}^{m}(\phi_n^j \times \Sigma_f^j \times V^j)} \tag{2.4}$$

where

Q_{fis}^{j} =average energy per fission for material j (MeV)

ϕ_n^j =value of flux of material j obtained from MCNP output file

Σ_f^j =macroscopic fission cross section of material j (cm^{-1})

V^j =total volume of all cells containing material j (cm^3)

m =number of materials being analysed .

The constant for normalizing to the desired power is calculated in MONTEBURNS as,

$$C = \frac{\nu \times P \times 10^6 W/MW}{FAC \times K_{eff} \times Q_{ave}} \tag{2.5}$$

$$\phi = \phi_n \times C \tag{2.6}$$

where

ϕ =flux normalized to system power

$FAC = 1.602 \times 10^{-13}$ J/MeV

ν = average number of neutrons produced per fission, *i.e.*

$$\nu = K_{eff} \times src/floss \tag{2.7}$$

where

src =weight of source neutrons and

$floss$ =weight of neutrons lost to fission

P =power defined by user for each material (in MW) and

K_{eff} =effective multiplication factor obtained by MCNP .

2.4.1.1 Modification in MONTEBURNS

We have modified the code MONTEBURNS to include energies from other reactions like capture and $(n, 2n)$. The Q_{ave} in Equation 2.4 will now be calculated using Equation 2.8,

which is

$$Q_{ave} = \sum_{j=1}^{m}((Q^j_{drfis} \times \phi^j_n \times \Sigma^j_f + Q^j_{drcap} \times \phi^j_n \times \Sigma^j_{cap} + Q^j_{drn2n} * \phi^j_n \times \Sigma^j_{n,2n}) \times V^j) \quad (2.8)$$

where

Q^j_{drfis} =average energy per fission for material j (MeV) provided by DRAGLIB

Q^j_{drcap} =average energy per capture for material j (MeV) provided by DRAGLIB

Q^j_{drn2n} =average energy per $(n, 2n)$ reaction for material j (MeV) provided by DRAGLIB

Σ^j_{cap} =macroscopic capture cross section of material j (cm^{-1})

$\Sigma^j_{n,2n}$ =macroscopic $(n, 2n)$ cross section of material j (cm^{-1})

The constant for normalizing to the desired power in modified version of MONTE-BURNS is calculated as,

$$C = \frac{(P - totdecay) \times 10^6 W/MW}{(1.602 \times 10^{-13} J/MeV) \times Q_{ave}} \quad (2.9)$$

where

totdecay = power from decay, contributed by all the elements considered in the mixture during the time interval. It is calculated as

$$totdecay = FAC \times \sum_{j=1}^{m} (Q^{j}_{decay} \times \lambda^{j} \times N^{j} \times V^{j}) \tag{2.10}$$

The value of C determined using Equation 2.9 is used to obtain the normalized flux using Equation 2.6. In the modification, we have introduced the energy contribution due to decay, which is calculated using Equation 2.10. This modification will help in determining the heat released from an irradiated fuel after shutdown of the reactor.

CHAPTER 3

PERFORMANCE OF ADVANCED SELF SHIELDING MODELS IN DRAGON FOR THE ESTIMATION OF CANDU-6 SAFETY PARAMETERS

Nuclear reactors are being built all around the world for more than half a century. Whenever a reactor of new design is to be built, it is a mandatory requirement for designers to study the safety related scenarios as accurately as possible. Several safety improvements have been incorporated in the design of modern nuclear stations leading to safe and reliable operation of these plants. Several reactor types have been built and are in operation in different regions in the world. The most common designs are the light water reactors (LWRs), mainly built by United States and France and Canada Deuterium Uranium (CANDU) reactors, which was first introduced by Canada and subsequently followed up in countries like India, China, and South Korea. The CANDU reactor is based on the pressure tube concept as opposed to pressure vessel concept used for LWRs. Heavy water is used as coolant and moderator in a CANDU reactor while light water is used in LWRs. In this chapter we will be focusing on the CANDU-6 lattice. CANDU-6 is the 700 MWe CANDU class reactor. The fuel bundle of CANDU-6 has 37 fuel pins that are made of natural uranium. It differs from the direct use of spent pressurized water reactor fuel in CANDU reactors [Lee 1993](DUPIC) fuel, which is a 43 element cluster with 1% enriched uranium and 0.45% ^{239}Pu, with central pin having 4.3% natural dysprosium [Choi 1999].

There have been several reports and publications which have already presented the studies on safety related scenarios of CANDU-6 reactor in detail. In this chapter we are revisiting most of the safety related parameters (SRP) that include the fuel temperature coefficient (FTC), coolant void reactivity (CVR), pressure tube ingression (PTI), which is essentially the filling of air gap between pressure tube and calandria tube by heavy water coolant,

and calandria tube ingression (CTI), which is essentially the filling of air gap between pressure tube and calandria tube by heavy water moderator, for a typical CANDU-6 lattice. In an earlier work [Roh 2000], lattice benchmark calculations were performed for the standard CANDU and DUPIC CANDU fuel lattices and the results were compared with the MCNP-4B code. A full fledged burnup calculation was performed using the lattice cell codes, WIMS-AECL [Donnelly 1986] and HELIOS [Casal 1991], and at specific burnup points comparison was made with MCNP-4B code. MCNP libraries were generated from ENDF/B-VI release 3. Major physics parameters such as burnup reactivity, CVR, FTC etc., were compared. The calculations showed that the physics parameters estimated by the lattice codes were consistent with those obtained using MCNP. The authors noted a tendency for the error to increase slightly when the fuel burnup is high. They also concluded that the WIMS-AECL produces reliable results for CANDU fuel analysis. In another earlier work [Lone 2001], a comprehensive discussion on the physics aspects related to estimation of FTC has been presented. The author has compared FTC results obtained using the code suite WIMS-AECL and MCNP4B. It was concluded that WIMS-AECL over-predicts FTC in the range of about 0.2 pcm/K when compared to that obtained using MCNP4B. The present study is following the same lines as those of Ref. [Roh 2000], with the difference that we have considered two more hypothetical safety related parameters and have focused on the effects of advanced self shielding models, that have been incorporated in DRAGON Version4 [Marleau 2006], on the estimation of safety related parameters. Another important aspect is that we have not done continuous burnup calculations, but have chosen two specific burnup points, and a reduced number of nuclides in the fuel.

3.1 Description of Problem

The safety related parameters FTC, CVR, PTI and CTI were estimated in a geometry representing a CANDU-6 unit cell, as depicted in Figure 3.1. It is a 37-rod cluster of natural

uranium pins, with zircalloy as clad. The pressure tube is made of zirconium-niobium and the calandria tube is made of zircalloy. The coolant and moderator are heavy water. Table 3.1 gives the isotopic composition of materials and description of cell geometry. The outermost boundary corresponding to a square pitch of 28.575 cm, was annularized and isotropic boundary condition was applied. We have considered four layers per fuel pin. This choice is based on the recommendations made in Santamarina 2004, in order to improve prediction of the distributed self shielding effects. The fuel pin will thus be divided in such a way that they have 50%, 30%, 15% and 5% volume in each layer, as depicted in Figure 3.2. Figure 3.3 shows the typical spectrum in a fuel pin in the CANDU-6 lattice. It can be observed that the peak of the Maxwellian spectrum is about 0.04 eV. This is due to scattering by coolant which is at higher temperature of 573.6 K.

Two burnup points were chosen as part of the analyses. The first burnup point corresponds to fresh fuel and the second point corresponds to typical CANDU-6 discharge burnup of 7993 MWd/T. The two points chosen are seen in the Figure 3.4, which is the typical infinite multiplication factor (k_∞) curve of CANDU-6 as a function of burnup. The two burnup points will henceforth be referred to as 'B0' and 'B1' respectively.

In the present analysis, we have considered only nine elements as part of the fuel. They are ^{235}U,^{238}U, ^{239}Pu, ^{240}Pu, ^{241}Pu, ^{242}Pu, ^{135}Xe, ^{149}Sm along with ^{16}O. Eventhough a large number of fission products and actinides are produced as a function of burnup, we have considered only those elements, that in our view play an important role in reactivity transients. The choice of these elements is based on the capture rate ratio given in Equation 3.1. It is the ratio of capture rate in the selected elements to capture rate in all the elements, in the energy range '677.29 eV to 2.7679 eV', which corresponds to resolved resonance energy

group.

$$Capture\ rate\ ratio = \frac{\sum_{i}^{9} \sum_{g=2.7679eV}^{677.29eV} N_i \sigma_g^i \varphi_g}{\sum_{i}^{M} \sum_{g=2.7679eV}^{677.29eV} N_i \sigma_g^i \varphi_g} \tag{3.1}$$

where M corresponds to all the actinides and fission products and σ_g corresponds to the cross section for (n, γ) reaction. Figure 3.5 shows the capture rate ratio as a function of burnup. It can be seen that the ratio changes from 100%, when the fuel is fresh, to 90% at discharge burnup. So it is a good enough assumption to choose these nine elements in order to study the effect of self shielding models on estimation of capture rate in the resolved resonance energy group. The choice would also help in understanding more effectively the influence of the resonances of individual elements. A further exhaustive study including all fission products and actinides may be performed as part of future studies.

We will now briefly describe the procedure followed to estimate the safety parameters. The FTC is essentially the change in reactivity per degree kelvin introduced due to variation in fuel temperature alone. The k_∞ is estimated at two different temperatures of fuel (841.3 K and 1041.3 K) and the FTC is estimated using the Equation 3.2

$$FTC = [1/k_\infty(T_1) - 1/k_\infty(T_2)]/\Delta T \tag{3.2}$$

where T_1 and T_2 are temperatures corresponding to 841.3 K and 1041.3 K respectively. The CVR is the reactivity introduced into the system when the coolant is not available to remove the heat produced in the fuel. The k_∞ is estimated at two different coolant densities (0.8 g/cc and 0.08 g/cc) and the CVR is estimated using the Equation 3.3

$$SRP\ (CVR/PTIR/CTIR) = [1/k_\infty(S_1) - 1/k_\infty(S_2)] \tag{3.3}$$

where S_1 and S_2 corresponds to presence and absence of coolant respectively.

PTI happens when there is a pressure tube breach. The hot coolant (573.6°K) has been considered to fill the gap between PT and CT. In reality it may become steam with very low density. We have however considered the coolant to maintain the same density. 'PTIR' stands for the reactivity associated with pressure tube ingression and is estimated using the Equation 3.3, where S_1 and S_2 corresponds to absence and presence of coolant in air gap respectively.

CTI happens when there is a calandria tube breach. During calandria tube ingression transient, the warm moderator (323.6°K) will fill the air gap and come in contact with PT, which is at a higher temperature. The heavy water will instantly vaporize and subsequently will also affect the temperature of the coolant. But in our studies, we have hypothetically considered that the moderator and coolant states do not change and they maintain the same density. 'CTIR' stands for the reactivity associated with calandria tube ingression and is estimated using the Equation 3.3, where S_1 and S_2 corresponds to absence and presence of moderator in air gap respectively.

3.2 Nuclear Data

3.2.1 MCNP Library Generation

A total of 29 elements were considered in this problem. This includes two moderator elements, 18 structural elements and 9 elements in fuel including oxygen. Table 3.2 gives the list of elements and evaluated datafiles that were considered for generation of library in ACE format, and the temperatures at which the cross sections were generated. The thermal scattering law data were generated for the two moderator mixtures, light water and heavy water, at two desired temperatures. The code NJOY99.90 [MacFarlane 2000] was used for

the library generation. The cross sections were generated from the evaluated datasets that were chosen on the basis of recommendations from IAEA co-ordinated research project, the WIMS Library Update Project (WLUP) [Leszczynski 2003], after several benchmark analyses.

3.2.2 Library in DRAGLIB Format

A multigroup microscopic cross section library in DRAGLIB [Hébert 2004] format has been generated for the nuclides pertinent to the present problem using available PENDF and GENDF files and processing them with the DRAGR [Hébert 1992] module. The 172 group library structure is in the European XMAS format. The weighting spectrum that was chosen to collapse the cross sections to 172 group corresponds to analytic thermal + 1/E + fission spectrum. The cross-section processing with the DRAGR [Hébert 1992] module is similar to the approach used in module MATXSR [MacFarlane 1992]. Isotopic depletion data, including burnup chains and radioactive decay constants, are also recovered by DRAGR and made available in the DRAGLIB.

3.3 Calculational methodology using MCNP5

The reference calculations were performed with MCNP5. The concentration of the nuclides were chosen differently for each ring in CANDU-6 cluster, considering distributed self shielding across all the pins in the bundle. The different concentrations were obtained by performing a DRAGON calculation for CANDU-6 cluster as a function of burnup. The number densities were thus obtained, at the two chosen burnup points for fuel pin in each ring. We however considered the concentration of nuclides in the four layers of a fuel pin to be identical, eventhough it will be different as a function of burnup. The number densities of the two fuel mixtures are provided in Table 3.3. We generated temperature dependent cross

sections for all the elements in the fuel, i.e. at 841.3, 941.3 and 1041.3K. We considered a total of 5000 batches of neutrons and each batch had 2000 neutrons. Fifty neutron batches were rejected before calculation of effective multiplication factor of the system. Therefore, a total of about 10 million neutron histories were used to obtain the final results. We performed separate Monte Carlo runs for each temperature and burnup state. The FTC was calculated using MCNP5 using Equation 3.2. The deviation for the FTC was calculated using Equation 3.4 [Roh 2000].

$$Deviation\ (MCNP5) = 1/\Delta T\sqrt{[\delta_2^2/k_\infty^4(T_2) + \delta_1^2/k_\infty^4(T_1)]} \tag{3.4}$$

where δ_1 is the standard deviation for $k_\infty(T_1)$ obtained using MCNP5, while δ_2 is the standard deviation for $k_\infty(T_2)$. The other parameters, i.e. CVR, PTI, and CTI were calculated by MCNP5 using Equation 3.3, and the deviation for CVR, PTIR and CTIR, was calculated using Equation 3.5.

$$Deviation\ (MCNP5) = \sqrt{[\delta_2^2/k_\infty^4(S_1) + \delta_1^2/k_\infty^4(S_2)]} \tag{3.5}$$

In the subsequent discussions, we will be using the following notations to represent the various self shielding models. The generalized Stamm'ler model (GSM) without Livolant-Jeanpierre (LJ) normalization [Hébert 1991] will henceforth be referred to as 'GSM0-NOLJ-X' and that with LJ normalization will be referred to as 'GSM0-LJ-X', where 'X' represents one of the burnup states, i.e. 'B0' or 'B1' as described earlier. The generalized Stamm'ler model with Nordheim model (GSM1) and no LJ normalization will henceforth be referred to as 'GSM1-NOLJ-X' and that with LJ normalization will be referred to as 'GSM1-LJ-X'. The generalized Stamm'ler model with Nordheim model and Riemann Integration (GSM2) and no LJ normalization will henceforth be referred to as 'GSM2-NOLJ-X' and that with LJ normalization will be referred to as 'GSM2-LJ-X'. The statistical self shielding model and the Ribon extended self-shielding model will be henceforth referred to as 'SUBG-X' and 'RIB-X' respectively.

3.4 Computational scheme used for DRAGON analysis

A custom cross-section library in DRAGLIB format [Hébert 2004] (172 group) was used by the `LIB:` module. APOLLO type transport correction based on the linearly anisotropic scattering cross sections was used for the total and isotropic scattering cross sections. This correction assumes that the micro-reversibility principle is valid for all energy groups. The geometry was tracked using the `EXCELT:` module, using angular quadrature parameter of 11 and track density of 50 lines per cm for both self shielding and flux calculations. One-twelfth symmetry was considered. The fuel was divided into four layers (50%, 30%, 15% and 5% by volume) based on the recommendations made in the Reference [Santamarina 2004]. Six meshes were considered in the coolant and ten meshes were considered in the moderator. Single mesh was considered in all the other regions. Outermost surface was annularized and isotropic reflection was considered. We used the default options for the `ASM:` module to generate collision probabilities. In the `FLU:` module, we used the option of criticality calculations *without* leakage effects. The reaction rates were obtained using the `EDI:` module in four broad groups, with energy limits being - 'fast' - 20 MeV to 4.076220E+05 eV; 'unresolved resonance' - 4.076220E+05 eV to 677.287 eV; 'resolved resonance' - 677.287 eV to 2.7679 eV; and 'thermal' - less than 2.7679 eV.

3.4.1 Calculational methodology in DRAGON

The FTC has been calculated along the same lines as Equation 3.2, and other SRPs were calculated according to Equation 3.3. In order to explain certain phenomena, we propose to define the following parameters,

$$\Delta K = k_{\infty}(ref) - k_{\infty}(model) \ , \tag{3.6}$$

$$\Delta SRP = SRP(ref) - SRP(model) \ . \tag{3.7}$$

3.5 Numerical Results

Table 3.4 gives the comparison of k_∞ and FTC calculated using MCNP5 and all the self shielding models, for the two burnup points. We have quoted the combined collision/ absorption/ track-length estimated k_∞ with 68% confidence as reference. In Smith 2004, it is mentioned that the reference MCNP solution with 98% confidence intervals would be used to determine whether the deterministic calculations are "in agreement" with the Monte Carlo reference solution. It can be seen in Table 3.4 that the basic k_∞ predicted by all models is not within the 98% confidence interval, except for 'GSM2-LJ-X', for burnup state B0. It can be seen in Table 3.4 that GSM1 and GSM2 results are poorer than GSM0 for both burnup points when NOLJ option is used. But when LJ option is used, it was observed that the results not only improves for GSM1 and GSM2, but in fact it becomes better than GSM0. It was also observed that the results for GSM2 with LJ normalization becomes even better than SUBG. Eventhough the basic k_∞ seems to be predicted better by 'GSM2' compared to all the models, the FTC seems to be predicted better by 'SUBG'. The FTC estimated by all the models is within 98% confidence interval for both the fuel states. It can also be observed in Table 3.4 that the deviation obtained for FTC using MCNP5, for fuel state corresponding to 7993 MWd/T, is almost half of that of the FTC itself. This is because the FTC estimated at this burnup step is quite small and the standard deviation should be lower than 0.014% that has been obtained for the basic k_∞ using 10 million histories. This can be improved when one follows larger number of histories, so that the standard deviation is reduced even further, which will be taken up in future studies. It can also be observed that the FTC is generally predicted to be more negative or less positive by all the models with respect to MCNP5. In Lone 2001, it was observed that WIMS-AECL over-predicts FTC in comparison to Monte Carlo reference calculation.

Table 3.5 gives the comparison of k_∞ for the various perturbation properties required

for CVR, PTI and CTI calculation. It is observed that the k_∞ is generally under-predicted by DRAGON. It can be seen again like in the case of FTC, that for all the cases GSM0 is better that GSM1 and GSM2 when NOLJ option is used. As seen before, using LJ option, GSM1 and GSM2 results become better than that of GSM0. It is interesting to note that 'GSM2-LJ-X' results are better than SUBG with coolant present. But when there is complete voiding, SUBG and RIB seems to predict k_∞ better than the GSM models.

Table 3.6 gives the values of reactivity associated with moderator/coolant ingression and coolant voiding. It is a well known fact that the CVR is positive for the present CANDU-6 lattice and can also be seen in Table 3.6. However the magnitude of CVR changes as a function of burnup, maximum being at fresh fuel stage and decreasing at higher burnups. The trend and the value of CVR is predicted well by all the self shielding models. The CVR is predicted well by the subgroup models, but the GSM1 and GSM2 models with LJ option seem to highly under-predict. Interestingly, the GSM2 which predicted the basic k_∞ better than SUBG at cold state, seem to deviate when voiding of coolant takes place. It was noted that all the self shielding models seem to under-predict the reactivity associated with coolant voiding.

It was interesting to study the behavior of the PTI transient as a function of burnup. PTIR values estimated using all the models is provided in Table 3.6. It was observed that for fresh fuel, the PTIR is negative and it increases as a function of burnup. At high burnups, it was observed that PTIR in fact becomes positive. It will be an interesting study to actually consider the kinetics of the situation with appropriate thermal hydraulics feedbacks to assess the safety of the reactor during such a transient. The PTIR is predicted well by all the models when the fuel is fresh, but curiously deviates at high burnup. It was noted that all the self shielding models under-predict the reactivity associated with PTI transient when the fuel is fresh and overpredict at higher burnup.

The next safety parameter that was studied was that of the coolant tube ingression. CTIR values estimated using all the models is provided in Table 3.6. It was observed that the CTIR is negative throughout, as a function of burnup. However the values continuously decrease. The estimation of reactivity in CTI transient seems to be predicted well by all the models. Like for the other safety parameters, all the self shielding models seem to under-predict the reactivity values associated with calandria tube ingression.

We will now focus on the effect of self shielding models on capture rate in the resolved resonance energy group. Tables 3.7 and 3.8 give comparison of capture rate in the resolved resonance energy group for CVR at two burnup states B0 and B1 respectively. It can be observed that the capture rate is not predicted well by GSM0 model both with LJ and NOLJ options. It is an intrinsic deficiency in the model, which calculates a single value of dilution for the whole fuel pin and cannot represent distributed self shielding well. GSM1 and GSM2 can represent distributed self shielding better than GSM0 and is reflected in the reduction in deviation with respect to MCNP5. In comparison to the GSM models, lower deviations are observed when one uses RIB and SUBG. It can however be observed in Tables 3.7 and 3.8, that RIB and SUBG also shows a large deviation, especially in the outermost layers of the inner fuel pins. It is surprising to note that GSM1 and GSM2 models seem to predict it better in the inner pins. But when one compares the capture rates in the outermost layer of the outermost fuel pin, the GSM models seem to grossly under-predict with respect to MCNP5. Figure 3.6 gives the comparison of capture rate with respect to MCNP5. One can clearly see from Figure 3.6, the effect of distributed self shielding, due to consideration of four layers within the fuel pin. It was however noted that there is a large amount of deviation in reaction rates when one considers four layers per fuel pin, which is the recommendation made for LWR pins [Santamarina 2004]. It will be interesting to find out the effect of splitting the fuel pin into two, three layers, and also four layers with volumes different from those we used, to

estimate the distributed self shielding within a fuel pin when the coolant and moderator are heavy water.

We next performed a study to estimate the capture rates of individual elements in the resolved resonance energy group in the outermost layer of the outermost ring. It can be seen in Table 3.9 that in both B0 and B1 cases, the main contribution to reaction rate is from ^{238}U and deviation is also maximum for this element. The relative deviation essentially filters out effect of number density and focuses mainly on the resonance effects. Next highest deviation can be observed to be of that of ^{240}Pu eventhough its contribution to actual reaction rate is low. But when the Pu vector becomes stronger, like in degraded MOX fuel, its role will become significant.

With the above studies, we next focused on ^{238}U to understand the contribution that comes from individual groups in resolved energy region. There are a total of thirty six groups in the 172 group structure between 677.29 eV and 2.7679 eV. It can be seen in Table3.10 the contribution towards capture rate by individual groups and relative error of all the self shielding models with respect to MCNP5. It can be observed that in energy ranges, 136.7 eV - 91.66 eV (group 67), 67.9 eV - 55.6 eV (group 70), 37.3 eV - 33.7 eV (group 76), 22.6 eV - 19.4 eV (group 81) and 7.5 eV - 6.2 eV (group 89), the deviations are maximum. These are the groups that correspond to the major resonances of ^{238}U. Figure 3.7 shows the capture cross section of ^{238}U in continuous and 172 energy group structure. It can be observed that for all the major resonances the deviations in capture rate estimated by 'GSM' models is quite high (76.6%) and is negative. A maximum deviation of 16.7% using 'SUBG' can be observed for group 70. In case of 'SUBG' we have used the 'Statistical' model for energy groups less than 81 and 'Wide Resonance' model for groups above 81. One could try to find the effect of tuning this parameter for better estimation of reaction rates, which is the scope of future study. The results obtained using 'RIB' was close to that obtained using 'SUBG'.

However this model needs "autolib data". It is thus evident that among all the self shielding models, 'SUBG' predicts results close to that of MCNP5.

3.6 Conclusions

We have attempted to calculate the safety related parameters using advanced self shielding models incorporated in DRAGON Version4. We have compared the infinite multiplication factor, reactivity values for safety related parameters and capture rates in the resonance energy group between 677.29 eV and 2.7679 eV using DRAGON Version4 and Monte Carlo code MCNP5.

The basic k_∞ values for all the safety related parameters are under-predicted by all the self shielding models. The Generalized Stamm'ler model incorporated in the official version of DRAGON predicts k_∞ better than the Generalized Stamm'ler model with Nordheim model and Riemann integration model, when no Livolant-Jeanpierre normalization is considered. But the trend is reversed when one considers Livolant-Jeanpierre normalization. In fact Generalized Stamm'ler model with Nordheim model and Riemann integration model with Livolant-Jeanpierre normalization performs better than subgroup models for all cases except when there is coolant voiding. The self shielding model based on subgroup approach using physical probability tables and mathematical probability tables performed on par in prediction of basic k_∞ value.

It was observed that, in general for CANDU-6 analyses, all the self shielding models seem to under-predict safety related parameters. This needs to be kept in mind while using the code for design purposes. The trend in safety related parameters as a function of burnup is correctly predicted by all the models. The coolant void reactivity was grossly under-predicted when Livolant Jeanpierre normalization was used with Generalized Stamm'ler model with Nordheim model and Riemann integration model. It was observed that all the safety related

parameters were estimated well by the models based on subgroup approach.

In general, the capture rate in resolved resonance group is estimated better by subgroup models in comparison to models based on equivalence in dilution. It was however observed that in the case of coolant voiding the capture rates are poorly estimated by all the models. The fuel pin was split into four layers based on recommendations for LWR, where the flux is expected to change quite rapidly between pins. As a future course of work, it would be interesting to evaluate the optimum number of layers required for a fuel pin in CANDU context. Overall, of all the self shielding models, the resonance self shielding model based on subgroup approach using physical probability tables, seems to perform well for all the situations. One could alternately use self shielding model based on subgroup approach using mathematical probability tables, but this model needs "autolib data".

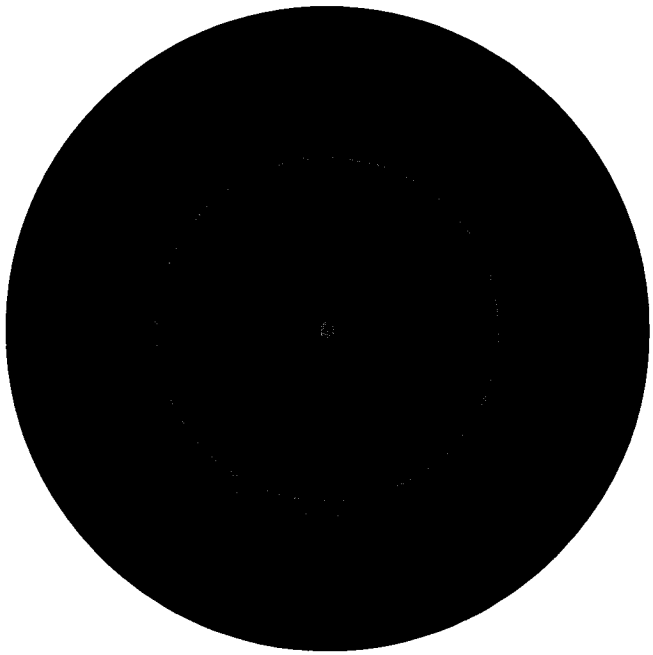

Figure 3.1 Cross section of 37 element fuel assembly

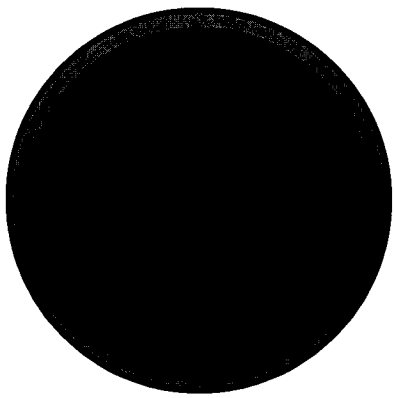

Figure 3.2 Single pin with 4 layers in fuel

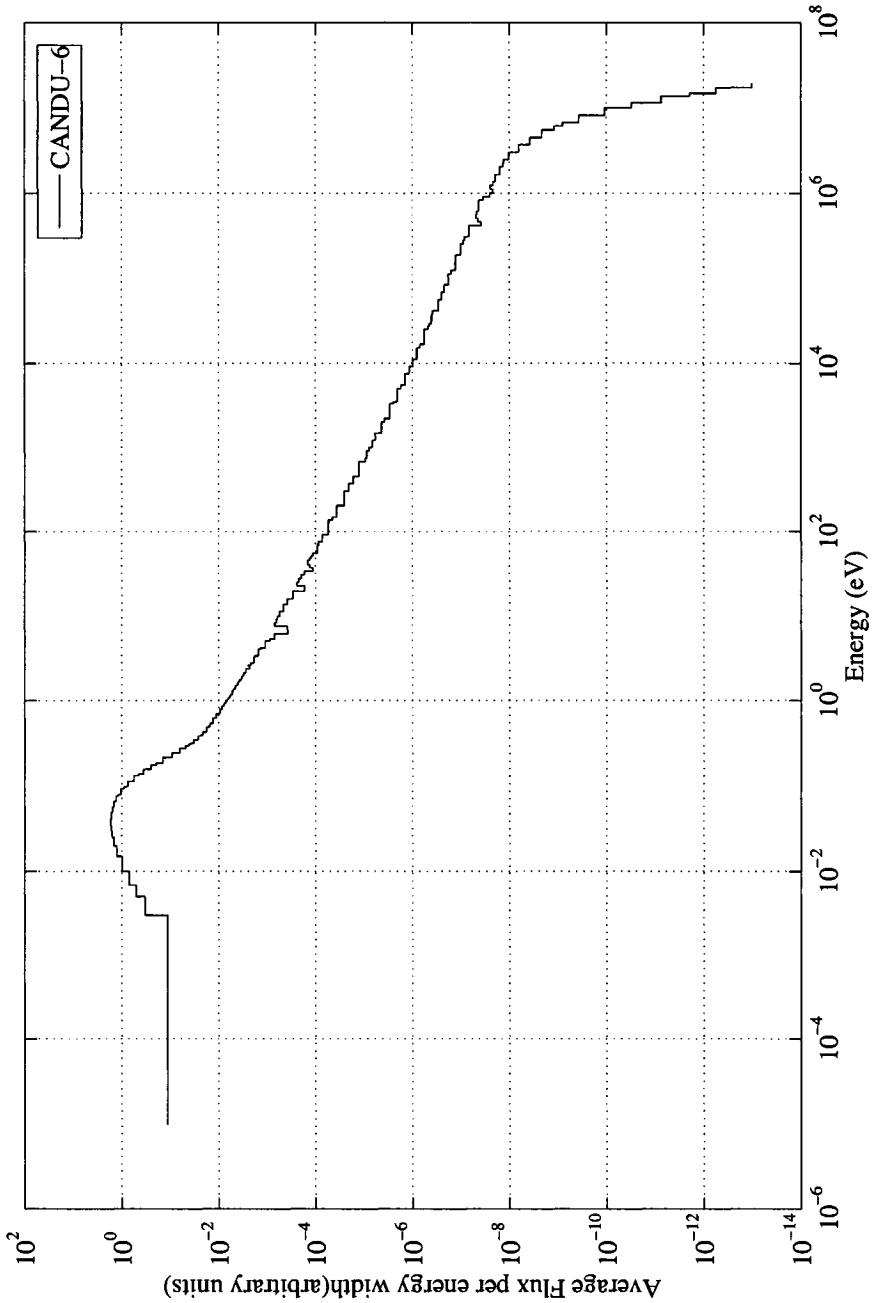

Figure 3.3 Typical spectrum in a CANDU-6 lattice

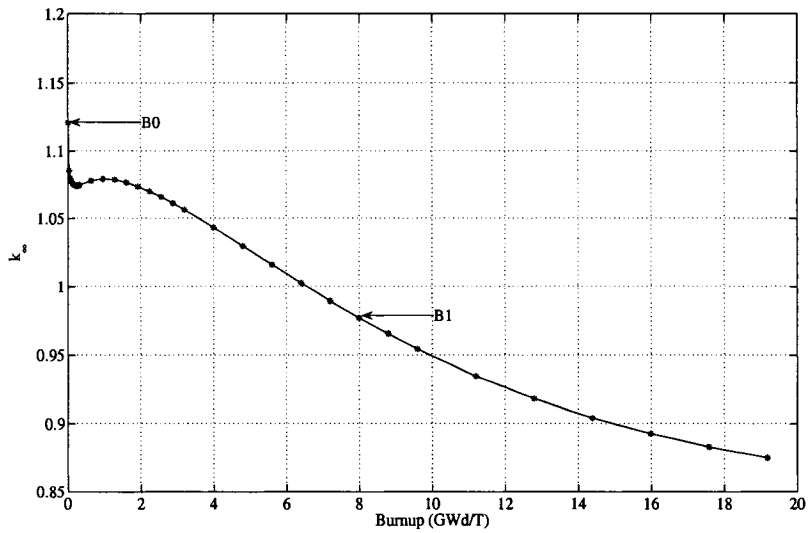

Figure 3.4 k_∞ curve for natural uranium CANDU fuel as a function of burnup

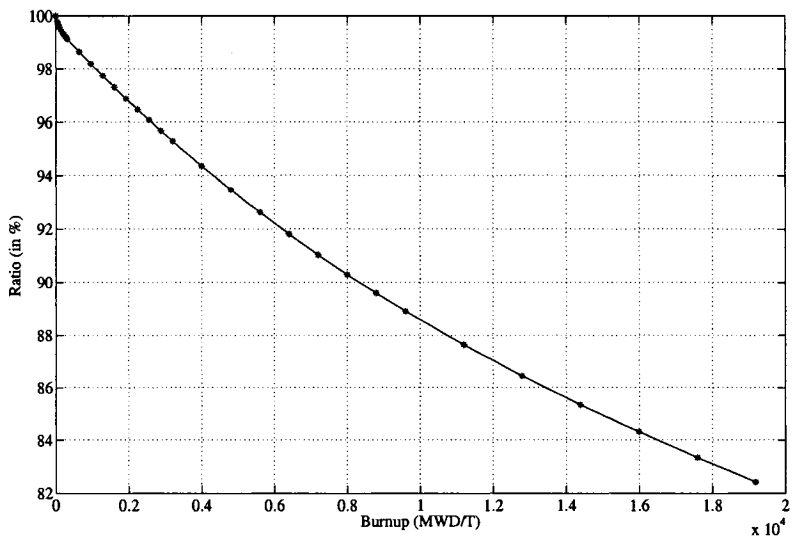

Figure 3.5 Ratio of capture rate in nine elements in fuel to all the elements as a function of burnup

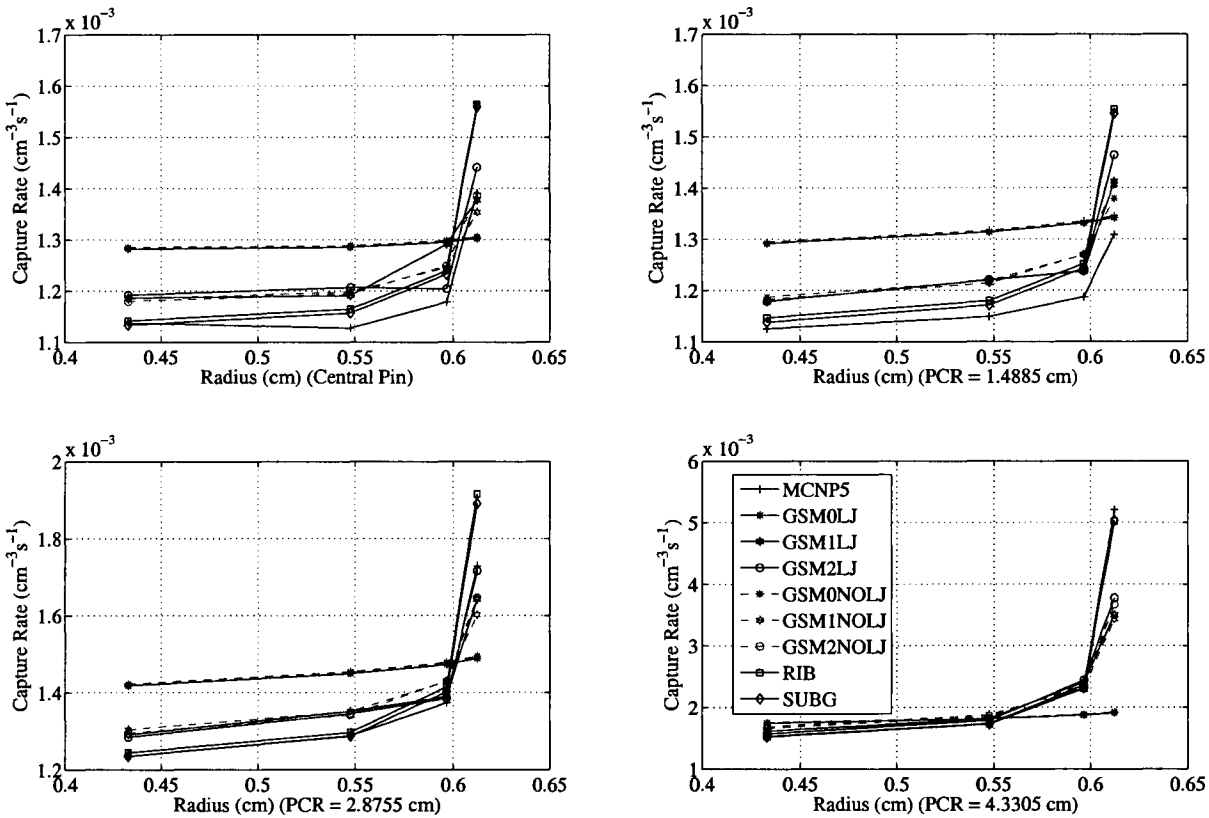

Figure 3.6 Comparison of capture rate for CVR at 'B0' in resolved resonance group for representative pins in CANDU-6 lattice

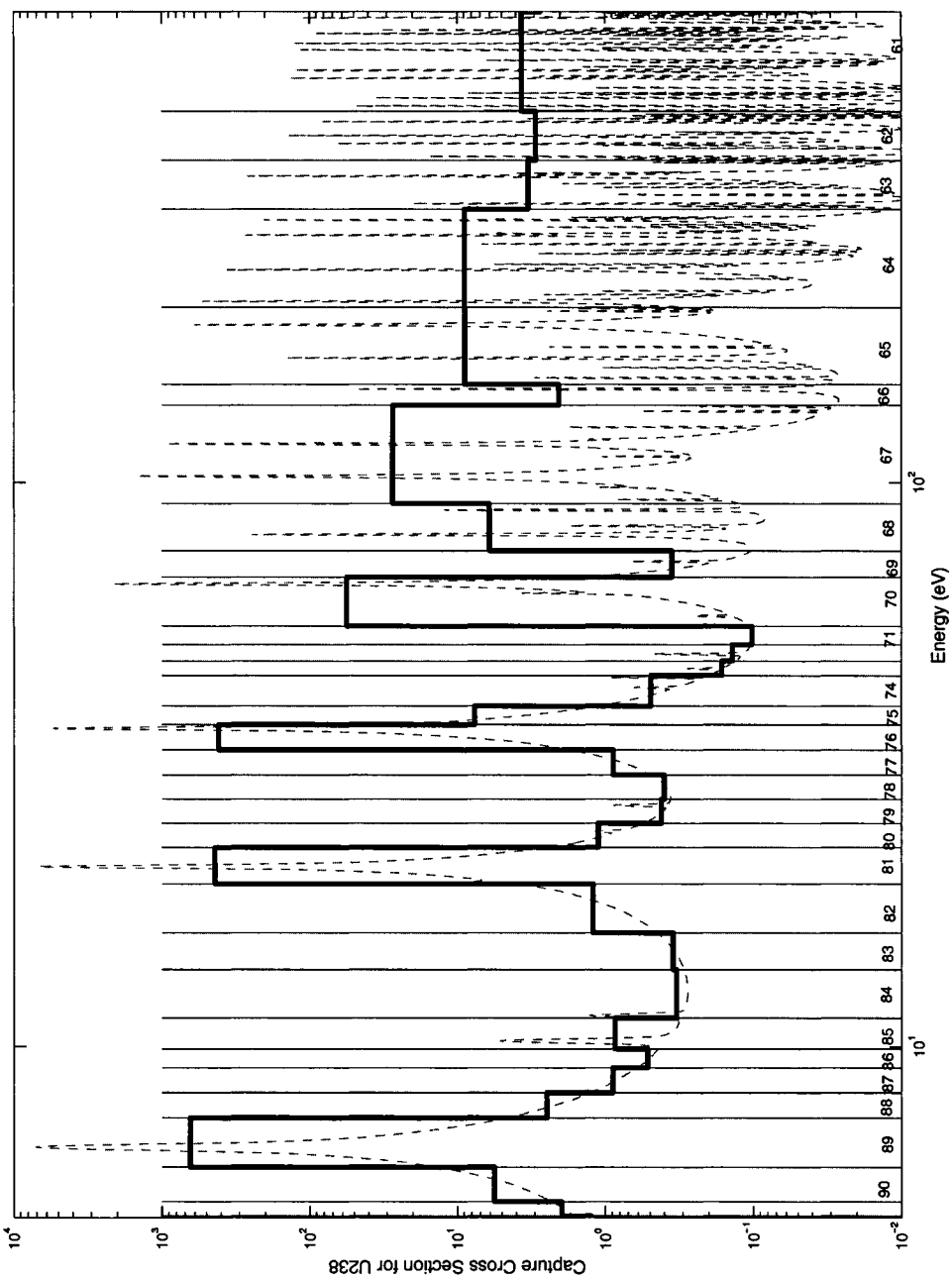

Figure 3.7 Capture cross section in resolved resonance group for ^{238}U

Table 3.1 CANDU benchmark specifications

Pitch (cm)	28.575 (square)
Number of rods	37 (1/6/12/18)
Radius of rod centers (cm)	0.0/1.4885/2.8755/4.3305
Fuel (OR)(cm)	0.6122
Clad (OR) (cm)	0.6540
IR/OR of pressure tube (cm)	5.1688/5.6032
IR/OR of calandria tube (cm)	6.4478/6.5874

Structure	Elements	Number density atoms per barn-cm
Clad (T=560.7 K) Calandria Tube (CT)(345.7 K)	Zr-nat	4.2373E-02
	^{10}B	2.2109E-07
	^{11}B	8.8992E-07
	^{54}Fe	6.5497E-06
	^{56}Fe	1.0182E-04
	^{57}Fe	2.3312E-06
	^{58}Fe	3.1083E-07
	^{50}Cr	3.5615E-06
	^{52}Cr	6.8681E-05
	^{53}Cr	7.7869E-06
	^{54}Cr	1.9385E-06
	^{58}Ni	2.7043E-05
	^{60}Ni	1.0339E-05
	^{61}Ni	4.4761E-07
	^{62}Ni	1.4221E-06
	^{64}Ni	3.6047E-07
Pressure Tube (PT) (T=560.7 K)	Zr-nat	4.2287E-02
	^{93}Nb	1.0641E-03
	^{10}B	1.5286E-07
	^{11}B	6.1526E-07
Coolant (T=573.6 K)	^{1}H	3.8016E-04
	^{2}D	4.8508E-02
	^{16}O	2.4444E-02
Coolant Voided state	^{1}H	3.8016E-06
	^{2}D	4.8508E-04
	^{16}O	2.4444E-04
Moderator (T=323.6 K)	^{1}H	5.7933E-05
	^{2}D	6.5084E-02
	^{16}O	3.2571E-02
Gap between PT and CT(T=353 K)	^{4}He	2.1064E-04

Table 3.2 Information on the elements used in the analysis

Nuclide	Source	Temperatures (in K)
^{1}H	JEF-2	323.6, 573.6
^{2}H	JEF-2	323.6, 573.6
^{4}He	JENDL-3.2	353.0
^{10}B	ENDF/B-VI R1	353.0,560.7
^{11}B	ENDF/B-VI R1	353.0,560.7
^{16}O	ENDF/B-VI R8	323.6, 573.6, 841.3,941.3,1041.3
^{50}Cr	ENDF/B-VI R8	345.7, 560.7
^{52}Cr	ENDF/B-VI R8	345.7, 560.7
^{53}Cr	ENDF/B-VI R8	345.7, 560.7
^{54}Cr	ENDF/B-VI R8	345.7, 560.7
^{54}Fe	ENDF/B-VI R8	345.7, 560.7
^{56}Fe	ENDF/B-VI R8	345.7, 560.7
^{57}Fe	ENDF/B-VI R8	345.7, 560.7
^{58}Fe	ENDF/B-VI R8	345.7, 560.7
^{58}Ni	ENDF/B-VI R8	345.7, 560.7
^{60}Ni	ENDF/B-VI R8	345.7, 560.7
^{61}Ni	ENDF/B-VI R8	345.7, 560.7
^{62}Ni	ENDF/B-VI R8	345.7, 560.7
^{64}Ni	ENDF/B-VI R8	345.7, 560.7
Zr-nat	JENDL-3.2	345.7, 560.7
^{93}Nb	ENDF/B-VI R6	560.7
^{135}Xe	JENDL-3.2	841.3,941.3,1041.3
^{149}Sm	ENDF/B-VI R0	841.3,941.3,1041.3
^{235}U	ENDF/B-VI R5	841.3,941.3,1041.3
^{238}U	CENDL-2 R1	841.3,941.3,1041.3
^{239}Pu	FOND-2.2	841.3,941.3,1041.3
^{240}Pu	FOND-2.2	841.3,941.3,1041.3
^{241}Pu	FOND-2.2	841.3,941.3,1041.3
^{242}Pu	FOND-2.2	841.3,941.3,1041.3

Table 3.3 Concentration of nuclides (in atoms per barn-cm) in each ring in fuel assembly of CANDU-6

Fuel Burnup (MWD/T)	Element	Ring-1	Ring-2	Ring-3	Ring-4
Fresh Fuel	^{16}O	4.6530E-02	4.6530E-02	4.6530E-02	4.6530E-02
	^{235}U	1.6770E-04	1.6770E-04	1.6770E-04	1.6770E-04
	^{238}U	2.3110E-02	2.3110E-02	2.3110E-02	2.3110E-02
7993 MWD/T	^{16}O	4.6530E-02	4.6530E-02	4.6530E-02	4.6530E-02
	^{235}U	6.8573E-05	6.5023E-05	5.5666E-05	4.0274E-05
	^{238}U	2.2948E-02	2.2943E-02	2.2927E-02	2.2893E-02
	^{239}Pu	5.5693E-05	5.5953E-05	5.7003E-05	5.8992E-05
	^{240}Pu	1.9359E-05	2.0321E-05	2.3007E-05	2.7743E-05
	^{241}Pu	3.7112E-06	3.9167E-06	4.6547E-06	6.3369E-06
	^{242}Pu	7.3871E-07	8.2943E-07	1.1558E-06	2.0701E-06
	^{135}Xe	2.1687E-09	2.1317E-09	2.0493E-09	1.9307E-09
	^{149}Sm	1.4396E-08	1.4215E-08	1.3880E-08	1.3601E-08

Table 3.4 FTC estimation for CANDU-6 using various self shielding models

Model	$k_\infty(T_1)$	$k_\infty(T_2)$	FTC (pcm/K)
M-1	1.12306± 0.00013	1.12030± 0.00013	-1.0968± 0.0731*
M-2	1.03105± 0.00014	1.03145± 0.00014	0.1881± 0.0931
A-1	279 +	309	-0.1273 !
A-2	313	331	-0.0854
B-1	318	349	-0.1289
B-2	349	371	-0.1020
C-1	289	329	-0.1655
C-2	329	349	-0.0948
D-1	204	234	-0.1220
D-2	244	261	-0.0809
E-1	56	89	-0.1315
E-2	113	133	-0.0971
F-1	26	49	-0.0946
F-2	90	102	-0.0566
G-1	108	126	-0.0748
G-2	159	166	-0.0325
H-1	91	101	-0.0405
H-2	144	143	0.0047

* - Standard deviation
+ - ΔK (in pcm) = k_∞(MCNP5) - k_∞(model)
! - ΔFTC(in pcm/K) = FTC(model) - FTC(MCNP5)

M - MCNP5; A - GSM0-NOLJ; B - GSM1-NOLJ; C - GSM2-NOLJ; D - GSM0-LJ; E - GSM1-LJ; F - GSM2-LJ; G - RIB; H - SUBG

'-1' - for fresh fuel; '-2' - for fuel at discharge burnup

Table 3.5 Comparison of k_∞ for various safety related parameters of CANDU-6

Model	k_∞ (Ref)	k_∞(CTI)	k_∞(PTI)	k_∞(CVR)
M-1	1.12149± 0.00013	1.12031± 0.00012	1.11882± 0.00012	1.14312± 0.00012
M-2	1.03111 ±0.00014	1.03078 ±0.00014	1.03417 ±0.00014	1.04568 ±0.00014
A-1	279 +	235	265	312
A-2	313	284	197	337
B-1	317	270	301	376
B-2	351	319	233	394
C-1	292	252	276	358
C-2	330	299	213	378
D-1	204	162	191	257
D-2	244	216	129	286
E-1	57	17	47	211
E-2	114	89	0	246
F-1	24	-16	14	174
F-2	88	64	-25	209
G-1	101	55	84	147
G-2	153	114	25	186
H-1	81	44	73	110
H-2	135	113	24	152

+ - ΔK (in pcm)= k_∞(MCNP5) - k_∞(model)

M - MCNP5; A - GSM0-NOLJ; B - GSM1-NOLJ; C - GSM2-NOLJ; D - GSM0-LJ; E - GSM1-LJ; F - GSM2-LJ; G - RIB; H - SUBG

'-1' - for fresh fuel; '-2' - for fuel at discharge burnup

Table 3.6 Comparison of CTIR, PTIR and CVR of CANDU-6 using various self shielding models

Model	CTIR (pcm)	PTIR(pcm)	CVR(pcm)
M-1	-94±14*	-213±14	1687±14
M-2	-31±19	287±19	1351±18
A-1	35 !	11	-17
A-2	27	111	-13
B-1	37	12	-36
B-2	30	113	-30
C-1	31	12	-42
C-2	29	112	-36
D-1	34	9	-35
D-2	26	109	-32
E-1	32	8	-116
E-2	24	107	-118
F-1	32	8	-114
F-2	23	106	-109
G-1	37	14	-32
G-2	36	120	-26
H-1	29	6	-20
H-2	20	105	-13

* - Standard deviation

! - ΔSRP(in pcm) = SRP(model) - SRP(MCNP5)

M - MCNP5; A - GSM0-NOLJ; B - GSM1-NOLJ; C - GSM2-NOLJ;
D - GSM0-LJ; E - GSM1-LJ; F - GSM2-LJ; G - RIB; H - SUBG

'-1' - for fresh fuel; '-2' - for fuel at discharge burnup

Table 3.7 Comparison of capture rate ($cm^{-3}s^{-1}$) in resolved resonance group for CVR at B0

Fuel Pin	Radius (cm)	Capture rate(B0) (MCNP5)	Relative error with respect to MCNP5 (in %)							
			A	B	C	D	E	F	G	H
1 (Central pin)	0.4329	1.1376E-03±0.0072*	13.0	4.1	3.7	12.7	4.3	4.8	0.4	-0.4
	0.5476	1.1272E-03±0.0073	14.3	6.3	6.0	14.0	5.6	7.1	3.3	2.6
	0.5967	1.1783E-03±0.0091	10.2	5.7	6.0	9.9	9.6	2.2	5.2	4.6
	0.6122	1.3912E-03±0.0167	-6.2	-2.7	-0.3	-6.4	-1.0	3.6	12.5	12.1
2 (PCR at 1.4885 cm)	0.4329	1.1252E-03±0.0070	15.1	5.5	5.1	14.8	4.8	4.8	1.9	1.1
	0.5476	1.1490E-03±0.0075	14.6	6.1	5.7	14.4	6.2	6.3	2.7	2.0
	0.5967	1.1873E-03±0.0088	12.4	6.9	7.0	12.2	4.2	4.3	5.5	4.7
	0.6122	1.3089E-03±0.0132	2.8	5.3	7.5	2.5	7.9	11.9	18.7	18.0
3 (PCR at 2.8755 cm)	0.4329	1.2351E-03±0.0070	15.2	5.6	4.9	14.8	4.5	4.0	0.7	0.0
	0.5476	1.2882E-03±0.0075	12.9	4.9	4.2	12.5	4.9	4.4	0.7	-0.1
	0.5967	1.3734E-03±0.0090	7.6	4.0	4.1	7.3	1.2	0.9	3.0	2.1
	0.6122	1.7287E-03±0.0152	-13.6	-7.3	-4.8	-13.9	-5.0	-0.7	10.8	9.4
4 (PCR at 4.3305 cm)	0.4329	1.5317E-03±0.0068	14.6	10.1	8.5	14.0	5.6	2.7	-0.2	-0.7
	0.5476	1.7369E-03±0.0069	5.3	8.3	6.8	4.7	4.7	3.1	-0.4	-0.4
	0.5967	2.3620E-03±0.0094	-20.1	-1.4	0.1	-20.6	2.0	3.4	-2.4	-1.9
	0.6122	5.2099E-03±0.0135	-63.1	-34.1	-29.5	-63.3	-32.7	-27.5	-3.6	-3.4

* - Relative error

A - GSM0-NOLJ B - GSM1-NOLJ C - GSM2-NOLJ D - GSM0-LJ

E - GSM1-LJ F - GSM2-LJ G - RIB H - SUBG

Table 3.8 Comparison of capture rate ($cm^{-3}s^{-1}$) in resolved resonance group for CVR at B1

Fuel Pin	Radius (cm)	Capture rate(B0) (MCNP5)	Relative error with respect to MCNP5 (in %)							
			A	B	C	D	E	F	G	H
1 (Central pin)	0.4329	1.1257E-03±0.0071*	15.3	6.3	5.8	15.0	6.5	6.9	2.4	1.7
	0.5476	1.1374E-03±0.0075	14.4	6.4	6.1	14.1	5.6	7.1	3.4	2.7
	0.5967	1.2041E-03±0.0094	8.9	4.4	4.8	8.6	8.3	0.9	3.9	3.4
	0.6122	1.4096E-03±0.0148	-6.5	-3.1	-0.6	-6.7	-1.2	3.8	11.9	11.6
2 (PCR at 1.4885 cm)	0.4329	1.1369E-03±0.0071	15.0	5.4	5.0	14.7	4.6	4.6	1.8	1.0
	0.5476	1.1614E-03±0.0074	14.4	5.9	5.5	14.2	6.0	6.0	2.5	1.8
	0.5967	1.1916E-03±0.0085	13.0	7.5	7.6	12.8	4.6	4.7	6.0	5.3
	0.6122	1.3800E-03±0.0157	-1.6	0.8	2.9	-1.9	3.3	7.6	13.4	12.8
3 (PCR at 2.8755 cm)	0.4329	1.2143E-03±0.0068	17.9	8.1	7.3	17.6	7.0	6.4	3.1	2.3
	0.5476	1.2754E-03±0.0072	14.7	6.6	5.9	14.4	6.6	6.0	2.3	1.5
	0.5967	1.3501E-03±0.0090	10.1	6.5	6.5	9.8	3.4	3.1	5.4	4.5
	0.6122	1.7000E-03±0.0154	-11.6	-5.2	-2.5	-11.9	-2.9	2.0	13.2	11.8
4 (PCR at 4.3305 cm)	0.4329	1.5179E-03±0.0067	15.8	11.3	9.5	15.1	6.6	3.5	0.8	0.3
	0.5476	1.7307E-03±0.0071	5.7	8.8	7.3	5.0	5.4	3.2	0.1	0.1
	0.5967	2.3577E-03±0.0092	-20.0	-1.1	0.5	-20.6	2.5	4.1	-2.2	-1.6
	0.6122	5.3863E-03±0.0133	-64.3	-36.5	-31.8	-64.6	-35.2	-29.3	-6.8	-6.6

∗ - Relative error

A - GSM0-NOLJ B - GSM1-NOLJ C - GSM2-NOLJ D - GSM0-LJ

E - GSM1-LJ F - GSM2-LJ G - RIB H - SUBG

Table 3.9 Elementwise contribution to capture rate ($cm^{-3}s^{-1}$) for CVR estimation of CANDU-6

Element	Capture rate (B0) (MCNP5)	Relative error with respect to MCNP5 (in %)							
		A	B	C	D	E	F	G	H
^{16}O	8.9834E-09±0.0029*	-1.4	-1.9	-1.9	-1.2	-1.3	-1.3	-1.2	-1.1
^{235}U	1.0275E-04±0.0047	-0.3	0.6	-1.1	-0.2	1.3	-0.7	0.2	0.4
^{238}U	5.1072E-03±0.0138	-64.3	-34.8	-30.0	-64.6	-33.4	-28.0	-3.6	-3.4
Element	Capture rate (B1)	D	E	F	A	B	C	G	H
^{16}O	8.9991E-09±0.0029	-1.0	-1.5	-1.5	-0.8	-1.0	-0.9	-0.8	-0.7
^{235}U	2.5214E-05±0.0047	0.4	0.0	-0.4	0.5	0.6	0.4	0.4	0.6
^{238}U	5.2830E-03±0.0136	-65.6	-37.2	-32.5	-65.9	-35.9	-29.9	-7.0	-6.7
^{239}Pu	5.1452E-05±0.0064	-1.9	-0.2	-1.7	-1.9	0.2	-1.4	-1.1	-1.0
^{240}Pu	1.9130E-05±0.0131	7.9	9.4	7.9	8.1	10.3	8.6	8.3	8.4
^{241}Pu	6.1915E-06±0.0068	-0.8	-1.0	-1.1	-0.6	-0.4	-0.5	-0.5	-0.3
^{242}Pu	1.2908E-06±0.0133	-1.8	-1.9	-1.8	-1.7	-1.6	-1.5	-1.5	-1.6
^{135}Xe	9.9561E-10±0.0061	-1.1	-1.4	-1.5	-1.0	-1.0	-0.9	-0.9	-0.8
^{149}Sm	7.6763E-08±0.0068	-1.2	-1.6	-1.6	-1.1	-1.2	-1.1	-1.0	-0.9

$*$ - Relative error
A - GSM0-NOLJ; B - GSM1-NOLJ; C - GSM2-NOLJ; D - GSM0-LJ;
E - GSM1-LJ; F - GSM2-LJ; G - RIB; H - SUBG

Table 3.10 Groupwise breakdown of capture rate ($cm^{-3}s^{-1}$) for ^{238}U for CVR case at B1 for outermost layer of outermost pin

Energy Limits (eV)	Capture rate(B1) (MCNP5)	Relative error with respect to MCNP5 (in %)							
		A	B	C	D	E	F	G	H
1.3674E+02 - 9.1661E+01	3.5172E-04 $\pm$ 0.0332*	-63.6	-21.6	-8.5	-63.8	-21.4	-8.1	-5.8	-8.3
6.7904E+01 - 5.5595E+01	3.4707E-04 $\pm$ 0.0445	-73.4	-34.0	-20.0	-73.7	-33.5	-19.5	-14.8	-16.7
3.7267E+01 - 3.3720E+01	7.2074E-04 $\pm$ 0.0366	-76.0	-49.5	-40.7	-76.3	-48.4	-37.9	-13.4	-10.3
2.2603E+01 - 1.9455E+01	1.0358E-03 $\pm$ 0.0348	-75.3	-48.7	-40.5	-75.6	-47.3	-37.7	-4.8	-4.5
7.5240E+00 - 6.1601E+00	1.8844E-03 $\pm$ 0.0276	-76.4	-54.1	-48.9	-76.6	-52.1	-44.7	-8.2	-7.6

* - Relative error

A - GSM0-NOLJ; B - GSM1-NOLJ; C - GSM2-NOLJ; D - GSM0-LJ;
E - GSM1-LJ; F - GSM2-LJ; G - RIB; H - SUBG

CHAPTER 4

ESTIMATION OF COOLANT VOID REACTIVITY FOR CANDU-NG LATTICE USING DRAGON AND VALIDATION USING MCNP5

The CANDU New Generation (CANDU-NG) lattice was proposed at an early stage of the Advanced CANDU Reactor (ACR) development and is now used for academic bench-marking [Chan 2001]. It does not comprise the detailed engineering features of the ACR that guarantee a negative CVR under all conditions. The CANDU-NG fuel bundle is a 43 element CANFLEX design which is one of the several proposals considered for the futuristic reactor to be built by Canada. The CANDU-NG lattice has some salient design features like central dysprosium pin, light water as coolant, square lattice pitch of 22 cm and a large calandria tube diameter, in order to reduce the heavy water moderator inventory. There was also a requirement that the design caters to higher burnup in comparison to the present CANDU-6 fuel, and hence there was a consideration for enriched uranium fuel. Several studies have been performed earlier to estimate the CVR for the evolving ACR design [Cotton 2005].

The central pin of the 43 rod cluster has dysprosium (4.6 %) in natural uranium. The central pin and seven pins in ring 1 are thicker (inner/outer diameter-0.627/0.675 cm) compared to fourteen pins in ring 2 and twenty-one pins in ring 3 (inner/outer diameter-0.533/0.575 cm). The fuel density of the inner eight pins is higher (10.12 g/cc) in comparison to the outer 35 pins (9.825 g/cc). The pressure tube dimension is the same as that of CANDU-6. An important geometrical change for ACR type lattice is the increase in the calandria tube inner/outer diameter (7.5/7.8 cm) in comparison to CANDU-6 (6.45/6.59 cm). As a result the air gap is much larger and the moderator volume is further reduced. The coolant is light water and the moderator is heavy water, and we have considered the air gap to be filled with

helium gas. Table 4.1 gives the geometric and material specifications of CANDU-NG lattice analysed. Figure 4.1 gives the cross section of a 43 element fuel assembly and a single pin with 4 layers (50%, 30%, 15% and 5% volume) considered in each fuel pin, which is based on the recommendations in Santamarina 2004. The subdivision is made in order to effectively predict the distributed self-shielding effects within a fuel pin.

4.1 Scope of study

In the present work, we will be focusing mainly on the performance of advanced self-shielding models based on "equivalence in dilution" or "subgroup approach" on estimation of CVR for CANDU-NG lattice in the presence of strong neutron absorber like dysprosium. Under equivalence in dilution models, we used the Generalised Stamm'ler model [Hébert 1991] with or without Riemann integration and Nordheim model [Hébert 2004a]. Among the subgroup approaches, we have used the Ribon extended and the statistical self-shielding models, which are both compatible with a characteristics solution of the subgroup equations [Hébert 2005].

Two sets of studies have been carried out as part of the present work. In the first set, CVR will be estimated for a single CANDU-NG unit cell using DRAGON. This study will include two varieties, where we will be considering, natural uranium/dysprosium in natural uranium, in the central pin. It will help in understanding the effect of dysprosium during coolant voiding, and performance of self-shielding models in the presence of strong neutron absorbers. In this study we also demonstrate the capability of DRAGON Version4 for estimation of CVR for an assembly in 2×2 pattern, which includes complete voiding and checkerboard voiding. Checkerboard voiding calculation is performed by considering void

in the diagonal cells and coolant in the other two cells.

In an earlier study [Cotton 2005] it has been mentioned that the CVR estimated for a checkerboard lattice for ACR is higher than that obtained for complete voiding. In a recent study, checkerboard voiding estimation has been carried out using DRAGON 3.04 [Marleau 2000] for a CANDU-6 and ACR type lattice, but with modifications to the basic lattice, where square pins were considered instead of annular pins [Talebi 2006].

In the present study the results obtained using DRAGON has been validated against that obtained using Monte Carlo code MCNP5. ACE libraries needed for analyses using MCNP5 [X-5 Monte Carlo Team 2003] were generated using NJOY99.90. A total of 10 million neutron histories were tracked using MCNP5. This validation process will help in identifying the appropriate self-shielding model that can be recommended for analysis of CANDU-NG type lattices using DRAGON. Apart from comparing the CVR values, we have also compared the capture rate in the resolved resonance energy group '677.29 eV to 2.7679 eV'.

4.2 Computational scheme used for DRAGON analysis

A custom cross-section library in DRAGLIB format [Hébert 2004] (172 group) was used by the `LIB:` module. The evaluated files for the elements chosen in the library were from JEF-2.2 evaluation. APOLLO type transport correction based on the linearly anisotropic scattering cross sections was used for the total and isotropic scattering cross sections. This correction assumes that the micro-reversibility principle is valid for all energy groups. The geometry was tracked using the `NXT:` [Marleau 2005] module, using angular quadrature pa-

rameter of 12 in [0,π/2] and track density of 50 lines per cm for both self shielding and flux calculations. The fuel was divided into four layers (50%, 30%, 15% and 5% by volume) based on the recommendations made in the Reference [Santamarina 2004]. The fuel pins were split into two in an inward/outward fashion. This splitting was done not only in terms of regions for the flux calculations but also in terms of correlated resonant mixtures for the space-dependent self-shielding treatment. This refinement of the self-shielding treatment has a noticeable effect (40 pcm) on the k_{∞} when the cell is voided. It also improved the resonant capture in the outer ring of fuel (about 2%) and has an overall effect of about 25 pcm on the CVR. This splitting in terms of regions for the flux calculation has also a noticeable effect on the thermal fission rate (about 1.5%). Thirty six meshes were considered in the light water coolant. Five annular meshes were considered in the moderator and seven cartesian meshes were chosen near the boundary. The mesh-splitting of Figure 4.1 produces 389 regions and 60 outer surfaces, each of them corresponding to an unknown of the main flux calculation. No mesh-splitting of the moderator was done for the self-shielding calculation, leading to 44 regions and 4 outer surfaces. The method of characteristics module (`MCCGT:`) [Le Tellier 2006] was used for the multigroup flux integration. For the 2 $\times$ 2 assembly calculation, isotropic translation boundary condition has been applied on the external surfaces of the lattice. Note that there is no approximation on the internal surfaces that couple the cells. The cross section of a 2 $\times$ 2 CANDU-NG assembly is shown in Figure 4.2. The reaction rates were obtained using the `EDI:` module in four broad groups, with energy limits being - 'fast' - 20 MeV to 4.076220E+05 eV; 'unresolved resonance' - 4.076220E+05 eV to 677.287 eV; 'resolved resonance' - 677.287 eV to 2.7679 eV; and 'thermal' - less than 2.7679 eV.

4.3 Results and Discussions

Figure 4.3 gives the typical spectrum seen by a fuel pin in CANDU-NG lattice. It can be seen that the peak of the Maxwellian spectrum is at about 0.08 eV. Eventhough the coolant temperature is close to CANDU-6 lattice, the peak is shifted mainly due to reduction in lattice pitch that is making the spectrum more hard in comparison to CANDU-6.

As a first step, the CANDU-NG cell was analyzed using Monte Carlo code MCNP5. The reference values obtained using MCNP5 is presented in Table 4.2. Four sets of calculations were performed. The sets included two varieties of fuel and two coolant states. The two varieties of fuel include natural uranium/ dysprosium in natural uranium in the central pin at two coolant densities of 0.714 g/cc and 0.001 g/cc each. The k_∞ was estimated for each of the states and the CVR for each variety was estimated using the Equation 4.1:

$$CVR = [1/k_\infty(S_1) - 1/k_\infty(S_2)] \tag{4.1}$$

where S_1 and S_2 corresponds to presence (0.714 g/cc) and absence (0.001 g/cc) of coolant respectively. The deviation for CVR was obtained using Equation 4.2,

$$Deviation\ (MCNP5) = \sqrt{[\delta_2^2/k_\infty^4(S_1) + \delta_1^2/k_\infty^4(S_2)]} \tag{4.2}$$

where δ_1 is the standard deviation for $k_\infty(T_1)$ obtained using MCNP5, while δ_2 is the standard deviation for $k_\infty(T_2)$.

In the following discussions, we will be using the following notations to represent the two varieties of assemblies analysed for the estimation of CVR. The first variety with central

pin having natural uranium will henceforth be referred to as 'V1' and that with dysprosium in natural uranium in central pin will be referred to as 'V2'.

Table 4.2 gives the k_∞ values and CVR obtained using MCNP5 and DRAGON Version4, for a single CANDU-NG lattice for 'V1' and 'V2', with and without coolant. It can be seen from Table 4.2 that the results obtained using the self-shielding models in DRAGON systematically under-predict basic k_∞ values with respect to that obtained using MCNP5. The results obtained using 'GSM1-NOLJ' show the maximum deviation, for both 'V1' and 'V2' for both cooled and voided states. k_∞ values predicted by GSM0 are better than GSM1 and GSM2 when NOLJ option is considered. This trend is reversed when LJ option is considered. However, the under prediction by all the GSM models is reduced when LJ option is considered. It is interesting to note that GSM2-LJ predicts basic k_∞ close to that of MCNP5 in the presence of coolant. Another interesting trend when there is voiding is that the GSM models without LJ predict k_∞ close to that of MCNP5 when compared to GSM models with LJ. When LJ is used, the trend is reversed for GSM2 for 'V1' and for all the GSM models for 'V2'. However, the subgroup models have a uniform trend of increased under-prediction during voiding for both 'V1' and 'V2'. The CVR is estimated to be positive for 'V1' and 'V2', but the magnitude is lower in case of 'V2'. It can be seen from Figure 4.4 that the capture rate is almost doubled when one considers dysprosium in the central pin. The capture rate gets further enhanced during voiding and thus Dy plays a crucial role in lowering the CVR. The CVR predicted using the various self-shielding models incorporated in DRAGON, are in close agreement with that estimated using MCNP5.

Tables 4.3 and 4.4 compare the capture rate for 'V1' and 'V2' respectively, in resolved resonance energy group obtained using MCNP5 and all the self-shielding models in DRAGON. It can be seen that the models based on a subgroup approach predicts the capture rate better than the models based on equivalence in dilution. Even though the k_∞ predicted

by GSM2LJ is better during voiding, it can be noted that the capture rate is over predicted. It was noted that the subgroup approach ('SUBG') based on physical probability tables seems to predict the basic k_∞, CVR and reaction rates better than all other models. This trend has been observed before on simpler validation tests [Hébert 2004a]. The Stamm'ler method is based on very crude approximations related to the calculation of the equivalent dilution in each resonant region and each resonant energy group. The subgroup method with physical probability tables is now considered as the recommended tool in state-of-the-art lattice codes and is compatible with the characteristics method. Finally, the Ribon extended method is more expensive and is required only in situations where the mutual shielding phenomenon is important. We have thus used 'SUBG' model for assembly calculations in 2×2 pattern.

Table 4.5 gives the k_∞ values for assembly calculation in 2×2 pattern, obtained using MCNP5 and DRAGON Version4 for fully cooled, fully voided and checkerboard voiding states. Translation boundary condition is applied on all the parallel surfaces in order to truly reflect the physical phenomena when there is a possibility of checkerboard voiding. It can be seen that the k_∞ and CVR values for 2×2 pattern matches quite well with that obtained for a single cell in Table 4.2. When all the four cells are cooled, it can be noticed that the difference from single cell calculation, using DRAGON, is about 15 pcm while it is about 40 pcm when all cells are voided. It is interesting to note that these differences are about half those obtained when one compares calculations with isotropic and specular boundary conditions for cooled and voided states using MCNP5 (about 30 pcm and 80 pcm). This is totally coherent as each cell in a 2×2 assembly has two outer surfaces out of four for which the isotropic/uniform boundary conditions are applied. One can expect that with an exact treatment of the boundary condition (i.e. a specular tracking obtained using translation boundary condition), DRAGON results will be closer to MCNP5 in estimation of CVR. This capability is currently under development in NXT: [Marleau 2005]. It is interesting to note from Table 4.5 that the CVR value during checkerboard voiding for 'V1' is lower than that

obtained for total coolant voiding. But for 'V2', the CVR obtained for checkerboard voiding is higher than that observed when there is total voiding. It can be seen from Table 4.5 that this trend is also observed using the code DRAGON. Tables 4.6 to 4.8 compare the capture rate in resolved resonance energy group obtained using MCNP5 and DRAGON for the three states - all 4 cells cooled, voided and checkerboard voiding. It can be observed that the capture rate estimated using "SUBG" model in DRAGON is predicted within a few percents of values obtained using MCNP5. The maximum discrepancy of 15% is found in the outermost layer of pins in second ring. It can also be noted in Tables 4.6and 4.7 that the capture rates are slightly unsymmetric. This may be due to statistical phenomena to obtain fluxes in various regions of problem domain and can possibly be improved by tracking more than ten million neutron histories.

4.4 Conclusions

Coolant void reactivity has been estimated for CANDU-NG lattice using various self shielding models incorporated in DRAGON Version4. The obtained results have been validated using Monte Carlo code MCNP5. It was observed that the self-shielding model based on subgroup approach using physical probability tables predicts the basic k_{∞}, CVR and reaction rates better than all the other models. This model was used for performing the assembly calculation in 2×2 pattern and the CVR for checkerboard voiding state was estimated. This calculation using DRAGON was made possible by the introduction of a new tracking module NXT: developed at École Polytechnique de Montréal. Using DRAGON, we have obtained the trend of a higher CVR for checkerboard voiding state when compared to complete voiding state for CANDU-NG lattice with dysprosium in the central pin.

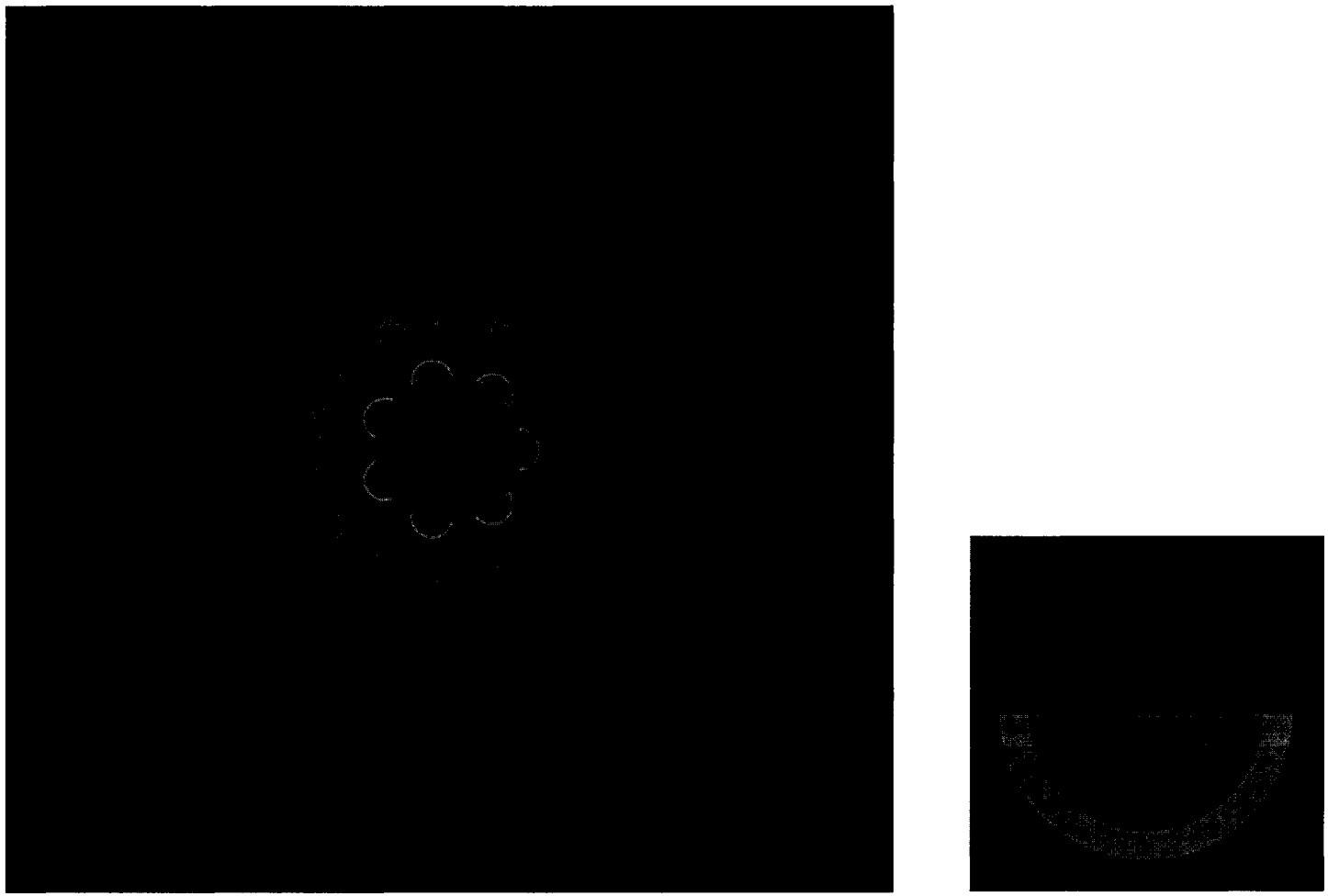

Figure 4.1 Cross section of CANDU-NG unit cell and single pin

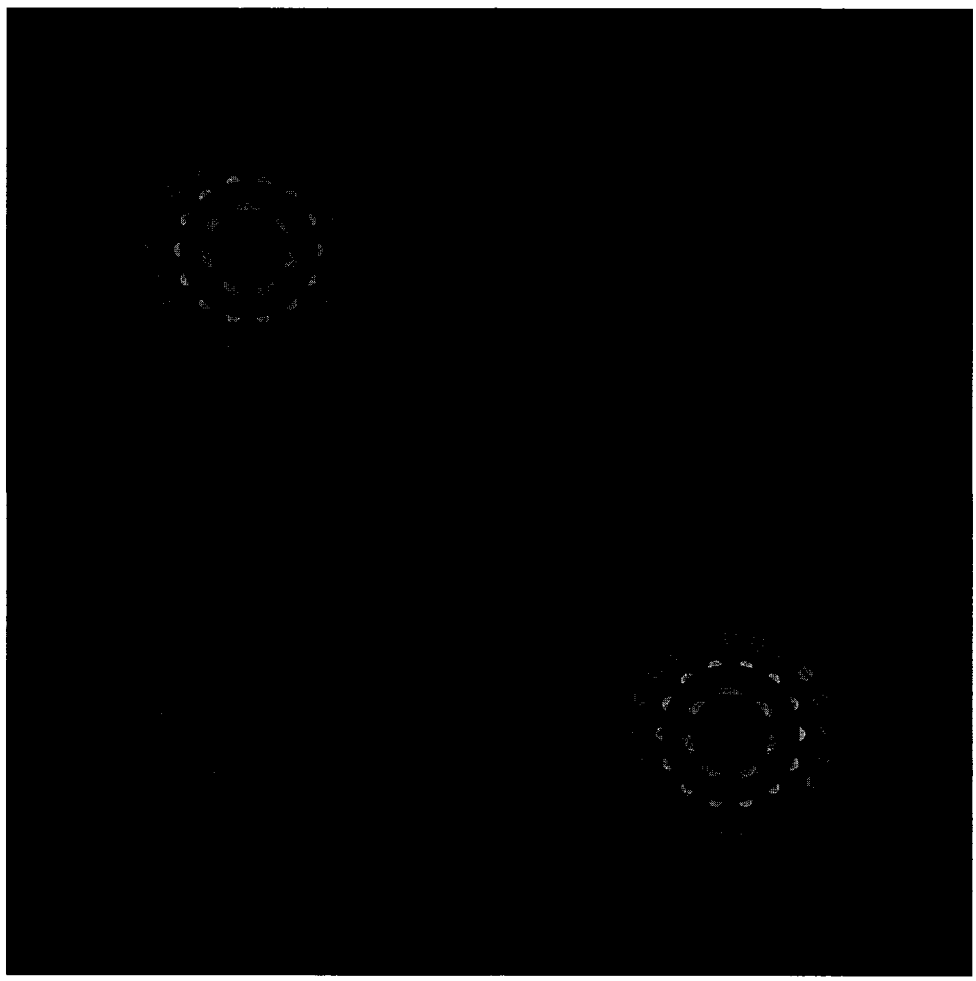

Figure 4.2 Cross section of 2 × 2 CANDU-NG assembly

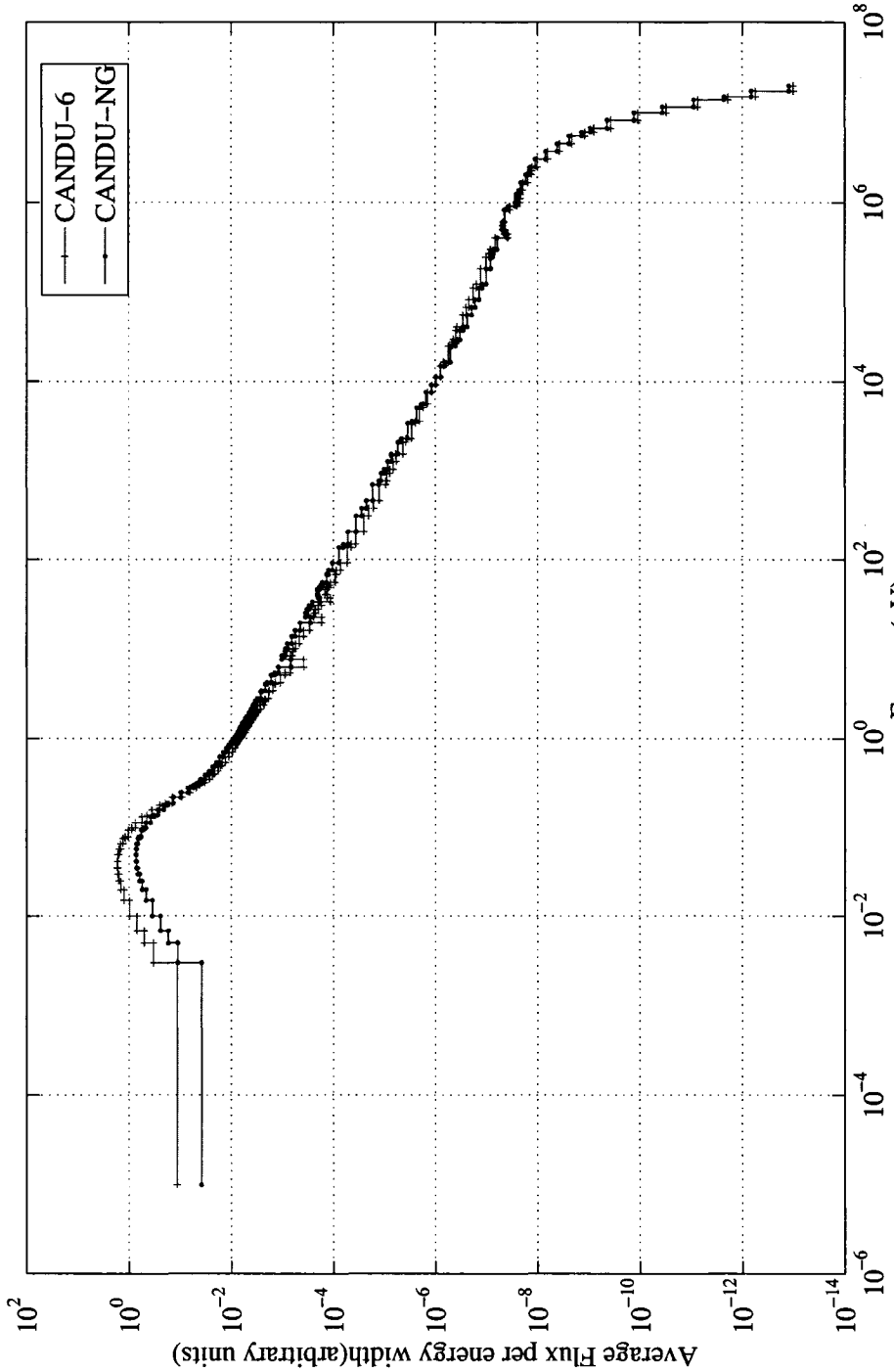

Figure 4.3 Typical spectrum in CANDU-NG lattice

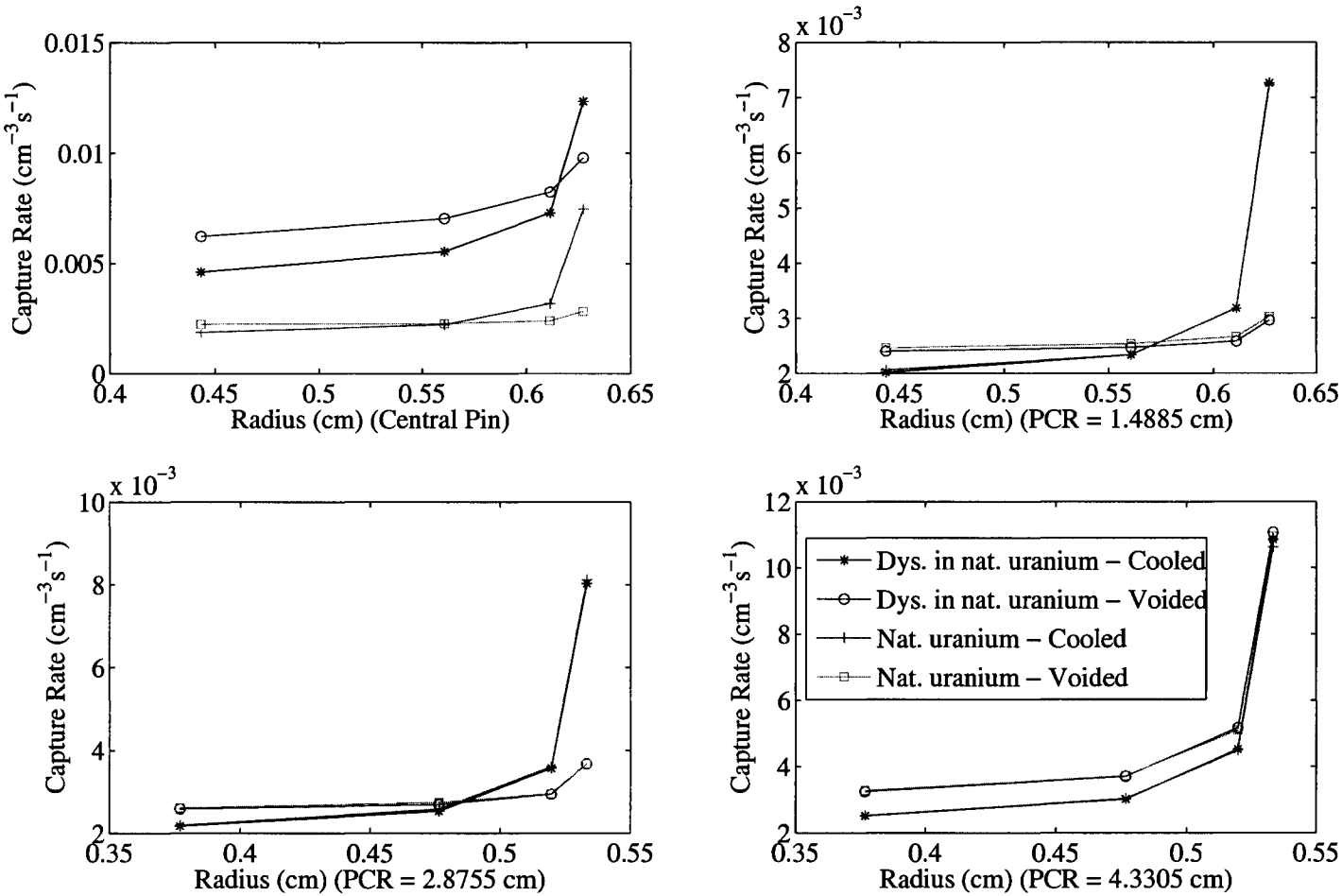

Figure 4.4 Capture rate in four layers of pins in four rings

Table 4.1 CANDU-NG benchmark Specifications

Pitch (cm)	22 (square)
Number of rods	43 (1/7/14/21)
Radius of rod centers (cm)	0.0/1.73/3.075/4.384
Fuel material	1.65 % enr UO_2
Density of fuel material(g/cm^3)	10.12 (inner 8 pins) 9.825 (outer 35 pins)
Radius of fuel rods (cm)	0.627 (inner 8 pins) 0.533 (outer 35 pins)
Clad Composition (%)	Zr-98.1813, Fe-0.21, Cr-0.1, Ni-0.007,^{10}B-5.962E-5
Density of Clad (g/cm^3)	7.55*
Outer radius of Clad (cm)	0.675 (inner 8 pins) 0.575 (outer 35 pins)
Coolant Composition	^{1}H-0.047720, ^{16}O-0.023803,^{2}D-4.7720E-7
Moderator Composition	^{1}H-6.4950E-5,^{16}O-0.032398,^{2}D-0.064886
Material Composition - PT(%)	Zr-97.3126, Nb-2.58, Fe-0.04678, Cr-0.008088, Ni-0.0035, ^{10}B-2.431E-5
Density of PT (g/cm^3)	6.57
Inner radius of PT (cm)	5.1689
Outer Radius of PT(cm)	5.7689
Material Composition - CT(%)	Zr-98.2083, Fe-0.135, Cr-0.1, Ni-0.055, ^{10}B-5.962E-5
Density of CT (g/cm^3)	6.44
Inner radius of CT (cm)	7.5
Outer Radius of CT(cm)	7.8
Fuel Temperature (K)	960.16
Clad Temperature (K)	573.16
Coolant Temperature (K)	573.16
Moderator Temperature (K)	353.16

* Artificial density to accommodate clad material of the end cap and spacers so as to account to 2.32 Kg/ bundle of the clad material.

Table 4.2 Comparison of k_∞ for single CANDU-NG lattice

Model	Central pin - Natural Uranium			Central pin - Dysprosium in Natural Uranium		
	k_∞(Cooled)	k_∞(Voided)	CVR(pcm)	k_∞(Cooled)	k_∞(Voided)	CVR(pcm)
M	1.30449±	1.32867±	1395±	1.25556±	1.26374±	516±
	0.00016	0.00017	13	0.00017	0.00018	16
A	885$^+$	689	-131*	842	649	-129
B	1096	945	-111	1043	883	-111
C	953	885	-60	918	842	-56
D	609	556	-43	567	507	-43
E	540	576	9	507	518	3
F	134	426	163	146	395	156
G	312	379	32	305	361	33
H	286	423	72	280	404	76

$^+$ - ΔK(in pcm) = (k_∞(MCNP5) - k_∞(model))
* - ΔCVR(in pcm) = (CVR(MCNP5) - CVR(model))
M-MCNP5; A-GSM0-NOLJ; B-GSM1-NOLJ; C-GSM2-NOLJ;
D-GSM0-LJ; E-GSM1-LJ; F-GSM2-LJ; G-SUBG; H-RIB

Table 4.3 Comparison of the capture rate in the resolved resonance energy group for single CANDU-NG lattice with natural uranium in the central pin

Central Pin	Ring	Layer	Capture rate ($cm^{-3}s^{-1}$) (MCNP5)	Relative error with respect to MCNP5 (in %)							
				A	B	C	D	E	F	G	H
Natural Uranium	1	1	4.6127E-03±0.037*	18.66	9.74	11.17	18.30	6.59	9.25	5.18	5.40
		2	5.5395E-03±0.037	10.14	6.20	6.96	8.88	2.79	5.42	3.05	2.99
		3	7.2948E-03±0.046	-8.67	-2.48	-0.55	-10.41	-2.11	2.51	1.37	1.04
		4	1.2344E-02±0.070	-42.72	-4.54	-4.59	-44.13	-1.93	-1.23	0.00	0.02
	2	5	2.0176E-03±0.054	29.71	12.48	11.06	28.95	7.98	4.90	1.91	2.34
		6	2.3350E-03±0.057	19.97	9.81	7.98	18.73	5.59	2.32	1.22	1.15
		7	3.1801E-03±0.075	-6.93	-1.33	-1.42	-8.25	0.20	-0.87	0.58	0.04
		8	7.2628E-03±0.111	-57.80	-25.06	-21.07	-58.51	-22.89	-17.16	-2.62	-2.57
	3	9	2.1742E-03±0.061	30.89	14.44	12.81	29.85	9.53	6.10	2.15	2.50
		10	2.5368E-03±0.063	19.01	11.09	9.18	17.60	7.66	3.80	1.25	1.10
		11	3.5682E-03±0.084	-11.34	-1.18	-0.51	-12.69	1.50	1.91	0.09	-0.58
		12	8.0317E-03±0.121	-59.38	-21.80	-17.67	-60.09	-19.67	-13.73	-3.49	-3.25
	4	13	2.5182E-03±0.059	30.74	16.06	13.96	29.16	9.64	5.06	1.29	1.47
		14	3.0229E-03±0.061	16.06	12.71	10.06	14.13	8.37	3.12	0.94	0.41
		15	4.5187E-03±0.082	-18.47	-0.11	0.32	-20.13	2.01	1.87	0.44	-0.65
		16	1.0857E-02±0.109	-65.01	-16.92	-13.87	-65.80	-15.37	-11.01	-0.83	-0.70

* - Relative error A-GSM0-NOLJ B-GSM1-NOLJ C-GSM2-NOLJ D-GSM0-LJ;
E-GSM1-LJ F-GSM2-LJ G-SUBG H-RIB

Table 4.4 Comparison of the capture rate in the resolved resonance energy group for single CANDU-NG lattice with dysprosium in natural uranium in the central pin

Central Pin	Ring	Layer	Capture rate ($cm^{-3}s^{-1}$) (MCNP5)	Relative error with respect to MCNP5 (in %)							
				A	B	C	D	E	F	G	H
Dysprosium in Natural Uranium	1	1	6.2208E-03±0.030*	9.35	4.39	6.34	9.19	2.49	5.93	3.61	3.79
		2	7.0400E-03±0.030	3.90	1.21	2.75	3.16	-0.32	3.94	1.26	1.37
		3	8.2389E-03±0.036	-5.69	-4.26	-2.56	-6.87	-3.25	0.44	-0.76	-0.73
		4	9.7927E-03±0.049	-17.36	4.50	0.60	-18.72	7.17	3.76	0.05	0.22
	2	5	2.4022E-03±0.045	15.27	5.74	5.27	15.14	5.23	4.23	1.66	2.24
		6	2.4713E-03±0.047	14.28	5.94	5.42	14.12	2.60	1.58	2.23	2.74
		7	2.5813E-03±0.055	10.99	5.85	5.75	10.81	10.01	10.86	4.52	4.94
		8	2.9633E-03±0.095	-2.50	1.91	3.75	-2.68	5.09	8.45	15.36	15.62
	3	9	2.5898E-03±0.050	17.45	8.02	7.43	17.19	6.82	7.16	1.63	2.17
		10	2.6958E-03±0.052	15.11	7.64	7.07	14.80	3.62	2.72	1.89	2.33
		11	2.9404E-03±0.070	7.08	4.79	5.12	6.75	9.88	8.82	2.45	2.74
		12	3.6744E-03±0.117	-13.46	-4.60	-1.86	-13.74	-1.88	2.58	9.35	9.83
	4	13	3.2472E-03±0.049	15.88	10.59	9.09	15.16	7.23	4.62	0.54	0.84
		14	3.7094E-03±0.052	5.13	8.19	6.55	4.37	5.24	1.43	0.40	0.19
		15	5.1698E-03±0.071	-22.55	-1.78	-0.65	-23.18	-0.44	1.85	-2.06	-2.77
		16	1.1074E-02±0.100	-63.27	-27.79	-24.16	-63.58	-26.58	-22.39	-5.27	-5.07

* - Relative error A-GSM0NOLJ B-GSM1NOLJ C-GSM2NOLJ D-GSM0LJ;
E-GSM1LJ F-GSM2LJ G-SUBG H-RIB

Table 4.5 Comparison of k_∞ for assembly calculation in 2×2 pattern for CANDU-NG

Central pin	Code	k_∞(A)	$k_\infty(B)$	CVR(A-B)	k_∞(C)	CVR(A-C)
Natural Uranium	MCNP5	1.30480±0.00016	1.32967±0.00017	1433±13	1.32497±0.00016	1167±13
	SUBG	330^+	435	53*	349	5
Dysprosium in Natural Uranium	MCNP5	1.25609±0.00017	1.26494±0.00018	557±16	1.26774±0.00018	732±16
	SUBG	344	443	59	379	18

A - All 4 cells cooled ; B - All 4 cells voided; C - Checkerboard voiding

$^+$ - ΔK(in pcm) = (k_∞(MCNP5) - k_∞(model))

* - ΔCVR(in pcm) = (CVR(MCNP5) - CVR(model))

Table 4.6 Comparison of capture rate in resolved resonance energy group for assembly calculation in 2x2 pattern (all cells cooled) for CANDU-NG with central pin having Dy in natural uranium

Ring	Layer	Capture rate ($cm^{-3}s^{-1}$) (MCNP5)	A	Layer	Capture rate ($cm^{-3}s^{-1}$) (MCNP5)	B
1	1	2.3100E-03±0.053*	4.93+	17	2.3220E-03±0.053*	4.39+
	2	2.7796E-03±0.053	2.46	18	2.7597E-03±0.053	3.20
	3	3.6598E-03±0.065	1.04	19	3.6552E-03±0.065	1.17
	4	6.3148E-03±0.103	-1.87	20	6.1635E-03±0.099	0.54
2	5	1.0230E-03±0.078	0.55	21	1.0063E-03±0.076	2.22
	6	1.1577E-03±0.078	2.11	22	1.1503E-03±0.080	2.76
	7	1.5995E-03±0.105	0.00	23	1.5609E-03±0.108	2.47
	8	3.6078E-03±0.160	-2.21	24	3.5303E-03±0.158	-0.06
3	9	1.1015E-03±0.086	0.81	25	1.0989E-03±0.086	1.05
	10	1.2674E-03±0.089	1.34	26	1.2788E-03±0.091	0.44
	11	1.8146E-03±0.124	-1.87	27	1.8265E-03±0.121	-2.51
	12	3.9253E-03±0.169	-1.18	28	4.0613E-03±0.171	-4.49
4	13	1.2682E-03±0.084	0.50	29	1.2548E-03±0.082	1.57
	14	1.5113E-03±0.086	0.87	30	1.5094E-03±0.088	1.00
	15	2.2366E-03±0.112	1.44	31	2.2730E-03±0.118	-0.18
	16	5.3172E-03±0.153	1.21	32	5.5005E-03±0.155	-2.16

* - Relative error A,D - Cooled; B,C - Cooled
+ - Deviation (in %) w.r.t MCNP5

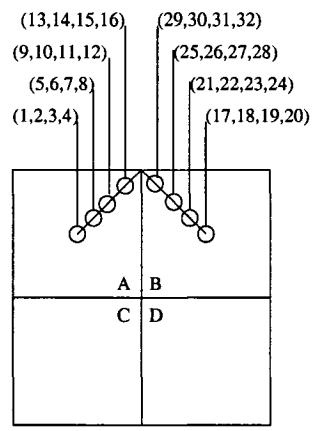

Table 4.7 Comparison of capture rate in resolved resonance energy group for assembly calculation in 2x2 pattern (all cells voided) for CANDU-NG with central pin having Dy in natural uranium

Ring	Layer	Capture rate ($cm^{-3}s^{-1}$) (MCNP5)	A	Layer	Capture rate ($cm^{-3}s^{-1}$) (MCNP5)	B
1	1	3.0968E-03±0.043*	3.89+	17	3.0908E-03±0.043*	4.09+
	2	3.5029E-03±0.043	1.52	18	3.4948E-03±0.043	1.76
	3	4.0835E-03±0.051	-0.04	19	4.0968E-03±0.050	-0.36
	4	4.7857E-03±0.066	2.67	20	4.8308E-03±0.066	1.71
2	5	1.2098E-03±0.065	0.84	21	1.2044E-03±0.065	1.30
	6	1.2273E-03±0.065	2.82	22	1.2275E-03±0.067	2.80
	7	1.2929E-03±0.081	4.23	23	1.3011E-03±0.084	3.57
	8	1.4852E-03±0.141	14.60	24	1.4937E-03±0.139	13.95
3	9	1.2811E-03±0.070	2.61	25	1.2937E-03±0.071	1.61
	10	1.3359E-03±0.073	2.67	26	1.3385E-03±0.073	2.47
	11	1.4337E-03±0.093	4.76	27	1.4522E-03±0.094	3.42
	12	1.8258E-03±0.158	9.86	28	1.8451E-03±0.172	8.71
4	13	1.6186E-03±0.069	0.69	29	1.6069E-03±0.070	1.42
	14	1.8801E-03±0.076	-1.15	30	1.8426E-03±0.073	0.86
	15	2.5785E-03±0.101	-2.02	31	2.5824E-03±0.102	-2.17
	16	5.4176E-03±0.141	-3.34	32	5.5332E-03±0.144	-5.35

* - Relative error A,D - Voided; B,C - Voided
+ - Deviation (in %) w.r.t MCNP5

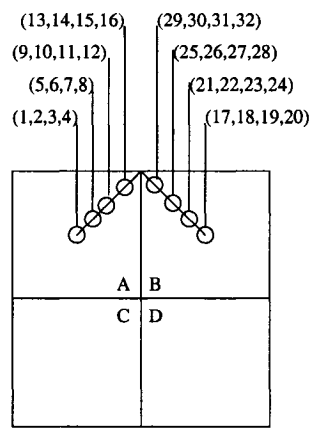

Table 4.8 Comparison of capture rate in resolved resonance energy group for assembly calculation in 2x2 pattern (checkerboard) for CANDU-NG with central pin having Dy in natural uranium

Ring	Layer	Capture rate ($cm^{-3}s^{-1}$) (MCNP5)	A	Layer	Capture rate ($cm^{-3}s^{-1}$) (MCNP5)	B
1	1	2.6629E-03±0.048*	5.40+	17	2.5172E-03±0.048*	4.32+
	2	3.2168E-03±0.049	2.50	18	2.8504E-03±0.048	1.89
	3	4.2173E-03±0.060	1.52	19	3.3522E-03±0.058	-0.48
	4	7.1955E-03±0.094	-0.29	20	3.9895E-03±0.076	0.71
2	5	1.1746E-03±0.071	1.57	21	9.7692E-04±0.071	1.73
	6	1.3503E-03±0.074	1.48	22	1.0018E-03±0.072	2.63
	7	1.8415E-03±0.099	0.67	23	1.0454E-03±0.087	5.04
	8	4.1642E-03±0.147	-1.69	24	1.2059E-03±0.146	15.06
3	9	1.2763E-03±0.080	1.58	25	1.0575E-03±0.081	1.30
	10	1.5021E-03±0.084	-0.19	26	1.1032E-03±0.086	1.33
	11	2.0892E-03±0.112	-0.51	27	1.1838E-03±0.106	3.44
	12	4.6210E-03±0.159	-1.91	28	1.4893E-03±0.188	9.88
4	13	1.4867E-03±0.077	1.04	29	1.3371E-03±0.079	-0.61
	14	1.7644E-03±0.080	1.82	30	1.5206E-03±0.083	-0.30
	15	2.6624E-03±0.106	0.44	31	2.0770E-03±0.112	-0.71
	16	6.4597E-03±0.139	-1.74	32	4.4611E-03±0.158	-4.03

* - Relative error A,D - Cooled; B,C - Voided
+ - Deviation (in %) w.r.t MCNP5

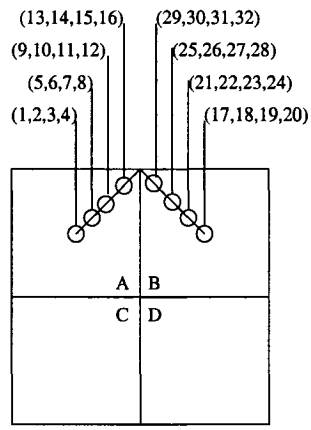

CHAPTER 5

HIGH CONVERSION LIGHT WATER REACTOR BENCHMARK

In this chapter we present the results of analysis of a high conversion light water reactor (HCLWR) benchmark [Hiroshi 1988]. This benchmark is of special interest as the main contribution to fission (46%) is from the resonance region. This lattice will be a good testing ground for the performance of all the self shielding models. Figure 5.1 shows the HCLWR lattice that has been analysed. Table 5.1 gives the geometrical description and material composition of the lattice.

It can be seen from the Table 5.1 that the fuel is enriched plutonium oxide (7%) in depleted uranium oxide. The hexagonal cell pitch is 1.2204 cm which is quite tight when compared to regular PWR pin pitch. The benchmark analysed was originally suggested as a burnup benchmark, which was performed for infinite hexagonal cells with V_m/V_f of 0.6 and 1.1. These calculations were performed for three voidage conditions at several burnup stages. Fifteen organizations from eight countries participated in this benchmark. One of the major conclusions were that one has to consider self-shielding of 2.67 eV resonance of ^{242}Pu, which was found to build to a high concentration as a function of burnup. It was also observed by various teams that self shielding effect on k_∞ decreases with increasing void fraction due to hardening of spectrum [Hiroshi 1988].

In the present work we have focused mainly on the analysis of hexagonal lattice with a V_m/V_f of 1.1 at zero burnup.

5.1 Reference solution

The reference solution was obtained using the code MCNP5 at zero burnup. A total of 10 million histories were tracked to obtain the k_∞ and reaction rates. White boundary condition was applied on the six surfaces of the hexagon. The fuel region was divided into four layers, each of volume 50%, 30%, 15% and 5% respectively from inside to outside, based on recommendations from Santamarina [Santamarina 2004]. The capture rate of each element in the fuel region was obtained for all the energy groups between 2.7679 eV and 677.287 eV.

5.2 Computational scheme used for DRAGON analysis

In the `LIB:` module we used library based on DRAGLIB format which included a total of nine elements. The evaluated nuclear data files for all the elements were chosen on the basis of recommendations from WLUP [Leszczynski 2003]. Under the `GEO:` module we considered the hexagonal pincell with isotropic reflective boundary condition on all surfaces. The geometry was tracked with an angular quadrature parameter of 11 and track density of 100 lines per cm. In the following section we discuss the effects of choice of angular quadrature and track density on the k_∞. Only one region was considered in the coolant for shielding and flux calculation, as there was minimal effect in estimation of k_∞. The tracking of the geometry was performed using the `EXCELT:` module. The APOLLO type transport correction based on the linearly anisotropic scattering cross sections was used for the total and isotropic scattering cross sections. We used the default options in `ASM:` module for generation of collision probabilities. In the `FLU:` module, we used the option of criticality calculations *without* leakage effects. The reaction rates were obtained using the `EDI:` module in four broad groups, with energy limits being - 'fast' - 20 MeV to 4.076220E+05 eV; 'unresolved resonance' - 4.076220E+05 eV to 677.287 eV; 'resolved resonance' - 677.287 eV to 2.7679

eV; and 'thermal' - less than 2.7679 eV.

5.3 Optimization studies

The optimization studies were carried out for the lattice by varying the angular quadrature parameter and track density. The k_∞ variation was observed until a saturated value was obtained. In the studies it was seen to that the error in volume was kept as minimum as possible. We chose the self shielding model 'SUBG' based on earlier experience for arriving at optimum angular quadrature parameter and track density. Table 5.2 gives the variation in k_∞ and volume error for various angular quadrature parameters and track densities. It can be observed that an angular quadrature parameter of 11 and track density of 100 was optimum for analysis of this lattice. The error in volume was found to be about 2%.

5.4 Results obtained using various self shielding models

Figure 5.2 gives the typical spectrum in a HCLWR lattice. It can be seen that the Maxwellian peak is at 0.08 eV. One can observe sharp dips in the spectrum at energies corresponding to resonances of plutonium isotopes (0.3 eV resonance of ^{239}Pu, 1.06 eV resonance of ^{240}Pu and 2.67 eV resonance of ^{242}Pu).

Table 5.3 gives the comparison of k_∞ obtained using the various self shielding models. It can be seen from the Table 5.3 that there is a broad range of values that have been obtained using each of the self shielding model. It can be seen that the lowest k_∞ is predicted using 'GSM1' with 'NOLJ' option. The k_∞ obtained using 'GSM0' is higher than 'GSM1' and slightly lower than 'GSM2' when 'NOLJ' option is used. But when 'LJ' option is used the

trend gets reversed and 'GSM2' with 'LJ' option being the highest. There is a substantial gain in k_∞, to the tune of 837 pcm when 'LJ' option is used as against the use of 'NOLJ' option with 'GSM2'. Such a gain is not seen with the other 'GSM' models eventhough the change is quite significant (371 pcm for 'GSM1' and 211 pcm for 'GSM0'). It can be observed that, when compared to the reference MCNP5 value, the k_∞ is highly under-predicted by all models based on "equivalence in dilution". It was noted that when models based on "subgroup approach", i. e. 'SUBG' and 'RIB' was used, the k_∞ was also under-predicted. But interestingly, when 'RIB' was used along with correlation model, henceforth referred to as 'RIB-CORR', there was a substantial gain in k_∞, to the tune of 508 pcm vis-à-vis the 'RIB' model. This is mainly due to the better treatment of mutual self shielding [Hébert 2005] between isotopes ^{238}U, ^{239}Pu and ^{240}Pu. It can be observed in Table 5.3 that when one considers pairs of nuclides, the k_∞ gradually improves, i.e. when correlation is applied between ^{238}U and ^{239}Pu, there is no major changed observed with respect to results obtained using 'RIB' model. But when correlation is applied between ^{239}Pu and ^{240}Pu, there is an improvement of 123 pcm and 362 pcm when correlation is applied between ^{238}U and ^{240}Pu. But when correlation is considered for ^{238}U, ^{239}Pu and ^{240}Pu, the results improves such that it is within 45 pcm of the results obtained using MCNP5. When correlation is considered for all isotopes, then the k_∞ slightly reduces by 85 pcm. No other self shielding model, except 'RIB' has the capability to treat mutual self shielding effect [Hébert 2005] and hence when there is a substantial amount of ^{239}Pu and ^{240}Pu in the system, one must consider the use of 'RIB-CORR' model for estimation of k_∞. A sensitivity study was carried out to assess the behaviour of 'RIB-CORR' model with ratio of ^{238}U and ^{240}Pu. This was done because the major contribution of correlation effects was due to these two isotopes. It can be seen from Figure 5.3 that when the ratio of ^{238}U to ^{240}Pu decreases, the difference between correlation and non-correlation model increases. For this exercise, all the number densities in Table 5.1 were kept constant except that of ^{240}Pu, which was artificially increased. Another exercise was carried out by maintaining the same composition in fuel as mentioned in Table 5.1 and increasing the lattice pitch. It was observed that the effect of mutual self shielding becomes

less prominent when the spectrum gets softer. It was thus noted that the mutual self shielding effect decreases with increase in V_m/V_f.

We next compared the reaction rates obtained using MCNP5 with that obtained using all the self shielding models. Figures 5.4 to 5.6 show the capture rate in ^{238}U, ^{239}Pu and ^{240}Pu, in each layer of the fuel pin in the resolved energy group. A high capture rate can be seen at all the major resonances of the respective isotopes. It can also be seen that the capture rate is highest for the outermost layer and reduces towards the inside. Table 5.4 gives a comparison of capture rate in resolved energy group and nu-fission rate in thermal energy group, obtained using all the self shielding models in DRAGON, with respect to MCNP5. It can be seen that the models based on subgroup approach, i.e. 'SUBG' and 'RIB' gives results close to that of MCNP5. The models based on "equivalence in dilution" shows a large deviation in capture rates w.r.t MCNP5. It can be seen that all the models under-predict the capture rate in outermost layer and the layer next to it, while in the inner two layers it is over-predicting the capture rate. Of all the models, RIB-CORR model seems to predict the capture rate close to that of MCNP5. It is interesting to note that eventhough the k_∞ predicted by GSM2-LJ was closer to MCNP5, the capture rate shows a larger deviation in all the layers when compared to 'SUBG' and 'RIB' models. The nu-fission rate was under-predicted by all the self shielding models in all the layers. It can be seen in Table 5.4, that of all the self shielding models, the nu-fission rate obtained using RIB-CORR model predicted close to that obtained using MCNP5.

Table 5.5 gives the contribution due to each element towards capture rate in each layer and in each of the four broad energy groups mentioned earlier. The values correspond to those obtained using 'RIB-CORR' model. It can be seen from Table 5.5 that the major elements that contribute towards capture rates are ^{238}U, ^{239}Pu and ^{240}Pu. It is logical mainly taking into consideration the fact that the fuel is highly enriched plutonium in depleted uranium. The spectrum is also hard taking into account the tight lattice pitch of 1.2204 cm. All this makes the resonances of these individual isotopes play a big role in affecting the lattice

characteristics. It was noted that almost 42% of absorption and 35% of fissions happen in resolved resonance group.

Tables 5.6 to 5.8 gives the comparison of capture rate for ^{238}U, ^{239}Pu, and ^{240}Pu in certain energy groups where a large deviation with MCNP5 was observed. It can be seen in general that among all the models the 'RIB-CORR' model predicted the capture rate for all the elements close to MCNP5. It can be seen in Figure 5.7 that there are overlap of resonances of ^{238}U and ^{240}Pu at 20.9 eV/20.45 eV, and 66 eV/66.2 eV respectively, as mentioned in Hébert 2005. Figure 5.8 shows the cross section variation of ^{239}Pu and ^{240}Pu. It can be seen that there are overlap of resonances of ^{239}Pu and ^{240}Pu at 41.66 eV/41.64 eV, 65.71 eV/66.65 eV respectively. It can be seen in Tables 5.6, 5.7 and 5.8, that at these energy groups the deviation in capture rate with respect to MCNP5 gets drastically reduced when 'RIB-CORR' model is used.

In order to get an insight into the effect of self shielding models the following was done. In the code DRAGON, the absorption rate is normalized to unity and the corresponding flux is used to obtain the fission rate and hence the k_∞. This procedure masks the effect of self shielding models, because the major contribution to change in k_∞ due to self shielding models is brought about by change in absorption rate. To substantiate this statement, we performed a calculation without self shielding. It was observed that for this lattice the nu-fission rate change was about 3% and change in absorption rate was about 35%. In another exercise, we artficially normalised the flux obtained from all the models to that of a reference value, which was chosen as 'RIB-CORR'. This was done with the basis that only this model predicted the k_∞ close to that of MCNP5. Using the normalization factors the absorption rate and nu-fission rate was calculated for all the groups and for all the models. These values are provided in Table 5.9. It can be observed that only in groups 2 and 3, there is a change in absorption rate and in group 4 for nu-fission rate. It can be noted that when GSM models are used with 'LJ' normalization, the maximum reduction in absortion rate is observed for 'GSM1', followed by 'GSM2' and 'GSM0'. It was also noted that the fission rate undergoes a change,

i.e there is a large reduction in fission rate when GSM1 is used with LJ option, followed by 'GSM0'. But when 'LJ' option is used with 'GSM2', the fission rate increases. This is the reason, for increase in k_∞ when 'GSM2' is used with 'LJ' option. The k_∞ also increases for 'GSM0' and 'GSM1', but the change is not appreciable, mainly due to reduction in fission rate being almost matched with reduction in absorption rate, when 'LJ' option is used with 'GSM0' and 'GSM1' models.

5.5 Conclusions

The high conversion light water reactor benchmark has been analysed at zero burnup with all the self shielding models incorporated in DRAGON Version4. It was noted that the k_∞ obtained using various models showed a large deviation when compared to MCNP5. The largest deviation was observed for generalized Stamm'ler model with Nordheim approximation and no Livolant Jeanpierre normalization. The least deviation was observed when Ribon extended self shielding model with mutual self shielding (correlation) between individual isotopes was used. In general, the models based on "subgroup approach" perform better than the models based on "equivalence in dilution". The k_∞ was found to increase when the generalized Stamm'ler models are used with the use of Livolant Jeanpierre normalization. The correlation effects depends upon two factors - the ratio of ^{238}U and ^{240}Pu number densities and the spectrum. For a hard spectrum, when the ratio of number densities is of the order of 300, one has to consider mutual self shielding of ^{238}U and ^{240}Pu. The mutual shielding of ^{239}Pu and ^{240}Pu also plays a role in improving the capture rate and k_∞. Correlation effects are to be considered for ^{238}U, ^{239}Pu and ^{240}Pu together to obtain good results. When the spectrum gets softer, the correlation effects become less prominent. An important observation is that the nu-fission rate reduces by a larger extent when generalized Stamm'ler model with Nordheim model is used with Livolant-Jeanpierre normalization in comparison to the other two generalized Stamm'ler models.

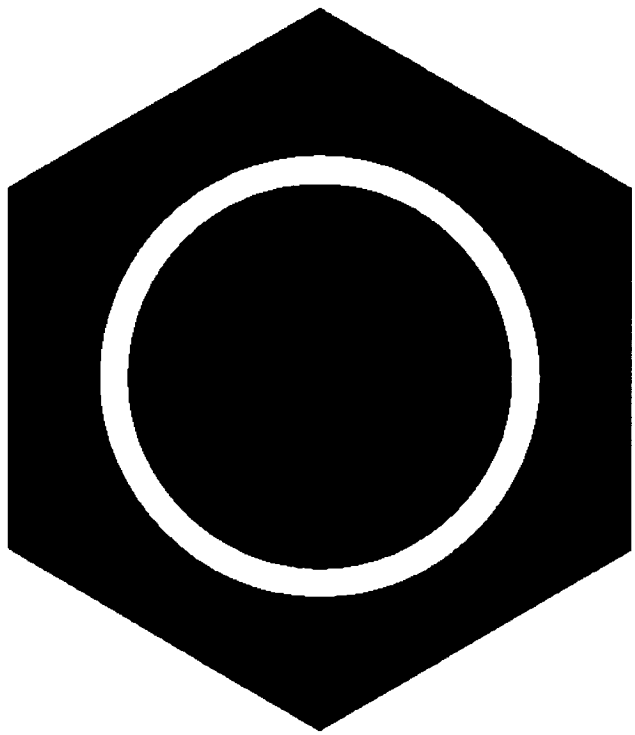

Figure 5.1 High conversion light water reactor lattice

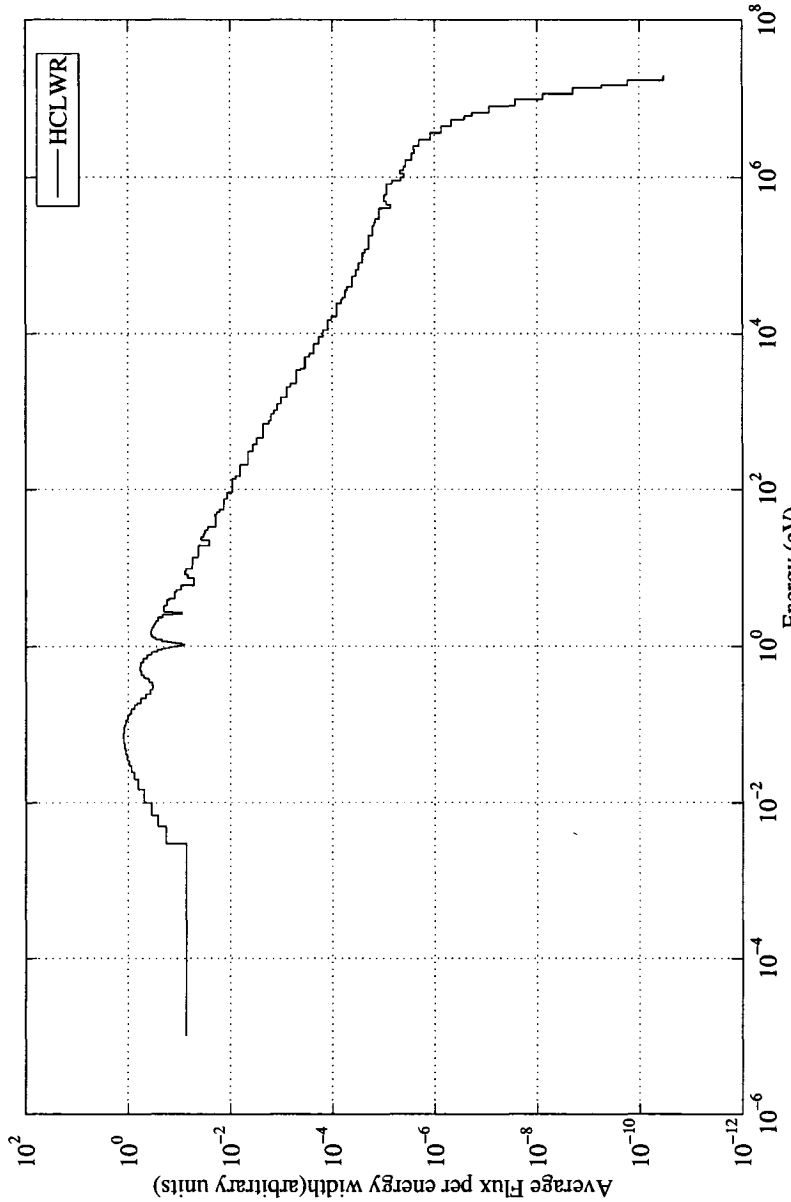

Figure 5.2 Typical spectrum in a high conversion light water reactor lattice

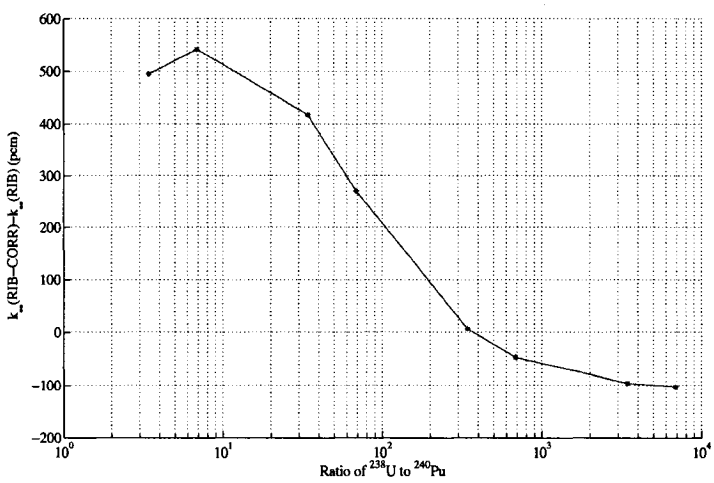

Figure 5.3 Variation of δK as a function of ratio of number densities of ^{238}U and ^{240}Pu

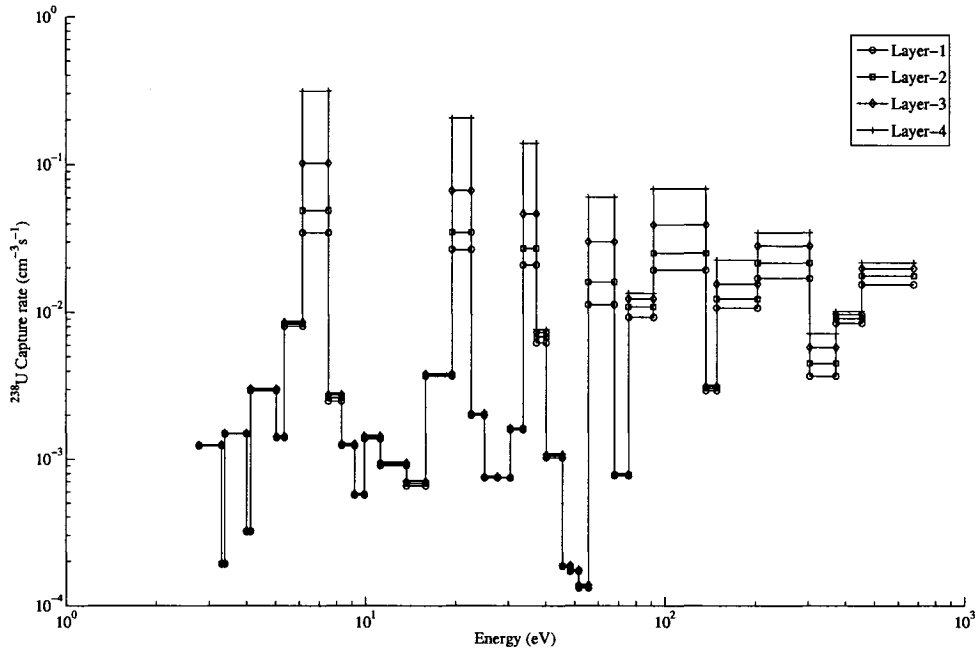

Figure 5.4 Capture rate in the resonances of ^{238}U in groups between 2.7679 eV and 677.287 eV

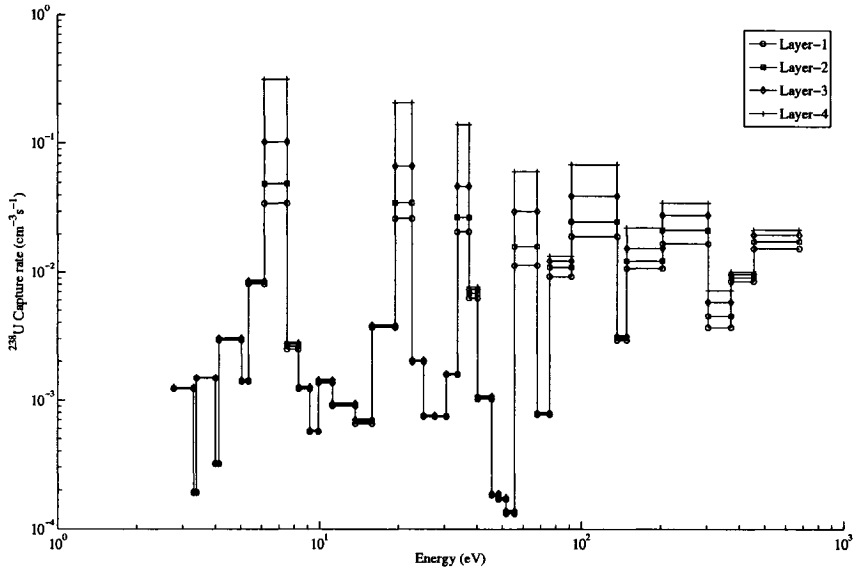

Figure 5.5 Capture rate in the resonances of ^{239}Pu in groups between 2.7679 eV and 677.287 eV

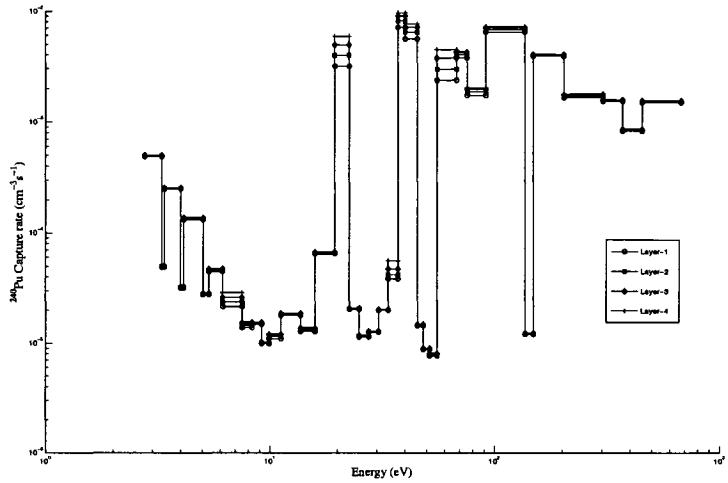

Figure 5.6 Capture rate in the resonances of ^{240}Pu in groups between 2.7679 eV and 677.287 eV

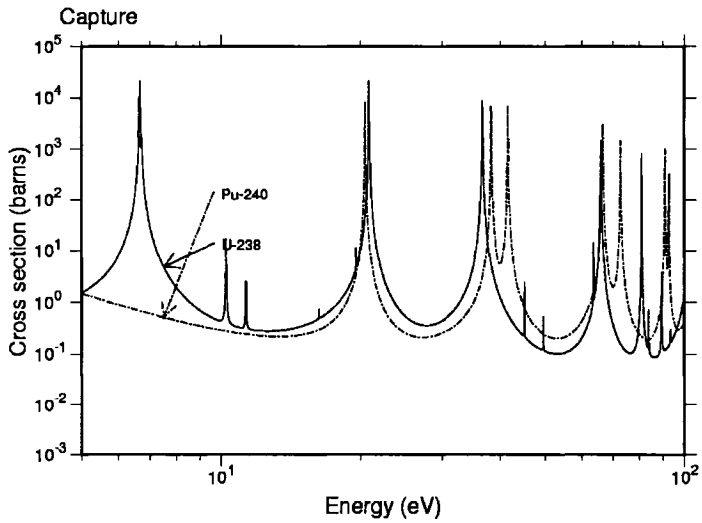

Figure 5.7 Resonances of ^{238}U and ^{240}Pu between 2.7 eV and 100 eV

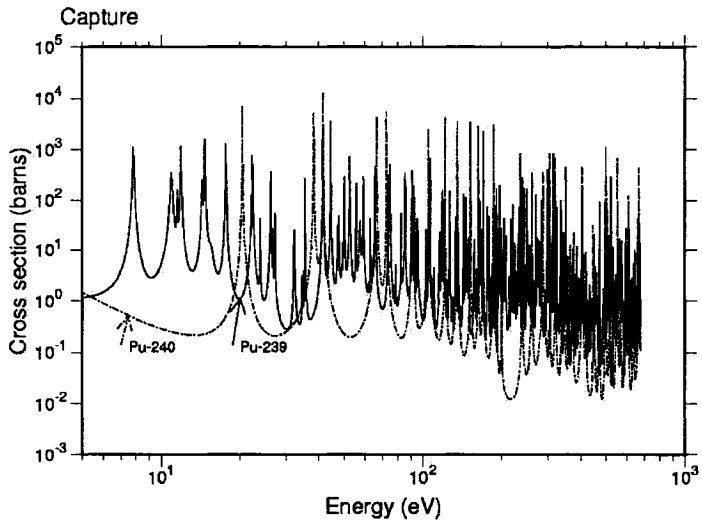

Figure 5.8 Resonances of ^{239}Pu and ^{240}Pu between 2.7 eV and 100 eV

Table 5.1 Modified high conversion light water reactor benchmark specifications

Region	Element	Fuel Rod
Fuel	U-235	6.194 E-05
	U-238	2.058 E-02
	Pu-239	1.367 E-03
	Pu-240	6.009 E-04
	Pu-241	2.418 E-04
	Pu-242	1.844 E-04
	O	4.608 E-02
Clad	Zr	3.702 E-02
Water	H	4.744 E-02
	O	2.372 E-02

All nuclear densities are given in atoms per barn-cm

Parameter	Hot Full Power
Fuel Temperature(K)	900
Cladding Temperature(K)	621
Coolant Temperature(K)	573.6
Fuel Pellet Radius (cm)	0.41
Cladding Outer Radius (cm)	0.475
Pin Pitch (cm)	1.2204

Table 5.2 Optimization of quadrature parameter and track density

Quadrature	Track density (lines/cm)	k_∞	Error in surface(%)	Error in Volume(%)
11	10	1.107863	6.08	188
11	50	1.109851	1.26	25.4
11	100	1.111531	0.60	2.08
11	200	1.110766	0.20	1.6
21	10	1.107553	4.70	188
21	50	1.109835	0.40	25.4
21	100	1.111512	0.08	2.08
21	200	1.110831	0.26	1.6
31	10	1.107756	4.96	188
31	50	1.109794	0.32	25.4
31	100	1.111485	0.12	2.08
31	200	1.110733	0.08	1.6

Table 5.3 k_∞ obtained using various self shielding models for HCLWR lattice

Model	k_∞	δ K (pcm)
MCNP5	1.11763±0.00021	–
GSM0-NOLJ	1.104315	-1332
GSM1-NOLJ	1.103078	-1455
GSM2-NOLJ	1.104541	-1309
GSM0-LJ	1.106426	-1120
GSM1-LJ	1.106784	-1085
GSM2-LJ	1.112906	-472
SUBG	1.111531	-610
RIB	1.112150	-548
RIB-CORR(A)	1.112107	-556
RIB-CORR(B)	1.113380	-425
RIB-CORR(C)	1.115766	-186
RIB-CORR(D)	1.117178	-45
RIB-CORR(E)	1.116325	-130

δ K = k_∞(MCNP5)-k_∞(model)

A - ^{238}U and ^{239}Pu
B - ^{239}Pu and ^{240}Pu
C - ^{238}U and ^{240}Pu
D - ^{238}U, ^{239}Pu and ^{240}Pu
E - All elements

Table 5.4 Capture rate in resolved resonance group and nu-fission rate in thermal group obtained using various self shielding models

Layer	Capture rate ($cm^{-3}s^{-1}$) (MCNP5)	Relative error with respect to MCNP5 (in %)								
		A	B	C	D	E	F	G	H	I
1	4.1997E-01±0.0500*	21.33	8.98	9.97	20.69	5.39	6.16	3.18	3.08	1.65
2	4.8558E-01±0.0500	10.06	5.84	6.02	9.27	3.83	3.31	1.70	1.41	0.28
3	6.4598E-01±0.0700	-14.19	-3.27	-3.40	-14.93	-1.41	-1.78	-0.21	-0.61	-1.17
4	1.1725E+00±0.1100	-51.84	-13.51	-15.35	-52.30	-11.86	-13.45	-3.60	-3.19	-2.98

Layer	Nu-fission rate ($cm^{-3}s^{-1}$) (MCNP5)	Relative error with respect to MCNP5 (in %)								
		A	B	C	D	E	F	G	H	I
1	6.7018E-01±0.0900*	-1.20	-0.99	-1.47	-0.62	0.53	-0.26	-0.45	-0.39	0.15
2	9.1462E-01±0.0700	-1.71	-1.51	-1.98	-1.13	0.01	-0.78	-0.97	-0.90	-0.37
3	1.1656E+00±0.0700	-1.82	-1.61	-2.08	-1.24	-0.10	-0.89	-1.07	-1.01	-0.47
4	1.3662E+00±0.0800	-3.57	-3.36	-3.83	-3.00	-1.88	-2.66	-2.84	-2.77	-2.25

* - Relative error

A - GSM0-NOLJ B - GSM1-NOLJ C - GSM2-NOLJ D - GSM0-LJ E - GSM1-LJ
F - GSM2-LJ G - SUBG H - RIB I - RIB-CORR

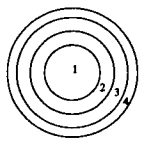

Table 5.5 Contribution (in %) to capture rate due to each element in each layer of fuel pin and in each broad energy group obtained using 'RIB-CORR' model

Layer	Group	^{235}U	^{238}U	^{239}Pu	^{240}Pu	^{241}Pu	^{242}Pu
1	1	0.3	90.8	3.8	3.2	1.0	0.9
	2	0.5	78.9	12.5	5.2	1.6	1.3
	3	1.2	52.1	27.9	9.9	6.0	2.8
	4	0.2	3.4	32.4	50.0	3.5	10.4
2	1	0.3	90.8	3.8	3.2	1.0	0.9
	2	0.5	79.3	12.2	5.1	1.6	1.2
	3	1.1	55.8	25.8	9.4	5.4	2.5
	4	0.2	2.9	34.1	49.6	3.5	9.7
3	1	0.3	90.8	3.8	3.2	1.0	0.9
	2	0.5	79.8	12.0	5.0	1.5	1.2
	3	0.9	64.7	20.5	7.7	4.2	1.9
	4	0.2	2.2	30.6	56.0	3.0	7.9
4	1	0.3	90.8	3.8	3.2	1.0	0.9
	2	0.5	80.1	11.8	4.9	1.5	1.2
	3	0.5	79.7	11.8	4.5	2.4	1.1
	4	0.1	1.6	23.4	67.0	2.2	5.7

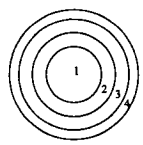

Table 5.6 Capture rate in ^{238}U in resolved resonance group obtained using various self shielding models

Fine Group in resolved resonance group	Capture rate in ^{238}U ($cm^{-3}s^{-1}$) (MCNP5)	Relative error with respect to MCNP5 (in %)									
		L	A	B	C	D	E	F	G	H	I
1	1.13E-02 ± 0.0037*	1	66.91	36.92	23.79	66.17	33.79	18.64	11.71	10.45	-1.64
2	2.66E-02 ± 0.0028		67.46	41.57	35.46	64.91	30.67	19.4	2.96	3.78	4.6
1	1.60E-02 ± 0.0037	2	23.01	15.5	8.9	22.43	14.26	6.48	6.1	2.82	-6.88
2	3.50E-02 ± 0.0028		39.85	30.33	22.29	37.3	24.23	11.19	3.01	2.38	3.32
1	3.00E-02 ± 0.0039	3	-32.9	-15.9	-11.02	-33.23	-14.71	-10.68	-3.11	-3.37	-8.02
2	6.69E-02 ± 0.0032		-21.45	-5.94	-6.48	-23.06	-2.44	-3.62	0.88	-1.06	0.41
1	6.07E-02 ± 0.0041	4	-66.39	-9.71	-8.52	-66.56	-9.04	-8.07	-7.42	-4.56	-5.44
2	2.05E-01 ± 0.0032		-73.5	-32.85	-24.58	-74.07	-31.39	-22.09	-4.96	-3.86	-2.02

* - Relative error L - Layer in pin

1 - 6.7904E+01 eV - 5.5595E+01 eV;

2 - 2.2603E+01 eV - 1.9455E+01 eV

A - GSM0-NOLJ B - GSM1-NOLJ C - GSM2-NOLJ D - GSM0-LJ

E - GSM1-LJ F - GSM2-LJ G - SUBG H - RIB I - RIB-CORR

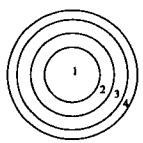

Table 5.7 Capture rate in ^{239}Pu in resolved resonance group obtained using various self shielding models

Fine Group in resolved resonance group	Capture rate in ^{239}Pu ($cm^{-3}s^{-1}$) (MCNP5)	Relative error with respect to MCNP5 (in %)									
		L	A	B	C	D	E	F	G	H	I
1	3.84E-03 ± 0.0023*	1	36.96	30.08	37.14	36.37	25.6	37.49	36.43	36.59	14.37
2	1.10E-02 ± 0.0031		12.48	3.44	11.12	11.92	0.25	11.05	10.28	10.37	2.08
1	4.17E-03 ± 0.0021	2	30.77	28.78	32.32	30.18	26.76	32.69	32.51	32.66	10.43
2	1.20E-02 ± 0.0028		5.56	3.58	7.59	5.02	1.99	7.66	7.58	7.66	0.47
1	4.62E-03 ± 0.0021	3	20.95	26.97	22.46	20.37	27.95	22.16	24.48	24.59	4.13
2	1.29E-02 ± 0.0029		0.39	9.84	4.5	-0.14	10.64	4.73	5.63	5.72	-0.51
1	5.16E-03 ± 0.0022	4	9.67	26.47	15.63	9.14	27.41	16.07	14.18	14.27	-3.42
2	1.35E-02 ± 0.0031		-3.22	22.15	4.86	-3.74	23.03	5.86	3.66	3.76	-1.87

* - Relative error L Layer in pin

1 - 6.7904E+01 eV - 5.5595E+01 eV;

2 - 4.5517E+01 eV - 4.0169E+01 eV

A - GSM0-NOLJ B - GSM1-NOLJ C - GSM2-NOLJ D - GSM0-LJ

E - GSM1-LJ F - GSM2-LJ G - SUBG H - RIB I - RIB-CORR

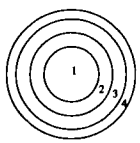

Table 5.8 Capture rate in ^{240}Pu in resolved resonance group obtained using various self shielding models

Fine Group in resolved resonance group	Capture rate in ^{240}Pu ($cm^{-3}s^{-1}$) (MCNP5)	Relative error with respect to MCNP5 (in %)									
		L	A	B	C	D	E	F	G	H	I
1	2.37E-03 ± 0.0054*	1	83.95	60.33	74.14	84.1	60.13	74.16	72.15	70.94	-5.71
2	5.59E-03 ± 0.0044		26.31	12.57	23.07	26.18	11.50	23.05	21.64	21.48	6.86
3	3.15E-03 ± 0.0051		61.98	54.03	62.54	64.18	56.71	70.01	70.84	70.95	17.62
1	2.96E-03 ± 0.0047	2	52.63	46.21	58.06	52.71	46.52	58.33	57.12	57.08	-5.35
2	6.41E-03 ± 0.0040		13.26	10.02	16.26	13.12	9.67	16.41	16.38	16.43	4.31
3	3.95E-03 ± 0.0044		42.11	37.57	42.64	43.61	40.17	47.02	47.72	47.94	8.05
1	3.74E-03 ± 0.0046	3	24.16	41.28	38.65	24.21	42.42	38.87	38.74	39.44	-8.18
2	7.16E-03 ± 0.0041		3.50	16.86	9.05	3.36	18.09	9.00	12.29	12.48	2.45
3	4.91E-03 ± 0.0042		22.63	24.7	22.86	23.64	28.08	26.56	26.64	26.82	-1.98
1	4.47E-03 ± 0.0050	4	5.01	62.84	20.12	5.04	64.00	21.19	23.55	24.64	-12.76
2	7.68E-03 ± 0.0045		-2.57	37.34	12.48	-2.71	38.3	12.85	9.03	9.32	0.56
3	5.86E-03 ± 0.0043		6.50	21.74	7.66	7.26	24.71	11.73	11.80	11.93	-10.03

* - Relative error L - Layer in pin

1 - 6.7904E+01 eV - 5.5595E+01 eV;

2 - 4.5517E+01 eV - 4.0169E+01 eV;

3 - 2.2603E+01 eV - 1.9455E+01 eV

A - GSM0-NOLJ B - GSM1-NOLJ C - GSM2-NOLJ D - GSM0-LJ

E - GSM1-LJ F - GSM2-LJ G - SUBG H - RIB I - RIB-CORR

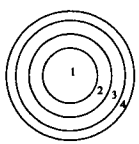

Table 5.9 Capture rate and nu-fission rate in four groups obtained using various self shielding models

Model	Capture rate ($cm^{-3}s^{-1}$)				Nu-fission rate ($cm^{-3}s^{-1}$)			
	1	2	3	4	1	2	3	4
GSM0-NOLJ	0.0803	0.1167	0.4217	0.3905	0.1911	0.0823	0.3917	0.4489
GSM1-NOLJ	0.0803	0.1161	0.4200	0.3904	0.1911	0.0823	0.3881	0.4488
GSM2-NOLJ	0.0803	0.1161	0.4234	0.3905	0.1911	0.0823	0.3931	0.4489
GSM0-LJ	0.0803	0.1164	0.4183	0.3905	0.1911	0.0823	0.3899	0.4489
GSM1-LJ	0.0803	0.1152	0.4112	0.3904	0.1911	0.0822	0.3817	0.4488
GSM2-LJ	0.0803	0.1152	0.4166	0.3905	0.1911	0.0822	0.3935	0.4489
SUBG	0.0803	0.1169	0.4164	0.3905	0.1911	0.0823	0.3935	0.4489
RIB	0.0803	0.1169	0.4160	0.3905	0.1911	0.0823	0.3937	0.4489
RIB-CORR	0.0803	0.1169	0.4123	0.3905	0.1911	0.0823	0.3941	0.4488

CHAPTER 6

DEPLETING A CANDU-6 FUEL ASSEMBLY USING DETAILED BURNUP DATA AND REACTIONWISE ENERGY RELEASE

Temporal behavior of reactor fuel assembly due to neutron exposure is an integral part of lattice analysis. It is important to estimate the production of actinides and fission products as a function of burnup so as to decide the quality of fuel for further energy production. It is also important from the point of view of post irradiation behavior of fuel. The information on heat production during and after irradiation helps in determining the amount of time a fuel assembly needs to be cooled before taking it up for storage or reprocessing. In the present study we have considered the CANDU-6 fuel assembly as reference which is depicted in Figure 3.1. Table 3.1 gives the isotopic composition of materials and description of cell geometry. For this analysis we used the number densities of the fresh fuel provided in Table 3.3.

6.1 Computational scheme used for DRAGON analysis

A custom cross-section library in DRAGLIB format [Hébert 2004] (172 group) was used by the `LIB:` module. The evaluated files for the elements chosen in the library are based on recommendations from the WLUP. APOLLO type transport correction based on the linearly anisotropic scattering cross sections was used for the total and isotropic scattering cross sections. This correction assumes that the micro-reversibility principle is valid for all energy groups. The geometry was tracked using the `EXCELT:` module, using angular quadrature parameter of 11 and track density of 50 lines per cm for both self shielding and flux

calculations. One-twelfth symmetry was considered. The fuel pin was divided into four layers (50%, 30%, 15% and 5% by volume) based on the recommendations made in Santamarina 2004. Six meshes were considered in the coolant and ten meshes were considered in the moderator. Single mesh was considered in all the other regions. Outermost surface was annularized and isotropic reflection was considered. `USS:` module i. e. Ribon extended self shielding model (RIB) was used for performing self shielding calculations. We used the default options for the `ASM:` module to generate collision probabilities. In the `FLU:` module, we used the option of criticality calculations *without* leakage effects. Under the `EVO:` module, we have considered the model where none of the fission products or actinides saturate. We obtained the solution of the Bateman equations using fourth order Kaps-Rentrop algorithm [Press 1994] without extrapolation of reaction rates at the beginning and end of burnup step. The Bateman equations are solved individually for each of four layers in each fuel ring. We have considered a value of 31.9713 kW/kg for power normalization.

6.2 Scope of study

In libraries generated under the auspices of WLUP, it is mentioned that the energy for normalization is calculated as a sum of fission energy minus neutrino energy, energy due to capture and incident neutron energy. Power normalization is performed in most of the codes using fission rate and associated energy (like that provided in WLUP). In the present study we have attempted to perform power normalization more explicitly considering decay energy and with most of neutron induced reactions and their associated energies. Three sets of studies were carried out. In the first and second study we prepared the complete burnup chain and included energies from all reactions. In the first study power normalization was done using energy from fuel alone, henceforth referred to as 'MODEL-1', while we considered energy from all mixtures in the lattice for the second study, henceforth referred to as 'GLOB'. In the third study we considered the recommended energy values for actinides from WLUP,

henceforth referred to as 'MODEL-2'. The recommended energy values were multiplied with the fission rate and used for power normalization.

For sake of continuity, we will now briefly present certain formulae that have been used for the analysis. These formulae were already mentioned in the chapter explaining the various self shielding and burnup models in DRAGON Version 4. Power normalization is done as

$$A\phi + D = B \tag{6.1}$$

where $A\phi$ is the contribution due to neutron induced reactions, D is the energy due to decay process and B is the power for normalization of fluxes. By considering decay energy as part of normalization, one can analyze the behavior of fuel assembly and heat generated thereof when it is cooled away from the reactor. In general,

$$A\phi = \sum_{m=1}^{MIX} \sum_{l=1}^{L} \sum_{x=1}^{NREAC} Q_{xlm} \langle \sigma_{\mathrm{x},lm}\phi \rangle N_{lm} \tag{6.2}$$

where Q_{xlm} is energy associated with reaction x for element l of mixture m, while $\sigma_{\mathrm{x},lm}$ is the microscopic cross section of element l for reaction x of mixture m and N_{lm} is the number density of element l of mixture m. $\langle \sigma_{\mathrm{x},lm}\phi \rangle$ represents summation of reaction rates over all energy groups. 'NREAC' represents the eleven types of reactions taken into consideration, as mentioned before. L represents all the fission products and actinides considered in burnup chain. MIX represents the different mixtures in the study, which includes fuel, coolant, clad, moderator, pressure tube, calandria tube and helium cover gas. In 'MODEL-1', MIX includes only the fuel mixture, but in 'GLOB' option it includes all the mixtures. In the 'MODEL-2',

$$A\phi = \sum_{m=1}^{MIX} \sum_{l=1}^{L} Q_{flm} \langle \sigma_{\mathrm{f},lm}\phi \rangle N_{lm} \tag{6.3}$$

where Q_{flm} is energy recommended by WLUP, while $\sigma_{\mathrm{f},lm}$ is the microscopic fission cross

section of actinides and N_{lm} is the number density of actinides considered in burnup chain. MIX represents only the fuel mixtures. The difference in k_∞ is calculated as

$$\delta k_\infty = k_\infty(MODEL-2) - k_\infty(MODEL-1 or GLOB) \ . \tag{6.4}$$

The difference in relative contribution of pin in each ring is defined as

$$\Delta E_p = (E_p(MODEL-2) - E_p(MODEL-1)) * 100/E_p(MODEL-1) \tag{6.5}$$

where $E_p(MODEL-2)$ and $E_p(MODEL-1)$ is the contribution to power normalization (in %) using 'MODEL-2' and 'MODEL-1' respectively.

6.3 Numerical results

Figure 6.1 gives the variation in k_∞ as a function of burnup for the three sets of calculations. Figure 6.2 gives the variation in Δk_∞ as a function of burnup for 'MODEL-2' with respect to 'MODEL-1' and 'GLOB' option. It can be observed in Figure 6.2 that Δk_∞ with respect to 'MODEL-1' is positive throughout as a function of burnup, the maximum being 1.66 mk at 8 GWd/T, which is typically the discharge burnup for CANDU-6 fuel. When we used the 'GLOB' option the Δk_∞ is still positive but lower compared to that using 'MODEL-1' with a maximum of 1.1 mk at 7 GWd/T. Figure 6.3 shows the variation in normalized flux as a function of burnup. Since the energy considered for fission reaction rate is higher ('MODEL-2'), the flux to produce the normalized power is lower. As a result, the depletion happens at a slower rate compared to the 'MODEL-1'. As a function of burnup the difference reduces and there is a crossover close to 20 GWd/T with flux from 'MODEL-1'. Similar such observation is made for 'GLOB' option, but the cross over with normalized flux from 'MODEL-2' occurs much earlier at 13 GWd/T. This seems to indicate for CANDU analysis,

the 'MODEL-2' data somewhat over estimates the energy produced. It may be due to consideration of PWR spectrum to quantify the energy, while in the present case it is a heavy water reactor spectrum. It will be interesting to see the effect of the different approaches on a PWR lattice.

In most of the reactor codes, power normalization is mainly done using energy from fuel alone. Hence in subsequent discussions, we have attempted to explain the effect of explicit treatment of energy channels on burnup behavior taking into consideration the 'MODEL-1'. Figures 6.4, 6.5 and 6.6 gives the variation with burnup of energy contribution from (n, f), (n, γ), $(n, 2n)$. It can be observed from Figure 6.4 that the contribution of (n, f) towards power normalization varies from 97.1% at zero burnup to 95.3% at 8 GWd/T, while the contribution by energy from (n, γ) reaction varies from 2.92% at zero burnup to 4.72%, as seen in Figure 6.5. A small contribution by $(n, 2n)$ reaction was observed in Figure 6.6 and it varies from -0.006% to -0.008%. Contributions from other reactions were observed to be very low, as most of them have a high threshold, and the number of such neutrons available in a thermal reactor is low. It would nevertheless be interesting to apply this model for intermediate or fast spectrum lattices and evaluate the contribution from these threshold reactions. Figures 6.7 and 6.8 shows the variation in contribution to power normalization due to (n, f) and (n, γ) respectively from actinides like ^{235}U, ^{238}U, ^{239}Pu, and ^{241}Pu. The contribution from ^{235}U varies from 92.6% at zero burnup to 25% at 8 GWd/T, while it varies from 4.5% to 5.8% for ^{238}U. The contribution from ^{239}Pu increases as a function of burnup and is close to 57% at 8 GWd/T while it is close to 7.2% from ^{241}Pu. It can be observed in Figure 6.8 that maximum contribution due to (n, γ) reaction towards power normalizations is from ^{238}U, which is around 2.4%. Figure 6.9 shows the contribution towards power normalization from a representative pin from each fuel ring in a CANDU-6 cluster. It is close to 2.1% for the central pin, 2.2% for pin in second ring, 2.5% for pin in the third ring and 3.1% for pin in the outermost ring. Figure 6.10 shows the relative contribution of pin in each ring towards power normalization between 'MODEL-1' and 'MODEL-2'. It can be seen in Figure

6.10 that energy contribution from outermost ring is under-predicted when one considers no explicit break up in energy contribution, while it is over-predicted in the other three rings.

6.4 Conclusions

A burnup analysis of CANDU-6 has been performed using DRAGON Version4. We have for the first time attempted to use detailed energy distribution from individual reactions towards power normalization. We observe that the k_{∞} is over-predicted as a function of burnup when one considers energy recommended by WLUP for power normalization. The maximum deviation with respect to 'MODEL-1' being 1.6 mk at, typical discharge burnup for CANDU-6, 8 GWd/T, and 1.1 mk with respect to 'GLOB' option at 7 GWd/T. We have estimated the contribution due to individual reactions towards power normalization. We observe at discharge burnup that 95.3% of energy contribution comes due to fission reaction, while 4.7% is due to capture, of which 0.8% is from fission products. There are no pseudo fission products in the burnup chain.

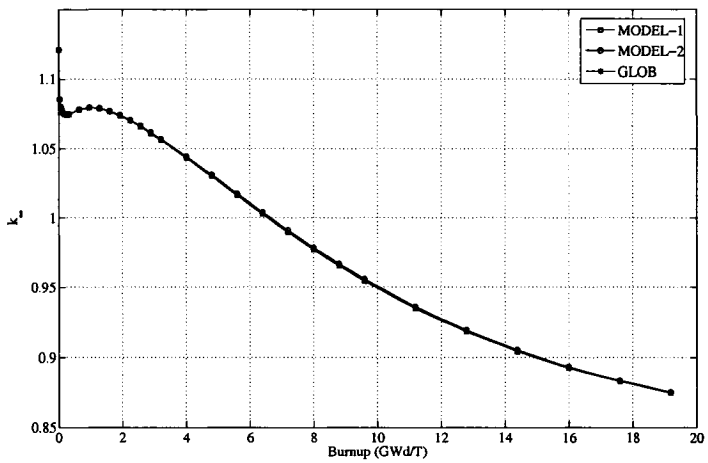

Figure 6.1 Variation in k_∞ as a function of burnup

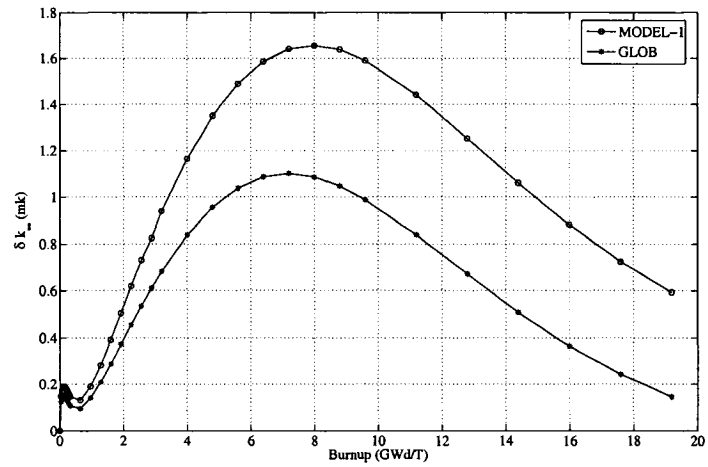

Figure 6.2 Variation in δk_∞ of 'MODEL-2' w.r.t 'MODEL-1' and 'GLOB' option as a function of burnup

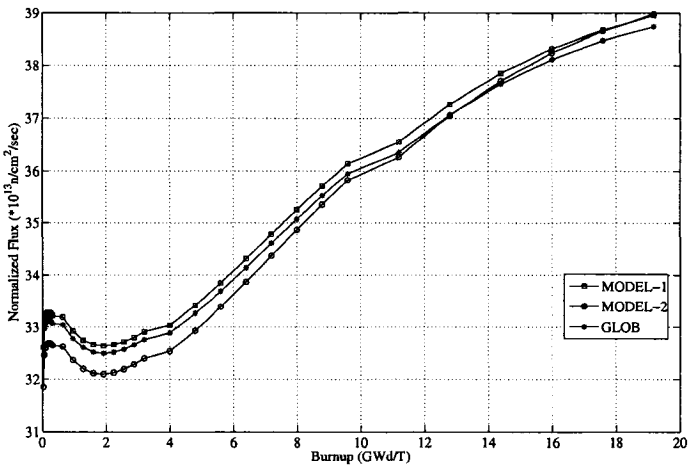

Figure 6.3 Variation in normalized flux as a function of burnup

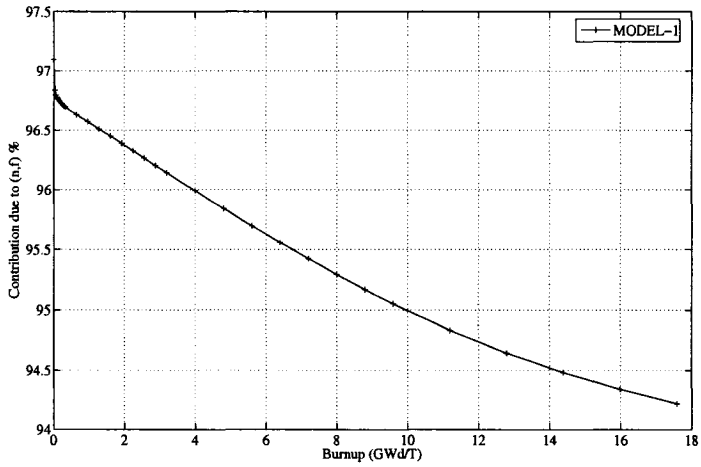

Figure 6.4 Contribution of (n, f) to power normalization ('MODEL-1') as a function of burnup

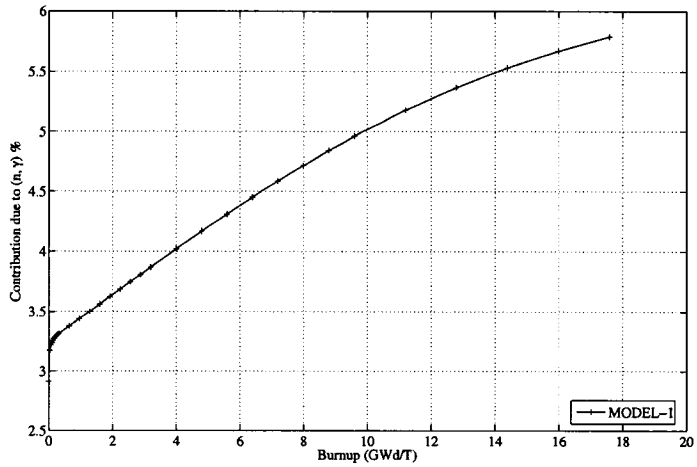

Figure 6.5 Contribution of (n, γ) to power normalization ('MODEL-1') as a function of burnup

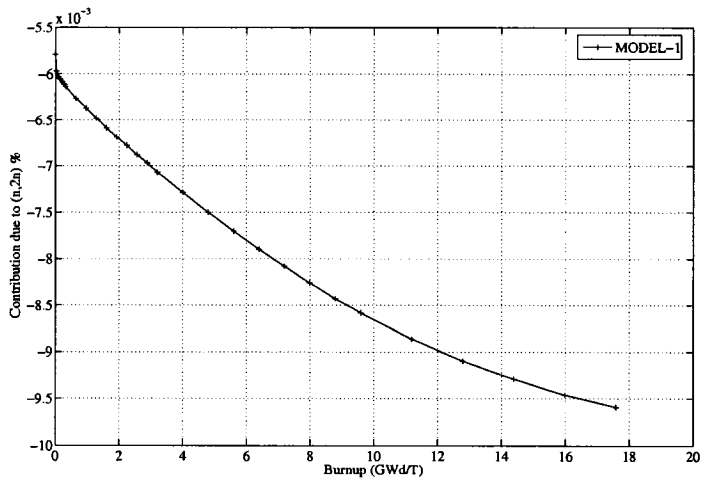

Figure 6.6 Contribution of $(n, 2n)$ to power normalization ('MODEL-1') as a function of burnup

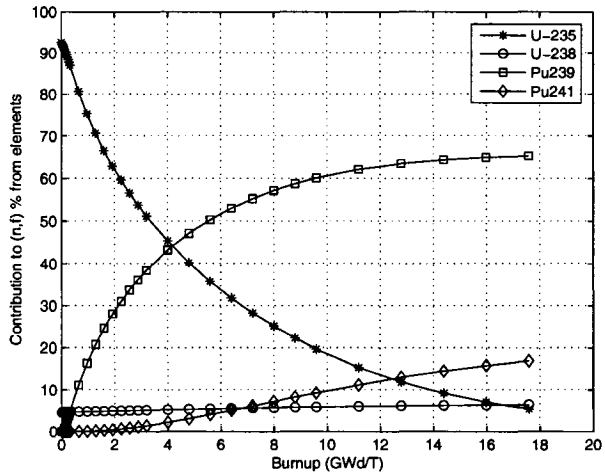

Figure 6.7 Contribution of (n, f) to power normalization by selected actinides ('MODEL-1') as a function of burnup

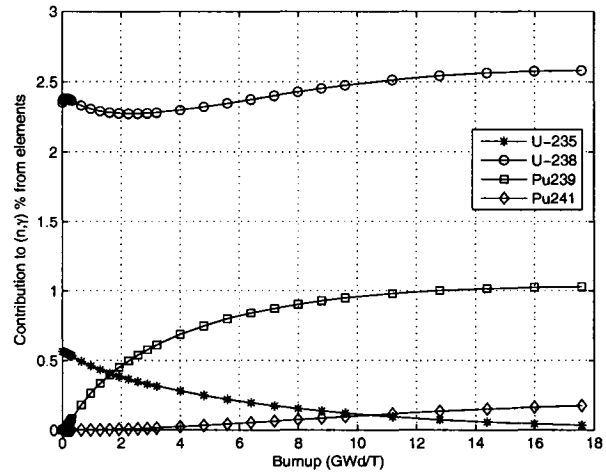

Figure 6.8 Contribution of (n, γ) to power normalization by selected actinides ('MODEL-1') as a function of burnup

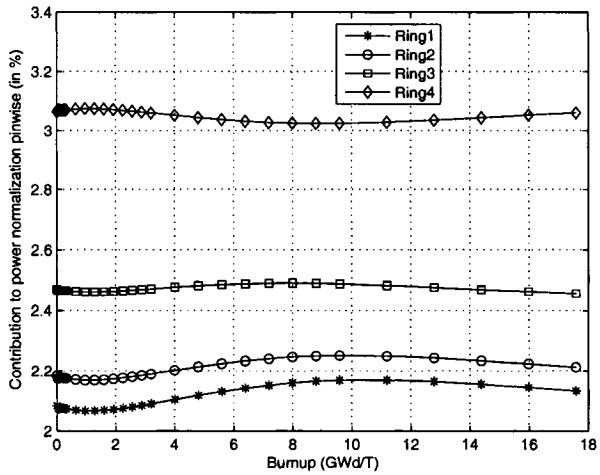

Figure 6.9 Pinwise contribution to power normalization ('MODEL-1') as a function of burnup

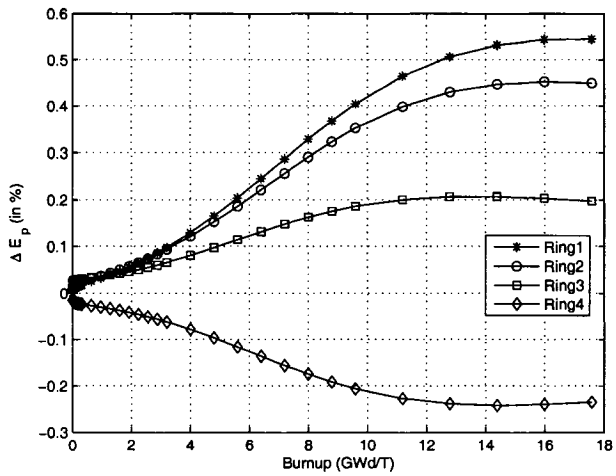

Figure 6.10 Variation in ΔE_p as a function of burnup

CHAPTER 7

DEPLETION OF A PWR THORIUM PINCELL USING DETAILED BURNUP DATA AND REACTIONWISE ENERGY RELEASE USING DRAGON AND VALIDATION WITH MONTEBURNS

Nuclear energy is being seriously considered as one of the safest options for future large scale energy production, owing to its minimal contribution to greenhouse emissions. Present nuclear reactors are fueled mainly by uranium and its various compounds, which include uranium oxide like for PWRs, CANDU and uranium carbide in the form of TRISO particles for high temperature reactors. Lots of studies are being performed with MOX fuels, which include utilization of reactor grade and weapon grade plutonium along with uranium fuels. There is always a constant fear of proliferation of these nuclear materials and there is a focus for fuel that can be proliferation resistant. Thorium fuel is thus gaining popularity and will become a necessary part of nuclear energy production, owing to the dwindling uranium resources. Research on thorium fuel and its ultimate use as reactor fuel is gaining grounds in countries like India, where new reactor concepts based on thorium are being studied/constructed. We have thus chosen the PWR pincell for our analysis, in order to study the effect of detailed burnup data and reactionwise energy release incorporated in DRAGON Version4 for fuels based on thorium.

In this chapter we will present the burnup dependent behaviour of a typical PWR thorium pincell. It is a pincell excised from a standard 17x17 pin assembly typical of large Westinghouse PWRs. This pincell benchmark was analysed earlier [Zhao 2000] using codes MOCUP (MCNP4B+ORIGEN2) and CASMO-4. Eigenvalue and isotope concentrations

were compared up to a very high burnup.

7.1 Computational scheme used for DRAGON analysis

In the LIB: module, we used library based on DRAGLIB format which included a total of 178 nuclides (25 actinides, 150 fission products and 3 structural elements). The evaluated nuclear data files for all the elements were chosen on the basis of recommendations from WLUP [Leszczynski 2003]. Under the GEO: module we considered the square pincell with mirror reflective boundary condition on all surfaces. The geometry was tracked with an angular quadrature parameter of 11 and track density of 50 lines per cm, which was found adequate. For the self shielding calculation, the coolant was not split into fine regions, while we considered ten regions in the coolant for flux calculation. We considered only one ring in the fuel. The tracking of the geometry was performed using the EXCELT: module. The APOLLO type transport correction based on the linearly anisotropic scattering cross sections was used for the total and isotropic scattering cross sections. We have used the 'SUBG' keyword to generate physical probability tables using temperature interpolated cross section as input. The intermediate resonance treatment of using statistical model up to 81 groups and wide resonance model beyond was used. We used the USS: module to perform self shielding calculations, which is the subgroup approach using physical probability tables. We used the default options in ASM: module for generation of collision probabilities. In the FLU: module, we used the option of criticality calculations *without* leakage effects. In the EVO: module we obtained the solution using the 4^{th} order Kaps-Rentrop algorithm. We didn't consider linear extrapolation of the microscopic reaction rates in the solution of the burnup equations. Saturated number densities were calculated without considering Dirac distribution model. Power was normalized to 38.1347 KW/KgHM and fluxes were estimated to deplete the fuel.

7.2 Scope of study

Table 7.1 gives the isotopic composition of materials and description of cell geometry. Figure 7.1 gives the pincell model used for the analysis. The depletion of PWR thorium pincell was carried out in three different ways. The first way was to deplete the pincell using the complete burnup chain and energies from all neutron induced reactions, henceforth referred to as 'MODEL-1'. In the second way we modified the library to include energy per fission as recommended by the WLUP. The energies of all other reactions and for all elements was set to zero. This energy together with fission rate will be used for power normalization and will henceforth be referred to as 'MODEL-2'. The third way was to use the code MONTEBURNS with modifications mentioned earlier and presented in Appendix V. The k_{∞}, number density of important actinides and fission products obtained using DRAGON have been compared with that obtained using the code MONTEBURNS.

7.3 Validation using MONTEBURNS

Four files are important for execution of MONTEBURNS. One is the MCNP input file, followed by MONTEBURNS input file which describes number of materials to burn, power for normalization, outer burn steps, inner burn steps between each outer burn step and number of predictor steps. The third file is the feed file which is used to describe the burn steps and also the material that is removed or fed into the system. The fourth file is the cross section file that is used by MCNP for analyses. For our analyses we generated ACE files using NJOY 99.90 for all the nuclides and have made a custom cross section library.

One million neutron histories were used to obtain the k_{∞} in MCNP5. For ORIGEN calculations, we considered ten outer burnup steps and forty inner burnup steps for each outer burnup step. We used the option in MONTEBURNS to determine the k_{∞} at intermediate

steps too. We also considered the option of tracking all the fission products and actinides which form part of the DRAGLIB library. An external library was provided with information related to half lives of all nuclides, decay energy and energies corresponding to most neutron induced reactions for each element. This file was used in the modified MONTEBURNS routine to calculate the normalization factor to obtain fluxes to deplete the fuel in code ORIGEN. We have provided the value of 0.0001692 MW for power normalization, which was obtained in the following way. The power density is 38.1347 KW/KgHM and the radius of the fuel pellet is 0.41274 cm. The oxide density of fuel is 9.424 g/cc. Therefore the power (in MW) supplied to MONTEBURNS is evaluated as

$$Power = \pi \times 0.41274 \times 0.41274 \times 9.424 \times 38.1347 \times 1e\text{-}6 \times 0.87974$$

$$= 0.0001692 \text{ MW}$$

where 0.87974 is the heavy metal fraction.

7.4 Numerical results

Figure 7.2 gives the typical spectrum seen by PWR thorium pincell. It can be seen that the peak of the Maxwellian spectrum is at about 0.067 eV. The shape beyond the Maxwellian is a typical 1/E shape with dips at major resonances of ^{232}Th and ^{238}U. Figure 7.3 shows the variation of k_∞ as a function of burnup obtained using MODEL-1 and MONTEBURNS. It can be seen that there is almost a linear fall in k_∞ as a function of burnup. For the sake of

discussion we define a quantity δK as

$$\delta K = [k_\infty(state) - k_\infty(ref)] \ . \tag{7.1}$$

Equation 7.1 is used to calculate the deviation in k_∞ with respect to a reference. The maximum difference in k_∞, when MONTEBURNS is taken as reference, is of the order of 6 mk but reduces close to end of burnup, as seen in Figure 7.4. The standard deviation obtained using MCNP5 is of the order of 50 pcm for all burnups. The zig zag nature of curve could possibly be smoothened when one considers larger number of histories. As each burnup step takes a lot of time due to tracking of many fission products and actinides, we have restricted the results to that obtained using one million histories.

Figure 7.4 also shows the variation of δK as a function of burnup, obtained using 'MODEL-2' as reference. It can be observed that the δK continuously decreases when one considers explicit division of energies and respective reaction rates as against combined energy and fission rate. Figure 7.5 shows the comparison of normalization flux obtained using the two modes of power normalization and that obtained using MONTEBURNS. It can be seen that the normalization flux obtained using 'MODEL-2' lies in between that of 'MODEL-1' and MONTEBURNS. Since the flux is higher when one considers 'MODEL-1', there is quicker depletion of fuel and hence lower k_∞.

We next compared the number densities obtained using 'MODEL-1' of DRAGON and MONTEBURNS. In order to justify the choice of nuclides that needs to be compared, we performed a study to determine the contribution towards absorption rate due to fission products and actinides, as a function of burnup. It can be observed from Figure 7.6 that the contribution to absorption rate due to actinides reduces from 100% to about 79% at the end of

burnup while the contribution to absorption rate due to fission products increases from zero to about 21%. The major contributor to absorption rate due to fission products is from ^{135}Xe (94.81%), ^{149}Sm (2.48%) and ^{105}Rh (1%), when fuel is relatively fresh. But as a function of burnup, other fission products begin to contribute and the main contributors at about 60,000 MWd/T are given in Table 7.2. The contribution to absorption rate due to the listed fission products is about 91% of the total contribution due to all fission products. Similarly Table 7.3 gives the contribution due to the actinides at 60,000 MWd/T. The listed actinides contribute almost 98% to the total absorption rate of actinides alone. It can be noted in general that the number densities of fission products estimated by both the codes match quite well. Large deviations are observed in prediction for ^{135}Cs. For certain other elements like ^{149}Sm and ^{150}Sm, the deviation in prediction is about 10-15%. The reason for the large deviation can be attributed to the fission product yields with respect to the considered isotopes and their respective parents between ORIGEN and DRAGON. We didn't modify the yields provided in ORIGEN libraries, as we were considering it as reference solution. It can be noted that in general, the relative difference in estimation of major actinides by DRAGON with respect to MONTEBURNS is within 5%. For certain minor actinides like ^{237}Np the deviation in estimation is slightly higher. The plutonium isotopes estimated by DRAGON is within 10% with respect to MONTEBURNS. Figures 7.7 to 7.13 give the burnup behaviour of selected nuclides obtained using DRAGON and MONTEBURNS. It can be observed that the burnup dependent behaviour of important nuclides compares well between the two codes.

Figures 7.14 to 7.19 give the power normalization contribution due to different reactions and nuclides, that are part of the burnup chain, obtained using DRAGON Version4. It can be observed in Figure 7.14 that the contribution to power normalization is predominantly due to (n, f) reaction and it varies from 97.5% to about 95% at about 60,000 MWd/T. Figure 7.15 shows the contribution to power normalization due to (n, γ) reaction. The contribution increases from 2.5% to about 5% at 60,000 MWd/T. The contribution to (n, γ) reaction by

fission products is about 1.3% at about 60,000 MWd/T. It is interesting to note that the energy released per (n, γ) reaction by fission products is about 6%, while for the actinides it is about 4.7% at 60,000 MWd/T. Figure 7.16 shows that there is a small negative contribution due to $(n, 2n)$ reaction. It varies from -0.01% to -0.014%. Figure 7.17 gives the contribution to (n, f) reaction due to individual actinides. It can be noted that maximum contribution is from ^{235}U. However it reduces as a function of burnup as expected. It is interesting to note the contribution from ^{233}U, which increases to about 40% at 60,000 MWd/T. In fact the contribution due to ^{233}U becomes more than ^{235}U close to 47,000 MWd/T. The contribution due to the fissile plutonium nuclides ^{239}Pu and ^{241}Pu is close to about 26% at 60,000 MWd/T. However it can be seen in Figure 7.18 that the (n, γ) contribution from ^{239}Pu is higher than that of ^{233}U as a function of burnup. This is mainly due to more radiative captures in ^{239}Pu when compared to ^{233}U. Figure 7.19 compares the contribution to (n, γ) reaction due to the two fertile elements ^{232}Th and ^{238}U. It is interesting to note that the ratio of number densities between ^{232}Th and ^{238}U is almost four, but the ratio of contribution to (n, γ) reaction is only two times. Table 7.4 compares the energy contribution towards power normalization obtained from the two codes MONTEBURNS and DRAGON. It can be observed that they match quite well as a function of burnup.

7.5 Conclusions

Burnup behaviour of a typical PWR thorium pincell was carried out using code DRAGON Version4. The power normalization was performed using energies from all neutron induced reactions. The results were validated with that obtained using MONTEBURNS. It was noticed that the k_∞ predicted by DRAGON was close to that obtained using MONTEBURNS. The number densities was predicted within 5% for most of the actinides. It can thus be concluded that the burnup dependent behaviour of a PWR thorium pincell is modelled correctly by DRAGON vis-à-vis MONTEBURNS. It was also noted that when energies from

all neutron induced reactions are considered, the depletion of the fuel was increased. Also, the energies for power normalization corresponding to fission, capture and $(n, 2n)$, obtained using the two different codes DRAGON and MONTEBURNS match quite well.

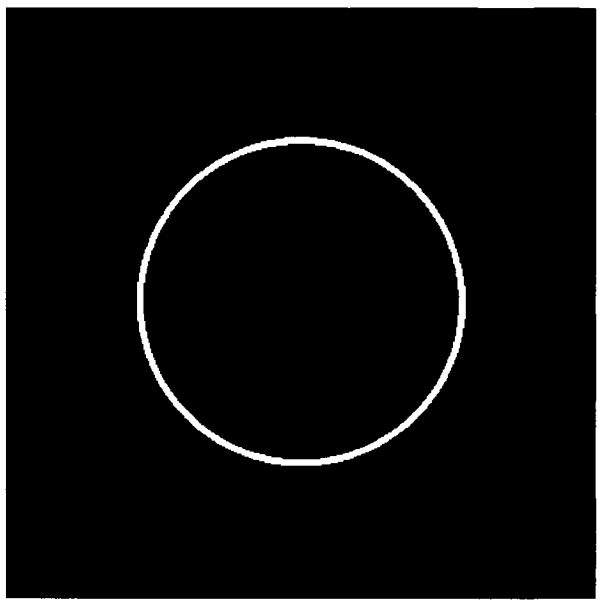

Figure 7.1 PWR thorium pincell

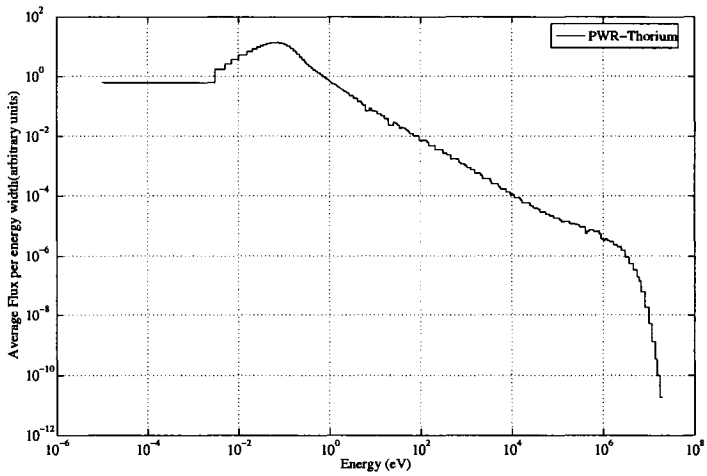

Figure 7.2 Typical spectrum in a PWR thorium pincell

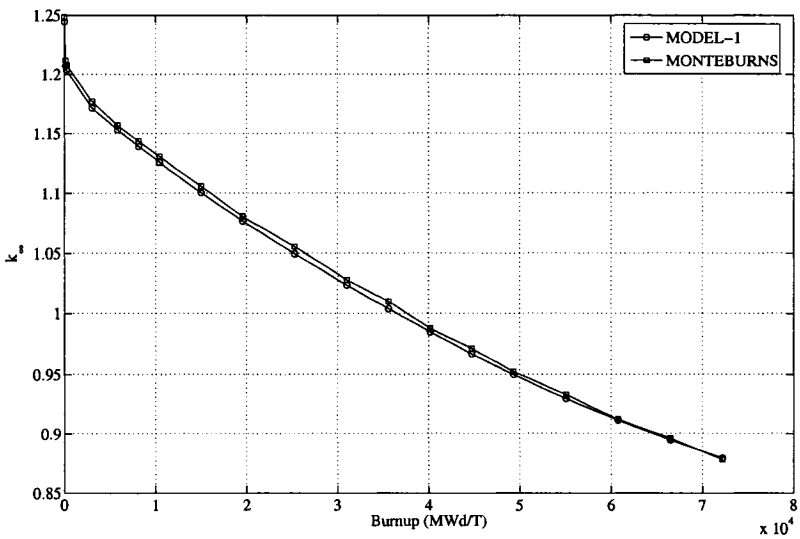

Figure 7.3 Variation of k_{∞} as a function of burnup

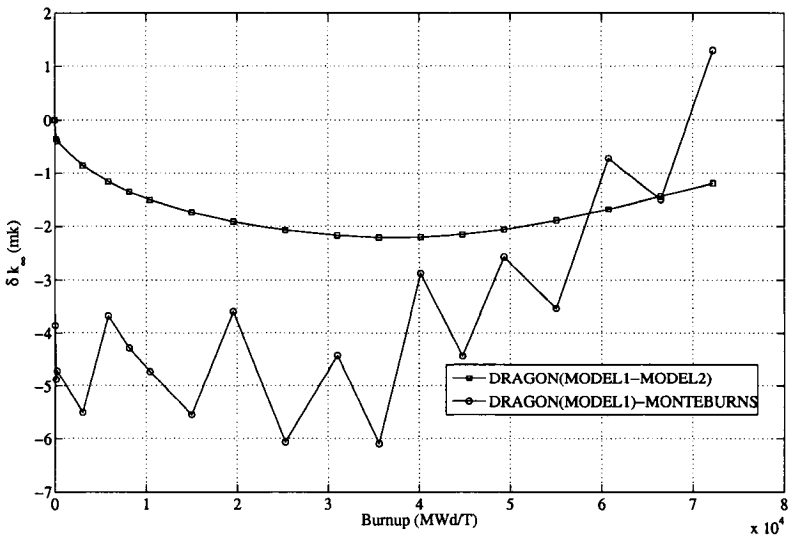

Figure 7.4 Variation of δk_{∞} as a function of burnup

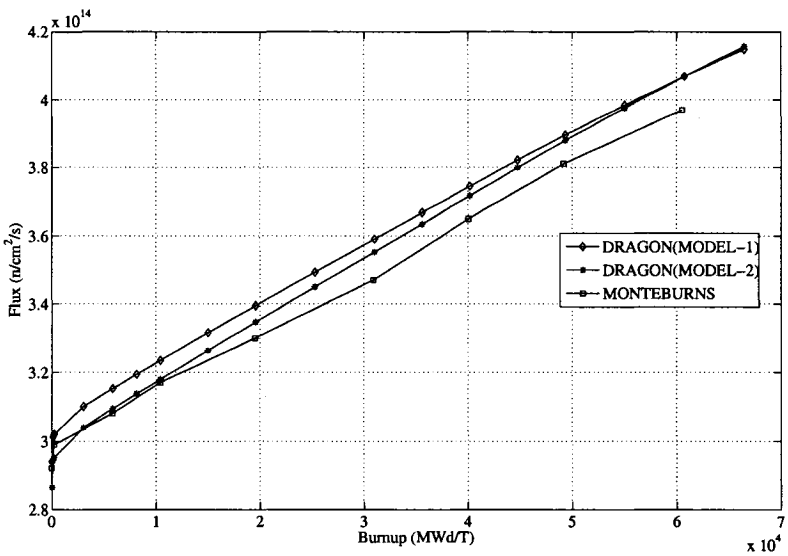

Figure 7.5 Comparison of fluxes as a function of burnup obtained using various models

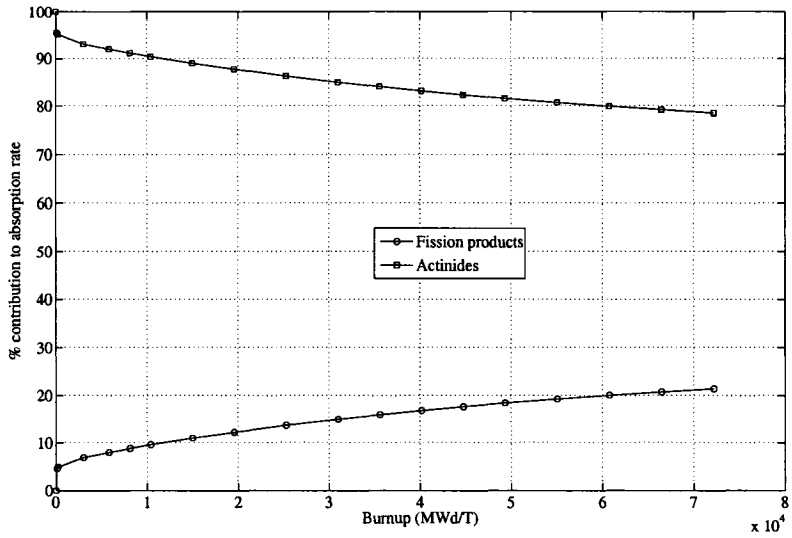

Figure 7.6 Contribution (in %) to absorption rate from fission products and actinides as a function of burnup

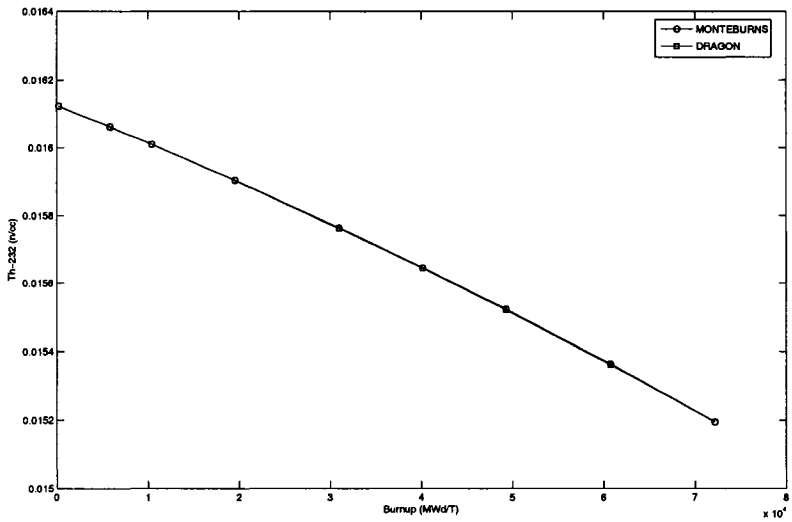

Figure 7.7 Comparison of ^{232}Th number density as a function of burnup

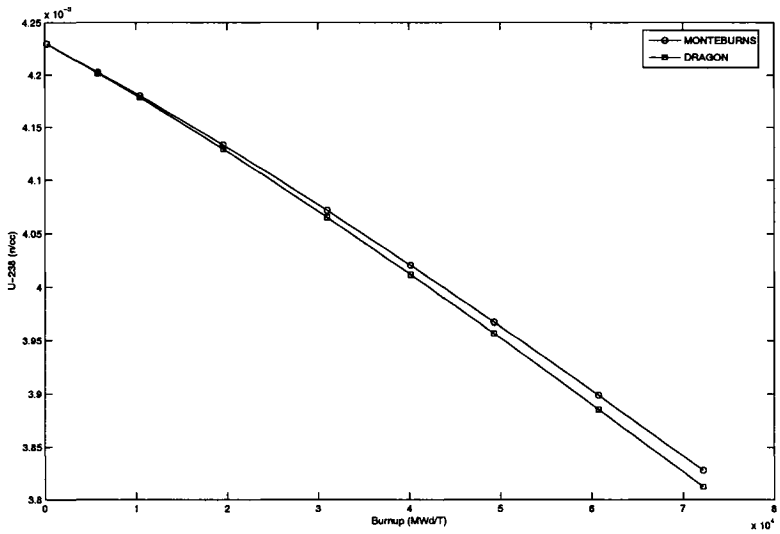

Figure 7.8 Comparison of ^{238}U number density as a function of burnup

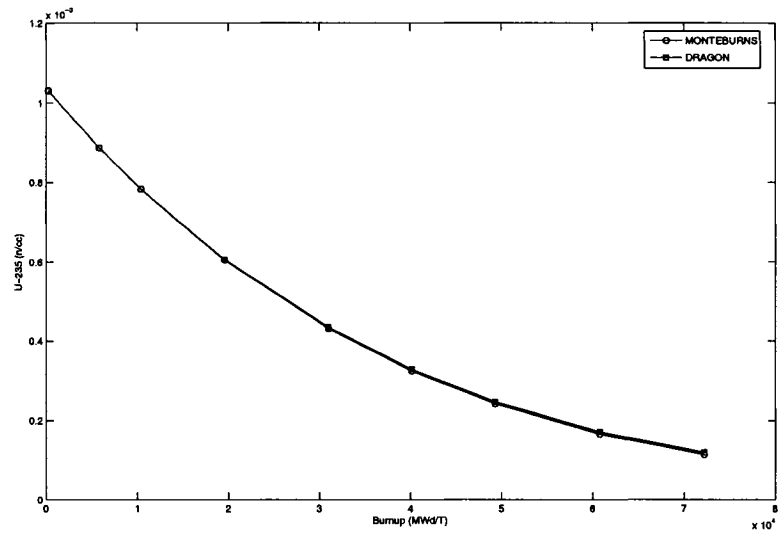

Figure 7.9 Comparison of ^{235}U number density as a function of burnup

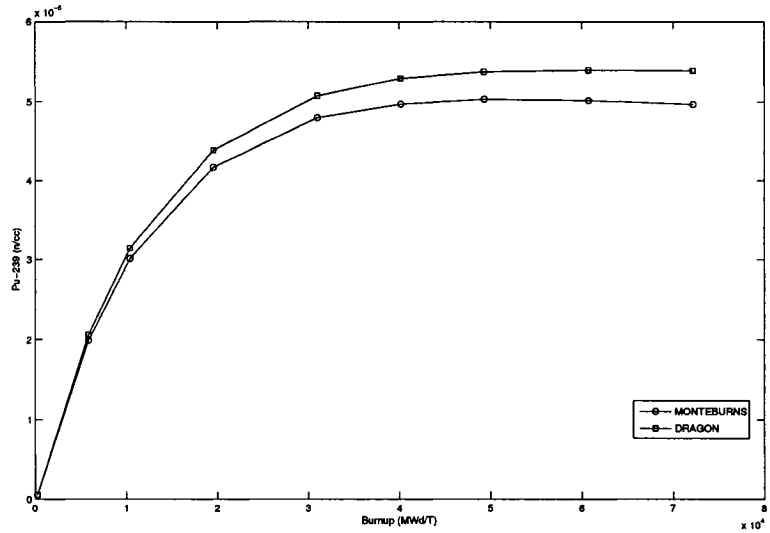

Figure 7.10 Comparison of ^{239}Pu number density as a function of burnup

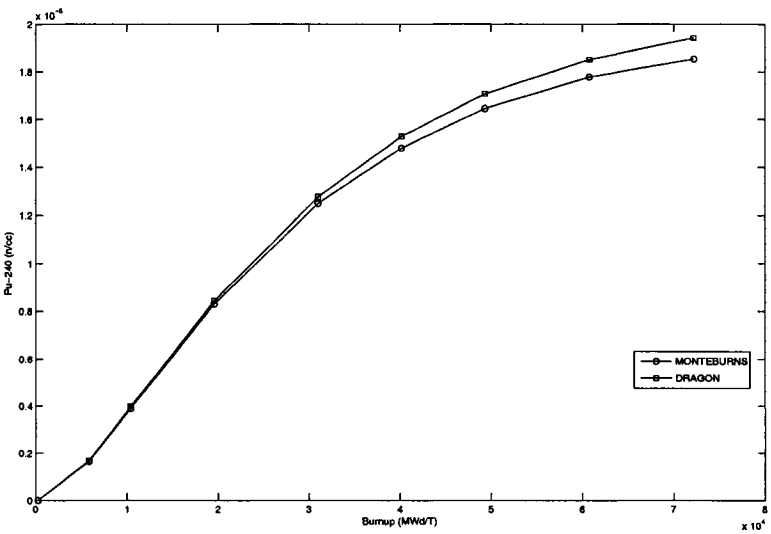

Figure 7.11 Comparison of ^{240}Pu number density as a function of burnup

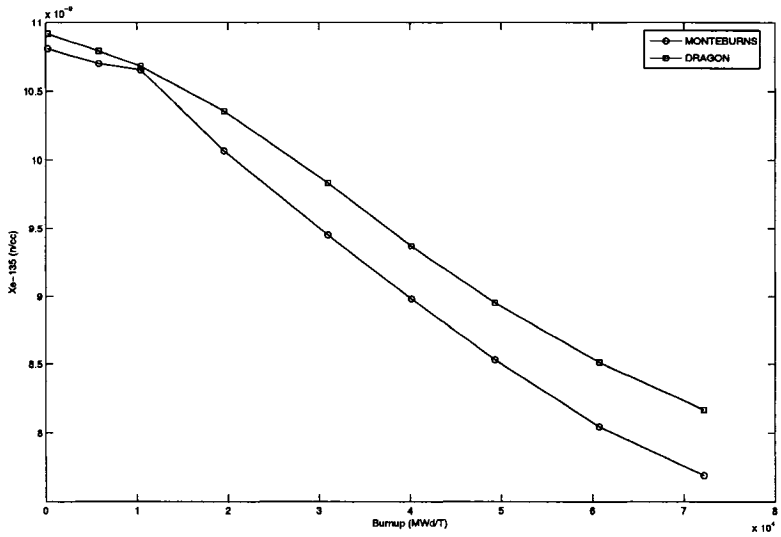

Figure 7.12 Comparison of ^{135}Xe number density as a function of burnup

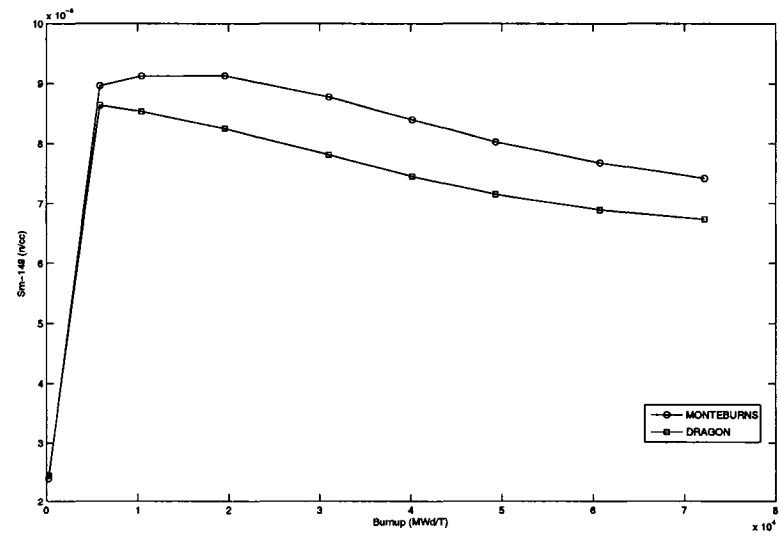

Figure 7.13 Comparison of ^{149}Sm number density as a function of burnup

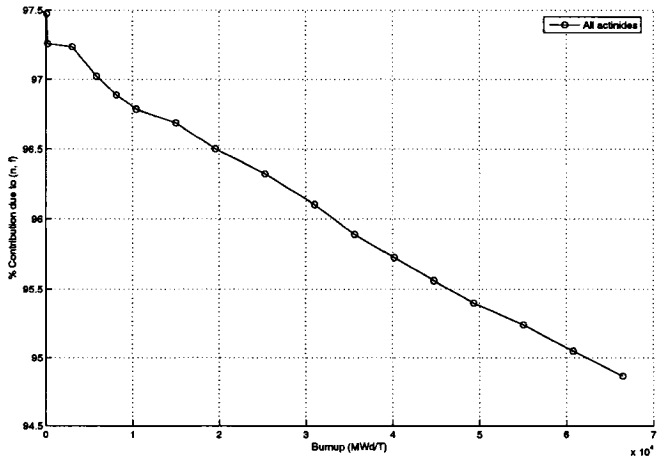

Figure 7.14 Contribution to power normalization due to energy from fission

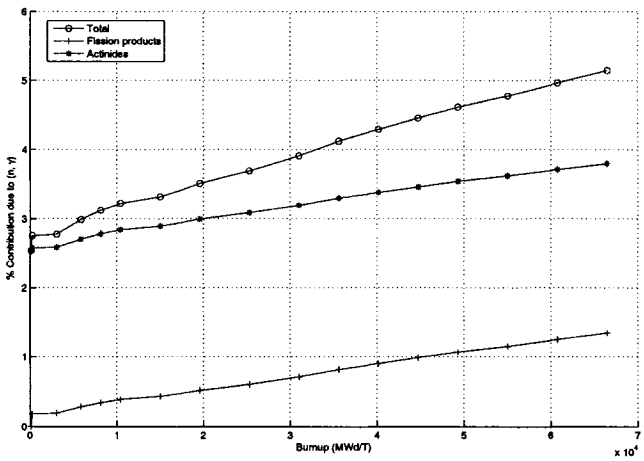

Figure 7.15 Contribution towards power normalization due to energy from (n, γ) reaction

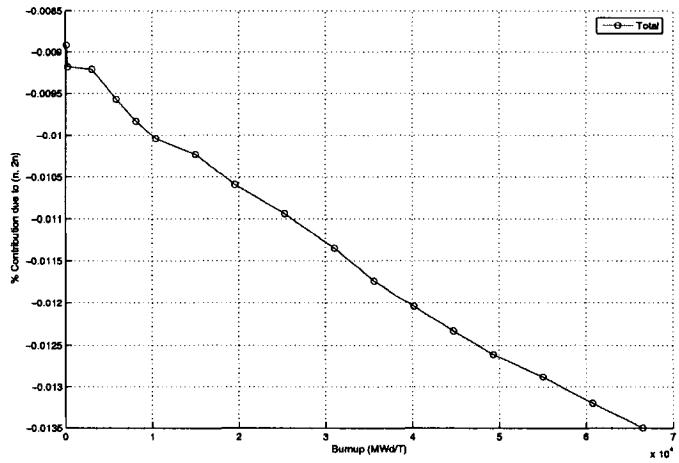

Figure 7.16 Contribution to power normalization due to energy from $(n, 2n)$ reaction

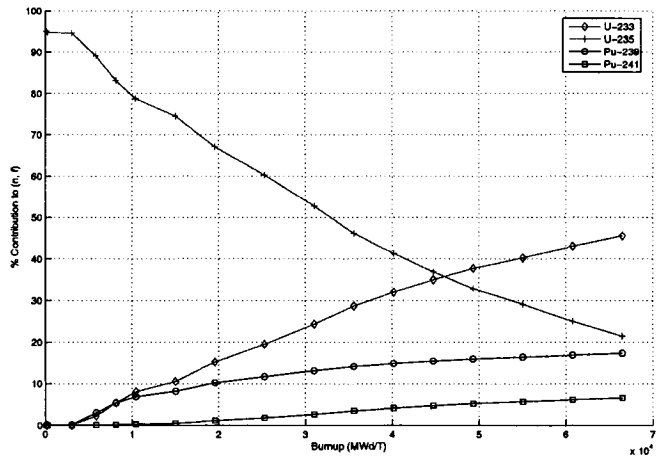

Figure 7.17 Contribution to power normalization due to energy from fission of important actinides

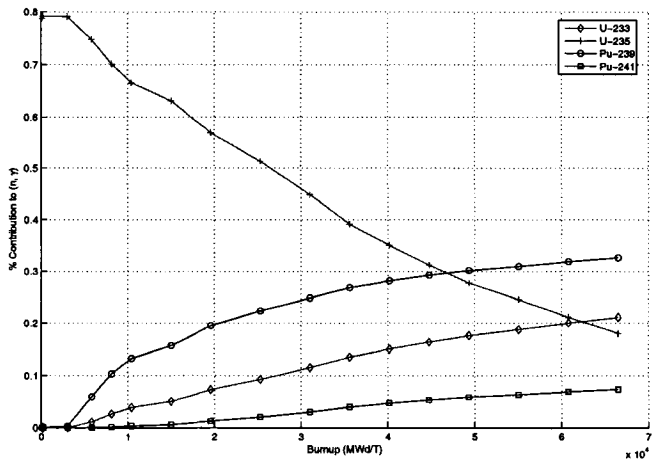

Figure 7.18 Contribution to power normalization due to energy from (n, γ) reaction of important actinides

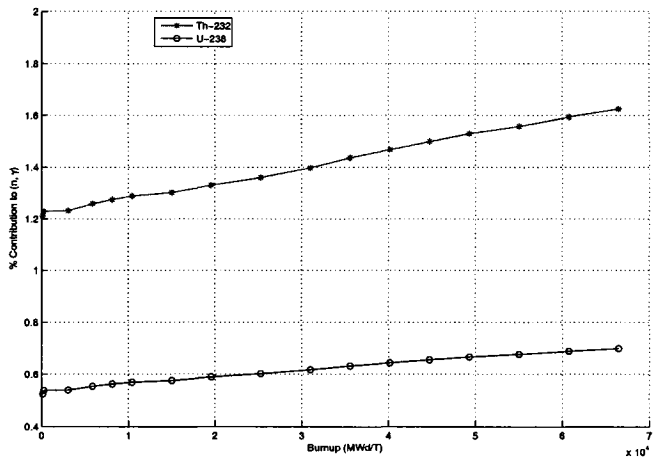

Figure 7.19 Contribution to power normalization due to energy from (n, γ) reaction of ^{232}Th and ^{238}U

Table 7.1 Modified PWR thorium pincell benchmark specifications

Parameter	Hot Full Power
Fuel Temperature(K)	900
Power Density (KW/KgHM)	38.1347
Fuel Density (g/cm^3)	9.424
Cladding Temperature(K)	621
Coolant Temperature(K)	573.6
Fuel Pellet Radius (cm)	0.41274
Cladding Inner Radius (mm)	0.41896
Cladding Outer Radius (mm)	0.47609
Pin Pitch (mm)	1.2626

Initial Compositions (at Hot Full Power Conditions)

Region	Nuclide	Weight Percent (%)	Number Density (atoms per barn-cm)
Fuel	Th-232	65.909	1.61215E-02
	U-234	0.034	8.24518E-06
	U-235	4.291	1.03615E-03
	U-238	17.74	4.22957E-03
	O-16	12.026	4.26835E-02
Cladding	Zirconium	100	4.31438E-02
Coolant	H-1	11.19	4.71053E-02
	O-16	88.81	2.35662E-02

Table 7.2 Comparison of number densities of fission products at 60,000 MWd/T

Element	ID No.	MONTEBURNS	C (in %)	D (in %)
Kr83	360830	6.7633E-06	1.01	-0.9
Zr93	400930	8.0984E-05	1.02	-1.5
Mo95	420950	6.7942E-05	3.52	0.5
Tc99	430990	6.5316E-05	5.16	-0.4
Ru101	441010	5.9176E-05	2.27	-0.9
Rh103	451030	2.2856E-05	7.25	-1.9
Ag109	471090	3.2796E-06	1.18	-9.0
Xe131	541310	2.5285E-05	7.21	-4.7
Xe135	541350	8.0444E-09	12.28	5.3
Cs133	551330	6.8161E-05	7.3	3.0
Cs134	551340	1.0621E-05	1.16	-5.7
Cs135	551350	2.8494E-05	1.43	93.2
Pr141	591410	7.6088E-05	1.09	-1.5
Nd143	601430	4.8694E-05	10.68	4.0
Nd145	601450	4.1037E-05	3.71	1.7
Pm147	611470	7.6699E-06	3.56	-5.4
Sm147	621470	4.3772E-06	1.19	-3.9
Sm149	621490	7.6754E-08	3.17	-10.7
Sm150	621500	1.3943E-05	1.61	-15.3
Sm151	621510	4.8380E-07	2.83	5.0
Sm152	621520	3.9115E-06	3.4	-0.2
Eu153	631530	5.3098E-06	2.83	2.0
Eu154	631540	1.3427E-06	2.94	2.1
Eu155	631550	2.7624E-07	3.04	0.4

C - Conribution to absorption due to fission products (in %)
D - Relative deviation (in %) of DRAGON w.r.t MONTEBURNS

Table 7.3 Comparison of number densities of actinides at 60,000 MWd/T

Element	ID No.	MONTEBURNS	C (in %)	D (in %)
Th232	902320	1.5363E-02	44.96	0.0
Pa233	912330	1.9547E-05	1.24	1.5
U233	922330	2.7622E-04	4.67	0.4
U234	922340	5.2584E-05	2.78	1.4
U235	922350	1.6577E-04	2.82	3.3
U236	922360	1.4518E-04	2.80	-3.4
U238	922380	3.8988E-03	19.20	-0.3
Np237	932370	1.7989E-05	2.03	16.3
Pu239	942390	5.0168E-05	7.32	6.3
Pu240	942400	1.7782E-05	7.10	2.5
Pu241	942410	1.8277E-05	1.79	5.8
Pu242	942420	1.0145E-05	1.03	3.5

C - Conribution to absorption due to actinides (in %)
D - Relative deviation (in %) of DRAGON w.r.t MONTEBURNS

Table 7.4 Comparison of energies for power normalization obtained from MONTEBURNS and DRAGON

Burnup	MONTEBURNS			DRAGON		
(MWd/T)	$(n,f)(\%)$	$(n,\gamma)(\%)$	$(n,2n)(\%)$	$(n,f)(\%)$	$(n,\gamma)(\%)$	$(n,2n)(\%)$
114.40	97.29	2.72	-0.0091	97.47	2.54	-0.0089
3031.71	97.07	2.94	-0.0093	97.23	2.78	-0.0092
8122.69	96.84	3.17	-0.0097	96.89	3.12	-0.0098
14986.94	96.56	3.45	-0.0105	96.69	3.32	-0.0102
25283.31	96.17	3.84	-0.0110	96.32	3.69	-0.0109
35579.68	95.80	4.22	-0.0117	95.89	4.12	-0.0117
44732.00	95.46	4.55	-0.0123	95.56	4.45	-0.0123
55028.38	95.12	4.90	-0.0127	95.24	4.77	-0.0129
66468.78	94.75	5.26	-0.0134	94.87	5.15	-0.0135

CHAPTER 8

GADOLINIUM PINCELL BURNUP BENCHMARK

This chapter will deal with the study of burnup behaviour of gadolinium pincell. Gadolinium is used in present day pressurized water reactors (PWRs) for suppression of initial excess reactivity. Gadolinium is composed of six naturally occurring isotopes - ^{154}Gd (2.1%), ^{155}Gd (14.8%),^{156}Gd (20.6%),^{157}Gd (15.7%),^{158}Gd (24.8%), ^{160}Gd (21.8%) [Friedlander 1981]. Of the six isotopes, ^{155}Gd and ^{157}Gd play a very important role in suppression of reactivity due to very high thermal absorption cross section. ^{155}Gd has a thermal absorption cross section (0.0253 eV) of 61,000 barns while ^{157}Gd has 2,55,000 barns. Gadolinium is generally mixed in a form compatible with that of the fuel. For eg. it is mixed as Gd_2O_3, when the fuel is in oxide form. Since gadolinium has a very large absorption cross section, the neutron mean free path is extremely small. As a result, the gadolinium pin burns like onion skin. It has been recommended by Santamarina [Santamarina 2004] that if the PWR assembly contains gadolinium pin, one has to consider eleven evolving concentric zones with discrete steps. In this chapter we discuss the various aspects of burnup behaviour of gadolinium pincell due to choice of number of concentric rings in fuel and size of burnup steps.

The benchmark analysed in this chapter is a hexagonal pincell of WWER type having gadolinium oxide in uranium oxide [IAEA 1996]. The dimensions of the pincell and composition are given in Table 8.1. The lattice analysed in the benchmark is shown in Figure 8.1. This benchmark is slightly modified from the original. The water temperature has been modified (575 K $\rightarrow$ 573.6 K) and clad temperature has been modified (600 K $\rightarrow$ 621 K). These modifications were chosen to be consistent with the nuclear data generated for analysis of burnup benchmarks. Also the S(α,β) data for light water in the chosen evaluated datafile was available at 573.6 K. It will be interesting to study the effect of heat generated in the pincell,

not only due to fission of ^{235}U but also due to heat generated due to capture of neutrons by gadolinium isotopes. In this study, the gadolinium pincell has been divided into single, four, six and ten equal volume regions. Burnup steps varying from 50, 100, 200, 250, 500 and 1000 MWd/T each has been considered. We have compared the k_{∞}, number densities of ^{155}Gd, ^{157}Gd, ^{235}U, ^{239}Pu, ^{240}Pu, ^{241}Pu, and ^{242}Pu under the various situations.

The pincell that has been considered has an hexagonal outer cell. Figure 8.2 gives the typical spectrum in a gadolinium pin. It can be observed that the peak of Maxwellian spectrum is at 0.4 eV when compared to 0.06 eV when there is no gadolinium. This is mainly due to high preferential absorption of thermal neutrons by gadolinium isotopes. As a result the spectrum is hard and this will aid in increased production of ^{239}Pu and higher isotopes, when ^{238}U is part of fuel.

8.1 Computational scheme used for DRAGON analysis

In the `LIB:` module we used library based on DRAGLIB format which included a total of 178 nuclides (25 actinides, 150 fission products and 3 structural elements). The evaluated nuclear data files for all the elements were chosen on the basis of recommendations from WLUP [Leszczynski 2003]. Under the `GEO:` module we considered the hexagonal pincell with isotropic reflective boundary condition on all surfaces. The geometry was tracked with an angular quadrature parameter of 11 and track density of 50 lines per cm, which was found adequate. Only one region was considered in the coolant for shielding and flux calculation, as there was minimal effect in estimation of k_{∞}. The tracking of the geometry was performed using the `EXCELT:` module. The APOLLO type transport correction based on the linearly anisotropic scattering cross sections was used for the total and isotropic scattering cross sections. We have used the 'SUBG' keyword to generate physical probability tables using temperature interpolated cross section as input. The intermediate resonance treatment

of using statistical model up to 81 groups and wide resonance model beyond was used. We used the USS: module to perform self shielding calculations, which is the subgroup approach using physical probability tables. We used the default options in ASM: module for generation of collision probabilities. In the FLU: module, we used the option of criticality calculations *without* leakage effects. In the EVO: module we obtained the solution using the 4^{th} order Kaps-Rentrop algorithm. We didn't consider linear extrapolation of the microscopic reaction rates in the solution of the burnup equations. Saturated number densities were calculated without considering Dirac distribution model. Power was normalized to 15.04312 KW/KgHM and fluxes were estimated to deplete the fuel.

8.2 Effect of burnup step

In an earlier work [Yamamoto 1985], burnup behaviour of a BWR lattice containing Gd rods was studied for various burnup steps. The lattice analysed was a 8×8 BWR lattice with one Gd pin. It was mentioned in the paper that a burnup step of 200 MWd/T initially and with coarse burnup steps of 500 MWd/T beyond 1000 MWd/T was considered as reference. The burnup behaviour of the BWR lattice will be primarily dictated by the uranium pins and hence coarse irradiation steps has given good results. But when one considers a pincell having fuel with Gd, it will be interesting to identify the burnup steps that needs to be considered. In the present work, we have studied the effect of coarse irradiation steps on the burnup of the gadolinium pincell at six irradiation steps of 50, 100, 200, 250, 500 and 1000 MWd/T each. The flux calculations are performed at these steps and number densities are updated. In general, it is assumed that the one group cross sections of the isotopes in fuel do not change much during the interval. The k_∞ obtained due the choice of coarse irradiation steps are shown in Figure 8.3. It can be observed that the k_∞ increases as a function of burnup up to 10,000 MWd/T. Beyond that it begins to fall. This is generally the property when gadolinium

is present. Gadolinium suppresses initial excess reactivity and subsequently releases it when it gets burnt. It is interesting to note that eventhough the trend in behaviour of k_∞ as a function of burnup is similar for all the coarse irradiation steps, there is a difference in values. It can also be noted that when the irradiation steps become small, the difference reduces. For the sake of discussion we define quantities ΔK as

$$\Delta K = [1/k_\infty(state) - 1/k_\infty(ref)] \ , \tag{8.1}$$

and δK

$$\delta K = [k_\infty(state) - k_\infty(ref)] \ . \tag{8.2}$$

We have compared the ΔK (obtained using Equation 8.1) for various coarse burnup steps and is shown in Figure 8.4. We have chosen the k_∞ values obtained using 50 MWd/T step as our reference. It can be noticed from Figure 8.4 that the ΔK is maximum when an irradiation step of 1000 MWd/T is chosen. ΔK goes on reducing when one considers smaller coarse steps of irradiation. This is mainly due to failure of assumption that the one group reaction rates remain unchanged within the burnup step. As mentioned earlier, the gadolinium cross sections are quite large and has to be updated in very short time intervals. It can thus be concluded that when gadolinium is present in the assembly, one has to consider fine steps of irradiation and observe the burnup of the gadolinium pin.

8.3 Effect of number of rings per pin

In a recent work [Matsumoto 2006], a study on depletion of PWR assemblies having Gd has been carried out using lattice code PARAGON [Ouisloumen 2003]. The authors have concluded that eight equal volume splitting model for Gd_2O_3 is acceptable in terms of accuracy and computation time. This again was performed for 17×17 PWR assembly having 16 gadolinium rods and the recommendations are made for the assembly. As mentioned before, in the present work we have focused on single gadolinium pincell and studied the effect of number of rings chosen within a pin on irradiation behaviour. For this study we considered a coarse irradiation step of 250 MWd/T. Figure 8.5 gives the deviation of k_∞ as a function of burnup when one, four, six and ten rings are chosen within a pin. It can be observed that the k_∞ obtained for single ring per pin is higher than that when more rings are chosen. Figure 8.6 shows the variation of ΔK for the various rings chosen within fuel pin, with the reference being 10 rings per pin. It can be observed that when single ring is considered, the k_∞ is higher up to 5000 MWd/T and becomes lower up to 12000 MWd/T. This trend is observed for 4 rings and 6 rings per pin but the deviation is lower.

Figure 8.7 shows the thermal absorption rate ($cm^{-3}s^{-1}$) as a function of number of rings per pin at zero burnup. It can be observed that the thermal absorption increases as a function of radius and is maximum towards the periphery. This clearly demonstrates the rim effect and can be observed only when the pin is subdivided into multiple rings. The thermal absorption rate at the periphery is more than three times when ten rings are considered as against a single ring per pin. This also explains the earlier observed phenomenon of lower k_∞ as a function of burnup when lesser number of rings are considered per pin. The lower thermal absorption leads to slower depletion of gadolinium.

Figure 8.8 shows the thermal absorption rate ($cm^{-3}s^{-1}$) as a function of burnup up to 10,000 MWd/T, when ten rings per pin are considered. It can be noticed that as a function of

burnup, the peak absorption rate moves towards the centre, till the gadolinium gets completely burnt. The thermal absorption rate peaks in the outermost ring at zero burnup and in the central ring at 6750 MWd/T. Figure 8.9 shows the thermal absorption rate ($cm^{-3}s^{-1}$) as a function of burnup beyond 10,000 MWd/T. It can be observed that after 10,000 MWd/T, the absorption rate increases as a function of burnup, in the outermost ring and decreases in the innermost ring.

Figure 8.10 shows the resonance absorption rate ($cm^{-3}s^{-1}$) as a function of number of rings per pin at zero burnup. It can be observed that in the periphery, the ratio of absorption rate when ten rings are considered instead of a single ring is about 2.3. The resonance absorption rate clearly shows the rim effect when one considers ten rings instead of single ring within fuel pin with gadolinium. But unlike thermal absorption rate, resonance absorption rate doesn't show moving boundary phenomenon with the depletion of gadolinium, as shown in Figure 8.11. Figure 8.12 shows the resonance absorption rate ($cm^{-3}s^{-1}$) as a function of burnup beyond 10,000 MWd/T. It can be observed that after 10,000 MWd/T, the absorption rate increases as a function of burnup, in the outermost ring.

8.4 Effect of gadolinium

A study was performed to assess the effect of gadolinium on burnup characteristics of fuel pin. In the study we artificially set the concentration of gadolinium isotopes to zero and performed the burnup study with the same power normalization as used for the pin with gadolinium. It can be observed from Figure 8.13 that the k_∞ is about 1.18 at zero burnup and reduces as a function of burnup. It can be seen that the burnup of gadolinium pin reaches a maximum of 1.006 and then falls almost parallel to curve of the fuel pin.

8.5 Burnup of important actinides

Figures 8.14 to 8.18 show the change in concentration of important actinides as a function of burnup. It was calculated as the difference in number densities at the end and beginning of a burnup step. It can be seen that in the presence of gadolinium, ^{235}U burnt slowly when compared to burnup in the absence of Gd. It is interesting to note that the plutonium isotopes form more rapidly in presence of Gd than its absence. This is mainly due to the spectrum that gets harder in the presence of Gd, as seen in Figure 8.2, and it aids in conversion of ^{238}U to ^{239}Pu and all the subsequent isotopes of plutonium.

8.6 Contribution due to different neutron induced reactions

Power normalization is performed usually with the fission rate and the energy associated with it. In this analysis, we have considered power normalization due to eleven neutron induced reactions and their corresponding energies. They are (n,γ), (n,f), $(n,2n)$, $(n,3n)$, $(n,4n)$, (n,α), (n,p), $(n,2\alpha)$, (n,np), (n,d), (n,t). A power normalization value of 15.04132 W/g has been considered. Figure 8.19 shows that the contribution to power normalization due to energy from fission is almost 73% initially and increases to 95% close to 9500 MWd/T. Almost 27% contribution towards power normalization comes due to energy from (n,γ) reaction, as shown in Figure 8.20. It is interesting to note that this value continuously decreases and reaches a saturation value of about 5% beyond 9500 MWd/T. It can also be noted from Figure 8.20 that an initial contribution of about 21% due to energy from (n,γ) reaction, is from elements other than the actinides.

The actinide contribution to power normalization due to energy from (n,γ) reaction, is about 5.6%. The contribution to power normalization due to energy from (n,γ) reaction from elements other than actinides reduces to about 1% beyond 9500 MWd/T, whereas it

is about 4% from actinides. It can be seen from Figure 8.21 that the major contribution to (n,γ) reaction from elements other than the actinides, is from ^{155}Gd and ^{157}Gd. Almost 15% contribution is from ^{157}Gd while about 6% contribution is from ^{155}Gd. This contribtion decreases as a function of burnup and becomes less than 1% at 6500 MWd/T for ^{157}Gd and 9500 MWd/T for ^{155}Gd. Other isotopes of gadolinium, i.e. ^{154}Gd,^{156}Gd and ^{158}Gd also contibutes towards power normalization due to (n,γ) reaction. It can be seen from Figure 8.22 that the contribution due to even isotopes of gadolinium towards power normalization due to (n,γ) reaction is about 0.5% initially and reduces to 0.25% beyond 9500 MWd/t.

Figure 8.23 shows the contribution to power normalization due to energy from fission of major actinides. It can be seen that the major contribution comes from ^{235}U initially, as expected. But the contribution from ^{239}Pu increases as a function of burnup and in fact exceeds the contribution from ^{235}U at about 4500 MWd/T and remains higher beyond. It is interesting to observe that ^{238}U contributes about 25% to fission energy, which suggests that the lattice is highly undermoderated with large number of neutrons still at higher energy. It can also be noted that the value reaches a saturation of about 8% beyond 10,000 MWd/T. The contribution from fission of ^{241}Pu increases upto 10% almost linearly as a function of burnup. One important thing that is to be noted is that the fission energy contribution from ^{235}U shows points of inflexion at 6000 MWd/T (minimum) and 9500 MWd/T (maximum). Coincidentally, these two points correspond to the burnout of ^{157}Gd and ^{155}Gd respectively.

Figure 8.24 shows the contribution from important actinides to power normalization due to energy from (n,γ) reaction . It can be observed that the major contribution is from ^{238}U, as expected. It is about 5% in the beginning and reduces to a constant value of about 2% beyond 10,000 MWd/T. This is again due to the presence of gadolinium, which pumps the neutrons into the resonances of ^{238}U. Other than (n,γ) and (n,f), there is a small contribution to power normalization from $(n,2n)$ reaction. Figure 8.25 shows the contribution to power normalization due to $(n,2n)$ reaction by all nuclides. The contribution is small, negative and it increases as a function of burnup, as it is a threshold reaction. The contribution changes

from -0.04% to -0.012% as a function of burnup.

8.7 Effect of power normalization

In this section we will study the effect of performing power normalization using energies from all neutron induced reactions and their respective reaction rates ('MODEL-1') vis-à-vis energy per fission and fission rate ('MODEL-2'). As mentioned in the earlier chapter, for calculation using 'MODEL-2', the library was modified to include energy per fission as recommended by the WLUP. The energies of all other reactions and for all elements was set to zero.

Figure 8.26 compares the k_∞ obtained for fuel pin with and without gadolinium, using the two above mentioned models. Figure 8.27 shows the variation of δK (see Equation 8.2) obtained with 'MODEL-2' as reference. It can be seen that for fuel pin without gadolinium, the δK decreases as a function of burnup. This indicates that when one uses 'MODEL-1', the depletion of fuel is faster and hence a lower k_∞. But when gadolinium becomes part of the fuel pin, the δK decreases drastically as a function of burnup. This phenomena can be understood by having a look at the flux obtained for depletion after power normalization procedure. Figure 8.28 shows the normalization flux obtained when one considers the two models of power normalization. It can be seen that the flux is much higher when one uses 'MODEL-2'. This is not the case for situations where there is no gadolinium in the fuel. It was earlier noted in the context of depletion of PWR thorium fuel, that the flux obtained during power normalization was lower when one considers 'MODEL-2' vis-à-vis 'MODEL-1' (see Figure 7.5). But in the present case, the higher flux obtained when one uses 'MODEL-2', leads to quicker and higher depletion of gadolinium isotopes, increased production of ^{239}Pu and hence a higher k_∞. This can be seen in Figures 8.29 to 8.32. This result thus

substantiates the need for use of energies from all neutron induced reactions for all elements that are part of the fuel for power normalization.

8.8 Reference solution using MCNP5 at zero burnup

A reference solution with MCNP5 was obtained at zero burnup. The hexagonal pincell was studied using MCNP5 by tracking two million neutron histories. Isotropic boundary condition was applied on the six surfaces. Table 8.2 gives the comparison of reference solution obtained using MCNP5 and all the self shielding models in DRAGON Version4. It can be seen that δK with respect to MCNP5, obtained by all the models, is more that 200 pcm. Models based on subgroup approach and GSM2 with LJ option show lower deviations compared to other models. In Table 8.3, we have compared the reaction rates corresponding to fission and capture between MCNP5 and 'SUBG' option in DRAGON. It can be seen that the capture rate and fission rates are predicted well by DRAGON Version4. We plan to perform full burnup calculation using MONTEBURNS and provide it as reference solution for burnup calculations using 'SUBG' model in DRAGON Version4.

8.9 Conclusions

Burnup dependent behaviour of gadolinium pincell has been studied using the code DRAGON Version4. It was noted that one has to consider at least ten rings of equal volume to obtain consistent behaviour as a function of burnup. Also one has to consider fine burnup steps of the order of 50 MWd/T, till gadolinium gets completely burnt. Two different models of power normalization was studied. It was noted that when energy from all neutron induced reactions was considered for power normalization, the fuel depletes faster due to higher flux. But when gadolinium is part of the fuel, this type of power normalization leads to slower

burning of gadolinium due to lower flux. This lower flux was due to energy contribution towards power normalization by capture of neutrons by gadolinium isotopes. This can be as high as 21% at the start of burnup. It is therfore important to include in the library, the energy released due to capture of neutrons by all the elements and perform power normalization.

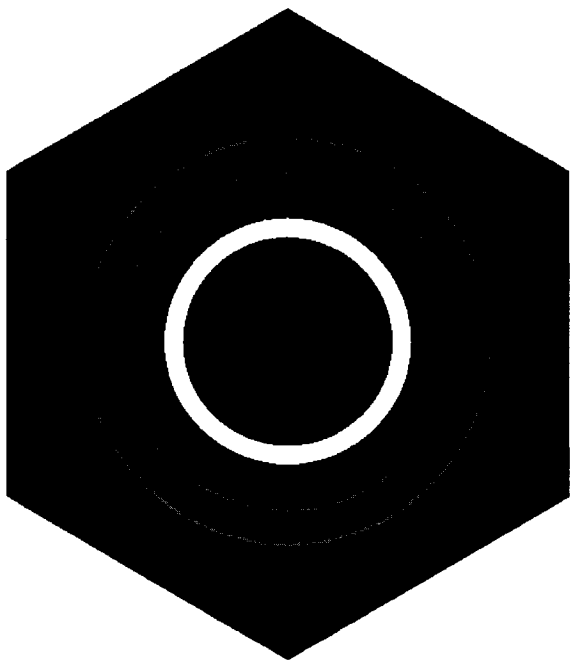

Figure 8.1 Sidorenko lattice

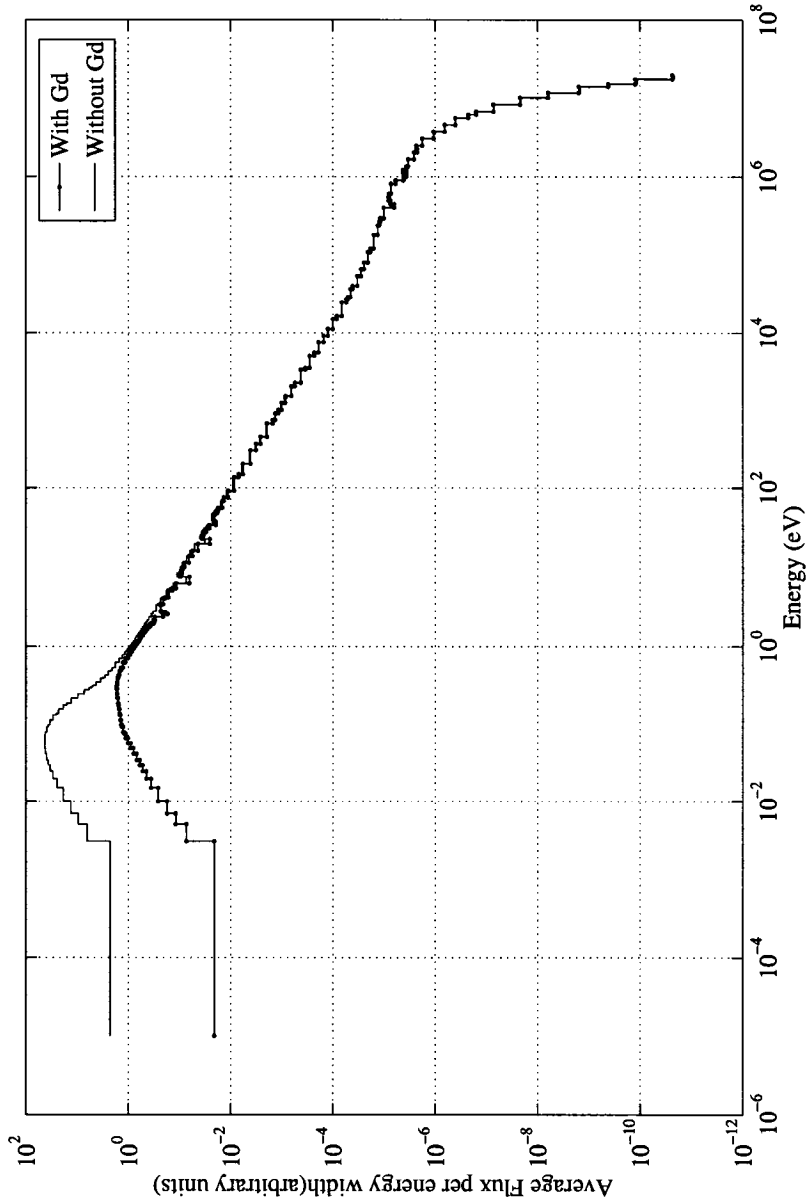

Figure 8.2 Typical spectrum in Sidorenko lattice

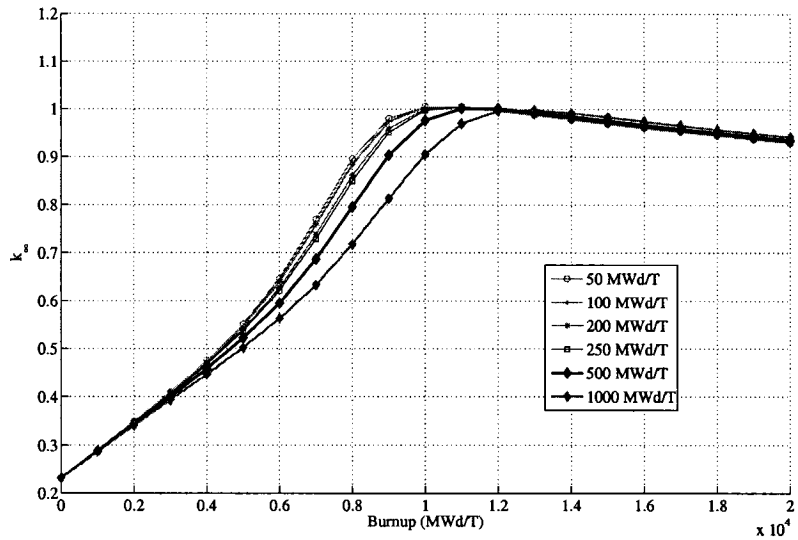

Figure 8.3 Dependence of k_{∞} on burnup step and its variation as a function of burnup

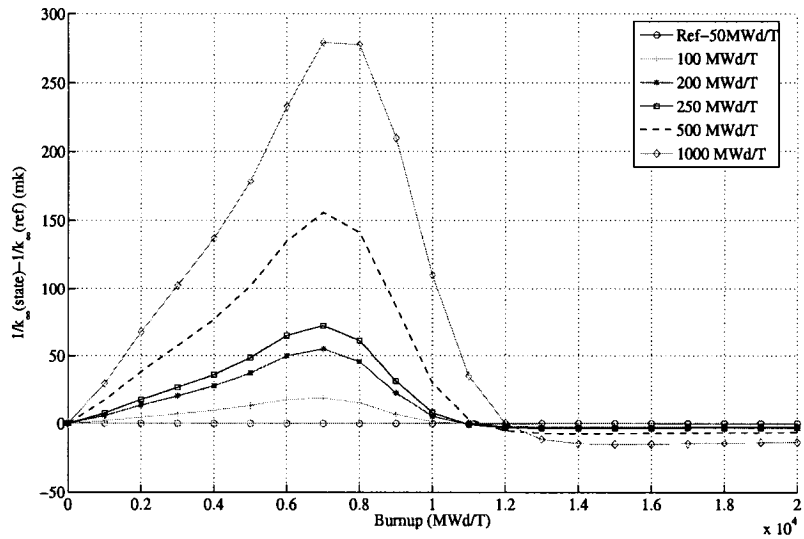

Figure 8.4 Variation of ΔK, with reference to 50 MWd/T burnup step, as a function of burnup

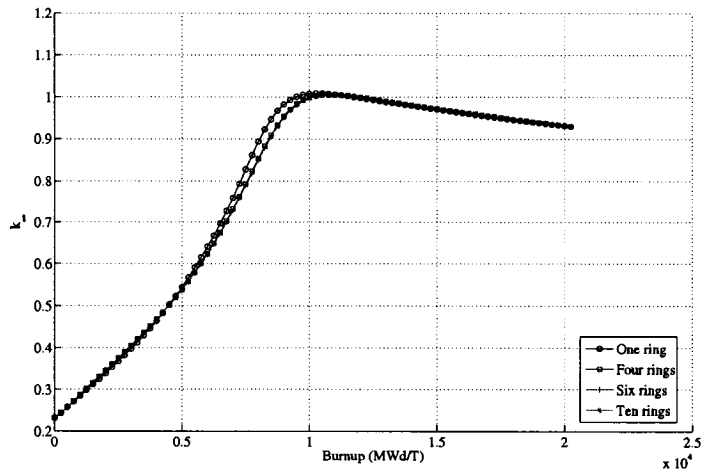

Figure 8.5 Dependence of k_∞ on choice of different rings per pin and its variation as a function of burnup

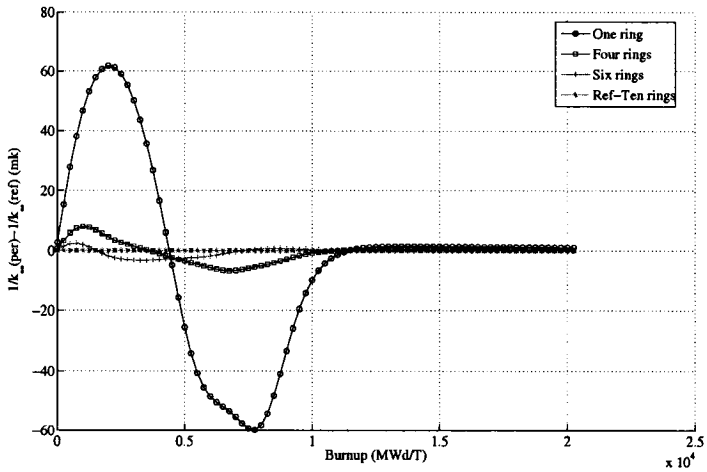

Figure 8.6 Variation of ΔK, with reference to ten rings per pin, as a function of burnup

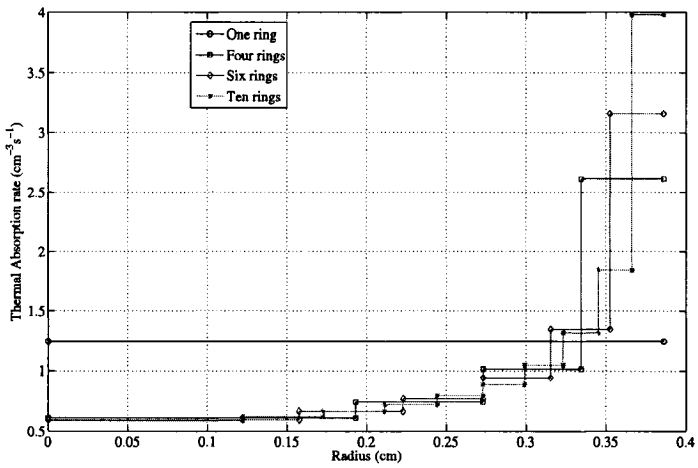

Figure 8.7 Thermal absorption rate ($cm^{-3}s^{-1}$) as a function of number of rings per pin

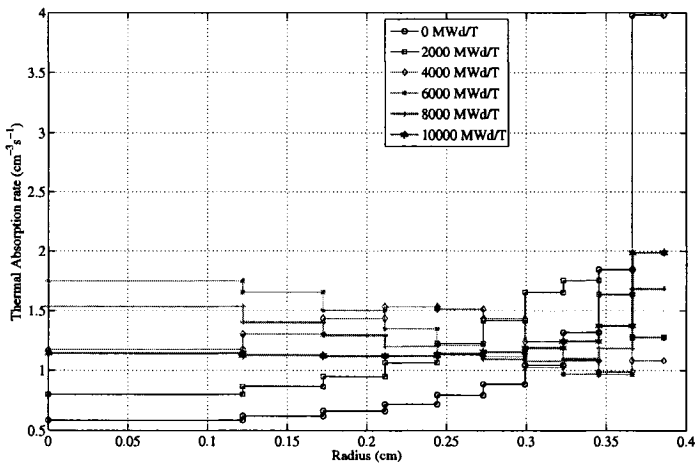

Figure 8.8 Thermal absorption rate ($cm^{-3}s^{-1}$) up to 10,000 MWd/T in fuel pin with 10 rings

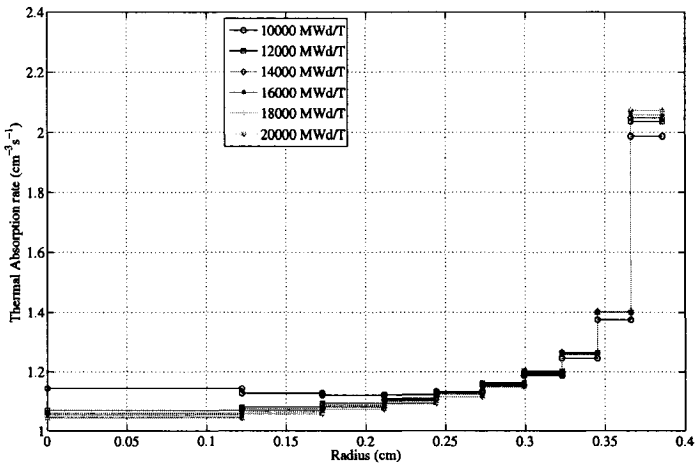

Figure 8.9 Thermal absorption rate ($cm^{-3}s^{-1}$) beyond 10,000 MWd/T in fuel pin with 10 rings

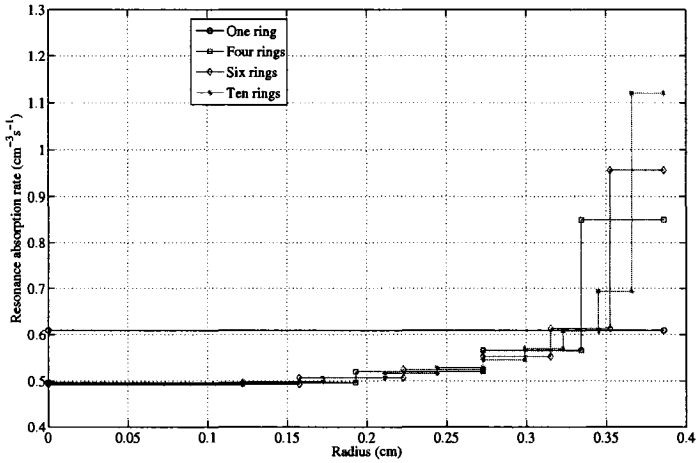

Figure 8.10 Resonance absorption rate ($cm^{-3}s^{-1}$) as a function of number of rings per pin

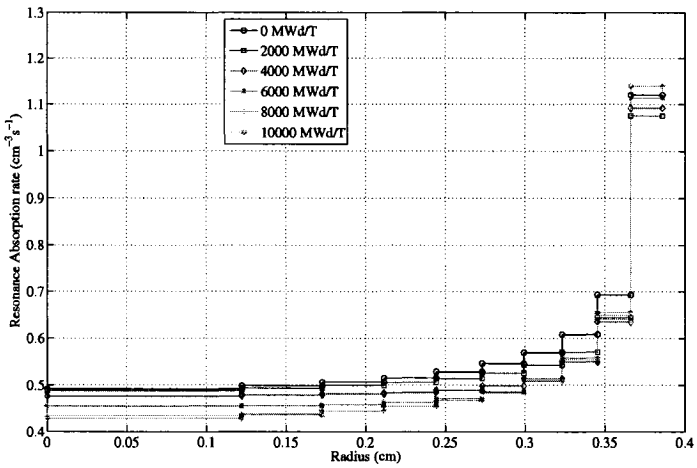

Figure 8.11 Resonance absorption rate ($cm^{-3}s^{-1}$) up to 10,000 MWd/T in fuel pin with 10 rings

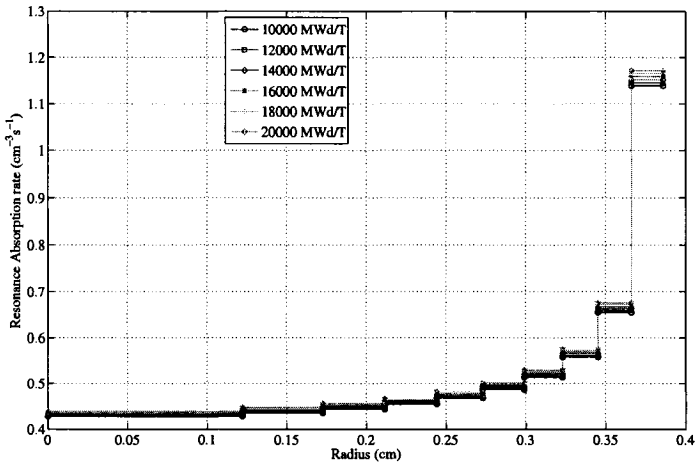

Figure 8.12 Resonance absorption rate ($cm^{-3}s^{-1}$) beyond 10,000 MWd/T in fuel pin with 10 rings

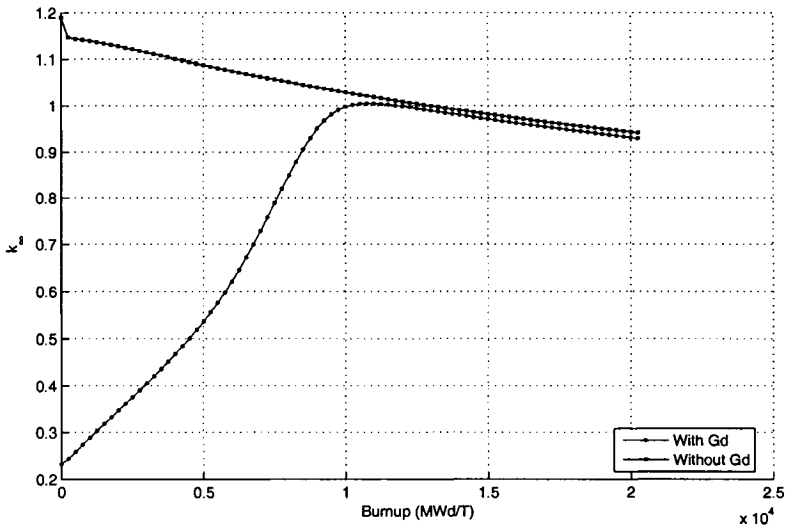

Figure 8.13 k_∞ variation as a function of burnup for pin with and without gadolinium

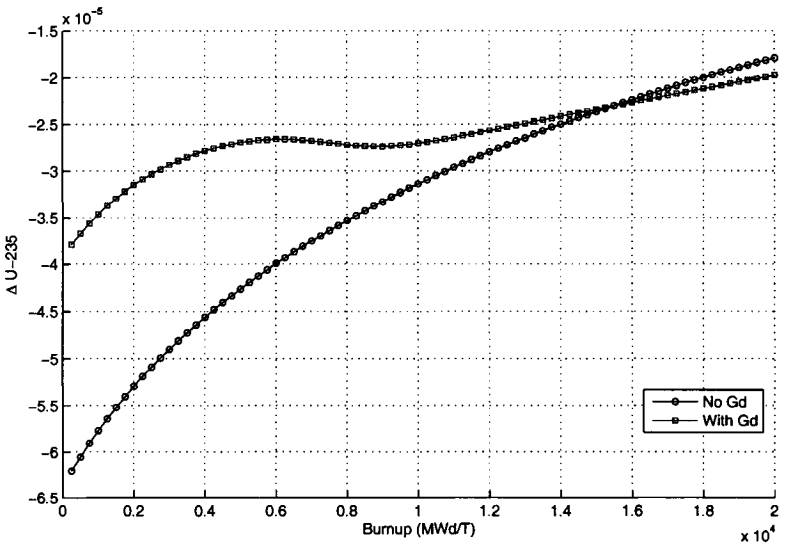

Figure 8.14 Δ^{235}U variation as a function of burnup for pin with and without gadolinium

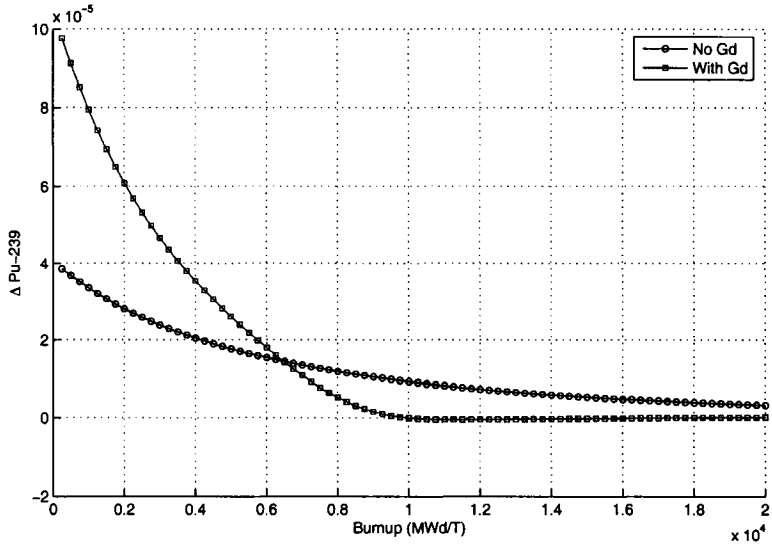

Figure 8.15 Δ^{239}Pu variation as a function of burnup for pin with and without gadolinium

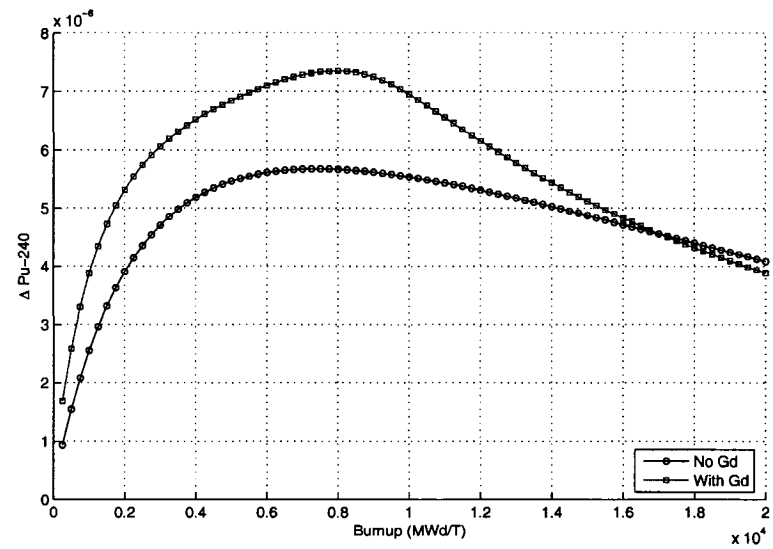

Figure 8.16 Δ^{240}Pu variation as a function of burnup for pin with and without gadolinium

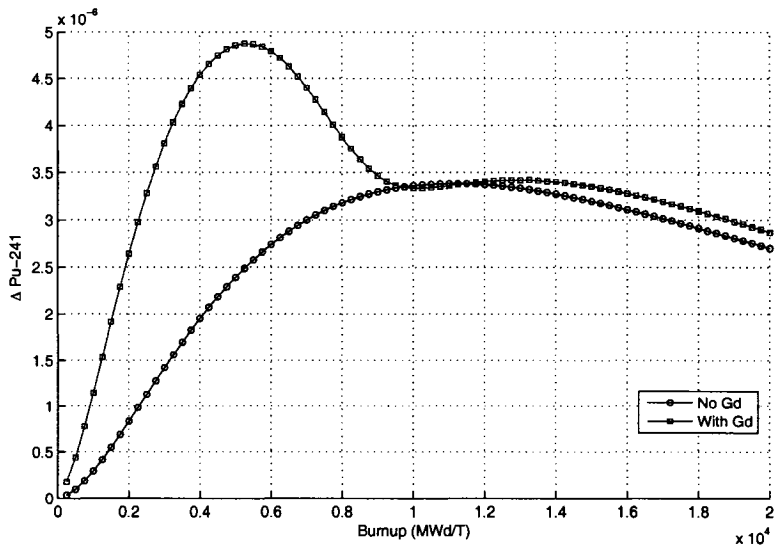

Figure 8.17 Δ^{241}Pu variation as a function of burnup for pin with and without gadolinium

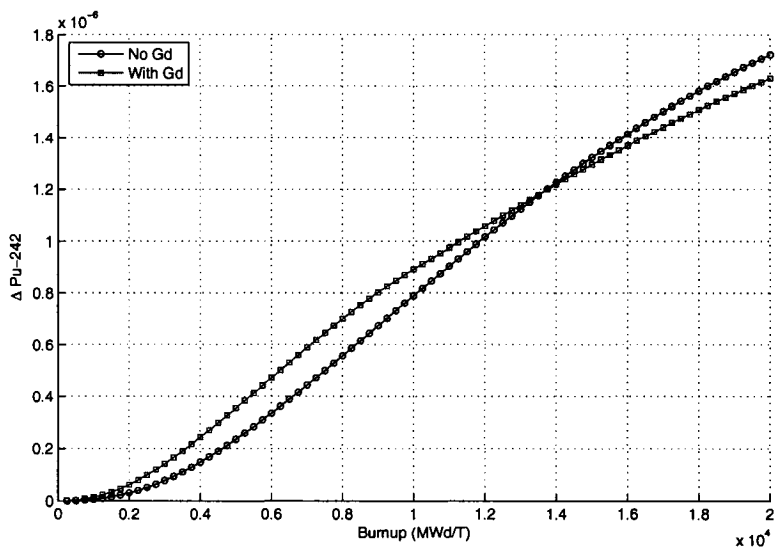

Figure 8.18 Δ^{242}Pu variation as a function of burnup for pin with and without gadolinium

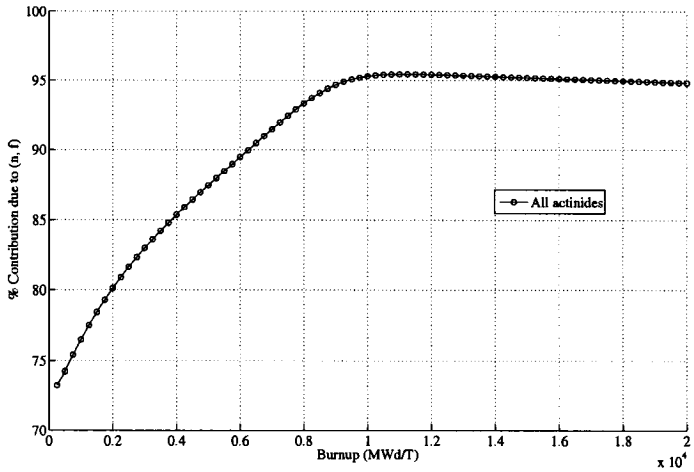

Figure 8.19 Contribution to power normalization due to energy from fission reaction

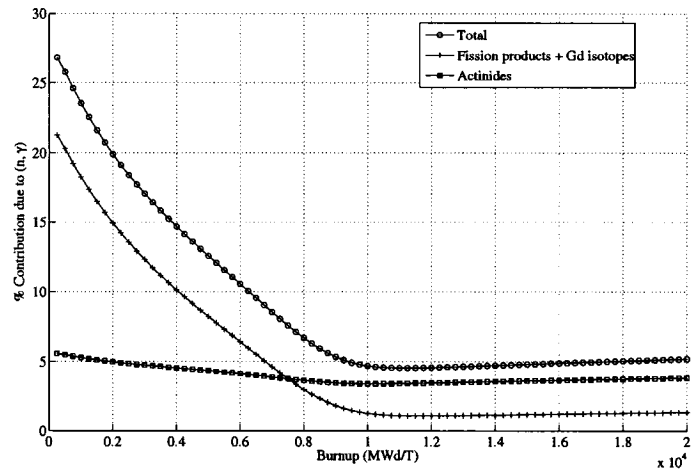

Figure 8.20 Contribution towards power normalization due to energy from (n, γ) reaction

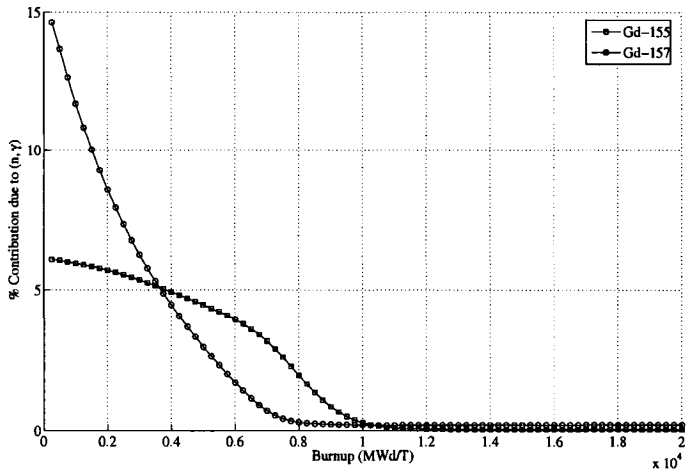

Figure 8.21 Contribution towards power normalization due to energy from (n, γ) reaction in ^{155}Gd and ^{157}Gd

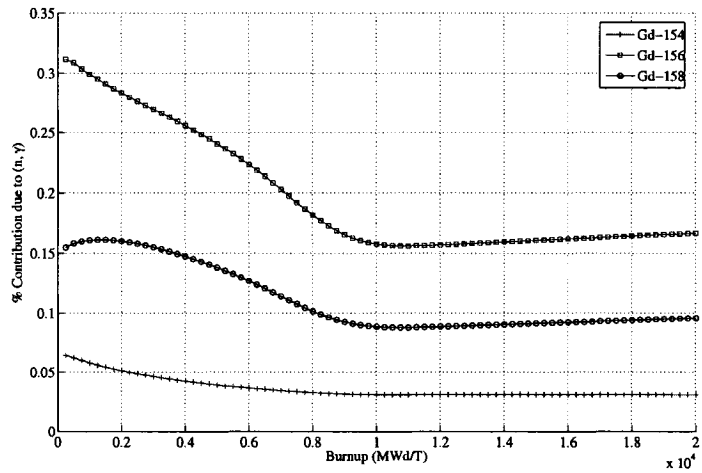

Figure 8.22 Contribution towards power normalization due to energy from (n, γ) reaction in ^{154}Gd,^{156}Gd and ^{158}Gd

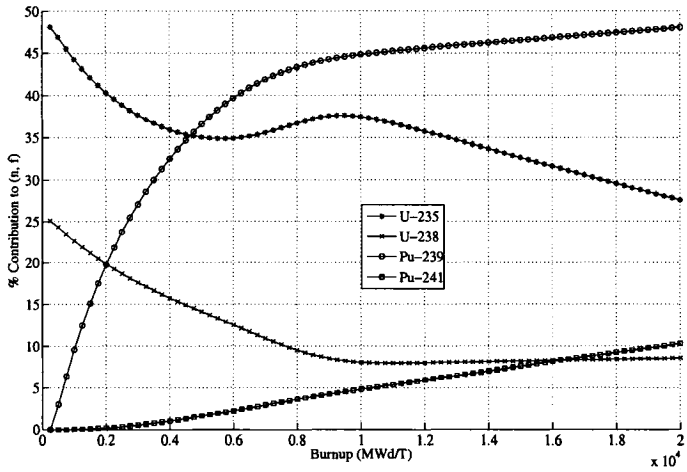

Figure 8.23 Contribution to power normalization due to energy from fission of important actinides

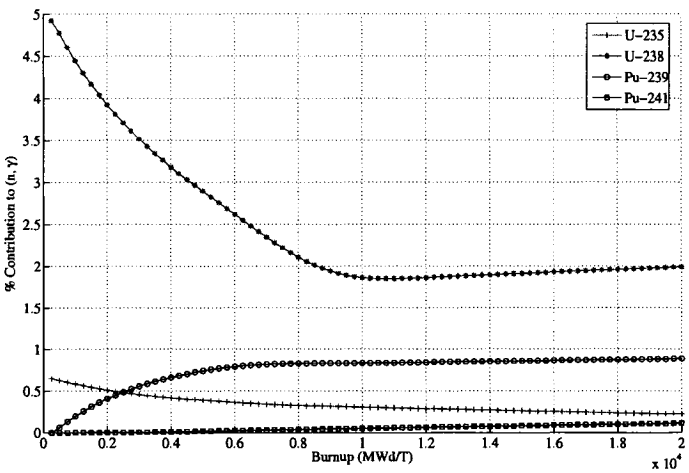

Figure 8.24 Contribution to power normalization due to energy from (n, γ) reaction of important actinides

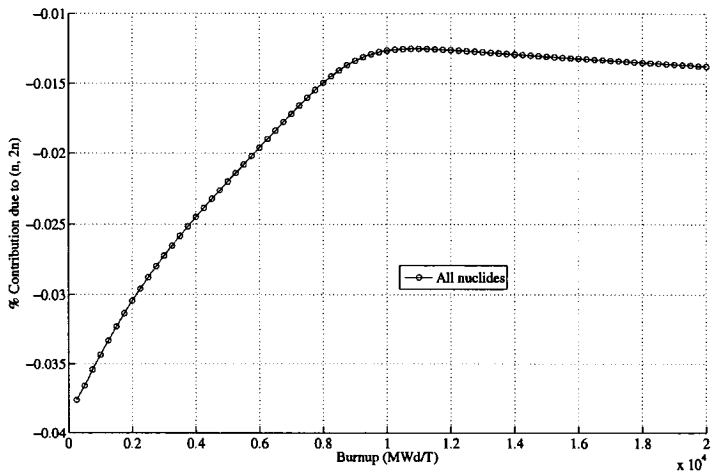

Figure 8.25 Contribution to power normalization due to energy from $(n, 2n)$ reaction

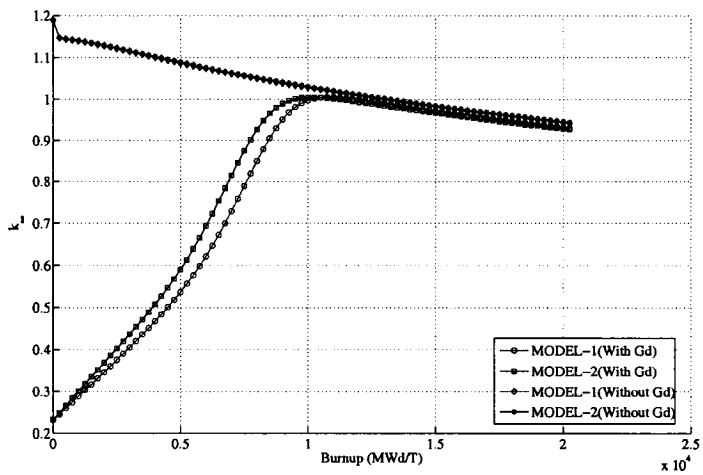

Figure 8.26 k_∞ variation as a function of burnup using two different models of power normalization

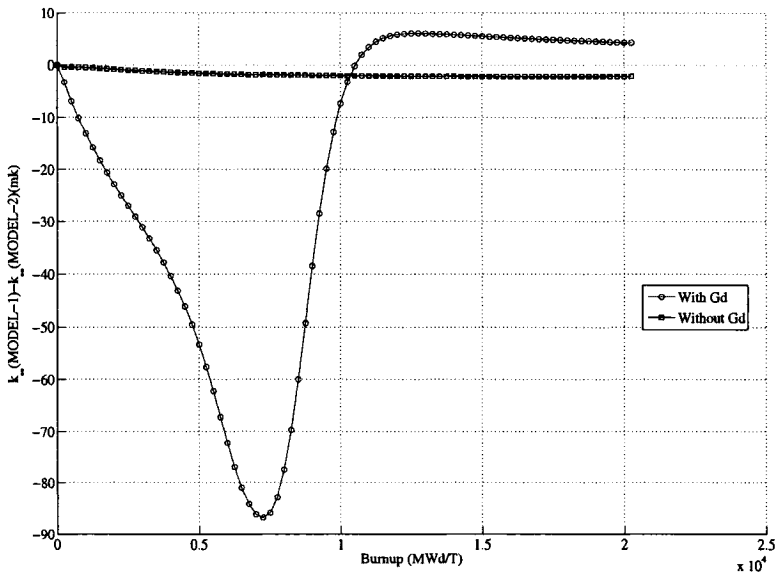

Figure 8.27 Variation of δK, with 'MODEL-2' as reference, as a function of burnup

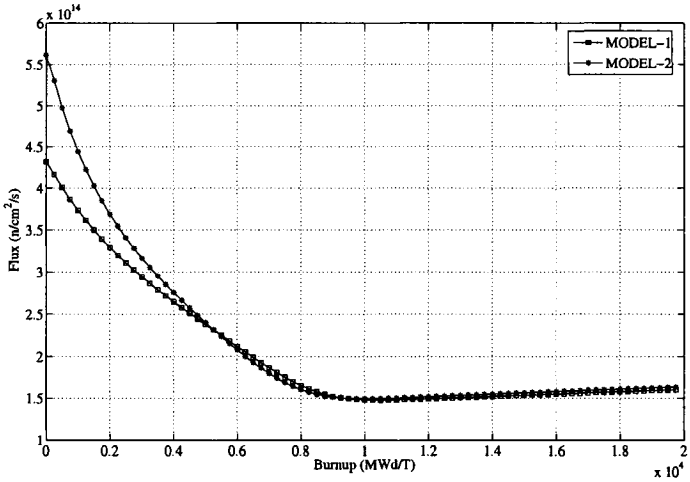

Figure 8.28 Comparison of normalization flux using two different models of power normalization

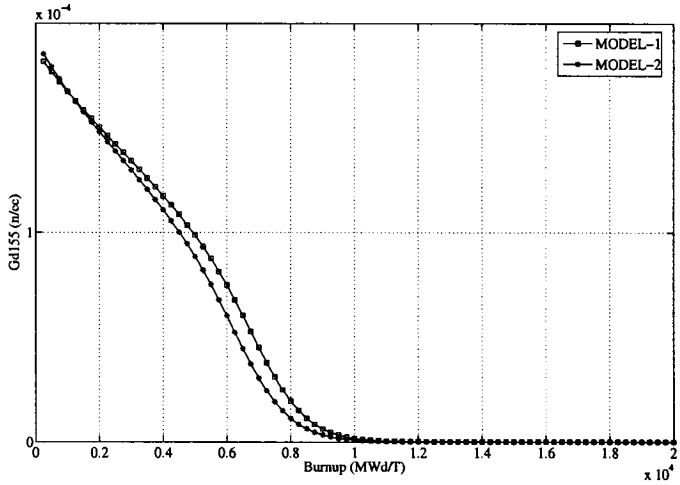

Figure 8.29 Comparison of ^{155}Gd number density using two different models of power normalization

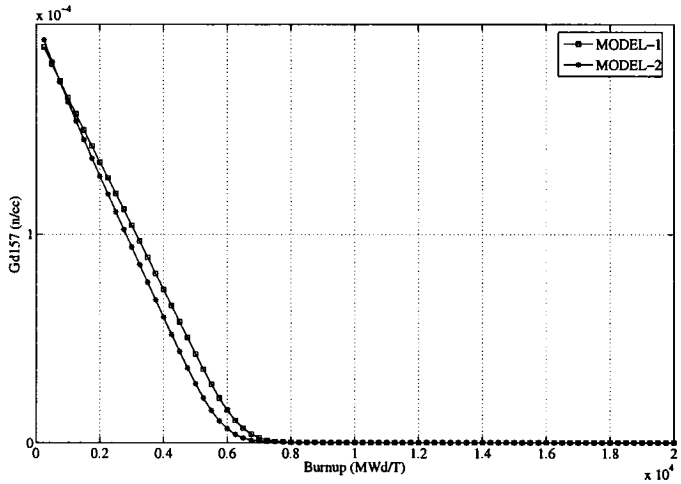

Figure 8.30 Comparison of ^{157}Gd number density using two different models of power normalization

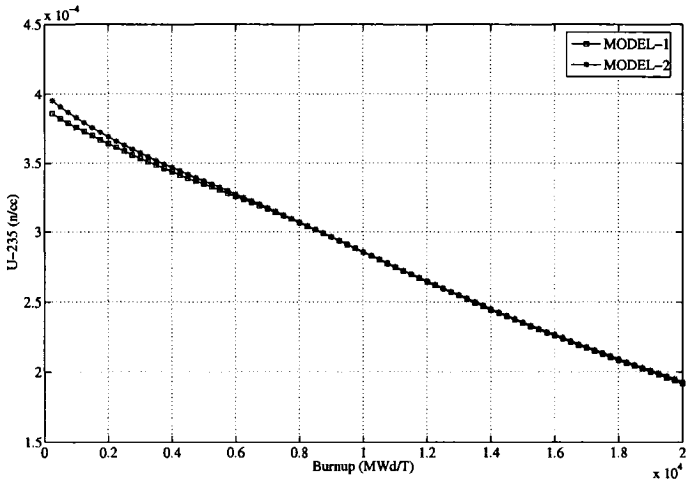

Figure 8.31 Comparison of ^{235}U number density using two different models of power normalization

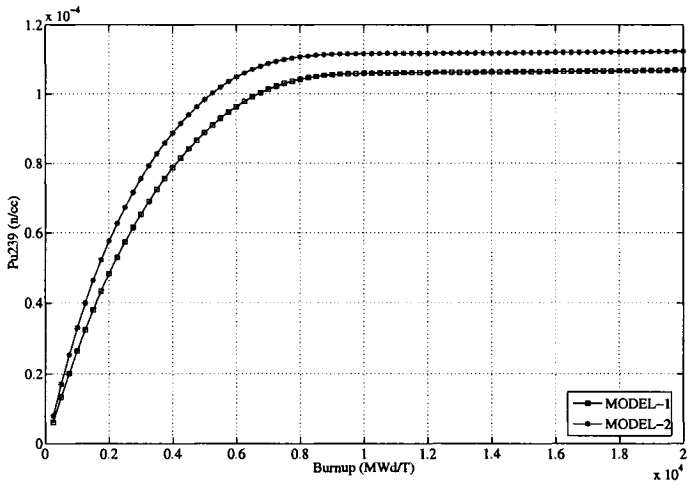

Figure 8.32 Comparison of ^{239}Pu number density using two different models of power normalization

Table 8.1 Modified Sidorenko benchmark specifications

Region	Element	Fuel Rod	BA Rod
Fuel	U-235	0.0004	0.0004
	U-238	0.0208	0.0208
	Gd-154	-	0.0000279
	Gd-155	-	0.000192
	Gd-156	-	0.000266
	Gd-157	-	0.000203
	Gd-158	-	0.000323
	O	0.0424	0.0424
Clad	Zr	0.0423	0.0423
Water	H	0.0482	
	O	0.0241	

All nuclear densities are given in atoms per barn-cm

Parameter	Hot Full Power
Fuel Temperature(K)	900
Power Density (W/gHM)	15.04312
Power Density (W/cc)	126
Cladding Temperature(K)	621.1
Coolant Temperature(K)	573.6
Fuel Pellet Radius (cm)	0.386
Cladding Outer Radius (cm)	0.455
Pin Pitch (cm)	1.275

Table 8.2 k_{∞} obtained using MCNP5 and δK (in pcm) with respect to MCNP5 obtained using various self shielding models

k_{∞}	δK with respect to MCNP5							
	A	B	C	D	E	F	G	H
0.23130±0.00012	-350	-368	-333	-317	-318	-219	-226	-222

A - GSM0-NOLJ B - GSM1-NOLJ C - GSM2-NOLJ D - GSM0-LJ
E - GSM1-LJ F - GSM2-LJ G - SUBG H - RIB

Table 8.3 Comparison of capture rate and fission rate (in $cm^{-3}s^{-1}$) in resolved resonance and thermal groups

Group	Radius(cm)	Capture rate ($cm^{-3}s^{-1}$) (MCNP5)	Devn. (%)	Fission rate ($cm^{-3}s^{-1}$) (MCNP5)	Devn. (%)
	1.2210E-01	4.2013E-01±0.0020	2.4	5.5260E-02±0.0015	-0.5
	1.7260E-01	4.2611E-01±0.0018	2.6	5.5462E-02±0.0013	-0.6
	2.1140E-01	4.3530E-01±0.0017	2.2	5.5616E-02±0.0012	-0.6
	2.4410E-01	4.4588E-01±0.0016	2.0	5.5924E-02±0.0012	-0.9
3	2.7290E-01	4.5783E-01±0.0016	2.0	5.6105E-02±0.0012	-1.0
	2.9900E-01	4.7379E-01±0.0015	2.0	5.6320E-02±0.0011	-0.9
	3.2300E-01	4.9718E-01±0.0015	2.0	5.6545E-02±0.0011	-1.0
	3.4520E-01	5.3743E-01±0.0016	1.5	5.6809E-02±0.0011	-1.1
	3.6620E-01	6.2996E-01±0.0018	0.1	5.7166E-02±0.0011	-1.1
	3.8600E-01	1.0725E+00±0.0022	-1.8	5.7706E-02±0.0010	-1.7
	1.2210E-01	5.4909E-01±0.0024	-0.8	4.7119E-02±0.0017	-1.1
	1.7260E-01	5.8422E-01±0.0020	-0.9	4.7974E-02±0.0015	-0.9
	2.1140E-01	6.2806E-01±0.0019	-1.2	4.9059E-02±0.0014	-1.1
	2.4410E-01	6.8291E-01±0.0018	-1.3	5.0219E-02±0.0013	-1.2
4	2.7290E-01	7.5484E-01±0.0017	-0.3	5.1579E-02±0.0012	-1.2
	2.9900E-01	8.5589E-01±0.0016	-1.4	5.3253E-02±0.0012	-0.9
	3.2300E-01	1.0097E+00±0.0016	-0.6	5.5341E-02±0.0011	-0.8
	3.4520E-01	1.2745E+00±0.0015	0.1	5.8261E-02±0.0011	-1.1
	3.6620E-01	1.8517E+00±0.0015	-2.5	6.2972E-02±0.0010	-0.7
	3.8600E-01	3.8726E+00±0.0012	1.2	7.4740E-02±0.0009	-1.2

CONCLUSION

This research is primarily aimed at validating the advanced self shielding and burnup models incorporated in the advanced lattice code "DRAGON Version4". The advanced self shielding models are based on two different approaches. They are models based on "equivalence in dilution" and "subgroup approach". Under the "equivalence in dilution" approach, we have studied Generalised Stamm'ler model, with and without Nordheim model and Riemann integration model. Under the "subgroup approach", we have studied two varieties based on physical probability tables and mathematical probability tables. Under the advanced burnup model we have studied the power normalization using energies from decay and from most of the neutron induced reactions. The models have been tested against a variety of lattices which covers a broad spectrum of fuel, clad, coolant/moderator and geometry.

NJOY99.90 was used for generation of cross section libraries for the elements included in the benchmarks. Multigroup cross section library in 172 group DRAGLIB format for analysis using DRAGON and in ACE (aka "A Compact ENDF") libraries for analysis using MCNP5 were generated in house. A Python script was prepared to generate the cross section libraries. This script also includes the possibility to verify the correctness of ACE libraries generated based on a procedure recommended by the International Atomic Energy Agency (IAEA). The evaluated datafiles for the elements in the library were chosen based on the recommendations of the IAEA co-ordinated research project on the WIMS Library Update Project (WLUP). Detailed cross section information for the total and P_0 scattering reactions, i.e. "autolib data" is essential for certain self shielding models and was obtained using DRAGR module.

Five infinite lattice benchmarks were chosen for the analysis. The lattices included

CANDU-6, CANDU-New generation (CANDU-NG), PWR thorium pincell, gadolinium pincell and high conversion light water reactor. The benchmark solutions were provided using Monte Carlo code MCNP5. We compared the infinite multiplication factor (k_∞), capture rate and nu-fission rate in four groups for validation of self shielding models. In the case of benchmarks to validate the burnup model, we compared the k_∞, number densities of important fission products and actinides. The validation of burnup model was performed using code MONTEBURNS, which link the codes MCNP5 and ORIGEN. Certain interesting trends have been observed during the analyses of these lattices.

In general it was observed that the self shielding models based on "subgroup approach" performed better in all situations in comparison to models based on "equivalence in dilution". The k_∞ and reaction rates were predicted closer to MCNP5 by models based on "subgroup approach". In some situations the generalized Stamm'ler model along with Nordheim model and Riemann integration model predicted k_∞ better than the models based on "subgroup approach", but the capture rates were not predicted as well. The safety related parameters like coolant void reactivity, fuel temperature coefficient, reactivity due to coolant tube ingression, pressure tube ingression were predicted well by models based on "subgroup approach". However all these values were lower than that predicted using MCNP5. It is thus important to make note of the fact that safety related parameters are generally underpredicted by DRAGON Version4. It was also noted that all the models based on "equivalence in dilution" uniformly performed better when one considered Livolant-Jeanpierre normalization.

The subgroup approach based on mathematical probability tables also performs as good as the subgroup approach based on physical probability tables, but requires "autolib data". However in situations where the fuel comprises a high concentration of ^{238}U, ^{239}Pu and ^{240}Pu, one has to consider subgroup approach based on mathematical probability tables along with correlation model. Only this model is capable of considering mutual self shielding effects.

It was observed that when the ratio of concentration of ^{238}U to ^{240}Pu is of the order of 300 or below, the correlation effects begin to dominate. The correlation effect however begins to fade with increase in V_m/V_f.

For validation of burnup model, an important change was made in the code MONTE-BURNS. This code was made capable of utilizing other than energy per fission, energies also from capture reaction and $(n, 2n)$ reaction, along with their respective reaction rates in order to perform power normalization. Earlier this code only had the capability to perform power normalization using energy per fission and the fission rate.

The burnup model was tested by creating an alternate library which included only modified fission energy for all the actinides which were part of the burnup chain. This modified fission energy for each actinide was including decay, fission energy and capture energy, as recommended by the WLUP. It was found during the benchmark studies that when one considers explicit treatment of reaction rates and their corresponding energies, the fuel depletion was faster. This effect is reversed when one considers a nuclide (other than actinide) that can contribute to power normalization with energy released from capture of neutron. In our case we have studied gadolinium, which is considered in burnable absorber rods for suppression of initial excess reactivity in light water reactors. Interestingly, when one considers explicit treatment of energies and their corresponding reaction rates, the gadolinium burnt slowly and fuel was found to be reactive beyond the burnup stage where the other model predicted total burnout of gadolinium.

The depletion behaviour of PWR thorium pincell using DRAGON was compared with the model incorporated in MONTEBURNS. It was found that the k_∞ predicted by DRAGON was within 0.5% of the value estimated by MONTEBURNS. The number densities of the

actinides matched well and was within 10%. Some of the fission products showed a large deviation. This was mainly due to the different yields provided in the cross section libraries that was supplied with ORIGEN code and that which was generated in house.

Interesting trends were observed when gadolinium forms part of the fuel pin. It is important to consider at least ten layers of equal volume within the fuel pin in order to simulate onion peel like burnup behaviour. The burnup steps should be as small as possible (say) 50 MWd/T till the gadolinium gets completely burnt. When gadolinium was used along with uranium, it enhanced the production of plutonium isotopes. This is due to hardening of spectrum, which leads to increased supply of neutrons to the resonances of ^{238}U.

We also obtained the contribution of each reaction towards power normalization. In situations where only actinides are present in the fuel, the contribution to power normalization due to energy from fission is of the order of 95-96%, while the remaining is from capture. In cases where gadolinium forms part of fuel, almost 25% of energy contribution is due to capture of neutrons by ^{155}Gd and ^{157}Gd. There is a small negative contribution to power normalization due to $(n, 2n)$ reaction. It is therefore important to introduce into the lattice codes, power normalization capability taking into consideration energy from fission, capture and $(n, 2n)$ reactions.

SCOPE FOR FUTURE STUDIES

It was observed in CANDU-NG lattice that the basic k_{∞} obtained even after using advanced self shielding models was different from that obtained using MCNP5. It will be interesting to propose a benchmark and obtain solutions for this lattice from other laboratories.

Almost all the benchmarks have been studied with the recommendations by Santamarina for use of four rings having volumes of 50%, 30%, 15% and 5% within fuel pin. It will be interesting to study the dependence of choice of number of rings and their respective volumes within the fuel pin on the spectrum of lattice.

We have used a 172 group mesh throughout our calculation. It will be interesting to implement 281 SHEM (Santamarina-Hfaiedh Energy Mesh) [Hfaiedh 2005] into GROUPR and study the effects of self shielding models. If the 172 group mesh is used, the lower limit of autolib data was fixed at 2.67 eV. It is exactly on the energy boundary of resonance of ^{242}Pu. As none of our benchmarks had a high concentration of ^{242}Pu, the effect due to this resonance was not observed. A benchmark with high concentration of ^{242}Pu, if studied, can bring out the importance of choice of energy group structure below 2.67 eV.

The self shielding models have not been tested for fast reactor benchmarks. It will be interesting to study the effect of choice of group structure in the unresolved resonance group.

The depletion calculations have been performed under the assumption that the gamma energy is deposited at its emission location. But in actual cases, it may be transported at another location in the lattice. It will be interesting to study the gamma transport ant its ef-

fect on power distribution. Also the depletion model needs to be tested on an infinite lattice of PWR/BWR fuel with many gadolinium rods. It will be interesting to study the depletion behaviour of CANDU-NG lattice which has dysprosium in the centre with the new burnup model. Dysprosium, like gadolinium has a high absorption cross section and magnitude of energy released by capture is as high as gadolinium. It will also be interesting to study the depletion behaviour of gadolinium when it is not mixed with fuel.

We have used 150 fission products in the depletion chain. There are no pseudo fission products. It was found during the studies, that the contribution by many fission products towards absorption was very negligible. It will be interesting to provide a unique choice of fission products that needs to be included as part of the depletion chain from reactivity considerations. It will still be important to include as many fission products and actinides from the radio toxicity study point of view.

The fission yields provided in libraries supplied with code ORIGEN needs to be looked into. In order to resolve the differences between DRAGON and MONTEBURNS, a study can be undertaken to artificially modify the fission yields in ORIGEN to that which is used in DRAGON.

It will be interesting to study the energy released from an irradiated fuel, when it is kept away from neutron field. It has also been modelled in MONTEBURNS. So a validation study on the out of core cooling behaviour of fuel assemblies can be studied and compared.

REFERENCES

Alcouffe, R. E., Baker, R. S., Brinkley, F. W., Marr, D. R., O'Dell, R. D., and Walters, W. F. (1995). DANTSYS: A Diffusion Accelerated Neutral Particle Transport Code System. LA-12969-M. Los Alamos National Laboratory, New Mexico, U.S.A.

Askew, J. R., Fayers, F. J., and Kemshell, P. B. (1966). A General Description of the Code WIMS. *J. British Nucl. Energy Soc.,5*(4), 564-584.

Both, J. P., and Peneliau, Y. (1996). The Monte Carlo code TRIPOLI-4 and its first benchmark interpretations. *Proc. on International Conference on the Physics of Reactors (PHYSOR 96), Mito, Japan.*

Casal, J. J., Stamm'ler, R. J. J., Villarino, E. A., and Ferri, A. A. (1991). HELIOS: Geometric Capabilities of a New Fuel-Assembly Program. *Proc. Int. Top. Mtg. on Advances in Mathematics, Computation, and Reactor Physics, Pittsburgh, U.S.A.*

Chan, P. S. W., Tsang, K. T., and Buss, D.B. (2001). Reactor Physics of NG CANDU. *22nd Annual Conference of the Canadian Nuclear Society, Toronto, Canada.*

Choi, H. B., Choi, J. W. and Yang, M. S. (1999). Composition Adjustment on Direct Use of Spent Pressurized Water Reactor Fuel in CANDU. *Nuclear Science and Engineering, 131*(1), 62-77.

Cotton, C. A., Lee, D. et. al. (2005). Physics Analysis of Coolant Voiding in the ACR-700 Lattice. *2005 ANS Annual Meeting - The Next 50 years : Creating opportunities, San Diego, California, U.S.A*

Croff, A. G. (1980). *A User's Manual for the ORIGEN2 Computer Code.* ORNL/TM-7175. Oak Ridge National Laboratory.

Cullen, D. E. (1977). *Calculation of Probability Table Parameters to Include Intermediate Resonance Self-Shielding.* Report UCRL-79761. Lawrence Livermore Laboratory, San Francisco, California, U.S.A.

Cullen, D. E. (2002). *PREPRO2002: The 2002 ENDF/B Pre-Processing Codes.* IAEA-NDS-39, Rev. 11. Nuclear Data Section, International Atomic Energy Agency, Vienna, Austria.

Donnelly, J. V. (1986). *WIMS-CRNL: A User's Manual for the Chalk River Version of WIMS.* AECL-8955. Atomic Energy of Canada Limited.

El Hajjami, S. (2001). Production d'une interface-librairie de section efficaces intégré au logiciel DRAGON. Mémoire de maîtrise, École Polytechnique de Montréal, Québec, Canada.

Engle Jr., W. W. (1967). ANISN, A One Dimensional Discrete Ordinates Transport Code with Anisotropic Scattering. K-1693, Oak Ridge Gaseous Diffusion Plant, U.S.A.

Friedlander, G., Kennedy, J. W., Macias, E. S., and Miller, J. M. (1981). *Nuclear and Radiochemistry.* 3^{rd} ed. Wiley-Interscience Publication. 684p.

Goldstein, R., and Cohen, E. R. (1962). Theory of Resonance Absorption of Neutrons. *Nuclear Science and Engineering, 13,* 132.

Halsall, M. J. (1996). WIMS7, An Overview. *Proc. on International Conference on the Physics of Reactors (PHYSOR 96), Mito, Japan.*

Hébert, A., and Marleau, G. (1991). Generalization of the Stamm'ler Method for the self shielding of resonant isotopes in arbitrary geometries. *Nuclear Science and Engineering, 108*(3), 230-239.

Hébert, A., and Saygin, H. (1992). Development of DRAGR for the Formatting of DRAGON Cross-section Libraries. *Seminar on NJOY-91 and THEMIS for the Processing of Evaluated Nuclear Data Files, NEA Data Bank, Saclay, France.*

Hébert, A. & Mathonnière, G. (1993). Development of a third-generation *Superhomogénéisation* method for the homogenization of a pressurized water reactor assembly. *Nuclear Science and Engineering, 115*(2), 129-141.

Hébert, A. (1998). A Comparison of Three Methods for Computing Probability Tables. *Proc. Int. Conf. on the Physics of Nuclear Science and Technology, Hauppage, New York, U.S.A.*

Hébert, A., and Coste, M. (2002). Computing Moment-Based Probability Tables for Self-Shielding Calculations in Lattice Codes. *Nuclear Science and Engineering, 142*(3), 245-257.

Hébert, A., Marleau, G. and Roy, R. (2006). *A Description of the DRAGON and TRIVAC Version4 Data Structures.* Report IGE-295. Institut de génie nucléaire, École Polytechnique de Montréal, Québec, Canada.

Hébert, A. (2004). Revisiting the Stamm'ler self shielding model. *25th CNS Annual Conference, Toronto, Canada.*

Hébert, A. (2005). A Presentation of the Ribon Extended Self Shielding Model. *Nuclear Science and Engineering, 151*(1). 1-24.

Hfaiedh, N. and Santamarina, A. (2005). Determination of the Optimized SHEM Mesh for Neutron Transport Calculations. *Proc. Int. Topical Meeting on Mathematics and Computation, Supercomputing, Reactor Physics, and Nuclear and Biological applications, M&C 2005, Avignon, France.*

Hiroshi, A., Ishiguro, Y., and Takano, H. (1988). *High conversion light water reactor lattices.* NEACRP-L-309. Japanese Atomic Energy Research Institute. Japan.

International Atomic Energy Agency. (1996). *Safe Core Management with Burnable Absorbers in WWERs.* IAEA-TECDOC-858.

Jagannathan, V., Usha Pal, Karthikeyan, R., Ganesan, S., Jain, R.P., and Kamat, S.U. (2001). A Thorium Breeder Reactor Concept for An Early Induction of Thorium in An Enriched Uranium Reactor. *Nuclear Technology, 133*(1), 1-32.

Kakodkar, A., Sinha, R. K., and Dhawan, M. L. (1998). General description of Advanced Heavy Water Reactor. *International symposium on trends in design and technology development for evolutionary water cooled reactors, Seoul, Korea.*

Le Tellier, R., Hébert, A., and Marleau, G. (2006). The implementation of a 3 D characteristics solver for the generation of incremental cross sections for reactivity devices in a CANDU reactor. *Topical Meeting on Advances in Nuclear Analysis and Simulation, Vancouver, Canada.*

Lebenhaft, J. R., and Treulle, H. R. (2003). Validation of MONTEBURNS for MOX Fuel Using ARIANE Experimental Results. *Nuclear Mathematical and Computational Sciences: A Century in Review, A Century Anew, Gatlinburg, Tennessee, U.S.A.*

Lee, J. S., Song, K. C., Yang, M. S., Chun, K. S., Rhee, B. W., Hong, J. S., Park, H. S., Rim, C. S. and Keil, H. (1993). Research and Development Program of KAERI for DUPIC (Direct Use of Spent PWR Fuel in CANDU Reactors. *Proc. Int. Conf. Future Nuclear Systems:Emerging Fuel Cycles and Waste Disposal Options(GLOBAL'93), Seattle, Washington, U.S.A.*

Leszcynski, F., Aldama, D. L., and Trkov, A. (2003). *WIMS-D Library Update Final report of a co-ordinated research project*, IAEA-TECDOC-Draft. 2003. http://www-nds.iaea.org/wimsd/download/tecdocdraft.pdf. (Page consulted on July 20, 2004).

Lone, M. A. (2001). Fuel Temperature Reactivity Coefficient of a CANDU Lattice - Numerical Benchmark of WIMS-AECL(2-5d) Against MCNP. *22nd CNS Annual Conference, Toronto, Canada.*

Loubière, S., Sanchez, R., Coste, M., Hébert, A., Stankovski, Z., Van Der Gucht, C., and Zmijarevic, I. (1999). APOLLO2, Twelve Years Later. *Int. Conf. on Mathematics and Computation, Reactor Physics and Environmental Analysis in Nuclear Applications, Madrid, Spain.*

MacFarlane, R. E. (1992). *TRANSX 2: A Code for Interfacing MATXS Cross-Section Libraries to Nuclear Transport Codes.* Report LA 12312 MS. Los Alamos National Laboratory, New Mexico, U.S.A.

MacFarlane, R. E. and Muir, D.W. (2000). *NJOY99.0 Code System for Producing Pointwise and Multigroup Neutron and Photon Cross Sections from ENDF/B Data.* PSR-480/NJOY99.0. Los Alamos National Laboratory, New Mexico, U.S.A.

Marleau, G., Hébert, A. and Roy, R. (2000). *A User Guide for DRAGON. Version DRAGON-000331 Release 3.04.* Report IGE-174 Rev.5. Institut de génie nucléaire, École Polytechnique de Montréal, Québec, Canada.

Marleau, G., Hébert, A. and Roy, R. (2006). *A User Guide for DRAGON 3.05C.* Report IGE-174 Rev.6C. Institut de génie nucléaire, École Polytechnique de Montréal, Québec, Canada.

Marleau, G., Hébert, A. and Roy, R. (2006). *A User Guide for DRAGON Version4.* Report IGE-294. Institut de génie nucléaire, École Polytechnique de Montréal, Québec, Canada.

Marleau, G. (2005). *New Geometries Processing in DRAGON: The NXT: Module.* Report IGE-260. Institut de génie nucléaire, École Polytechnique de Montréal, Québec, Canada.

Matsumoto, H., Ouisloumen, M., Yamaji, K., and Takeda, T. (2006). Depletion Calculations for PWR Assemblies including Burnable Absorbers with Lattice Code PARAGON. *Journal of Nuclear Science and Technology, 43*(2), 179-188.

Members of the Cross Section Evaluation Working Group. (2001). *ENDF-102 Data Formats and Procedures for the Evaluated Nuclear Data File ENDF-6.* BNL-NCS-44945-01/04-Rev. Brookhaven National Laboratory, Brookhaven, U. S. A.

Mosteller, R. D., Eisenhart, L. D.,Little, R. C., Eich, W. J., Chao, J. (1991). Benchmark Calculations for the Doppler Coefficient of Reactivity. *Nuclear Science and Engineering, 107*(3), 265-271.

Nordheim, L. W. (1961). The Theory of Resonance Absorption. *Proc. Symp. Applied Mathematics, Vol. XI: Nuclear Reactor Theory*, p.58, G. Birkhoff and E. P. Wigner, Eds., American Nuclear Society, 1961.

Ouisloumen, M. et al. (2003). The new lattice code PARAGON and its qualification for PWR core applications. *Proc. Int. Conf. on Supercomputing in Nuclear Applications, SNA'2003, Paris, France.*

Poston, D. I. and Trellue, H. R. (1999). *User's Manual, Version 2.0, for MONTEBURNS, Version 1.0.* LA-UR-99-4999. Los Alamos National Laboratory, New Mexico, U.S.A.

Press, W. H., Flannery, B. P., Teukolsky, S. A., and Vetterling, W. T. (1994). *Numerical Recipes in Fortran 77: The Art of Scientific Computing.* 2^{nd} ed. Cambridge: Cambridge University Press. 933p.

Reuss, P., and Coste-Declaux, M. (2003). Development of Computational Models Used in France for Neutron Resonance Absorption in Light Water Lattices". *Progress in Nuclear Energy, 42*(3), 237-282.

Rhoades, W. A. and Chiids, R. L. (1988). The DORT Two.Dimensional Discrete Ordinates Transport Code. *Nuclear Science and Engineering, 99*(1), 88-89.

Ribon, P. (1989). Statistical Probability Tables. CALENDF Program. *Proc. of the Seminar on NJOY and THEMIS, Saclay, France.* OECD/NEA Data Bank, P.220-232.

Roh, G. and Choi, H. (2000). Benchmark Calculations for Standard and DUPIC CANDU Fuel Lattices Compared with the MCNP-4B Code. *Nuclear Technology, 132*(1), 128-151.

Rowlands, J., Benslimane-Bouland, A., Bernnat, W., Cathalau, S., Coste, M. et al. (1999). *LWR Pin Cell Benchmark Intercomparisons.* An Intercomparison study organized by the JEF Project, with contributions by Britain, France, Germany, The Netherlands, Slovenia and the USA. JEF Report to be published. OECD/NEA Databank.

Santamarina, A., Collignon, C., and Garat, C. (2004). French Calculation Schemes for Light Water Reactor Analysis. *PHYSOR 2004 -The Physics of Fuel Cycles and Advanced Nuclear Systems: Global Developments, Chicago, U.S.A.*

Saygin, H., and Hébert, A. (1996). A New Self-Shielding Method Based on a Detailed Cross-Section Representation in the Resolved Energy Domain. *Nuclear Science and Engineering, 122*(2), 276-282.

Smith, M. A., Lewis, E. E., and Byung-Chan Na. (2004). Benchmark on Deterministic 2-D MOX Fuel Assembly Transport Calculations without Spatial Homogenization. *Progress in Nuclear Energy, 45*(2-4), 107-118.

Stamm'ler, R. J. J., and Abbate, M. J. (1983). *Methods of steady-state reactor physics in nuclear design.* London ; New York : Academic Press, 1983. 506p.

Talebi, F., Marleau, G., and Koclas, J. (2006). A model for coolant void reactivity evaluation in assemblies of CANDU cells. *Annals of Nuclear Energy, 33*(11-12), 975-983.

Trkov, A. (2005). Guidelines for nuclear data verification and validation. INDC(SEC)-0107. IAEA, Vienna, Austria.

X-5 Monte Carlo Team. (2003). MCNP- A General Monte Carlo N-Particle Transport Code, Version 5. LA-CP-03-0245. Los Alamos National Laboratory, New Mexico, U.S.A.

Yamamoto, M. (1985). Coarse Time-Step Integration Method for Burnup Calculation of LWR Lattice Containing Gadolinium-Poisoned Rods. *Journal of Nuclear Science and Technology, 22*(1), 1-15.

Zhao, X., Pilat, E. E., Weaver, K. D., and Hejzlar, P. (2000). A PWR Thorium Pin Cell Burnup Benchmark. *PHYSOR 2000 International Conference (ANS) International Topical Meeting on Advances in Reactor Physics and Mathematics and Computation into the Next Millennium, Pittsburgh, Pennsylvania, U.S.A.*

APPENDIX I

NUCLEAR DATA USED IN RESEARCH

Table I.1 Temperature (in K) at which cross sections were generated

ID	Temperature (in K)
T1	293.6, 323.6, 573.6
T2	345.7, 353.0, 560.7, 573.0
T3	293.6, 323.6, 573.6, 600.0, 841.3, 900.0, 941.3, 960.0, 1041.3, 1100.0
T4	293.0, 300.0, 560.0, 600.0, 841.3, 900.0, 941.3, 960.0, 1041.3, 1100.0
T5	353.0
T6	293.0, 300.0, 345.7, 353.0, 560.7, 573.0, 600.0, 610.0, 621.1

Table I.2 Dilutions (in barns) chosen for cross section generation

ID	Dilution (in barns)
D1	1.e10, 10000.0, 3549.18335, 1259.67004, 447.079956, 158.676849, 56.3173141, 19.9880447, 7.09412289, 2.51783395
D2	1.e10, 10000.0, 5957.50244, 3549.18335, 2114.42676, 1259.67004, 750.448669, 447.079956, 266.347961, 158.676849, 94.5317612, 56.3173141, 33.5510521, 19.9880447, 11.9078817, 7.09412289, 4.22632504, 2.51783395, 1.5
D3	1.e10, 10000.0, 5957.50244, 3549.18335, 2114.42676, 1259.67004, 750.448669, 447.079956, 266.347961, 158.676849, 94.5317612, 56.3173141, 33.5510521, 19.9880447, 11.9078817, 7.09412289, 4.22632504
D4	1.e10, 10000.0, 5957.50244, 3549.18335, 2114.42676, 1259.67004, 750.448669, 447.079956, 266.347961, 158.676849, 94.5317612, 56.3173141, 33.5510521, 19.9880447, 11.9078817, 7.09412289, 4.22632504, 2.51783395
D5	1.e10, 10000.0, 3549.18335, 1259.67004, 447.079956, 158.676849, 56.3173141

Table I.3 Elements in the library without dilution

Element	ID	Evaluation	Temps.	Element	ID	Evaluation	Temps.
H1	125	JEF2	T1	H1 in H2O	1	JEF2	
H2	128	JEF2	T1	H2 in D2O	11	JEF2	
He4	228	JENDL-3.2	T5	B10	525	ENDF/B-VI R1	T2
B11	528	ENDF/B-VI R8	T2	O16	825	ENDF/B-VI R8	T3
Cr50	2425	ENDF/B-VI R8	T2	Cr52	2431	ENDF/B-VI R8	T2
Cr53	2434	ENDF/B-VI R8	T2	Cr54	2437	ENDF/B-VI R8	T2
Fe54	2625	ENDF/B-VI R8	T2	Fe56	2631	ENDF/B-VI R8	T2
Fe57	2634	ENDF/B-VI R8	T2	Fe58	2637	ENDF/B-VI R8	T2
Ni58	2825	ENDF/B-VI R8	T2	Ni60	2831	ENDF/B-VI R8	T2
Ni61	2834	ENDF/B-VI R8	T2	Ni62	2837	ENDF/B-VI R8	T2
Ni64	2843	ENDF/B-VI R8	T2	Nb93	4125	ENDF/B-VI R6	T2
Ge72	3231	ENDF/B-VI R0	T4	Ge73	3234	ENDF/B-VI R2	T4
Ge74	3237	ENDF/B-VI R0	T4	Ge76	3243	ENDF/B-VI R0	T4
As75	3325	ENDF/B-VI R0	T4	Se76	3431	ENDF/B-VI R0	T4
Se77	3434	ENDF/B-VI R0	T4	Se78	3437	ENDF/B-VI R0	T4
Se79	3440	JEFF-3.0	T4	Se80	3443	ENDF/B-VI R0	T4
Se82	3449	ENDF/B-VI R0	T4	Br79	3525	ENDF/B-VI R0	T4
Br81	3531	ENDF/B-VI R0	T4	Kr80	3631	ENDF/B-VI R0	T4
Kr82	3637	ENDF/B-VI R0	T4	Kr83	3640	JENDL-3.2	T4
Kr84	3643	ENDF/B-VI R0	T4	Kr85	3646	ENDF/B-VI R0	T4
Kr86	3649	ENDF/B-VI R0	T4	Rb85	3725	JEF2	T4
Rb87	3731	ENDF/B-VI R8	T4	Sr86	3831	ENDF/B-VI R0	T4
Sr87	3834	ENDF/B-VI R0	T4	Sr88	3837	ENDF/B-VI R0	T4
Sr89	3840	JEFF-3.0	T4	Sr90	3843	JEFF-3.0	T4
Y89	3925	ENDF/B-VI R4	T4	Y91	3931	JEFF-3.0	T4
Zr90	4025	ENDF/B-VI R8	T4	Zr91	4028	ENDF/B-VI R8	T4
Zr92	4031	ENDF/B-VI R8	T4	Zr93	4034	ENDF/B-VI R0	T4
Zr94	4037	ENDF/B-VI R8	T4	Zr95	4040	ENDF/B-VI R0	T4
Zr96	4043	ENDF/B-VI R8	T4	Nb94	4128	ENDF/B-VI R0	T4
Nb95	4131	JEF2	T4	Mo95	4234	JENDL-3.2	T4
Mo96	4237	ENDF/B-VI R0	T4	Mo97	4240	ENDF/B-VI R0	T4
Tc99	4331	JENDL-3.2	T4	Ru99	4434	ENDF/B-VI R0	T4
Ru100	4437	ENDF/B-VI R0	T4	Ru101	4440	JENDL-3.2	T4
Ru102	4443	ENDF/B-VI R2	T4	Ru103	4446	JENDL-3.2	T4
Ru104	4449	ENDF/B-VI R0	T4	Ru106	4455	JENDL-3.2	T4
Rh103	4525	JENDL-3.2	T4	Rh105	4531	JENDL-3.2	T4
Pd104	4631	ENDF/B-VI R5	T4	Pd105	4634	ENDF/B-VI R8	T4

continued, on next page

continued, from previous page

Element	ID	Evaluation	Temps.	Element	ID	Evaluation	Temps.
Pd106	4637	ENDF/B-VI R5	T4	Pd107	4640	ENDF/B-VI R0	T4
Pd108	4643	ENDF/B-VI R5	T4	Pd110	4649	ENDF/B-VI R5	T4
Ag109	4731	JENDL-3.2	T4	Cd111	4840	ENDF/B-VI R0	T4
Cd112	4843	ENDF/B-VI R4	T4	Cd113	4846	ENDF/B-VI R0	T4
Cd114	4849	ENDF/B-VI R4	T4	Cd115m	4852	JEF2	T4
Cd116	4855	ENDF/B-VI R4	T4	In113	4925	ENDF/B-VI R0	T4
In115	4931	JENDL-3.2	T4	Sn115	5034	ENDF/B-VI R0	T4
Sn117	5040	ENDF/B-VI R0	T4	Sn118	5043	ENDF/B-VI R0	T4
Sn119	5046	ENDF/B-VI R0	T4	Sn121m	5053	ENDF/B-VI R0	T4
Sn123	5058	JEFF-3.0	T4	Sn126	5067	ENDF/B-VI R0	T4
Sb121	5125	ENDF/B-VI R8	T4	Sb123	5131	ENDF/B-VI R8	T4
Sb124	5134	JEFF-3.0	T4	Sb125	5137	JENDL-3.2	T4
Te122	5231	JEF2	T4	Te123	5234	JEF2	T4
Te124	5237	JEF2	T4	Te125	5240	JEF2	T4
Te126	5243	JEF2	T4	Te127m	5247	JENDL-3.2	T4
Te128	5249	JEF2	T4	Te129m	5253	JEFF-3.0	T4
Te130	5255	JEF2	T4	I127	5325	ENDF/B-VI R2	T4
I129	5331	ENDF/B-VI R0	T4	I135	5349	JEF2	T4
Xe128	5437	ENDF/B-VI R0	T4	Xe130	5443	ENDF/B-VI R0	T4
Xe131	5446	JENDL-3.2	T4	Xe132	5449	ENDF/B-VI R0	T4
Xe134	5455	JENDL-3.2	T4	Xe135	5458	JENDL-3.2	T4
Xe136	5461	JENDL-3.2	T4	Cs133	5525	ENDF/B-VI R0	T4
Cs134	5528	ENDF/B-VI R0	T4	Cs135	5531	ENDF/B-VI R0	T4
Cs137	5537	JENDL-3.2	T4	Ba134	5637	ENDF/B-VI R0	T4
Ba135	5640	ENDF/B-VI R0	T4	Ba136	5643	ENDF/B-VI R0	T4
Ba137	5646	ENDF/B-VI R0	T4	Ba138	5649	ENDF/B-VI R1	T4
La138	5725	JEFF-3.0	T4	Ce140	5837	ENDF/B-VI R0	T4
Ce141	5840	JEFF-3.0	T4	Ce142	5843	ENDF/B-VI R0	T4
Ce144	5849	JEFF-3.0	T4	Pr141	5925	ENDF/B-VI R0	T4
Nd142	6025	ENDF/B-VI R0	T4	Nd143	6028	JENDL-3.2	T4
Nd144	6031	ENDF/B-VI R0	T4	Nd145	6034	JENDL-3.2	T4
Nd146	6037	ENDF/B-VI R0	T4	Nd148	6043	ENDF/B-VI R0	T4
Nd150	6049	ENDF/B-VI R0	T4	Pm147	6149	JENDL-3.2	T4
Pm148	6152	JENDL-3.2	T4	Pm148m	6153	ENDF/B-VI R0	T4
Pm149	6155	JENDL-3.2	T4	Sm147	6234	JENDL-3.2	T4
Sm148	6237	JENDL-3.2	T4	Sm149	6240	ENDF/B-VI R0	T4
Sm150	6243	JENDL-3.2	T4	Sm151	6246	JENDL-3.2	T4
Sm152	6249	JENDL-3.2	T4	Sm154	6255	ENDF/B-VI R0	T4
Eu151	6325	ENDF/B-VI R0	T4	Eu152	6328	JENDL-3.2	T4

continued, on next page

continued, from previous page

Element	ID	Evaluation	Temps.	Element	ID	Evaluation	Temps.
Eu153	6331	ENDF/B-VI R0	T4	Eu154	6334	ENDF/B-VI R0	T4
Eu155	6337	ENDF/B-VI R1	T4	Tb159	6525	ENDF/B-VI R0	T4
Tb160	6528	ENDF/B-VI R0	T4	Ho165	6725	ENDF/B-VI R5	T4
Er166	6837	ENDF/B-VI R0	T4	Er167	6840	ENDF/B-VI R0	T4

Table I.4 Elements in the library with dilution

Element	ID	Evaluation	Temps.	Pot sctg	Dilutions
Zr0	4000	JENDL-3.2	T6	6.5144	D1
Gd152	6425	ENDF/B-VI R8	T4	5.8107	D1
Gd154	6431	JENDL-3.2	T4	7.6744	D1
Gd155	6434	JENDL-3.2	T4	5.7493	D1
Gd156	6437	JENDL-3.2	T4	7.9722	D1
Gd157	6440	JENDL-3.2	T4	4.1863	D1
Gd158	6443	JENDL-3.2	T4	5.3521	D1
Gd160	6449	JENDL-3.2	T4	5.8107	D1
Dy160	6637	JEF2	T4	5.3896	D1
Dy161	6640	JEF2	T4	5.4120	D1
Dy162	6643	JEF2	T4	5.4347	D1
Dy163	6646	JEF2	T4	5.4570	D1
Dy164	6649	JEF2	T4	7.2936	D1
Th230	9034	JENDL-3.2	T4	8.7040	D1
Th232	9040	JENDL-3.2	T4	11.8699	D2
Pa231	9131	JENDL-3.2	T4	8.7266	D1
Pa233	9137	JENDL-3.2	T4	9.9950	D1
U232	9219	JENDL-3.2	T4	12.0687	D1
U233	9222	ENDF/B-VI R0	T4	12.2989	D1
U234	9225	JENDL-3.2	T4	12.0113	D1
U235	9228	ENDF/B-VI R5	T4	11.6070	D2
U236	9231	JENDL-3.2	T4	11.2615	D1
U237	9234	JENDL-3.2	T4	11.3949	D1
U238	2922	CENDL-2.6	T4	11.8237	D2
Np237	9346	ENDF/B-VI R1	T4	11.4369	D1
Np239	9352	ENDF/B-VI R0	T4	10.4979	D1
Pu238	9438	FOND-2.294	T4	10.9999	D2
Pu239	9439	FOND-2.294	T4	10.7600	D3
Pu240	9440	FOND-2.294	T4	9.2474	D2
Pu241	9441	FOND-2.294	T4	12.0000	D4
Pu242	9442	FOND-2.294	T4	10.5000	D2
Am241	9541	FOND-2.295	T4	11.0329	D2
Am242	9542	FOND-2.295	T4	11.4369	D1
Am242m	9512	FOND-2.2	T4	11.7694	D5
Am243	9543	FOND-2.2	T4	10.6144	D1
Cm242	9631	JENDL-3.2	T4	10.7518	D5
Cm243	9634	JENDL-3.2	T4	12.2668	D5
Cm244	9637	JENDL-3.2	T4	14.2109	D5

APPENDIX II

GROUP STRUCTURE FOR DRAGLIB

Table II.1 French XMAS neutron energy group structure (in eV)

Group	Energy range (eV)	Group	Energy range (eV)
1	1.96403E+07 - 1.73325E+07	32	1.83156E+05 - 1.22773E+05
2	1.73325E+07 - 1.49182E+07	33	1.22773E+05 - 1.11090E+05
3	1.49182E+07 - 1.38403E+07	34	1.11090E+05 - 8.22975E+04
4	1.38403E+07 - 1.16183E+07	35	8.22975E+04 - 6.73795E+04
5	1.16183E+07 - 1.00000E+07	36	6.73795E+04 - 5.51656E+04
6	1.00000E+07 - 8.18731E+06	37	5.51656E+04 - 4.08677E+04
7	8.18731E+06 - 6.70320E+06	38	4.08677E+04 - 3.69786E+04
8	6.70320E+06 - 6.06531E+06	39	3.69786E+04 - 2.92830E+04
9	6.06531E+06 - 5.48812E+06	40	2.92830E+04 - 2.73944E+04
10	5.48812E+06 - 4.49329E+06	41	2.73944E+04 - 2.47875E+04
11	4.49329E+06 - 3.67879E+06	42	2.47875E+04 - 1.66156E+04
12	3.67879E+06 - 3.01194E+06	43	1.66156E+04 - 1.50344E+04
13	3.01194E+06 - 2.46597E+06	44	1.50344E+04 - 1.11378E+04
14	2.46597E+06 - 2.23130E+06	45	1.11378E+04 - 9.11882E+03
15	2.23130E+06 - 2.01896E+06	46	9.11882E+03 - 7.46586E+03
16	2.01896E+06 - 1.65299E+06	47	7.46586E+03 - 5.53084E+03
17	1.65299E+06 - 1.35335E+06	48	5.53084E+03 - 5.00451E+03
18	1.35335E+06 - 1.22456E+06	49	5.00451E+03 - 3.52662E+03
19	1.22456E+06 - 1.10803E+06	50	3.52662E+03 - 3.35463E+03
20	1.10803E+06 - 1.00259E+06	51	3.35463E+03 - 2.24867E+03
21	1.00259E+06 - 9.07180E+05	52	2.24867E+03 - 2.03468E+03
22	9.07180E+05 - 8.20850E+05	53	2.03468E+03 - 1.50733E+03
23	8.20850E+05 - 6.08101E+05	54	1.50733E+03 - 1.43382E+03
24	6.08101E+05 - 5.50232E+05	55	1.43382E+03 - 1.23410E+03
25	5.50232E+05 - 4.97871E+05	56	1.23410E+03 - 1.01039E+03
26	4.97871E+05 - 4.50492E+05	57	1.01039E+03 - 9.14242E+02
27	4.50492E+05 - 4.07622E+05	58	9.14242E+02 - 7.48518E+02
28	4.07622E+05 - 3.01974E+05	59	7.48518E+02 - 6.77287E+02
29	3.01974E+05 - 2.73237E+05	60	6.77287E+02 - 4.53999E+02
30	2.73237E+05 - 2.47235E+05	61	4.53999E+02 - 3.71703E+02
31	2.47235E+05 - 1.83156E+05	62	3.71703E+02 - 3.04325E+02

continued, on next page

continued, from previous page

Group	Energy range (eV)	Group	Energy range (eV)
63	3.04325E+02 - 2.03995E+02	102	2.13000E+00 - 2.10000E+00
64	2.03995E+02 - 1.48625E+02	103	2.10000E+00 - 2.02000E+00
65	1.48625E+02 - 1.36742E+02	104	2.02000E+00 - 1.93000E+00
66	1.36742E+02 - 9.16609E+01	105	1.93000E+00 - 1.84000E+00
67	9.16609E+01 - 7.56736E+01	106	1.84000E+00 - 1.75500E+00
68	7.56736E+01 - 6.79041E+01	107	1.75500E+00 - 1.67000E+00
69	6.79041E+01 - 5.55951E+01	108	1.67000E+00 - 1.59000E+00
70	5.55951E+01 - 5.15780E+01	109	1.59000E+00 - 1.50000E+00
71	5.15780E+01 - 4.82516E+01	110	1.50000E+00 - 1.47500E+00
72	4.82516E+01 - 4.55174E+01	111	1.47500E+00 - 1.44000E+00
73	4.55174E+01 - 4.01690E+01	112	1.44000E+00 - 1.37000E+00
74	4.01690E+01 - 3.72665E+01	113	1.37000E+00 - 1.33750E+00
75	3.72665E+01 - 3.37201E+01	114	1.33750E+00 - 1.30000E+00
76	3.37201E+01 - 3.05113E+01	115	1.30000E+00 - 1.23500E+00
77	3.05113E+01 - 2.76077E+01	116	1.23500E+00 - 1.17000E+00
78	2.76077E+01 - 2.49805E+01	117	1.17000E+00 - 1.15000E+00
79	2.49805E+01 - 2.26033E+01	118	1.15000E+00 - 1.12300E+00
80	2.26033E+01 - 1.94548E+01	119	1.12300E+00 - 1.11000E+00
81	1.94548E+01 - 1.59283E+01	120	1.11000E+00 - 1.09700E+00
82	1.59283E+01 - 1.37096E+01	121	1.09700E+00 - 1.07100E+00
83	1.37096E+01 - 1.12245E+01	122	1.07100E+00 - 1.04500E+00
84	1.12245E+01 - 9.90555E+00	123	1.04500E+00 - 1.03500E+00
85	9.90555E+00 - 9.18981E+00	124	1.03500E+00 - 1.02000E+00
86	9.18981E+00 - 8.31529E+00	125	1.02000E+00 - 9.96000E-01
87	8.31529E+00 - 7.52398E+00	126	9.96000E-01 - 9.86000E-01
88	7.52398E+00 - 6.16012E+00	127	9.86000E-01 - 9.72000E-01
89	6.16012E+00 - 5.34643E+00	128	9.72000E-01 - 9.50000E-01
90	5.34643E+00 - 5.04348E+00	129	9.50000E-01 - 9.30000E-01
91	5.04348E+00 - 4.12925E+00	130	9.30000E-01 - 9.10000E-01
92	4.12925E+00 - 4.00000E+00	131	9.10000E-01 - 8.60000E-01
93	4.00000E+00 - 3.38075E+00	132	8.60000E-01 - 8.50000E-01
94	3.38075E+00 - 3.30000E+00	133	8.50000E-01 - 7.90000E-01
95	3.30000E+00 - 2.76792E+00	134	7.90000E-01 - 7.80000E-01
96	2.76792E+00 - 2.72000E+00	135	7.80000E-01 - 7.05000E-01
97	2.72000E+00 - 2.60000E+00	136	7.05000E-01 - 6.25000E-01
98	2.60000E+00 - 2.55000E+00	137	6.25000E-01 - 5.40000E-01
99	2.55000E+00 - 2.36000E+00	138	5.40000E-01 - 5.00000E-01
100	2.36000E+00 - 2.13000E+00	139	5.00000E-01 - 4.85000E-01
101	2.13000E+00 - 2.10000E+00	140	4.85000E-01 - 4.33000E-01

continued, on next page

continued, from previous page

Group	Energy range (eV)	Group	Energy range (eV)
141	4.00000E-01 - 3.91000E-01	157	9.50000E-02 - 8.00000E-02
142	3.91000E-01 - 3.50000E-01	158	8.00000E-02 - 7.70000E-02
143	3.50000E-01 - 3.20000E-01	159	7.70000E-02 - 6.70000E-02
144	3.20000E-01 - 3.14500E-01	160	6.70000E-02 - 5.80000E-02
145	3.14500E-01 - 3.00000E-01	161	5.80000E-02 - 5.00000E-02
146	3.00000E-01 - 2.80000E-01	162	5.00000E-02 - 4.20000E-02
147	2.80000E-01 - 2.48000E-01	163	4.20000E-02 - 3.50000E-02
148	2.48000E-01 - 2.20000E-01	164	3.50000E-02 - 3.00000E-02
149	2.20000E-01 - 1.89000E-01	165	3.00000E-02 - 2.50000E-02
150	1.89000E-01 - 1.80000E-01	166	2.50000E-02 - 2.00000E-02
151	1.80000E-01 - 1.60000E-01	167	2.00000E-02 - 1.50000E-02
152	1.60000E-01 - 1.40000E-01	168	1.50000E-02 - 1.00000E-02
153	1.40000E-01 - 1.34000E-01	169	1.00000E-02 - 6.90000E-03
154	1.34000E-01 - 1.15000E-01	170	6.90000E-03 - 5.00000E-03
155	1.15000E-01 - 1.00000E-01	171	5.00000E-03 - 3.00000E-03
156	1.00000E-01 - 9.50000E-02	172	3.00000E-03 - 1.00001E-05

APPENDIX III

PYTHON SCRIPT TO GENERATE DRAGLIB AND ACELIB

This chapter will describe the procedure for generation of cross section libraries in DRAGLIB format and ACE format. DRAGLIB format libraries will be used for lattice analysis using the code DRAGON and ACE formatted libraries will be used for the analysis using Monte Carlo code MCNP5. Both the sets of libraries have been generated starting from the same evaluated datafiles, that were recommended by the IAEA WIMS Library Update Project (WLUP) [Leszczynski 2003]. A total of 200 nuclides have been used for analysis in this thesis. The libraries have been generated by using a Python script. The script is seen in Figure 1. The input for selected nuclides is presented in Figure 2. Another interesting addition to the script is to compare the generated ACELIB, with the PENDF tape generated by an alternate procedure as recommended by IAEA [Trkov 2005]. This involves regeneration of the PENDF file from the ACELIB using a code package called ACELST. Modules from PREPRO code system developed by Red Cullen are subsequently used on the evaluated data files and PENDF tape is generated. The modules used are LINEAR, RECENT, SIGMA1. Subsequently one can do a comparison of the two PENDF files using COMPLOT, which is another important module of PREPRO code system.

This chapter has three main sections. First section will give a general description of instance variables and methods needed to generate the various libraries. The second section will describe the steps needed to generate DRAGLIB. The third section will describe the generation of ACELIB and the final section will describe verification of generated ACE libraries by procedure recommended by IAEA.

PyNjoy Script

The generation of libraries has been made simple by the use of Python script. A complete processing of an evaluated datafile is done by invoking modules of NJOY through an object oriented Python script. A unique class named PyNjoy contains the various instance variables and methods required to use NJOY in the simplest possible way. Any modification of this model is possible in order to accommodate various processing requirements.

PyNjoy instance variables

Python parameters used in the input are described in this section.

`self.evaluationName` - Name of directory where you want to store the draglib and acelib files

`self.legendre` - Order of Legendre polynomials (=1 for LINEAR anisotropy in LAB – default)

`self.nstr` - Option for a particular group structure (=22 for the XMAS 172–group structure)

`self.iwt` - Type of flux weighting in GROUPR (=1 for user-defined spectra; =3 for $1/E$ weighting; =4 recommended/default)

`self.wght` - User-defined weighting spectra to be used if `self.iwt` $= 1$. Given as `" " "`–delimited string.

`self.autolib` - Two-component tuple containing the energy limits of the autolibs (must correspond to energy-group limits)

`self.temperatures` - Value of temperatures at which the cross sections are generated

`self.hmat` - Material name that is included in the DRAGLIB - User dependent

`self.mat` - `mat` number of nuclide under consideration

`self.za` - ZA number, mainly required for generation of S(alpha, beta) cross section in ACER

`self.scatName` - Name of S(α, β) cross section identifier for inclusion in xsdir

`self.suff` - The suffix to be attached to nuclide in ACELIB - User dependent

`self.evaluationFile` - Path of the evaluated datafile

`self.scatteringLaw` - Path of file having thermal scattering data (default = `None`)

`self.scatteringMat` - `mat` number in scattering data file

`self.fission` - Choice for including delayed neutron fission data in GROUPR module

`self.ss` - Two-component tuple containing energy limits in eV for recovering of punctual (autolib) data

`self.potential` - Value of the potential cross section used in the flux calculator of GROUPR

`self.dilutions` Tuple containing the dilution values that need to be considered for calculation of resonance integrals and probability tables

`self.dirName` - Directory name to store data for independent verification of ACELIB.

`self.tempace` - Temperature at which ACELIB needs to be generated.

`self.eFiss` - Fission energy in MeV. Used in cases where this value is not available in the evaluation.

`self.branchingNG` - Radiative capture isomeric branching ratio (default = `None`). If you use this value, don't forget to reset it to `None` after the isotope is completed.

`self.branchingN2N` - N2N isomeric branching ratio (default = `None`). If you use this value, don't forget to reset it to `None` after the isotope is completed.

PyNjoy methods

`self.pendf()` - To generate point ENDF file (to be used as starting point for all other data type generations including DRAGLIB, ACE, WIMSD etc., using the modules MODER,

RECONR, BROADR, PURR (if dilutions present), THERMR.

`self.gendf()` - To generate group ENDF file using the modules MODER and GROUPR.

`self.draglib([fp])` - To generate a DRAGLIB file using the modules MODER, DRAGR and add/update the new isotopic data in the DRAGLIB file. If `fp=1`, the scattering information are stored as diagonal matrices in the DRAGLIB.

`self.matxs()` - To generate an ascii MATXS file using the modules MODER and MATXSR.

`self.makeFp()` - call `self.pendf()`, `self.gendf()` and `self.draglib (fp=1)` for a single fission product.

`self.burnup()` - Process burnup data for the complete library. An important file that is needed while generating the burnup data is named as "chain(self)", for e.g. if self is candu then the file is named `chaincandu`. This file contains the information of energy from all isotopes generated using single DRAGR runs. This file is now generated automatically.

`self.acer()` - To generate ACELIB using the modules MODER, RECONR, BROADR, PURR (if dilutions present), THERMR and ACER.

`self.comp()` - To run the verification test using the modules ACELST, LINEAR, RECENT, SIGMA1, FIXUP and COMPLOT.

DRAGLIB Library Generation

The modules that will be used in the generation of DRAGLIB are MODER, RECONR, BROADR, PURR (if dilutions present), THERMR, GROUPR and DRAGR. Figure 2.1 gives the flow chart for generation of DRAGLIB formatted library. It is important to identify the nuclides that are needed to be included as part of library and corresponding evaluated datafiles from respective data centres need to be compiled in a particular directory. This will help in cross verification and assessment at any stage of library generation. In this section, specific examples of elements will be provided to understand the nuances of DRAGLIB library generation. The examples will be such that all the reactor type materials will be chosen. They are scattering

material (heavy water), structural material (Zirconium), fission product (Xe135), Actinide (U-235). A special example for burnup dependent data will also be provided. For isotopes that have resonances and whose presence in fuel can alter the flux in the energy region between 2.76792 eV and 1.66156e4 eV, cross sections are generated at specific dilution values. The choice of dilution values is shown in Table I.2. The value for potential scattering cross section is obtained using the Fortran code `getmf2.f` which is provided at IAEA website "http://www-nds.iaea.org/wimsd/". Using this code, and the evaluated datafile for the particular element, one can obtain the value for `self.potential`. In general we cannot provide more than ten temperature values and ten dilution values. If one has to generate cross sections for more than ten dilution values, it has to be split, as shown in example for U-235. After each "`self.dragr()`" run, one will obtain a file "`out_draglib_elementname`". Energy information is recovered from this ascii file by method `self.burnup()` and is collected in a file named `'chain' + self.evaluationName` (stored on directory `self.evaluationName`). Sometimes, it is likely that fission energy is not provided in the tape. In that case one obtains "`????????`" in the "`out_draglib_elementname`" file. In that case, one has to obtain the energy value from some other source (typically, from another evaluation) and provide it using the `self.eFiss` instance variable, even if one doesn't use the tape for generation of multigroup data.

File 8 of ENDF evaluation contains half-lives, decay modes, decay energies, and radiation spectra for most isotopes. Information concerning the decay of the reaction products is also given in this file. In addition, fission product yield data (MT=454 and 459) for fissionable materials and spontaneous radioactive decay data (MT=457) for the nucleus are included.

The File 8 is processed by module DRAGR. A large number of fission products are included in the evaluated file for each element capable of undergoing fission. For example, in the fission product yield data file included in ENDF/B-VI rel. 8, one can notice that there are information of 1232 fission products for 0.0253 eV fission of ^{233}U, 1247 fission products for 0.0253 eV fission of ^{235}U etc. But the evaluations are not available for all the nuclides, as most of them

have very short half-lives and in the reactor context, can be considered insignificant. They are subsequently lumped by a procedure that is built in DRAGR. If there are nuclides with long half lives, but are not available as evaluated files, a warning is provided before lumping the corresponding element. The DRAGR user has the complete control over the lumping process. DRAGR currently has no capability to produce pseudo fission product, i.e., custom library isotopes made from the combination of many minor ENDF fission products. All the isotopes missing in the `'chain' + self.evaluationName` file are tested against a lumping criterion and are lumped. The criterion for lumping a depleting isotope is a half life less than thirty days and a fission yield less than 0.01%. The lumping process incorporated in DRAGR is shown in Figure III.1.

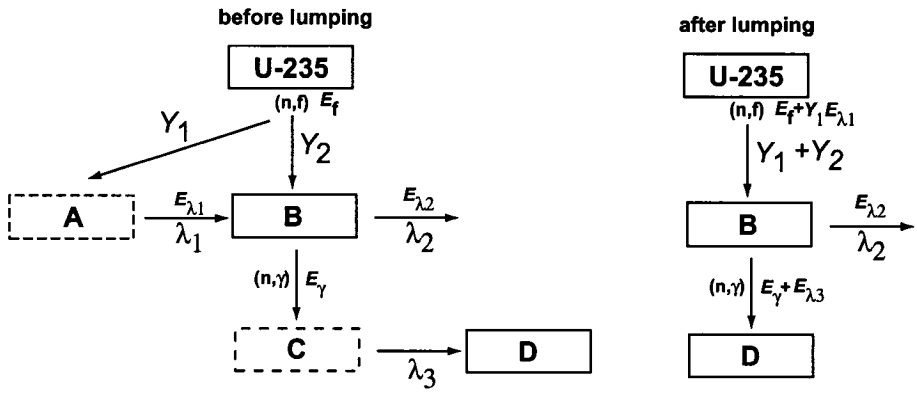

Figure III.1 Lumping of isotopes in DRAGR

Information on energies for various reaction types like (n,γ), (n,f), $(n,2n)$, $(n,3n)$, $(n,4n)$, (n,α), (n,p), $(n,2\alpha)$, (n,np), (n,d), (n,t) are recovered from earlier DRAGR single-isotope calculations and used for inclusion in relevant depletion data in DRAGLIB format. The fission energy (n,f) is obtained from MF1 MT458 and the energy from delayed betas and gammas are subtracted from it. Information regarding energies for other reactions are derived by DRAGR from MF3. The corresponding MT numbers for the above mentioned reactions (other than (n,f) are 102, 16, 17, 37, 107, 103, 108, 28, 104, 105 respectively. The complete information required to do the depletion calculations is provided in ten specific records of the DRAGLIB file. Appendix IV gives the energies corresponding to neutron induced reactions

with elements which are part of the library.

Heavy water

Heavy water is used in CANDU reactors as moderator and coolant. So it is important to generate consistent data for efficient analysis of CANDU lattices. The instance variables and methods that will be used are

candu.hmat = "H2_D2O"

candu.temperatures = (293.6, 323.6, 573.6,)

candu.mat = 128

candu.evaluationFile = "/home/develop/Tripoli4/JEF2/eval/jef2.neutron.H2.bcd"

candu.scatteringLaw = "/home/develop/Tripoli4/JEF2/eval/jef2.neutron.D_D2O.bcd.therm"

candu.scatteringMat = 11

candu.fission = None

candu.dilutions = None

candu.pendf()

candu.gendf()

candu.draglib()

Zirconium

Zirconium is used in CANDU reactors as cladding material and also for pressure tube and calandria tube. Zirconium has some resonances and as a result of this it is important to generate the cross sections of zirconium for certain dilution values. The instance variables and methods that will be used are

candu.hmat = "Zr0"

candu.temperatures = (293.6, 323.6, 573.6,)

candu.mat = 4000

candu.evaluationFile = "/home/karam/Njoy99/evaluations/database/jendl306.asc"

candu.fission = None

candu.ss = (2.76792, 1.66156e4)

candu.potential = 6.5144

candu.dilutions = (1.e10, 10000.0, 3549.18335, 1259.67004, 447.079956, 158.676849, 56.3173141, 19.9880447, 7.09412289, 2.51783395)

candu.pendf()

candu.gendf()

candu.draglib()

Xe135

Xenon is a very important fission product in nuclear reactors. It is very important to estimate the number density of this nuclide as a function of burnup. This will help in estimating reactivity variations due to change in concentration of the nuclide. By using makeFp option, we avoid generating scattering matrices in (NG X NG) format, where NG is number of groups. We instead generate only the scattering matrices along the diagonal.

candu.hmat = "Xe135"

candu.temperatures = (293.6, 323.6, 573.6,)

candu.scatteringLaw = None

candu.legendre = 0

candu.fission = None

candu.dilutions = None

candu.mat = 5458

candu.evaluationFile = "/home/karam/Njoy99/evaluations/database/jendl310.asc"

candu.makeFp()

U235

U-235 is one of the most prevalently used fissile material for energy production. In case of CANDU reactors, natural uranium is used as fuel, where weight (%) of U-235 is 0.711.

candu.hmat = "U235"

candu.temperatures = (293.6, 323.6, 573.6,)

candu.mat = 9228

candu.evaluationFile = "/home/karam/Njoy99/evaluations/database/U-235"

candu.fission = 2

candu.ss = (2.76792, 1.22773e5)

candu.potential = 11.6070

candu.dilutions = (1.e10, 94.5317612, 56.3173141, 33.5510521, 19.9880447, 11.9078817, 7.09412289, 4.22632504, 2.51783395, 1.5)

candu.pendf()

candu.gendf()

candu.draglib()

candu.dilutions = (1.e10, 10000.0, 5957.50244, 3549.18335, 2114.42676, 1259.67004, 750.448669, 447.079956, 266.347961, 158.676849)

candu.pendf()

candu.gendf()

candu.draglib()

Process burnup

It is important to identify the tapes provided by evaluators which contains information on fission yields and decay chains. These files are provided as mentioned below, along with the chain(self) file mentioned already.

candu.fissionFile = "/home/karam/Njoy99/evaluations/database/TAPE.107"
candu.decayFile = "/home/karam/Njoy99/evaluations/database/TAPE.106"
candu.burnup()

ACELIB Library Generation

The modules that will be used in the generation of ACELIB are MODER, RECONR, BROADR, PURR(if dilutions present), THERMR and ACER. Figure 3 gives the flow chart for generation of ACE formatted library. In this section specific examples of elements will be provided to understand the nuances of ACELIB library generation. The examples will be along the same lines as that for DRAGLIB library generation, i.e scattering material (heavy water), structural material (Zirconium), fission product (Xe135), Actinide (U-235). The present script is such that the ACELIBs are appended in a single file named "acecandu" and is available in the same directory as the draglib file. The other important file that is generated is the "acexsdir", which contains the information about the nuclides for which the cross sections are generated and the temperature at which the ACELIB is generated. A small code has been written-"append.f", which will read the file acecandu and acexsdir and create the file "myxsdir". This file has to be appended to existing xsdir file provided with MCNP5 data. It is important to provide suffix values "`self.suff`" for different temperatures. This will be automatically appended to the ZA value and written in main ACELIB and xsdir file. Care should be taken not to repeat the ".suff" value already used in xsdir file for other evaluations. For each temperature provide different "`self.dirName`" so that all the required data for comparison with PENDF tape generated using PREPRO code is made possible. The "`self.comp()`" does the task of verifying the ACELIBs generated, and is described in the next section. The example provided here helps in generating ACELIB alone. In case a DRAGLIB file also is to be generated, please refer to Figure 2.

Heavy water

```
candu.hmat = "H2_D2O"
candu.temperatures = ( 293.6, 323.6, 573.6, )
candu.mat = 128
candu.za = 1002
candu.scatName = "hwtr"
candu.evaluationFile = "/home/develop/Tripoli4/JEF2/eval/jef2.neutron.H2.bcd"
candu.scatteringLaw = "/home/develop/Tripoli4/JEF2/eval/jef2.neutron.D_D2O.bcd.therm"
candu.scatteringMat = 11
candu.fission = None
candu.dilutions = None
candu.pendf()
candu.dirName = "D2O-1"
candu.tempace = ( 293.6,)
candu.suff=0.20
candu.acer()
candu.comp()
candu.dirName = "D2O-2"
candu.tempace = ( 323.6,)
candu.suff=0.21
candu.acer()
candu.comp()
candu.dirName = "D2O-3" candu.tempace = ( 573.6,)
candu.suff=0.22
candu.acer()
candu.comp()
```

Zirconium

```
candu.hmat = "Zr0"
candu.temperatures = ( 293.6, 323.6, 573.6, )
candu.mat = 4000
candu.za = 40000
candu.evaluationFile = "/home/karam/Njoy99/evaluations/database/jendl306.asc"
candu.fission = None
candu.dilutions = ( 1.e10, 10000.0, 3549.18335, 1259.67004, 447.079956,
158.676849, 56.3173141, 19.9880447, 7.09412289, 2.51783395 )
candu.pendf()
candu.dirName = "Zr-1"
candu.tempace = ( 293.6,)
candu.suff=0.20
candu.acer()
candu.comp()
candu.dirName = "Zr-2"
candu.tempace = ( 323.6,)
candu.suff=0.21
candu.acer()
candu.comp()
candu.dirName = "Zr-3"
candu.tempace = ( 573.6,)
candu.suff=0.22
candu.acer()
candu.comp()
```

Xe135

```
candu.hmat = "Xe135"
candu.temperatures = ( 293.6, 323.6, 573.6, )
candu.scatteringLaw = None
candu.legendre = 0
candu.fission = None
candu.dilutions = None
candu.mat = 5458
candu.za = 54135
candu.evaluationFile = "/home/karam/Njoy99/evaluations/database/jendl310.asc"
candu.makeFp()
candu.dirName = "Xe135-1"
candu.tempace = ( 293.6,)
candu.suff=0.20
candu.acer()
candu.comp()
candu.dirName = "Xe135-2"
candu.tempace = ( 323.6,)
candu.suff=0.21
candu.acer()
candu.comp()
candu.dirName = "Xe135-3"
candu.tempace = ( 573.6,)
candu.suff=0.22
candu.acer()
candu.comp()
```

U235

```
candu.hmat = "U235"
candu.temperatures = ( 293.6, 323.6, 573.6, )
candu.mat = 9228
candu.za = 92235
candu.scatteringLaw = None
candu.legendre = 0
candu.evaluationFile = "/home/karam/Njoy99/evaluations/database/U-235"
candu.fission = 2
candu.dilutions = ( 1.e10, 10000.0, 5957.50244, 3549.18335, 2114.42676,
1259.67004, 750.448669, 447.079956, 266.347961, 158.676849 )
candu.dirName = "U235-1"
candu.tempace = ( 293.6,)
candu.suff=0.20
candu.acer()
candu.comp()
candu.dirName = "U235-2"
candu.tempace = ( 323.6,)
candu.suff=0.21
candu.acer()
candu.comp()
candu.dirName = "U235-3"
candu.tempace = ( 573.6,)
candu.suff=0.22
candu.acer()
candu.comp()
```

Verification of ACELIB

Cross section processing verification is described in Trkov 2005, where the steps involved are mentioned in detail. For the sake of completeness, we have presented the discussion as part of this chapter. The ACE ("A Compact ENDF") libraries produced by the NJOY nuclear data processing system, involves some data processing, which is susceptible to code errors. It is important to verify the ACELIB by comparing it with an independently processed data set. This may highlight possible errors due to linearization of data, resonance reconstruction from the resonance parameters included as part of the ENDF tape, and conversion of data representation for angular and energy distributions, where applicable. ENDF pre-processing codes included as part of PREPRO code system is independent to NJOY and can be considered for the data verification tasks

At the outset let us consider that the ACELIB has already been generated. The flow chart that needs to be subsequently followed for data verification is as under:

1. Run ACELST to generate the ACELIB summary of contents and to convert the data as much as possible into pointwise ENDF format.
2. Retrieve the basic evaluated nuclear data file from which the ACE library was generated.
3. Run LINEAR on the tested file to linearise any non-linear interpolation laws.
4. Run RECENT on the output of LINEAR to reconstruct cross sections from the resonance parameters.
5. Run SIGMA1 on the output of RECENT to Doppler-broaden the cross sections to the same temperature that is specified in the ACELIB.
6. Run FIXUP on the output of SIGMA1 to reconstruct the redundant cross sections.
7. Run COMPLOT to compare the output of ACELST and SIGMA1.

Each of the tasks above serves a specific purpose and provides useful information. The ACELST code is included in the SIGACE code package, which has been developed to generate high temperature ACELIBs from already provided low temperature files for use in MCNP.

This code provides a compact listing of the contents of the ACELIB, which is useful when insufficient information is provided on how the file was generated. The COMPLOT comparison of the ACELST and SIGMA1 output can reveal any inconsistency in the redundant reactions. For example, the total cross section in the ACELST output from the ACELIB is given by the sum of the partials, but in SIGMA1 it is calculated directly from the total cross section. An inconsistency in the resonance range might indicate that the implied competitive widths in the resonance parameters are inconsistent with the pointwise data in file MF3 for the competing reaction (usually the inelastic cross section).

The codes are LINEAR, RECENT, SIGMA1, FIXUP, COMPLOT are provided free of cost at the website "http://www-nds.iaea.org/ndspub/endf/prepro/". The code ACELST.f is included in SIGACE code package, which can be downloaded from "http://www-nds.iaea.org/fendl21/downloads/". All the tolerances are within 0.1% for data generation using PREPRO. It is important that this value is the same as that is used for PENDF file generation to make DRAGLIB or ACELIB.

Figures III.2 to III.4 gives the comparison of plots obtained using COMPLOT. It shows the magnitude of difference between generated ACELIB and PENDF generated using PREPRO. It was noted that the large difference in cross section is at the interface of resolved resonance and unresolved resonance group. This is not a major cause of concern though.

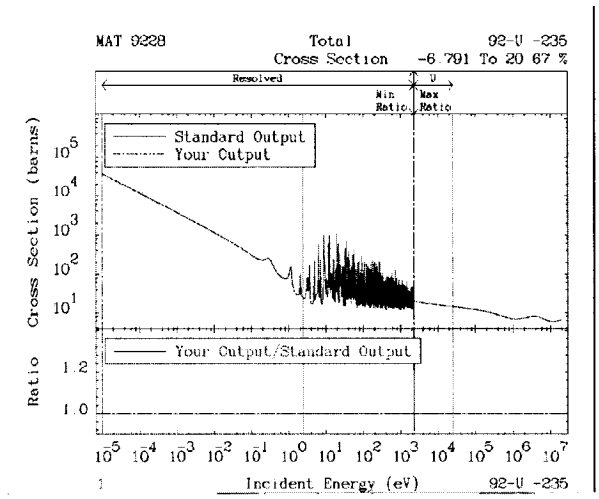

Figure III.2 COMPLOT - Total cross section of ^{235}U

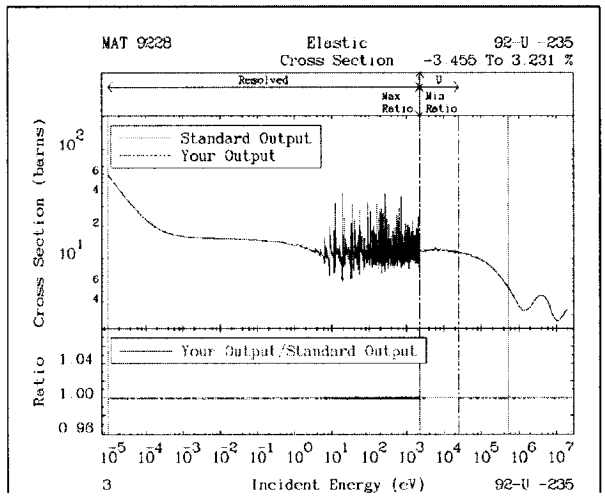

Figure III.3 COMPLOT - Elastic cross section of ^{235}U

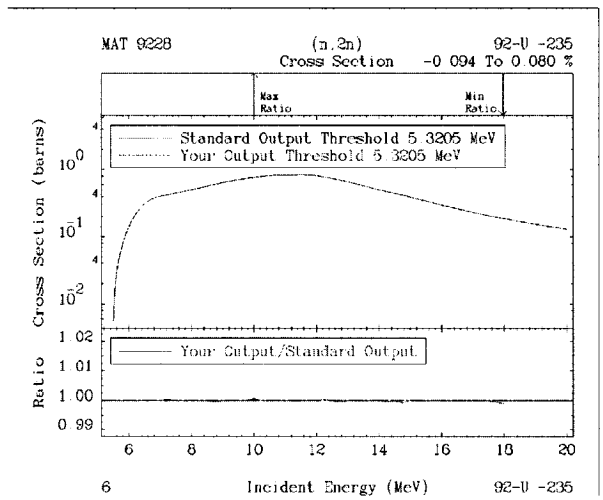

Figure III.4 COMPLOT - N,2N cross section of ^{235}U

APPENDIX IV

ENERGY FOR NORMALIZATION OF POWER IN BURNUP CALCULATIONS

Table IV.1 Energy(in MeV) from various neutron induced reactions on respective elements

Element	Decay	(n,f)	(n,γ)	(n,2n)	(n,3n)	(n,4n)	(n,α)	(n, p)	(n,2α)	(n,np)	(n, d)	(n,t)
H1(B)	0.00	0.00	2.22	0.00	0.00	0.00	0.00	0.00	0.00	0.00	0.00	0.00
(A)	0.00	0.00	2.22	0.00	0.00	0.00	0.00	0.00	0.00	0.00	0.00	0.00
H1 in H2O	0.00	0.00	2.22	0.00	0.00	0.00	0.00	0.00	0.00	0.00	0.00	0.00
	0.00	0.00	2.22	0.00	0.00	0.00	0.00	0.00	0.00	0.00	0.00	0.00
H2	0.00	0.00	6.26	-2.22	0.00	0.00	0.00	0.00	0.00	0.00	0.00	0.00
	0.00	0.00	6.26	-2.22	0.00	0.00	0.00	0.00	0.00	0.00	0.00	0.00
H2 in D2O	0.00	0.00	6.26	-2.22	0.00	0.00	0.00	0.00	0.00	0.00	0.00	0.00
	0.00	0.00	6.26	-2.22	0.00	0.00	0.00	0.00	0.00	0.00	0.00	0.00
He4	0.00	0.00	0.00	0.00	0.00	0.00	0.00	0.00	0.00	0.00	0.00	0.00
	0.00	0.00	0.00	0.00	0.00	0.00	0.00	0.00	0.00	0.00	0.00	0.00
Be9	0.00	0.00	6.81	0.00	0.00	0.00	-0.60	-12.82	0.00	0.00	-14.66	-10.44
	0.00	0.00	7.01	0.00	0.00	0.00	-0.60	-12.82	0.00	0.00	-4.40	-10.44
B10	0.00	0.00	11.46	0.00	0.00	0.00	2.79	0.23	0.00	0.00	-4.36	0.00
	0.00	0.00	11.46	0.00	0.00	0.00	2.79	0.43	0.00	0.00	-4.36	0.00
B11	0.00	0.00	3.37	-11.45	0.00	0.00	-6.63	-10.72	0.00	-11.23	0.00	-9.56
	0.00	0.00	3.37	-11.45	0.00	0.00	3.63	-10.72	0.00	-11.03	0.00	-9.56
O16	0.00	0.00	4.14	-15.66	0.00	0.00	-2.21	-9.64	-12.86	-12.13	-9.90	-14.48
	0.00	0.00	4.14	-15.66	0.00	0.00	-2.21	-2.38	-12.86	-12.13	-9.90	-14.48
Al27	0.00	0.00	7.72	-13.06	0.00	0.00	-3.13	-1.83	0.00	0.00	-6.05	-10.88
	0.00	0.00	7.72	-13.06	0.00	0.00	-3.13	-0.23	0.00	0.00	-6.05	-10.88
Cr50	0.00	0.00	9.26	-13.00	0.00	0.00	0.32	-0.26	0.00	-9.59	-7.36	0.00
	0.00	0.00	9.26	-13.00	0.00	0.00	0.32	-0.26	0.00	-9.59	-7.36	0.00
Cr52	0.00	0.00	7.94	-12.04	0.00	0.00	-1.21	-3.19	0.00	-10.51	0.00	0.00
	0.00	0.00	7.94	-12.04	0.00	0.00	-1.21	-0.68	0.00	-10.51	0.00	0.00
Cr53	0.00	0.00	9.72	-7.94	0.00	0.00	1.79	-2.64	0.00	-11.13	0.00	0.00
	0.00	0.00	9.72	-7.94	0.00	0.00	1.79	-2.64	0.00	-8.62	0.00	0.00
Cr54	0.00	0.00	6.25	-9.72	0.00	0.00	-1.55	-6.21	0.00	0.00	0.00	0.00
	0.00	0.00	6.25	-9.72	0.00	0.00	-1.55	-6.21	0.00	0.00	0.00	0.00
Fe54	0.00	0.00	9.30	-13.38	0.00	0.00	0.84	0.09	0.00	-8.85	-6.63	0.00
	0.00	0.00	9.30	-13.38	0.00	0.00	0.84	0.93	0.00	-8.85	-6.62	0.00
Fe56	0.00	0.00	7.65	-11.20	0.00	0.00	0.33	-2.91	0.00	-10.18	-7.96	-11.93
	0.00	0.00	7.65	-11.20	0.00	0.00	0.33	-0.39	0.00	-10.18	-7.96	-11.09
Fe57	0.00	0.00	10.05	-7.65	0.00	0.00	2.40	-1.91	0.00	-10.56	0.00	0.00
	0.00	0.00	10.05	-7.65	0.00	0.00	2.40	-1.91	0.00	-8.04	0.00	0.00
Fe58	0.00	0.00	6.58	-10.04	0.00	0.00	-1.40	-5.16	0.00	-11.95	0.00	0.00
	0.00	0.00	6.58	-10.04	0.00	0.00	-1.40	-5.16	0.00	-11.95	0.00	0.00
Ni58	0.00	0.00	9.00	-12.20	0.00	0.00	2.90	0.40	0.00	-8.17	-5.95	0.00
	0.00	0.00	9.00	-9.97	0.00	0.00	2.90	1.41	0.00	-8.04	-5.81	0.00
Ni60	0.00	0.00	7.82	-11.39	0.00	0.00	1.36	-2.04	0.00	-9.53	-7.31	0.00
	0.00	0.00	7.82	-11.39	0.00	0.00	1.36	0.56	0.00	-9.53	-7.31	0.00
Ni61	0.00	0.00	10.60	-7.82	0.00	0.00	3.58	-0.54	0.00	-9.86	0.00	0.00
	0.00	0.00	10.60	-7.82	0.00	0.00	3.58	-0.54	0.00	-7.26	0.00	0.00
Ni62	0.00	0.00	6.84	-10.60	0.00	0.00	-0.44	-4.46	0.00	-11.14	-8.91	0.00
	0.00	0.00	6.84	-10.60	0.00	0.00	-0.44	-4.46	0.00	-11.14	-8.91	0.00
Ni64 (B)	0.00	0.00	6.10	-9.66	0.00	0.00	-2.44	-6.52	0.00	-12.54	-10.31	0.00

B-Before lumping A-After lumping

continued, on next page

continued, from previous page

Element	Decay	(n,f)	(n,γ)	(n,2n)	(n,3n)	(n,4n)	(n,α)	(n, p)	(n,2α)	(n,np)	(n, d)	(n,t)
(A)	0.00	0.00	6.10	-9.66	0.00	0.00	-2.44	-6.52	0.00	-12.54	-10.31	0.00
Ge72	0.00	0.00	6.78	0.00	0.00	0.00	0.00	0.00	0.00	0.00	0.00	0.00
	0.00	0.00	6.78	0.00	0.00	0.00	0.00	0.00	0.00	0.00	0.00	0.00
Ge73	0.00	0.00	10.20	0.00	0.00	0.00	0.00	0.00	0.00	0.00	0.00	0.00
	0.00	0.00	10.20	0.00	0.00	0.00	0.00	0.00	0.00	0.00	0.00	0.00
Ge74	0.00	0.00	6.51	0.00	0.00	0.00	0.00	0.00	0.00	0.00	0.00	0.00
	0.00	0.00	6.96	0.00	0.00	0.00	0.00	0.00	0.00	0.00	0.00	0.00
Ge76	0.00	0.00	6.07	0.00	0.00	0.00	0.00	0.00	0.00	0.00	0.00	0.00
	0.00	0.00	7.99	0.00	0.00	0.00	0.00	0.00	0.00	0.00	0.00	0.00
As75	0.00	0.00	7.33	0.00	0.00	0.00	0.00	0.00	0.00	0.00	0.00	0.00
	0.00	0.00	8.81	0.00	0.00	0.00	0.00	0.00	0.00	0.00	0.00	0.00
Se76	0.00	0.00	7.42	0.00	0.00	0.00	0.00	0.00	0.00	0.00	0.00	0.00
	0.00	0.00	7.42	0.00	0.00	0.00	0.00	0.00	0.00	0.00	0.00	0.00
Se77	0.00	0.00	10.50	0.00	0.00	0.00	0.00	0.00	0.00	0.00	0.00	0.00
	0.00	0.00	10.50	0.00	0.00	0.00	0.00	0.00	0.00	0.00	0.00	0.00
Se78	0.00	0.00	6.98	0.00	0.00	0.00	0.00	0.00	0.00	0.00	0.00	0.00
	0.00	0.00	6.98	0.00	0.00	0.00	0.00	0.00	0.00	0.00	0.00	0.00
Se79	0.00	0.00	9.91	-6.97	-17.47	0.00	2.95	-1.42	0.00	-10.47	-8.16	-8.88
	0.05	0.00	9.91	-6.97	-17.47	0.00	2.95	-0.45	0.00	-7.89	-5.59	-8.65
Se80	0.00	0.00	6.70	0.00	0.00	0.00	0.00	0.00	0.00	0.00	0.00	0.00
	0.00	0.00	7.32	0.00	0.00	0.00	0.00	0.00	0.00	0.00	0.00	0.00
Se82	0.00	0.00	5.93	0.00	0.00	0.00	0.00	0.00	0.00	0.00	0.00	0.00
	0.00	0.00	9.35	0.00	0.00	0.00	0.00	0.00	0.00	0.00	0.00	0.00
Br79	0.00	0.00	7.88	0.00	0.00	0.00	0.00	0.00	0.00	0.00	0.00	0.00
	0.00	0.00	8.68	0.00	0.00	0.00	0.00	0.00	0.00	0.00	0.00	0.00
Br81	0.00	0.00	7.60	0.00	0.00	0.00	0.00	0.00	0.00	0.00	0.00	0.00
	0.00	0.00	10.38	0.00	0.00	0.00	0.00	0.00	0.00	0.00	0.00	0.00
Kr80	0.00	0.00	7.85	-11.52	0.00	0.00	0.97	-1.23	0.00	0.00	-6.89	-11.32
	0.00	0.00	7.87	-11.24	0.00	0.00	0.97	-0.43	0.00	0.00	-6.89	-11.32
Kr82	0.00	0.00	7.47	-10.98	0.00	0.00	1.11	-2.31	0.00	0.00	-7.77	-11.59
	0.00	0.00	7.47	-10.96	0.00	0.00	1.11	0.48	0.00	0.00	-7.77	-10.78
Kr83	0.00	0.00	10.52	-7.47	-18.43	0.00	3.43	-0.18	0.00	-9.78	-7.47	-8.88
	0.00	0.00	10.52	-7.47	-18.41	0.00	3.43	0.19	0.00	-7.00	-4.69	-8.88
Kr84	0.00	0.00	7.11	-10.52	0.00	0.00	1.17	-3.92	0.00	0.00	-8.48	-11.81
	0.00	0.00	7.11	-10.52	0.00	0.00	1.79	-0.93	0.00	0.00	-8.11	-9.02
Kr85	0.00	0.00	9.98	0.00	0.00	0.00	1.76	-2.02	0.00	0.00	-8.77	-9.32
	0.25	0.00	9.98	0.00	0.00	0.00	1.76	-0.50	0.00	0.00	-5.79	-8.95
Kr86	0.00	0.00	5.51	-9.86	-16.97	0.00	0.00	-6.52	0.00	0.00	-9.66	-12.41
	0.00	0.00	7.63	-9.86	-16.97	0.00	0.00	-1.18	0.00	0.00	-8.14	-9.42
Rb85	0.00	0.00	8.65	0.00	0.00	0.00	0.99	0.10	0.00	0.00	-4.79	-9.05
	0.00	0.00	9.41	0.00	0.00	0.00	3.77	0.10	0.00	0.00	-4.79	-9.05
Rb87	0.00	0.00	6.08	-9.92	0.00	0.00	-1.21	-3.11	0.00	-8.62	-6.39	-9.99
	0.08	0.00	8.79	-9.16	0.00	0.00	1.77	-0.99	0.00	-8.62	-6.39	-9.99
Sr86	0.00	0.00	8.43	0.00	0.00	0.00	0.00	0.00	0.00	0.00	0.00	0.00
	0.00	0.00	8.43	0.00	0.00	0.00	0.00	0.00	0.00	0.00	0.00	0.00
Sr87	0.00	0.00	11.11	0.00	0.00	0.00	0.00	0.00	0.00	0.00	0.00	0.00
	0.00	0.00	11.11	0.00	0.00	0.00	0.00	0.00	0.00	0.00	0.00	0.00
Sr88	0.00	0.00	6.36	0.00	0.00	0.00	0.00	0.00	0.00	0.00	0.00	0.00
	0.00	0.00	6.36	0.00	0.00	0.00	0.00	0.00	0.00	0.00	0.00	0.00
Sr89	0.00	0.00	7.71	0.00	0.00	0.00	2.71	-3.70	0.00	0.00	-8.66	-8.48
	0.58	0.00	7.71	0.00	0.00	0.00	2.71	-0.61	0.00	0.00	-5.95	-8.48
Sr90	0.00	0.00	5.96	0.00	0.00	0.00	0.42	-5.58	0.00	0.00	-9.28	-10.21
	1.13	0.00	7.63	0.00	0.00	0.00	2.54	-1.42	0.00	0.00	-6.19	-7.50
Y89 (B)	0.00	0.00	6.86	-11.47	0.00	0.00	0.69	-0.71	0.00	-7.07	-4.85	-9.70
(A)	0.00	0.00	7.79	-11.47	0.00	0.00	1.45	-0.71	0.00	-7.07	-4.85	-9.70

B-Before lumping A-After lumping

continued, on next page

continued, from previous page

Element	Decay	(n,f)	(n,γ)	(n,2n)	(n,3n)	(n,4n)	(n,α)	(n, p)	(n,2α)	(n,np)	(n, d)	(n,t)
Y91	0.00	0.00	6.50	0.00	0.00	0.00	1.90	0.00	0.00	0.00	-5.48	-7.02
	0.61	0.00	8.19	0.00	0.00	0.00	4.61	0.00	0.00	0.00	-5.48	-7.02
Zr0	0.00	0.00	8.04	-7.20	-14.30	0.00	5.66	-0.76	0.00	-8.36	-6.05	-7.09
	0.00	0.00	8.04	-7.20	-14.30	0.00	5.66	-0.76	0.00	-8.36	-6.05	-7.09
Zr90	0.00	0.00	7.98	-11.99	0.00	0.00	1.74	-1.51	0.00	0.00	0.00	0.00
	0.00	0.00	7.98	-10.73	0.00	0.00	1.74	-0.58	0.00	0.00	0.00	0.00
Zr91	0.00	0.00	7.98	-7.19	0.00	0.00	5.66	-0.76	0.00	0.00	0.00	0.00
	0.00	0.00	7.98	-7.19	0.00	0.00	5.66	-0.76	0.00	0.00	0.00	0.00
Zr92	0.00	0.00	7.98	-8.64	0.00	0.00	3.39	-2.84	0.00	0.00	0.00	0.00
	0.00	0.00	7.98	-8.64	0.00	0.00	3.39	-1.15	0.00	0.00	0.00	0.00
Zr93	0.00	0.00	8.19	0.00	0.00	0.00	0.00	0.00	0.00	0.00	0.00	0.00
	0.05	0.00	8.19	0.00	0.00	0.00	0.00	0.00	0.00	0.00	0.00	0.00
Zr94	0.00	0.00	7.98	-8.19	0.00	0.00	2.06	-4.22	0.00	0.00	0.00	0.00
	0.00	0.00	7.98	-8.19	0.00	0.00	3.73	-1.64	0.00	0.00	0.00	0.00
Zr95	0.00	0.00	7.94	0.00	0.00	0.00	0.00	0.00	0.00	0.00	0.00	0.00
	0.85	0.00	7.94	0.00	0.00	0.00	0.00	0.00	0.00	0.00	0.00	0.00
Zr96	0.00	0.00	7.98	-7.84	0.00	0.00	0.17	0.00	0.00	0.00	0.00	0.00
	0.00	0.00	10.70	-7.84	0.00	0.00	4.78	0.00	0.00	0.00	0.00	0.00
Nb93	0.00	0.00	7.21	-8.83	-16.72	0.00	4.92	0.69	0.00	-6.04	-3.82	-6.20
	0.00	0.00	7.21	-7.32	-16.70	0.00	5.85	0.69	0.00	-6.04	-3.82	-6.20
Nb94	0.00	0.00	8.50	0.00	0.00	0.00	0.00	0.00	0.00	0.00	0.00	0.00
	1.72	0.00	8.50	0.00	0.00	0.00	0.00	0.00	0.00	0.00	0.00	0.00
Nb95	0.00	0.00	6.93	-8.51	0.00	0.00	3.68	-0.34	0.00	0.00	-4.59	-6.55
	0.81	0.00	9.65	-8.51	0.00	0.00	5.37	-0.34	0.00	0.00	-4.59	-6.55
Mo95	0.00	0.00	9.15	-7.38	-17.05	0.00	6.40	-0.14	0.00	-8.64	-6.33	-7.38
	0.00	0.00	9.15	-7.38	-17.01	0.00	6.40	-0.14	0.00	-8.64	-6.33	-7.38
Mo96	0.00	0.00	6.82	0.00	0.00	0.00	0.00	0.00	0.00	0.00	0.00	0.00
	0.00	0.00	6.82	0.00	0.00	0.00	0.00	0.00	0.00	0.00	0.00	0.00
Mo97	0.00	0.00	8.64	0.00	0.00	0.00	0.00	0.00	0.00	0.00	0.00	0.00
	0.00	0.00	8.64	0.00	0.00	0.00	0.00	0.00	0.00	0.00	0.00	0.00
Tc99	0.00	0.00	6.76	-8.97	-16.25	0.00	3.94	-0.57	0.00	-6.50	-4.19	-6.66
	0.08	0.00	8.16	-8.97	-16.24	0.00	6.65	0.24	0.00	-6.50	-4.19	-6.66
Ru99	0.00	0.00	9.67	0.00	0.00	0.00	0.00	0.00	0.00	0.00	0.00	0.00
	0.00	0.00	9.67	0.00	0.00	0.00	0.00	0.00	0.00	0.00	0.00	0.00
Ru100	0.00	0.00	6.80	0.00	0.00	0.00	0.00	0.00	0.00	0.00	0.00	0.00
	0.00	0.00	6.80	0.00	0.00	0.00	0.00	0.00	0.00	0.00	0.00	0.00
Ru101	0.00	0.00	9.22	-6.81	-16.48	0.00	5.82	-0.84	0.00	-9.23	-6.92	-7.50
	0.00	0.00	9.22	-6.81	-16.48	0.00	5.82	-0.03	0.00	-7.83	-5.52	-7.50
Ru102	0.00	0.00	6.22	0.00	0.00	0.00	0.00	0.00	0.00	0.00	0.00	0.00
	0.00	0.00	6.22	0.00	0.00	0.00	0.00	0.00	0.00	0.00	0.00	0.00
Ru103	0.00	0.00	8.91	-6.24	-15.46	0.00	4.58	-1.57	0.00	-9.95	-7.64	-7.81
	0.60	0.00	8.91	-6.24	-15.46	0.00	4.58	-0.31	0.00	-7.34	-5.03	-7.00
Ru104	0.00	0.00	5.91	0.00	0.00	0.00	0.00	0.00	0.00	0.00	0.00	0.00
	0.00	0.00	7.09	0.00	0.00	0.00	0.00	0.00	0.00	0.00	0.00	0.00
Ru106	0.00	0.00	5.45	-8.47	-14.39	0.00	-0.07	-5.52	0.00	-11.09	-8.78	-10.51
	1.63	0.00	7.85	-7.29	-14.39	0.00	3.47	-0.89	0.00	-7.91	-5.60	-6.81
Rh103	0.00	0.00	7.00	-9.32	-16.77	0.00	3.65	0.02	0.00	-6.22	-3.91	-6.95
	0.00	0.00	8.00	-9.32	-16.77	0.00	5.05	0.02	0.00	-6.22	-3.91	-6.95
Rh105	0.00	0.00	6.59	-8.98	-15.98	0.00	2.40	-1.13	0.00	-7.05	-4.74	-7.47
	0.23	0.00	8.21	-7.98	-15.98	0.00	5.01	0.05	0.00	-7.05	-4.74	-7.47
Pd104	0.00	0.00	7.09	-9.99	-17.62	-28.18	4.20	-1.66	0.00	-8.66	-6.43	0.00
	0.00	0.00	7.09	-9.94	-17.62	-28.18	4.20	-0.66	0.00	-8.66	-6.43	0.00
Pd105	0.00	0.00	9.56	-7.09	-17.09	-24.71	6.33	0.22	0.00	-8.75	-6.53	0.00
	0.00	0.00	9.56	-7.09	-17.03	-24.71	6.33	0.22	0.00	-7.75	-5.53	0.00
Pd106 (B)	0.00	0.00	6.54	-9.56	-16.66	-26.65	3.00	-2.76	0.00	-9.35	-7.12	0.00

B-Before lumping A-After lumping

continued, on next page

continued, from previous page

Element	Decay	(n,f)	(n,γ)	(n,2n)	(n,3n)	(n,4n)	(n,α)	(n, p)	(n,2α)	(n,np)	(n, d)	(n,t)
(A)	0.00	0.00	6.54	-9.56	-16.66	-26.59	3.00	-1.14	0.00	-9.35	-7.12	0.00
Pd107	0.00	0.00	9.21	0.00	0.00	0.00	0.00	0.00	0.00	0.00	0.00	0.00
	0.01	0.00	9.21	0.00	0.00	0.00	0.00	0.00	0.00	0.00	0.00	0.00
Pd108	0.00	0.00	6.15	-9.22	-15.76	-25.32	2.06	-3.66	0.00	-9.95	-7.73	0.00
	0.00	0.00	6.60	-9.22	-15.76	-25.32	3.24	-1.02	0.00	-9.20	-6.98	0.00
Pd110	0.00	0.00	5.76	-8.81	-14.97	-24.18	1.01	-4.62	0.00	-10.61	-8.39	0.00
	0.00	0.00	7.07	-8.37	-14.97	-24.18	3.41	-1.63	0.00	-8.93	-6.71	0.00
Ag109	0.00	0.00	7.27	-9.19	-16.46	0.00	3.30	-0.33	0.00	-6.49	0.00	0.00
	0.00	0.00	8.48	-8.56	-16.46	0.00	4.91	0.11	0.00	-6.49	0.00	0.00
Cd111	0.00	0.00	9.40	0.00	0.00	0.00	0.00	0.00	0.00	0.00	0.00	0.00
	0.00	0.00	9.40	0.00	0.00	0.00	0.00	0.00	0.00	0.00	0.00	0.00
Cd112	0.00	0.00	6.54	-9.40	-16.37	0.00	2.70	-3.18	0.00	-9.64	-7.42	-10.00
	0.00	0.00	6.54	-9.40	-16.37	0.00	3.14	-1.09	0.00	-9.26	-7.04	-8.79
Cd113	0.00	0.00	9.04	-6.54	-15.94	0.00	5.31	-1.23	0.00	-9.72	-7.50	-7.70
	0.09	0.00	9.04	-6.54	-15.94	0.00	5.31	-0.39	0.00	-7.63	-5.41	-7.32
Cd114	0.00	0.00	6.15	-9.04	-15.58	0.00	1.67	-4.08	0.00	-10.27	-8.04	-10.28
	0.00	0.00	6.99	-9.04	-15.58	0.00	2.99	-1.82	0.00	-9.43	-7.21	-8.19
Cd115m	0.00	0.00	8.79	0.00	0.00	0.00	3.70	-2.58	0.00	0.00	-8.18	-8.11
	0.64	0.00	8.79	0.00	0.00	0.00	5.88	-0.20	0.00	0.00	-5.92	-7.27
Cd116	0.00	0.00	5.76	-8.70	-14.84	0.00	0.57	-5.32	0.00	-11.09	-8.87	-10.44
	0.00	0.00	8.25	-7.86	-14.84	0.00	3.13	-1.53	0.00	-8.72	-6.50	-8.18
In113	0.00	0.00	7.31	0.00	0.00	0.00	0.00	0.00	0.00	0.00	0.00	0.00
	0.00	0.00	8.09	0.00	0.00	0.00	0.00	0.00	0.00	0.00	0.00	0.00
In115	0.00	0.00	6.78	-9.04	-16.32	0.00	2.73	-0.67	0.00	-6.82	-4.50	-7.37
	0.15	0.00	6.78	-8.27	-16.32	0.00	4.82	0.18	0.00	-6.82	-4.50	-7.37
Sn115	0.00	0.00	9.57	0.00	0.00	0.00	0.00	0.00	0.00	0.00	0.00	0.00
	0.00	0.00	9.57	0.00	0.00	0.00	0.00	0.00	0.00	0.00	0.00	0.00
Sn117	0.00	0.00	9.33	0.00	0.00	0.00	0.00	0.00	0.00	0.00	0.00	0.00
	0.00	0.00	9.33	0.00	0.00	0.00	0.00	0.00	0.00	0.00	0.00	0.00
Sn118	0.00	0.00	6.49	0.00	0.00	0.00	0.00	0.00	0.00	0.00	0.00	0.00
	0.00	0.00	6.49	0.00	0.00	0.00	0.00	0.00	0.00	0.00	0.00	0.00
Sn119	0.00	0.00	9.10	0.00	0.00	0.00	0.00	0.00	0.00	0.00	0.00	0.00
	0.00	0.00	9.10	0.00	0.00	0.00	0.00	0.00	0.00	0.00	0.00	0.00
Sn121m	0.00	0.00	9.10	0.00	0.00	0.00	0.00	0.00	0.00	0.00	0.00	0.00
	0.13	0.00	9.10	0.00	0.00	0.00	0.00	0.00	0.00	0.00	0.00	0.00
Sn123	0.00	0.00	8.56	0.00	0.00	0.00	1.81	-3.60	0.00	0.00	-9.28	-8.85
	0.53	0.00	8.56	0.00	0.00	0.00	1.81	-0.53	0.00	0.00	-9.28	-6.84
Sn126	0.00	0.00	5.62	0.00	0.00	0.00	0.00	0.00	0.00	0.00	0.00	0.00
	2.90	0.00	9.20	0.00	0.00	0.00	0.00	0.00	0.00	0.00	0.00	0.00
Sb121	0.00	0.00	8.31	-9.24	-16.25	-25.84	0.35	0.40	0.00	-5.78	0.00	0.00
	0.00	0.00	9.31	-9.24	-16.25	-25.84	2.20	0.51	0.00	-5.78	0.00	0.00
Sb123	0.00	0.00	6.47	-8.97	-15.77	-25.01	2.16	-0.61	0.00	-6.56	0.00	0.00
	0.00	0.00	6.47	-7.96	-15.77	-25.01	2.16	-0.61	0.00	-6.56	0.00	0.00
Sb124	0.00	0.00	8.77	0.00	0.00	0.00	3.87	1.41	0.00	0.00	-4.85	-4.54
	2.24	0.00	8.77	0.00	0.00	0.00	5.89	1.41	0.00	0.00	-4.85	-4.54
Sb125	0.00	0.00	6.22	-8.71	-15.19	0.00	1.00	-1.57	0.00	-7.31	-5.00	-7.31
	0.57	0.00	9.34	-8.71	-15.19	0.00	1.00	-0.44	0.00	-7.31	-5.00	-7.31
Te122	0.00	0.00	6.93	0.00	0.00	0.00	5.41	-1.20	0.00	0.00	-5.78	-8.76
	0.00	0.00	6.93	0.00	0.00	0.00	5.41	-0.20	0.00	0.00	-5.78	-8.76
Te123	0.00	0.00	9.42	0.00	0.00	0.00	7.58	0.83	0.00	0.00	-5.90	-6.45
	0.02	0.00	9.42	0.00	0.00	0.00	7.58	0.83	0.00	0.00	-4.90	-6.45
Te124	0.00	0.00	6.58	0.00	0.00	0.00	4.33	-2.12	0.00	0.00	-6.36	-9.07
	0.00	0.00	6.58	0.00	0.00	0.00	4.44	-2.12	0.00	0.00	-6.36	-8.07
Te125 (B)	0.00	0.00	9.11	0.00	0.00	0.00	6.57	0.02	0.00	0.00	-6.47	-6.68
(A)	0.00	0.00	9.11	0.00	0.00	0.00	6.57	0.02	0.00	0.00	-6.47	-6.68

B-Before lumping A-After lumping

continued, on next page

continued, from previous page

Element	Decay	(n,f)	(n,γ)	(n,2n)	(n,3n)	(n,4n)	(n,α)	(n, p)	(n,2α)	(n,np)	(n, d)	(n,t)
Te126	0.00	0.00	6.29	0.00	0.00	0.00	3.40	-2.88	0.00	0.00	-6.88	-9.33
	0.00	0.00	6.52	0.00	0.00	0.00	3.40	0.24	0.00	0.00	-6.88	-9.33
Te127m	0.00	0.00	8.87	-6.30	-15.42	0.00	5.61	-0.80	0.00	-9.18	-6.87	-6.91
	0.31	0.00	8.87	-6.30	-15.42	0.00	5.61	0.37	0.00	-6.06	-3.75	-6.91
Te128	0.00	0.00	6.09	0.00	0.00	0.00	2.56	-3.48	0.00	0.00	-7.35	-9.47
	0.00	0.00	6.69	0.00	0.00	0.00	3.68	0.10	0.00	0.00	-6.18	-6.35
Te129m	0.00	0.00	8.41	0.00	0.00	0.00	4.56	-1.70	0.00	0.00	-7.44	-7.28
	0.69	0.00	8.41	0.00	0.00	0.00	4.56	0.54	0.00	0.00	-3.87	-6.12
Te130	0.00	0.00	5.93	0.00	0.00	0.00	1.90	-4.18	0.00	0.00	-7.78	-9.49
	0.00	0.00	7.64	0.00	0.00	0.00	5.48	-0.22	0.00	0.00	-5.54	-5.91
I127	0.00	0.00	6.83	-9.14	-16.28	-25.83	4.28	0.09	0.00	-6.20	0.00	0.00
	0.00	0.00	7.65	-8.53	-16.22	-25.83	4.28	0.32	0.00	-6.20	0.00	0.00
I129	0.00	0.00	6.46	0.00	0.00	0.00	0.00	0.00	0.00	0.00	0.00	0.00
	0.08	0.00	8.88	0.00	0.00	0.00	0.00	0.00	0.00	0.00	0.00	0.00
I135	0.00	0.00	3.95	0.00	0.00	0.00	0.00	0.00	0.00	0.00	0.00	0.00
	2.03	0.00	8.29	0.00	0.00	0.00	0.00	0.00	0.00	0.00	0.00	0.00
Xe128	0.00	0.00	6.91	-9.61	-16.84	0.00	4.81	-1.34	0.00	0.00	-5.94	-8.82
	0.00	0.00	6.91	-9.30	-16.84	0.00	4.81	-0.51	0.00	0.00	-5.94	-8.22
Xe130	0.00	0.00	6.61	-9.26	-16.16	0.00	4.05	-2.21	0.00	0.00	-6.44	-9.02
	0.00	0.00	6.61	-9.26	-16.16	0.00	4.28	0.22	0.00	0.00	-6.44	-8.19
Xe131	0.00	0.00	8.94	-6.62	-15.88	0.00	6.23	-0.19	0.00	-8.82	-6.51	-6.79
	0.00	0.00	8.94	-6.62	-15.88	0.00	6.23	0.39	0.00	-6.39	-4.08	-6.79
Xe132	0.00	0.00	6.45	-8.94	-15.54	0.00	3.37	-2.80	0.00	0.00	-6.90	-9.27
	0.00	0.00	6.64	-8.94	-15.54	0.00	3.97	-0.02	0.00	0.00	-6.32	-6.84
Xe134	0.00	0.00	6.45	-8.54	-14.99	0.00	2.73	-3.37	0.00	-9.52	-7.21	-9.29
	0.00	0.00	6.45	-8.36	-14.99	0.00	4.45	-0.15	0.00	-8.31	-6.00	-6.52
Xe135	0.00	0.00	7.99	-6.46	-15.00	0.00	4.36	-1.93	0.00	-9.83	-7.52	-7.48
	0.57	0.00	7.99	-6.46	-14.81	0.00	7.47	-1.93	0.00	-6.60	-4.29	-6.27
Xe136	0.00	0.00	3.86	-8.00	-14.45	0.00	2.16	-6.21	0.00	-9.92	-7.61	-9.33
	0.00	0.00	5.75	-8.00	-14.45	0.00	5.25	-1.87	0.00	-9.92	-7.61	-6.10
Cs133	0.00	0.00	6.70	-9.04	0.00	0.00	3.69	0.12	0.00	0.00	0.00	0.00
	0.00	0.00	6.70	-9.04	0.00	0.00	6.12	0.30	0.00	0.00	0.00	0.00
Cs134	0.00	0.00	8.83	0.00	0.00	0.00	0.00	0.00	0.00	0.00	0.00	0.00
	1.72	0.00	8.83	0.00	0.00	0.00	0.00	0.00	0.00	0.00	0.00	0.00
Cs135	0.00	0.00	6.55	0.00	0.00	0.00	0.00	0.00	0.00	0.00	0.00	0.00
	0.06	0.00	8.83	0.00	0.00	0.00	0.00	0.00	0.00	0.00	0.00	0.00
Cs137	0.00	0.00	4.28	-8.28	-15.05	0.00	3.06	-3.56	0.00	-7.43	-5.12	-6.93
	0.81	0.00	7.89	-6.00	-15.05	0.00	6.29	-1.67	0.00	-7.43	-5.12	-6.93
Ba134	0.00	0.00	6.98	0.00	0.00	0.00	0.00	0.00	0.00	0.00	0.00	0.00
	0.00	0.00	6.98	0.00	0.00	0.00	0.00	0.00	0.00	0.00	0.00	0.00
Ba135	0.00	0.00	9.11	0.00	0.00	0.00	0.00	0.00	0.00	0.00	0.00	0.00
	0.00	0.00	9.11	0.00	0.00	0.00	0.00	0.00	0.00	0.00	0.00	0.00
Ba136	0.00	0.00	6.90	0.00	0.00	0.00	0.00	0.00	0.00	0.00	0.00	0.00
	0.00	0.00	6.90	0.00	0.00	0.00	0.00	0.00	0.00	0.00	0.00	0.00
Ba137	0.00	0.00	8.61	0.00	0.00	0.00	0.00	0.00	0.00	0.00	0.00	0.00
	0.00	0.00	8.61	0.00	0.00	0.00	0.00	0.00	0.00	0.00	0.00	0.00
Ba138	0.00	0.00	4.71	-8.59	-15.54	0.00	3.87	-4.04	0.00	0.00	0.00	0.00
	0.00	0.00	4.71	-8.59	-15.54	0.00	3.87	-0.44	0.00	0.00	0.00	0.00
La138	0.00	0.00	8.78	-7.47	-16.64	0.00	6.80	2.53	0.00	-6.08	-3.77	-4.49
	1.26	0.00	8.78	-7.44	-16.64	0.00	6.80	2.53	0.00	-6.08	-3.77	-4.49
Ce140	0.00	0.00	5.43	0.00	0.00	0.00	0.00	0.00	0.00	0.00	0.00	0.00
	0.00	0.00	5.43	0.00	0.00	0.00	0.00	0.00	0.00	0.00	0.00	0.00
Ce141	0.00	0.00	7.21	-5.44	0.00	0.00	8.48	-1.65	0.00	0.00	-6.18	-5.08
	0.25	0.00	7.21	-5.44	0.00	0.00	8.48	-0.65	0.00	0.00	-3.35	-5.08
Ce142 (B)	0.00	0.00	5.18	0.00	0.00	0.00	0.00	0.00	0.00	0.00	0.00	0.00

B-Before lumping A-After lumping

continued, on next page

continued, from previous page

Element	Decay	(n,f)	(n,γ)	(n,2n)	(n,3n)	(n,4n)	(n,α)	(n, p)	(n,2α)	(n,np)	(n, d)	(n,t)
(A)	0.00	0.00	6.20	0.00	0.00	0.00	0.00	0.00	0.00	0.00	0.00	0.00
Ce144	0.00	0.00	4.64	-6.89	-12.00	0.00	5.19	-4.72	0.00	0.00	-7.18	-7.29
	1.35	0.00	6.88	-5.87	-12.00	0.00	7.92	-1.05	0.00	0.00	-4.78	-4.06
Pr141	0.00	0.00	5.84	-8.94	-17.38	0.00	6.14	0.20	0.00	-4.96	-6.95	-10.43
	0.00	0.00	6.71	-8.94	-17.38	0.00	6.14	0.20	0.00	-4.96	-6.95	-10.43
Nd142	0.00	0.00	6.13	0.00	0.00	0.00	0.00	0.00	0.00	0.00	0.00	0.00
	0.00	0.00	6.13	0.00	0.00	0.00	0.00	0.00	0.00	0.00	0.00	0.00
Nd143	0.00	0.00	7.82	-6.13	-15.95	0.00	9.74	-0.15	0.00	-7.50	-5.19	-4.86
	0.00	0.00	7.82	-6.13	-15.95	0.00	9.74	0.16	0.00	-6.64	-4.33	-4.86
Nd144	0.00	0.00	5.76	0.00	0.00	0.00	0.00	0.00	0.00	0.00	0.00	0.00
	1.91	0.00	5.76	0.00	0.00	0.00	0.00	0.00	0.00	0.00	0.00	0.00
Nd145	0.00	0.00	7.56	-5.76	-13.58	0.00	8.76	-1.02	0.00	-7.97	-5.66	-5.24
	0.00	0.00	7.56	-5.76	-13.58	0.00	8.76	-0.33	0.00	-6.74	-4.43	-4.92
Nd146	0.00	0.00	5.30	-7.45	-12.91	0.00	6.35	-6.95	0.00	-8.44	-10.43	-11.42
	0.00	0.00	5.71	-7.45	-12.91	0.00	7.37	-4.62	0.00	-7.75	-9.73	-10.18
Nd148	0.00	0.00	5.07	-6.95	-12.41	0.00	5.38	-7.95	0.00	-8.94	-10.93	-11.92
	0.00	0.00	5.94	-6.54	-12.41	0.00	7.61	-5.15	0.00	-6.91	-8.90	-9.59
Nd150	0.00	0.00	5.31	-6.95	-12.42	0.00	4.22	-7.95	0.00	-9.44	-11.42	-12.91
	0.00	0.00	7.41	-6.08	-12.42	0.00	8.19	-4.85	0.00	-7.00	-8.98	-10.12
Pm147	0.00	0.00	5.90	-7.67	-13.92	0.00	7.36	-0.11	0.00	-5.41	-3.10	-4.48
	0.06	0.00	5.90	-5.97	-13.88	0.00	8.60	0.29	0.00	-5.41	-3.10	-4.48
Pm148	0.00	0.00	7.26	-5.91	-13.58	0.00	8.41	1.32	0.00	-6.02	-3.71	-2.82
	1.30	0.00	7.26	-5.91	-11.88	0.00	9.10	1.32	0.00	-5.61	-3.30	-2.82
Pm148m	0.00	0.00	7.27	0.00	0.00	0.00	0.00	0.00	0.00	0.00	0.00	0.00
	2.16	0.00	7.27	0.00	0.00	0.00	0.00	0.00	0.00	0.00	0.00	0.00
Pm149	0.00	0.00	5.56	-7.27	-13.18	0.00	6.43	-0.91	0.00	-5.95	-3.64	-4.79
	0.38	0.00	7.81	-7.27	-13.18	0.00	8.76	-0.04	0.00	-5.95	-3.64	-4.39
Sm147	0.00	0.00	8.14	-6.36	-14.76	0.00	10.14	0.56	0.00	-7.12	-4.81	-4.87
	2.31	0.00	8.14	-3.81	-14.62	0.00	10.14	0.56	0.00	-5.41	-3.10	-4.83
Sm148	0.00	0.00	5.87	-8.15	-14.50	0.00	7.75	-1.68	0.00	-7.59	-5.28	-6.77
	1.99	0.00	5.87	-8.15	-11.96	0.00	7.75	-1.68	0.00	-7.59	-5.28	-5.06
Sm149	0.00	0.00	7.98	-5.86	-14.07	0.00	9.60	-0.28	0.00	0.00	0.00	0.00
	0.00	0.00	7.98	-5.86	-14.07	0.00	9.60	-0.28	0.00	0.00	0.00	0.00
Sm150	0.00	0.00	5.60	-7.99	-13.87	0.00	6.75	-2.72	0.00	-8.28	-5.97	-7.05
	0.00	0.00	5.60	-7.99	-13.87	0.00	7.16	-0.47	0.00	-8.28	-5.97	-7.05
Sm151	0.00	0.00	8.26	-5.60	-13.59	0.00	8.49	-0.41	0.00	-8.32	-6.01	-5.39
	0.02	0.00	8.26	-5.60	-13.59	0.00	8.49	0.21	0.00	-6.07	-3.76	-5.39
Sm152	0.00	0.00	5.87	-8.26	-13.86	0.00	5.27	-2.69	0.00	-8.67	-6.36	-8.09
	0.00	0.00	6.20	-8.26	-13.86	0.00	6.14	-1.14	0.00	-8.05	-5.74	-5.84
Sm154	0.00	0.00	5.81	0.00	0.00	0.00	0.00	0.00	0.00	0.00	0.00	0.00
	0.00	0.00	6.48	0.00	0.00	0.00	0.00	0.00	0.00	0.00	0.00	0.00
Eu151	0.00	0.00	6.31	-7.97	-14.35	0.00	7.87	-0.02	0.00	0.00	-2.67	-4.39
	0.00	0.00	6.31	-6.41	-14.35	0.00	7.87	-0.02	0.00	0.00	-2.67	-4.39
Eu152	0.00	0.00	8.55	-6.31	-14.28	0.00	8.83	2.66	0.00	-5.60	-3.29	-2.71
	1.29	0.00	8.55	-6.31	-12.72	0.00	8.83	2.66	0.00	-5.60	-3.29	-2.71
Eu153	0.00	0.00	6.44	-8.45	-14.70	0.00	5.83	-0.03	0.00	0.00	-3.67	-5.67
	0.00	0.00	6.44	-8.45	-14.70	0.00	8.08	0.31	0.00	0.00	-3.67	-5.67
Eu154	0.00	0.00	8.17	-6.44	-14.99	0.00	7.30	1.51	0.00	-6.47	-4.24	-3.85
	1.53	0.00	8.17	-6.44	-14.99	0.00	7.92	1.51	0.00	-6.13	-3.91	-3.85
Eu155	0.00	0.00	6.49	-7.95	-14.41	0.00	5.08	-4.97	0.00	-6.46	-8.94	-10.93
	0.13	0.00	8.19	-7.95	-14.41	0.00	6.62	-4.30	0.00	-6.46	-8.94	-10.59
Gd152	0.00	0.00	6.49	-8.61	-15.09	0.00	8.14	-1.04	0.00	-7.35	-5.04	-6.82
	2.21	0.00	6.64	-8.61	-9.75	0.00	8.14	-1.04	0.00	-7.35	-5.04	-5.26
Gd154 (B)	0.00	0.00	6.44	-8.66	-15.15	0.00	6.52	-1.20	0.00	-7.63	-5.32	-7.69
(A)	0.00	0.00	6.44	-8.51	-15.15	0.00	6.52	-1.20	0.00	-7.63	-5.32	-7.69

B-Before lumping A-After lumping

continued, on next page

continued, from previous page

Element	Decay	(n,f)	(n,γ)	(n,2n)	(n,3n)	(n,4n)	(n,α)	(n, p)	(n,2α)	(n,np)	(n, d)	(n,t)
Gd155	0.00	0.00	8.54	-6.44	-15.10	0.00	8.34	0.54	0.00	-7.64	-5.33	-5.58
	0.00	0.00	8.54	-6.44	-14.96	0.00	8.34	0.54	0.00	-7.64	-5.33	-5.58
Gd156	0.00	0.00	6.36	-8.54	-14.98	0.00	5.68	-1.67	0.00	-8.00	-5.69	-7.68
	0.00	0.00	6.36	-8.54	-14.98	0.00	6.01	0.02	0.00	-8.00	-5.69	-7.68
Gd157	0.00	0.00	7.94	-6.37	-14.91	0.00	7.28	-0.58	0.00	-8.04	-5.73	-5.87
	0.00	0.00	7.94	-6.37	-14.91	0.00	7.28	0.08	0.00	-6.34	-4.03	-5.87
Gd158	0.00	0.00	5.94	-7.94	-14.31	0.00	5.16	-2.67	0.00	-8.52	-6.21	-7.48
	0.00	0.00	6.30	-7.94	-14.31	0.00	5.83	-0.62	0.00	-7.86	-5.55	-5.79
Gd160	0.00	0.00	5.64	-7.46	-13.40	0.00	4.57	-3.62	0.00	-9.31	-7.00	-7.58
	0.00	0.00	6.84	-7.10	-13.40	0.00	6.50	-0.56	0.00	-7.67	-5.36	-5.53
Tb159	0.00	0.00	6.38	0.00	0.00	0.00	0.00	0.00	0.00	0.00	0.00	0.00
	0.00	0.00	6.38	0.00	0.00	0.00	0.00	0.00	0.00	0.00	0.00	0.00
Tb160	0.00	0.00	7.85	0.00	0.00	0.00	0.00	0.00	0.00	0.00	0.00	0.00
	1.48	0.00	8.08	0.00	0.00	0.00	0.00	0.00	0.00	0.00	0.00	0.00
Dy160	0.00	0.00	6.45	0.00	0.00	0.00	0.00	0.00	0.00	0.00	0.00	0.00
	0.00	0.00	6.45	0.00	0.00	0.00	0.00	0.00	0.00	0.00	0.00	0.00
Dy161	0.00	0.00	8.19	0.00	0.00	0.00	0.00	0.00	0.00	0.00	0.00	0.00
	0.00	0.00	8.19	0.00	0.00	0.00	0.00	0.00	0.00	0.00	0.00	0.00
Dy162	0.00	0.00	6.27	0.00	0.00	0.00	0.00	0.00	0.00	0.00	0.00	0.00
	0.00	0.00	6.27	0.00	0.00	0.00	0.00	0.00	0.00	0.00	0.00	0.00
Dy163	0.00	0.00	7.65	0.00	0.00	0.00	0.00	0.00	0.00	0.00	0.00	0.00
	0.00	0.00	7.65	0.00	0.00	0.00	0.00	0.00	0.00	0.00	0.00	0.00
Dy164	0.00	0.00	5.63	-7.64	-13.94	0.00	5.19	-2.97	0.00	0.00	0.00	0.00
	0.00	0.00	6.11	-7.64	-13.94	0.00	6.39	0.08	0.00	0.00	0.00	0.00
Ho165	0.00	0.00	6.24	-8.03	-14.66	-23.06	0.00	0.00	0.00	0.00	0.00	0.00
	0.00	0.00	6.97	-8.03	-14.66	-23.06	0.00	0.00	0.00	0.00	0.00	0.00
Er166	0.00	0.00	6.44	0.00	0.00	0.00	0.00	0.00	0.00	0.00	0.00	0.00
	0.00	0.00	6.44	0.00	0.00	0.00	0.00	0.00	0.00	0.00	0.00	0.00
Er167	0.00	0.00	7.77	0.00	0.00	0.00	0.00	0.00	0.00	0.00	0.00	0.00
	0.00	0.00	7.77	0.00	0.00	0.00	0.00	0.00	0.00	0.00	0.00	0.00
Th230	0.00	174.06	5.13	-6.79	-12.04	0.00	0.00	0.00	0.00	0.00	0.00	0.00
	4.76	174.06	5.31	-6.79	-12.04	0.00	0.00	0.00	0.00	0.00	0.00	0.00
(WLUP)		193.40										
Th232	0.00	171.93	4.79	-6.44	-11.56	0.00	0.00	0.00	0.00	0.00	0.00	0.00
	4.09	187.70	5.24	-6.25	-11.56	0.00	0.00	0.00	0.00	0.00	0.00	0.00
		193.40										
Pa231	0.00	170.00	5.56	-6.81	-12.61	0.00	0.00	0.00	0.00	0.00	0.00	0.00
	5.13	179.84	6.67	-6.81	-12.61	0.00	0.00	0.00	0.00	0.00	0.00	0.00
		203.04										
Pa233	0.00	175.58	5.21	-6.52	-12.08	0.00	0.00	0.00	0.00	0.00	0.00	0.00
	0.43	175.58	7.68	-5.41	-12.08	0.00	0.00	0.00	0.00	0.00	0.00	0.00
		203.04										
U232	0.00	180.00	5.74	-7.25	-13.15	0.00	0.00	0.00	0.00	0.00	0.00	0.00
	5.41	187.47	5.74	-7.25	-13.15	0.00	0.00	0.00	0.00	0.00	0.00	0.00
		199.62										
U233	0.00	180.87	6.84	-5.74	-13.01	0.00	0.00	0.00	0.00	0.00	0.00	0.00
	4.91	189.82	6.84	-5.74	-13.01	0.00	0.00	0.00	0.00	0.00	0.00	0.00
		200.16										
U234	0.00	179.46	5.30	-6.84	-12.60	0.00	0.00	0.00	0.00	0.00	0.00	0.00
	4.86	189.38	5.30	-6.84	-12.60	0.00	0.00	0.00	0.00	0.00	0.00	0.00
		203.34										
U235	0.00	180.89	6.55	-5.30	-12.14	-17.89	0.00	0.00	0.00	0.00	0.00	0.00
	4.86	192.31	6.55	-5.30	-12.14	-17.89	0.00	0.00	0.00	0.00	0.00	0.00
		202.53										
U236 (B)	0.00	179.51	5.12	-6.55	-11.85	0.00	0.00	0.00	0.00	0.00	0.00	0.00

B-Before lumping A-After lumping

continued, on next page

continued, from previous page

Element	Decay	(n,f)	(n,γ)	(n,2n)	(n,3n)	(n,4n)	(n,α)	(n, p)	(n,2α)	(n,np)	(n, d)	(n,t)
(A)	4.57	192.12	5.12	-6.55	-11.85	0.00	0.00	0.00	0.00	0.00	0.00	0.00
(WLUP)		200.15										
U237	0.00	180.00	6.15	-5.10	-11.66	0.00	0.00	0.00	0.00	0.00	0.00	0.00
	0.33	193.98	6.15	-5.10	-11.66	0.00	0.00	0.00	0.00	0.00	0.00	0.00
		205.42										
U238	0.00	181.33	4.80	-6.15	-11.28	0.00	0.00	0.00	0.00	0.00	0.00	0.00
	5.17	196.51	5.26	-6.15	-11.28	0.00	0.00	0.00	0.00	0.00	0.00	0.00
		212.06										
Np237	0.00	183.68	5.48	-6.57	-12.31	-19.30	0.00	0.00	0.00	0.00	0.00	0.00
	4.81	195.17	6.32	-5.71	-12.31	-19.30	0.00	0.00	0.00	0.00	0.00	0.00
		210.17										
Np239	0.00	190.00	5.17	-6.23	-11.71	0.00	0.00	0.00	0.00	0.00	0.00	0.00
(A)	0.43	190.00	6.79	-5.39	-11.71	0.00	0.00	0.00	0.00	0.00	0.00	0.00
		203.04										
Pu238	0.00	186.65	5.65	-7.00	-12.86	0.00	0.00	0.00	0.00	0.00	0.00	0.00
	5.59	195.97	5.65	-6.93	-6.99	0.00	0.00	0.00	0.00	0.00	0.00	0.00
		209.78										
Pu239	0.00	189.44	6.53	-5.65	-12.65	-18.51	0.00	0.00	0.00	0.00	0.00	0.00
	5.24	198.70	6.53	-5.65	-12.58	-12.64	0.00	0.00	0.00	0.00	0.00	0.00
		211.33										
Pu240	0.00	186.36	5.24	-6.54	-12.19	0.00	0.00	0.00	0.00	0.00	0.00	0.00
	5.25	196.87	5.24	-6.54	-12.19	0.00	0.00	0.00	0.00	0.00	0.00	0.00
		213.97										
Pu241	0.00	189.00	6.31	-5.24	-11.77	0.00	0.00	0.00	0.00	0.00	0.00	0.00
	0.01	200.74	6.31	-5.24	-11.77	0.00	0.00	0.00	0.00	0.00	0.00	0.00
		213.89										
Pu242	0.00	185.99	5.03	-6.30	-11.54	0.00	0.00	0.00	0.00	0.00	0.00	0.00
	4.98	198.93	5.23	-6.30	-11.54	0.00	0.00	0.00	0.00	0.00	0.00	0.00
		216.88										
Am241	0.00	190.83	5.54	-6.64	-12.57	0.00	0.00	0.00	0.00	0.00	0.00	0.00
	5.63	199.78	5.54	-5.54	-12.57	0.00	0.00	0.00	0.00	0.00	0.00	0.00
		216.96										
Am242	0.00	200.00	6.36	-5.49	-12.07	0.00	0.00	0.00	0.00	0.00	0.00	0.00
	0.19	200.00	6.36	-5.49	-10.98	0.00	0.00	0.00	0.00	0.00	0.00	0.00
		216.09										
Am242m	0.00	187.59	6.41	-5.54	-12.17	0.00	0.00	0.00	0.00	0.00	0.00	0.00
	0.07	197.47	6.41	-5.54	-11.07	0.00	0.00	0.00	0.00	0.00	0.00	0.00
		216.09										
Am243	0.00	190.25	5.36	-6.36	-11.91	-18.49	0.00	0.00	0.00	0.00	0.00	0.00
	5.43	200.19	6.49	-6.36	-11.91	-17.39	0.00	0.00	0.00	0.00	0.00	0.00
		222.12										
Cm242	0.00	191.42	5.70	-6.97	-13.05	0.00	0.00	0.00	0.00	0.00	0.00	0.00
	6.15	197.98	5.70	-6.28	-13.05	0.00	0.00	0.00	0.00	0.00	0.00	0.00
		212.69										
Cm243	0.00	191.54	6.80	-5.70	-12.66	-18.75	0.00	0.00	0.00	0.00	0.00	0.00
	6.17	199.73	6.80	-5.70	-11.98	-18.75	0.00	0.00	0.00	0.00	0.00	0.00
		213.12										
Cm244	0.00	190.49	5.52	-6.80	-12.49	0.00	0.00	0.00	0.00	0.00	0.00	0.00
	5.90	199.05	11.14	-6.80	-12.49	0.00	0.00	0.00	0.00	0.00	0.00	0.00
		213.17										

APPENDIX V

MODIFICATIONS IN MONTEBURNS

Modifications in the code monteb.f was done to make it capable to read the energies corresponding to (n, γ) and $(n, 2n)$ reactions. The power normalization was appropriately modified to include contributions from capture and $(n, 2n)$ reactions. Also, we have introduced in the code, the capability to calculate energy released due to decay of elements which are part of the fuel. We provide an external library with all the relevant information like energies from most of neutron induced reactions. The file also includes half life (in 10^{-8} seconds) and energy released due to decay. In the following text all the lines between '****' with numbers indicate the modifications. The comments after '****' indicate the reason for introduction of the modifications.

```
      subroutine worxs
c
      common /mbinp/nmat,mt(49),voli(49),pow,qu235,days,nouter,ninner,
     & npre,nrst,frimp,nauto(49),ntot(49),nkeff,mbxs,nisn(999,49),
     & nisnr(999,49)
      common /mbinp2/niso(999,49),nisor(999,49),title,olib,locale,posit,
     &     tmpfile,machin,CALC
      character niso*10,nisor*6,title*72,olib*10,locale*72,posit*1,
     &          machin*4,tmpfile*10,filen*21,ju30*30,char10*10,filec*11,
     &          tal*3,nm*2,file8*22,file6*22,fname*22,fname2*23,char9*9,
     &          ju17*17,char7*7,CALC*6,
     &          tape9*12,t9tmp*15,file1*22,file2*22,file3*22,file1t*22,
     &          ju10*10,ju80*80,ju3*3,tape7*12,ju6*6,blanks*4,mtuf*20,
     &          vers*2,filednz*9,ncell*6,f2name*22,char72*724,file18*22
      dimension xs(999,5,49),eflx(7,49),day(999),nfeed(99,49),flx(49),
     &        gf1(999,49),gf2(999,49),nf(3,999,49),rf(3,999,49),
     &        nmt(49),nisq(49),gad(49),fismac(49),tmst(999),pfra(999),
     &        qfis(49),flux(49),flux2(49),fiscap(999),vol(49),pwr(49),
     &        absmac(49),frfast(49),xsg(63,999,5,49),
     &        burnup(0:999,49),fluxy(49),fluxy2(49),pwrden(49),
     &        nuc(9999),iu(9999),thalf(9999),fbx(9999),aden(49),
     &        fpec(9999),fpecx(9999),fa(9999),fit(9999),grams(9999),
     &        fsf(9999),fn(9999),qrec(9999),abund(9999),frth(49),
     &        arcg(9999),wrcg(9999),gramat(9999),grmatf(9999),
     &        act(9999),nucl(9999),atomwe(9999),nucli(9999),xsh(999,49),
     &        xsec(6,9999),nuclf(9999),cflx(63,49),nisotop(9999,49),
     &        th(9999,49),thal(9999),nj(49),nis(3400),trit(63),
     &        totaval(49),totavalact(49),tmpval(999),frerr(999,49),
     &    xsdr(999,5,49),xsecdr(6,9999),drene(197,12),
     &    fismacdr(49),absmacdr(49),ndrag(197),
     &    fisenedr(49),absenedr(49),decaydr(49),decayc(197)
```

```
      real li6(49),li7(49),mtrit6(63,49),mtrit7(63,49)
      real*8 atperbcm(3500,49)
      real number(9999),htld(9999),inha(9999),inge(9999),nperp,
     &keff,nu,macfis,macabs,macn2n,mtu(49),ratio,mfis(9999,49,63),
     &mafis(63,49),mifis(9999),numb(9999,49),halflife(9999),
     &macab,macf,kinf2,n2nmac(49),n2nmacdr(49),n2nenedr(49),
     &n2npowr,n2ntot
      integer  ihit(999,49),delay
c
c...First obtain data from feed input file
c
c****************************  1  ************************************
c Following lines were introduced so as to read relevant energy information
c and decay constants needed to calculate decay energy from file called
c ''energymb.dat''
c
      write(*,888)CALC
 888  format('calc',a6)
      if (CALC.eq.'DRAGON') then
         open (66, file='energymb.dat')
         write(*,*)'reading file energymb.dat'
         do 777 i=1,197
            read(66,778)ndrag(i),decayc(i),(drene(i,k),k=1,12)
            write(*,*)i,ndrag(i),decayc(i),(drene(i,k),k=1,12)
 778        format(i10,2x,13(f11.5))
 777        continue
            endif
c****************************  1  ************************************

c
c obtain 1grp xs after dividing cross section with flux
c
c****************************  2  ************************************
c Obtaining the one-group cross sections for all elements of all mixtures

      xsdr(i,m,j)=xs(i,m,j)
c****************************  2  ************************************

      xs(i,m,j)=xs(i,m,j)/flx(j)
      if (nisn(i,j).ge.89000) iflag = 1

c
c for actinides in the mixture (eg m9901)
c
        read (11,'(17x,1pe11.5)') xs(ntot(j)+1,m,j)
c****************************  3  ************************************
c Obtaining the one-group cross sections for actinides in the mixture

        xsdr(ntot(j)+1,m,j)=xs(ntot(j)+1,m,j)
c****************************  3  ************************************
        xs(ntot(j)+1,m,j)=xs(ntot(j)+1,m,j)/flx(j)
c
c for whole mixture (eg m1)
c
       read (11,'(17x,1pe11.5)') xs(ntot(j)+2,m,j)
c****************************  4  ************************************
c Obtaining the one-group cross sections for whole mixture

       xsdr(ntot(j)+2,m,j)=xs(ntot(j)+2,m,j)
c****************************  4  ************************************
       xs(ntot(j)+2,m,j)=xs(ntot(j)+2,m,j)/flx(j)
   86 continue
```

```
         xsec(1,mn) = xs(i,1,j)
         xsec(2,mn) = xs(i,2,j)
         xsec(3,mn) = xs(i,3,j)
         xsec(4,mn) = xs(i,4,j)
c*****************************  5  ************************************
c Equating the one-group cross sections for particular reactions
c 1 - capture, 2-(n,2n), 3- (n,alpha), 4- (n, fission)

         xsecdr(1,mn) = xsdr(i,1,j)
         xsecdr(2,mn) = xsdr(i,2,j)
         xsecdr(3,mn) = xsdr(i,3,j)
         xsecdr(4,mn) = xsdr(i,4,j)
c*****************************  5  ************************************

c
c...  Read nuclide compositions from tape7
c
  220 read (16,911,err=220,end=250) kxs,(nisq(m),gad(m),m=1,4)
      write(*,*)'KXS',kxs,(nisq(m),gad(m),m=1,4)
      do 240 m=1,4
       ixs=0
       do 235 k=1,mn
         if (nucli(k).eq.nisq(m)) then
            write(*,*)'CHK1',k,m,nucli(k),nisq(m)
           ixs=1
           xs1 = xsec(1,k)
           xs2 = xsec(2,k)
           xs4 = xsec(4,k)
c*****************************  6  ************************************
           xsdr1 = xsecdr(1,k)
           xsdr2 = xsecdr(2,k)
           xsdr4 = xsecdr(4,k)
            write(*,*)'CHK2',xs1,xs2,xs4,xsdr1,xsdr2,xsdr4
c*****************************  6  ************************************
           goto 236
         endif
  235  continue
c*****************************  7  ************************************
c Obtaining energies corresponding to each reaction for each element
c drene1 - decay energy ; drene2 - fission energy; drene3 - capture energy
c drene4 - energy due to (n, 2n) reaction
c
 236   do 245 k=1,197
         if (ndrag(k).eq.nisq(m)) then
            write(*,*)'drag1',k,m,ndrag(k),nisq(m)
            drene1=drene(k,1)*decayc(k)
            drene2=drene(k,2)
            drene3=drene(k,3)
            drene4=drene(k,4)
            write(*,*)'energy',drene1,drene2,drene3,drene4
           goto 237
            endif
 245        continue
c*****************************  7  ************************************

  237  if (ixs.eq.0) then
c         write (6,*) 'Warning:  Isotope',nisq(m),
c     &               ' not found in xs lib'
       else
c
         if (voli(j).eq.0.0) voli(j) = vol(j)
         aval = gad(m)*0.6022/voli(j)
```

```
          totaval(j) = totaval(j) + aval
          if (nisq(m).ge.890000) totavalact(j) =
     &           totavalact(j) + aval
          absmac(j) = absmac(j) + aval*xs1
          n2nmac(j) = n2nmac(j) + aval*xs2
c*****************************  8  ************************************
c Calculating energies corresponding to decay, capture, (n, 2n) reactions
c for each element for power normalization

          absmacdr(j) = absmacdr(j) + aval*xsdr1
          n2nmacdr(j) = n2nmacdr(j) + aval*xsdr2
          absenedr(j) = absenedr(j) + aval*xsdr1*drene3
          n2nenedr(j) = n2nenedr(j) + aval*xsdr2*drene4
          decaydr(j)=decaydr(j)+aval*drene1*1.60217653e-3
          write(*,*)'drag2',j,absmacdr(j), n2nmacdr(j),absenedr(j),
     &    n2nenedr(j),decaydr(j)
c*****************************  8  ************************************

          if (kxs.eq.2) then
            fismac(j) = fismac(j) + aval*xs4
c*****************************  9  ************************************
c Calculating energies corresponding to fission reaction for  actinides
c for power normalization

            fismacdr(j) = fismacdr(j) + aval*xsdr4
            fisenedr(j) = fisenedr(j) + aval*xsdr4*drene2
            write(*,*)'drag3',j,fismacdr(j),fisenedr(j)
c*****************************  9  ************************************

          endif


c*****************************  10  ***********************************
c Calculating Qave using fission, capture and (n, 2n) reactions
c for power normalization

       if (CALC.eq.'DRAGON') then
       write(*,*)'i have reached here - 1c   ',CALC
       fispowr=fispowr+fisenedr(j)*voli(j)
       abspowr=abspowr+absenedr(j)*voli(j)
       n2npowr=n2npowr+n2nenedr(j)*voli(j)
       fistot=fistot+fismacdr(j)*voli(j)
       abstot=abstot+absmacdr(j)*voli(j)
       n2ntot=n2ntot+n2nmacdr(j)*voli(j)
       write(*,*)'glob1',fispowr,abspowr,n2npowr,fistot,abstot,n2ntot
       qave = fispowr+abspowr+n2npowr
       totdecay=totdecay+decaydr(j)*voli(j)
       ttt1=fispowr/fistot
       ttt2=abspowr/abstot
       ttt3=n2npowr/n2ntot
       write(*,*)'glob2',qave,ttt1,ttt2,ttt3
       goto 302
       endif
c*****************************  10  ***********************************


c
c... Normalize the flux obtained from MCNP by using the factors "nu"
c... power, energy per fission, and k-eff
c
       if (pow.lt.0.0) then
         fnorm =  (abs(pow)/1.0e+03)*pfrac1/1.602e-19
         f2norm = (abs(pow)/1.0e+03)*pfrac2/1.602e-19
```

```
      elseif (fsrc.eq.0.) then
c*****************************  11  ************************************
c Calculating normalization constant for multiplying with flux

         if (CALC.eq.'DRAGON')then
c       fnorm = nu*1.0e+6*(pow-totdecay)*pfrac1/1.602e-13/qave/keff
        fnorm = 1.0e+6*(pow-totdecay)*pfrac1/1.602e-13/qave
         write(*,*)'IHRHD2',nu,pow,totdecay,pfrac1,qave,keff,fnorm
c       f2norm = nu*1.0e+6*(pow-totdecay)*pfrac2/1.602e-13/qave/keff
        f2norm =1.0e+6*(pow-totdecay)*pfrac2/1.602e-13/qave
         write(*,*)'IHRHD3',nu,pow,totdecay,pfrac2,qave,keff,f2norm
         else
c*****************************  11  ************************************

        fnorm = nu*1.0e+6*pow*pfrac1/1.602e-13/qave/keff
         write(*,*)'IHRH2',nu,pow,pfrac1,qave,keff,fnorm
        f2norm = nu*1.0e+6*pow*pfrac2/1.602e-13/qave/keff
         write(*,*)'IHRH3',nu,pow,pfrac2,qave,keff,f2norm
         endif
      else
        fnorm = src*1.0e+6*pow*pfrac1/1.602e-13/qave/floss
        f2norm = src*1.0e+6*pow*pfrac2/1.602e-13/qave/floss
      endif

c      ENDIF
c
c... Write mcnp output to mb1t.out
c
  120 flux(j)=fnorm*flx(j)
      flux2(j)=f2norm*flx(j)
c*****************************  12  ************************************
c Re-calculating power produced

      if (CALC.eq.'DRAGON') then
      pwr(j)=(fisenedr(j)+absenedr(j)+n2nenedr(j)+decaydr(j))*
     &fnorm*voli(j)*1.602e-13/1.0e+6
c*****************************  12  ************************************

      else
      pwr(j)=qfis(j)*flux(j)*fismac(j)*voli(j)*1.602e-13/1.0e+6
      endif
      eli6 = 4.7838
      eli7 = 3.35
      pwr(j) = pwr(j) + (li6(j)*eli6 + li7(j)*eli7)*voli(j)
     &         *flux(j)*1.602e-13/1.0e+6

***************************** end ************************************

Change to be done in MONTEBURNS input file

Sidorenko single Gd pin
UNHP       ! Type of Operating System
*************************  introduce this in the input ******************
DRAGON     ! This entry is new (from original) it can either DRAGON or ORIGEN
**********************************************************************
10         ! Number of MCNP materials to burn
1          ! Material #1
```